An Abstract of the Thesis of

Michael Appel for the degree of Master of Science in Geology presented on June 15, 2001. Title: Alkaline and Peraluminous Intrusives in the Clarno Formation around Mitchell, Oregon: Ramifications on Magma Genesis and Subduction Tectonics.

Abstract approved: _____

Edward M. Taylor

The Clarno Formation is a series of volcanic, volcaniclastic, and related intrusive rocks located in central Oregon. It is the westernmost extent of a broader Eocene magmatic belt that covers much the western United States. The magmatic belt stretches eastward from Oregon to western South Dakota, and from the Canadian Yukon to northern Nevada. While once attributed to subduction of the Farallon Plate under North America, more recent work suggests that a more complex tectonic regime involving extension was in place during the early Cenozoic.

In the vicinity of Mitchell, Oregon, the Clarno Formation is well represented along with Mesozoic metamorphic and sedimentary units, and younger Tertiary volcanic and volcaniclastic units. In this area, Clarno volcanic activity occurred from ~ 52-42 Ma, producing mostly andesites and related volcaniclastic rocks. The Mitchell area is also underlain by related intrusive bodies ranging from basalt to rhyolite in composition. The Clarno was most active at ~ 49 Ma, and is dominantly calc-alkaline. In addition, there are several coeval alkaline and peraluminous intrusives also scattered throughout the Clarno Formation. While these suites are less voluminous than the calc-alkaline magmatism, they offer insight into the tectonic and magmatic processes at work in this area during the Eocene.

Whereas silicic intrusions are common in the Clarno, the high-silica rhyolite dike on the south face of Scott Butte is unusual due to its large garnet phenocrysts. The existence of primary garnet in rhyolitic magmas precludes middle to upper crustal genesis, a common source for silicic magmas. $^{40}Ar/^{39}Ar$ age determinations of the

biotite indicate an age of ~ 51 Ma. This is after andesitic volcanism had commenced, but prior to the most active period of extrusion. The presence of the almandine garnet indicates that the dike represents partial melting of lower crustal (18-25 km) material. The presence of a high field strength element (HFSE) depletion commonly associated with subduction arc magmatism indicates that either the source material had previously been metasomatised, or that some subduction melts/fluids (heat source) mixed with the crustal melt.

Two alkaline suites, a high-K calc-alkaline basanite (Marshall and Corporate Buttes) and alkaline minette/kersantite lamprophyres (near Black Butte and Mud Creek), were emplaced ~ 49 Ma, during the height of calc-alkaline activity. The basanite lacks the HFSE depletion common in the other Clarno rocks. Instead it has a HIMU-type (eg. St Helena) ocean island basalt affinity, resulting from partial melting of enriched asthenospheric mantle. In contrast, the lamprophyres represent hydrous partial melts of metasomatized lithospheric mantle veins and bodies.

Alkaline magmatism was not limited to the most active periods of calc-alkaline activity. The emplacement of an alkali basalt (Hudspeth Mill intrusion) at ~ 45 Ma occurred four million years after the largest pulse of volcanism, but still during calc-alkaline activity. This alkali basalt represents partial melting of metasomatized lithospheric mantle.

The occurrence of these alkaline suites coeval with the calc-alkaline activity is significant in that it disputes prior subduction theories for the broader Eocene magmatism that are based on spatial and temporal variations from calc-alkaline to alkaline magmatism. These suites also give further insight into the complex tectonic regime that existed in Oregon during the Eocene. The occurrence of asthenospheric melts not caused by fluid fluxing, along with lower lithospheric alkaline melts, are normally associated with extension. Extension provides these magmas with both the mechanism for melting, and the ability to reach shallow crust with little or no contamination. Extension is in agreement with both White and Robinson's (1992) interpretation that most Clarno Formation deposition occurred in extensional basins, and with other provinces in the broader Eocene magmatic belt.

Alkaline and Peraluminous Intrusives in the Clarno Formation around Mitchell, Oregon: Ramifications on Magma Genesis and Subduction Tectonics

by

Michael Appel

A THESIS

submitted to

Oregon State University

in partial fulfillment of
the requirements for the
degree of

Master of Science

Presented: June 15, 2001
Commencement June 2002

Master of Science thesis of Michael Appel presented on June 15, 2001

APPROVED

Redacted for Privacy

Major professor, representing Geology

Redacted for Privacy

Chair of Department of Geosciences

Redacted for Privacy

Dean of Graduate School

I understand that my thesis will become part of the permanent collection of Oregon State University Libraries. My signature below authorizes release of my thesis to any reader upon request.

Redacted for Privacy

Michael Appel, Author

Acknowledgement

I wish to thank several people, all of whom have played a significant role in the completion of this thesis. Thanks to my advisor Ed Taylor, for not only showing me that there is something interesting even out in the middle of nowhere, but that over 40 years in the field can instill tremendous amounts of information for that area; many thanks to Roger Nielsen, who not only was crucial in the collection of data and writing of this thesis, but who was the first to make sure that myself and my fellow graduate students were supported and progressing at all times; to Larry Snee who sponsored my work in the Ar/Ar Geochronology Lab at the U.S.G.S. facility in Denver, and to Dan Miggins who was instrumental in the laboratory work in Denver; to Chris Russo, Vaughn Balzer, and Andy Unger, for their help with acquiring data; to Jillian for all the help both directly on the thesis and in many other ways in my daily life; to my fellow graduate and undergraduate students for keeping me sain; and to Austin Powers for allowing me to constantly quote him. This thesis is dedicated to my father (whom I wish could have been around to see its completion) and my mother for sparking my interest in the natural world and for providing me with their greatest gift, their genes.

Table of Contents

Table of Contents (continued)

Table of Contents (continued)

List of Figures

List of Figures (continued)

List of Figures (continued)

List of Figures (continued)

List of Tables

List of Appendices

List of Appendices (continued)

Alkaline and Peraluminous Intrusives in the Clarno Formation around Mitchell, Oregon: Ramifications of Magma Genesis and Subduction Tectonics

Chapter 1: Subduction and Central Oregon

Introduction

In the past, much effort has been spent studying divergent margins and the processes that occur there. However, in more recent years, focus has shifted away from divergent margins toward the study of convergent margins and especially subduction zones. The Cascade Range is one such subduction zone that has been subjected to this increased study. Yet, the Cascades are only part of a much longer history of subduction and accretion of various plates beneath the western coast of the North American Plate. While much of the attention has been focused on the formation of the Cascades, this only covers the last ~ 40 million years. Prior to the Cascades, subduction was occurring, but both the trench and the resulting arc were further east. To gain a complete understanding of long–term effects of Tertiary subduction, pre-Cascadian subduction events must also be considered.

Tectonic reconstructions of the western margin of North America suggest that subduction has occurred almost continuously throughout the Cenozoic, with separate events in the Mesozoic and Paleozoic. Rocks exposed east of the Cascades are an important record of the early Cenozoic subduction. This holds especially true for the widespread igneous rocks of Eocene age.

During the Eocene, the trench, now 200 miles west of the current coast, was probably located under what is now the eastern Willamette Valley or the Western Cascades (Rogers and Novitsky-Evans, 1977). Because of this, the volcanic activity was focused east of the Cascades. The Clarno Formation is a series of calc-alkaline volcanic and intrusive rocks located in central Oregon. It marks the western edge of a

large group of Eocene-aged igneous rocks stretching from the Canadian Yukon in the north to northern Nevada in the south and as far east as the Black Hills of South Dakota (Dudás and Harlan, 1999). Traditionally, these rocks have been interpreted as a magmatic arc resulting from subduction of the Farallon Plate underneath the North American Plate.

Unfortunately, a simple subduction zone fails to explain the overall width of the magmatic activity, over 1500 km from the trench to the Black Hills (Dudás, 1991). Instead it was believed that a migrating subduction zone or a shallow, low-inclination slab resulted in the wider area of activity (Lipman, 1980; Armstrong, 1988). Such a migration would result in progressively younger volcanic rocks to the west, and a switch from arc calc-alkaline rocks to back-arc alkaline suites at a given location with time. Initial examination suggested that both trends were observable in the western US, and so it was thought that the arc must have migrated from the east into Oregon during the Eocene. However, recent work on many of the Eocene rocks have brought this interpretation into doubt. While many of the suites in Canada can still be interpreted as resulting from normal subduction (Dostal et al., 1998), much of the activity in the United States appears to be more complex.

Part of the reason for this shift in interpretation is that many of these new studies utilize recent advances in geochemistry and geochronology to better resolve the source material and the timing of magmatic activity. First, more detailed sampling and dating shows that in most places, calc-alkaline rocks appear in close proximity with coeval alkaline rocks (Dudás, 1991). This differs from a migrating arc, which would result in a progression from calc-alkaline to alkaline rocks as the locus of magmatism moved away from a given location. Secondly, as more of the suites are being re-dated using more accurate $^{40}Ar/^{39}Ar$ geochronology, the younging westward trend is less obvious (Armstrong, 1988). Finally, more recent trace-element and isotope studies suggest that there were other significant events, such as extension and isostatic rebound, taking place that could have played a major, if not dominant role, in the igneous activity (Norman and Mertzman, 1991; Dudás, 1991; Carlson et al., 1991). Many of the investigators suggest that a subduction signature seen in many of

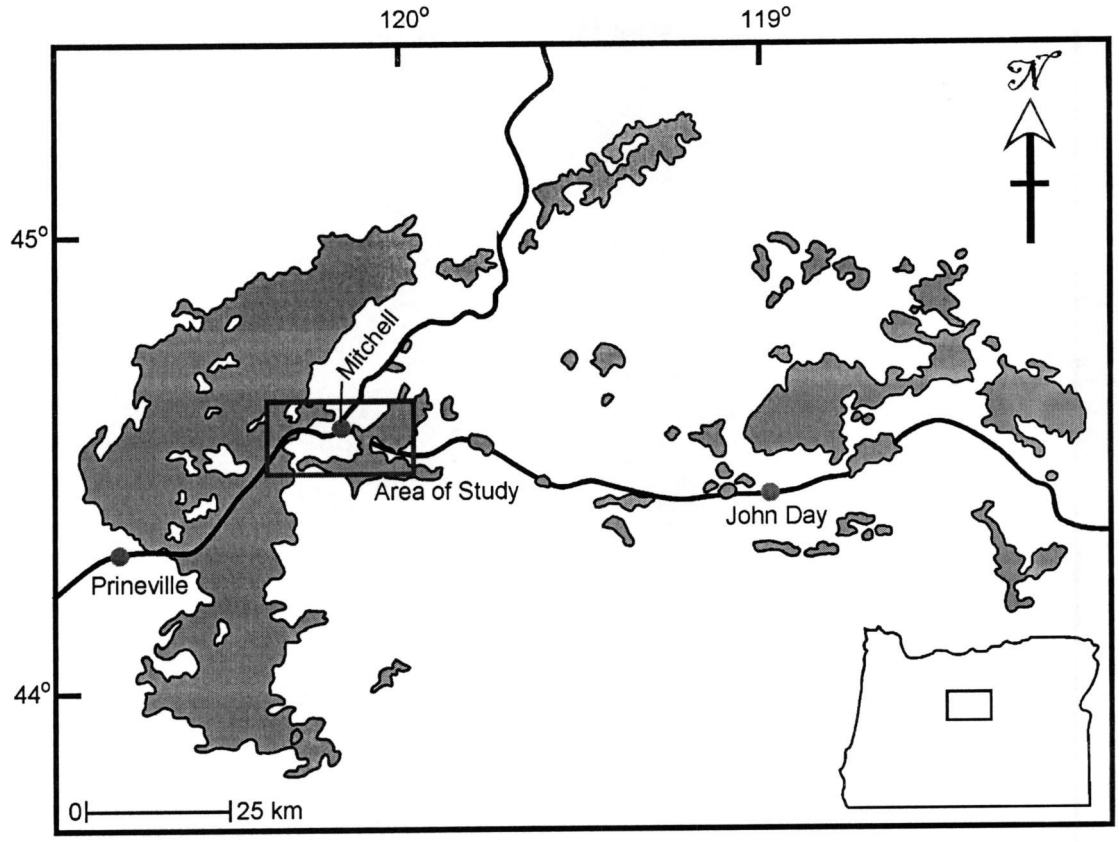

Figure 1.1: Map of central Oregon showing the distribution of the Eocene Clarno Formation (after Suayah and Rogers, 1991). This study will focus on several intrusive bodies in the area around Mitchell.

the suites may have resulted from minor fluxes of fluids (Dostal et al., 1998) or been inherited from older Mesozoic events (Norman and Mertzman, 1991, O'Brien et al., 1991). This differs from the idea that the signatures reflects the dominance of subduction-related fluid fluxing as the cause of the magmatism.

While the Clarno Formation has been studied for over 40 years, the quality of data obtained is marginal by today's standards. A better understanding of the evolution and geochronology of the Clarno Formation can help to resolve the magmatic and tectonic questions that persist about the Eocene activity in central Oregon.

Previous workers on the Eocene volcanic rocks throughout the northwestern United States have normally focused on larger, more abundant suites that constitute

the majority of the activity. Recent studies consider many of the less abundant, but equally important, suites of rocks. Commonly these smaller suites contain more mafic or other unusual rocks in which the source characteristics have not been destroyed by modification or mixing. These rocks allow for a more accurate investigation of magma sources and genesis.

Within the Clarno Formation there are several smaller suites of rocks that have not been well studied. These smaller suites appear to coincide with the main Clarno Formation, but are not representative of the larger volcanism. Instead they are either more alkaline or more aluminous than comparable Clarno rocks. Understanding the relationships between these small suites and the larger dominant volcanism may help to increase the understanding of the magmatic processes and perhaps the tectonic setting that created the Clarno Formation. Several intrusive bodies that represent these smaller suites are present near Mitchell, in central Oregon (Figure 1.1). These intrusive bodies often form topographic relief structures, and are thought to be intrusive plugs, dikes, or sills that are contemporaneous with the larger-scale volcanism.

This project focused on several of these intrusives thought to date from the period of Clarno activity. Preliminary unpublished work by Dr. Edward Taylor shows their petrography and geochemisty differs from the main Clarno activity. These rocks are clearly intrusive in nature and often cross-cut the surrounding strata. If these rocks are related to the Clarno Formation, then an understanding of their relationship to the more dominant activity is crucial. Comparisons with similar types of rocks in other areas of the western U.S. and throughout the world can be used to better understand the processes taking place during the Eocene and perhaps to even help reevaluate the current model of a subduction arc on a thin continental margin (Rogers and Novitsky-Evans, 1977).

Geologic Setting

In central Oregon, the Tertiary geologic record is dominated by volcanic activity. Wheeler County, in central Oregon, has large exposures of the Eocene Clarno Forma-

tion, the Oligocene John Day Formation, and the Miocene Columbia River Basalt Group. This study focused on several suites near the small town of Mitchell in Wheeler County. While previous workers have focused on the main units of these three periods, only cursory mention of several alkaline and peraluminous suites has been made.

In the Mitchell area, the most abundant rocks are the Tertiary volcanics of the Clarno, John Day, and Picture Gorge (Columbia River Basalt) Formations. In addition to the Tertiary volcanics, there are also pre-Cretaceous metamorphic and Cretaceous sedimentary rocks present in the area.

The oldest rocks in the area are a mélange of pre-Cretaceous metasediments consisting of phyllite, blueschist, chert, serpentinite, crystalline limestone, and marble, with some metavolcanics (mostly meta-pillow basalts) also interspersed. These rocks have been intensely deformed during the Triassic or Early Jurassic. The blueschist common in these rocks was probably formed in a subduction environment (Swanson, 1969). This suggests subduction was likely active along this margin in the early to middle Mesozoic.

The oldest non-metamorphosed sedimentary rocks in the area are the Hudspeth and Gable Creek Formations. These are Cretaceous marine rocks, originally classified as fluvial-deltaic and shallow marine by Oles and Enlows (1971), but are more likely of turbiditic origin (Kleinhans et al., 1984). The Hudspeth Formation is predominantly mudstone, with siltstone and thin beds of sandstone interspersed. The Gable Creek Formation is a series of conglomerate and coarse-grained sandstone units. These two formations are interfingered together repeatedly throughout the stratigraphic sequence (Oles, 1973).

The Hudspeth and Gable Creek Formations are unconformably overlain by the Clarno Formation. This represents the first of the three main volcanic periods. It is up to 2 kilometers thick and spatially heterogeneous (White and Robinson, 1992). The Clarno Formation is dominantly andesitic volcanics with compositions ranging from basalt to rhyolite. In addition to lavas, the formation also includes large mudflows, volcanic breccias, ash flows, and related tuffaceous sediments (Noblett, 1981). Plugs,

sills, and dikes that range in composition from basaltic to rhyolitic also heavily intrude the area (Oles and Enlows, 1971).

Oles and Enlows (1971) informally divided the Clarno Group into two formations, the lower and upper, on the basis of a large angular unconformity and differences in the sequences. This terminology was never formally adopted and instead most authors have referred to the upper and lower sections of the Clarno Formation.

The lower section of the Clarno makes up most of the Clarno rocks in the Mitchell area. The lavas grade from porphyritic two-pyroxene andesite to nonporphyritic quartz-bearing andesite, with some basaltic lavas also present. The lavas make up the majority of the lower portion with tuffs and breccias also present. The upper portion is much less abundant and appears to be missing in some areas. In the Mitchell area, Oles and Enlows (1971) separated a series of mudflows, andesites, and tuffs thought to have originated at Keyes Mountain as the upper section of the Clarno. However, these are more likely part of the lower section.

As previously mentioned, the Clarno Formation coincides with a broader group of calc-alkaline and alkaline suites extending across the northwest as far east as the Black Hills of South Dakota. These provinces, the Coville complex, the Challis complex, the Absaroka province, the Black Hills, and many smaller areas throughout Montana all exhibit a similar chemical affinity and were all active throughout the Eocene. These are often referred to as the Challis volcanic arc (see chapter 2).

Obtaining accurate radiometric dates on the Clarno lavas has been a recurring problem due to widespread alteration and weathering. Dates range from 30 Ma (Enlows and Parker, 1972) to 54 Ma (Bestland et al., 1999). Yet, despite this large range, most workers place Clarno activity completely within the Eocene, with most of the activity at 49 Ma. A decrease in subduction in the late Eocene, possibly caused by further reorganization of the Pacific Plate system, caused a sudden shift in volcanism about 40 million years ago along the western margin of the North American Plate. This caused the magmatic arc to jump from the Clarno area to the western Cascades (Robinson et al., 1984).

The John Day Formation followed the Clarno Formation in late Eocene and during most of the Oligocene. With the shift in volcanism to the Cascades around 40 Ma, the lithology of the deposits in the Mitchell area also changed. The John Day Formation is dominated by fluvial and lacustrine tuffs that are preserved as paleosols. It also contains early lavas, several ignimbrites, and a variety of back-arc intrusives. The John Day Formation air-fall tuffs are the distal deposits from the Cascades (White and Robinson, 1992).

The third and final Tertiary volcanic unit is the Miocene Columbia River Basalt Group. This group covers most of the northwestern part of the 15-minute Mitchell quadrangle. It consists almost entirely of flood basalt flows, most of which belong to the Picture Gorge Formation. While this formation once covered most of the area, subsequent uplift and erosion has removed it from much of the study area.

Chapter 2: The Clarno and other Eocene Magmatism

Summery of Previous Work

The traditional petrogenetic model for the widespread Eocene igneous activity that stretched from central Oregon to the Black Hills of South Dakota relates it to a subduction arc (Figure 2.1). At the time this model was proposed, the data available indicated both a succession of younger rocks to west and an increase in K_2O eastward

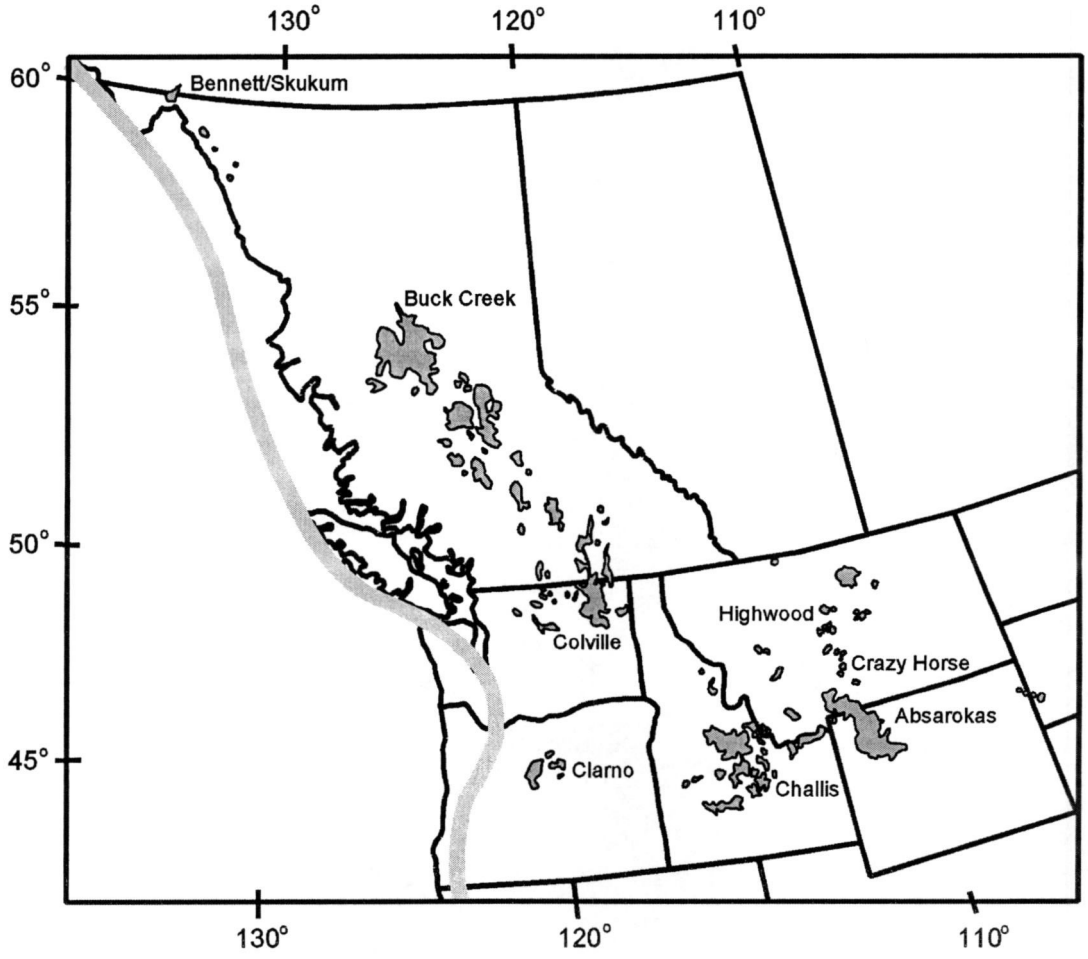

Figure 2.1: Map of western North America showing the distribution of Eocene igneous rocks. Several centers on which recent studies have been conducted are labeled on the map. The gray line represents the likely location of the Eocene trench.

(Dickenson, 1979; Lipman, 1980). Both features thought to be typical in subduction zones. However, more recent data have resulted in less defined temporal and geochemical patterns.

In Canada, the volcanism looked more like a traditional active continental margin. Here the arc is only 250-400 km wide and fairly continuous from west to east. The width was slightly larger than an average subduction zone due to rapid convergence and a shallow dip on the slab (Dostal et al., 1998). The arc also seems to show a chemical zonation with more alkalic rocks further to the east (Dudás, 1991). The Buck Creek Formation is one of the large exposures of high-K calc-alkaline rocks erupted around 50 Ma in British Columbia (Dostal et al., 1998). Rocks from Buck Creek show large-ion lithophile enrichments and Nb and Ta depletions, a typical signature of subduction zone volcanics. Yet, the overlying basalts record a transition to an intraplate extensional environment. Much of the Buck Creek volcanic deposits are located in extensional grabens that were active during magmatism.

Further south in the United States, the igneous activity was spread over an area almost 1000 km wide (Dudás, 1991). Even if this magmatic arc was once continuous across the entire area, today only scattered provinces remain.

The Colville complex of northeastern Washington contains high-K calc-alkaline rocks intermediate to felsic in composition (Carlson et al., 1991). These rocks range from 53-47 Ma, with the majority around 49 Ma. Additionally, there are less abundant alkali-rich felsic intrusives that range from 61-51 Ma. Both suites appear to have been emplaced during tectonic extension. Extension appears to have started about 61 Ma and reached a maximum at about 49 Ma. This led to abundant faulting and grabens into which much of the volcanism was deposited. As extension increased, the residence times of magmas in the crust shortened allowing for less crustal contamination (ibid). This allowed more primitive material to reach the surface. The trace elements and mineralogy from these rocks suggest a lithospheric mantle source. Yet, while this material shows a subduction signature, Sr isotopes suggest that this may be due to an earlier enrichment event and not contemporaneous subduction. Instead, melting may have been in response to extensional rebound of overthickened crust.

Large sections of Idaho are covered by volcanic and plutonic rocks commonly referred to as the Challis Formation. These rocks were erupted or emplaced between 51-40 Ma (Norman and Mertzman, 1991). Recent work by Lewis and Kiilsgaard (1991) shows that large areas of intrusive rocks originally believed to be part of the Cretaceous Idaho batholith are instead Challis rocks. These intrusives range in age from 50 Ma to 44 Ma. Two main suites were recognized, inferred to have two distinct sources and magmatic histories. One appears to represent a lower crustal melt on the basis of Sr isotopes, while the other represents an upper mantle melt with subsequent crustal assimilation due to its trace-element and Sr isotopic signatures. Lead isotopes suggest a source more similar to the Snake River Basalts than typical subduction magmas.

Similar results have been proposed for much of the Challis volcanics. While the Challis volcanics erupted on an evolving convergent margin, the Challis rocks do not appear to be direct products of a subduction-generated magma (Norman and Mertzman, 1991). As in the Challis-age intrusives, the magma generation appears to be in the lower crust and lithospheric mantle. While no reason was given for the melting that generated the intrusives (Lewis and Kiilsgaard, 1991), Norman and Mertzman (1991) suggest that tectonic thickening of the crust and subsequent extension resulted in the Challis volcanics.

Further east in the Highwood Mountains of Montana (54-50 Ma), the picture becomes even more complex because older crustal rocks become involved. High-K rocks suggest an asthenospheric source mixed with heterogeneous lithospheric mantle of Archean age (O'Brien et al., 1991). In order to explain the Rb and Sr isotopic results, the rocks must also contain a source enriched in large-ion lithophile elements. This was presumed to be due to subduction-related fluid of Eocene or late Cretaceous age. Similar rocks have been found in western Mexico and other subduction centers also undergoing extension. This reinforces the idea that even though subduction was occurring, extension was likely occurring also. O'Brien et al.'s favored model suggests that a devolitizing subducted slab caused asthenospheric melts in the mantle wedge, which in turn assimilated older Wyoming craton mantle. While subduction

has be used to explain the Highwood Mountain compositions, additional areas in Montana and Wyoming disagree with this conclusion.

The Absaroka Mountains in southwestern Montana and northwestern Wyoming form another large province of volcanic and plutonic rocks ranging from 53-43 Ma (Hiza, 1999). As in many of the other locales throughout the Eocene magmatic province, both alkalic and calc-alkaline rocks that overlap each other in age are found here. Once again, a lack of both an age progression and a shift toward more alkalic products suggests that subduction is not the cause, but that extension may be.

Dudás (1991) provides the best summary of concerns relating to a subduction source for the entire area from Oregon to South Dakota in his work on the Crazy Mountains of Montana. While trace-element geochemical evidence suggests a subduction source, other geologic and tectonic constraints seem to dispute this. Most importantly, the previously suggested chemical zonation and age progression in the magmatic belt have become less clear with additional geochemical studies and age determinations. Not only does it appear that many of the centers were active at the same time across the entire belt, but both calc-alkaline and alkaline rocks were emplaced in many of the centers at the same time. Yet these patterns were basis for the hypothesis of a migrating subduction arc. Likewise, the hypothesis of a near flat slab cannot account for the needed thermal input to create the necessary volcanism without the presence of hot asthenosphere. However, most models of flat slab subduction, including those in the Andes, infer direct contact between the descending slab and the lithosphere. This precludes the existence of a mantle wedge of hot asthenosphere in contact with the lithosphere. Furthermore, the hypothesis is made more difficult by the thick Wyoming craton, which would force the slab deeper than the calc-alkaline chemistry would allow. Instead alternate hypotheses for the melting could be by mantle upwelling, or by rebound from earlier uplift and crustal thickening (ibid).

The Clarno Formation is the western extent of the Eocene calc-alkaline magmatic activity. The current tectonic model is that it resulted from subduction zone volcanism on the edge of a thin continental margin, 20-30 km thick, under conditions intermediate between an Andean-style continental arc and an island-arc (Rogers and No-

vitsky-Evans, 1977; Noblett, 1981). The volcanism resulted from subduction of the Pacific Farallon Plate underneath the North American Plate along a trench located under the current western Cascades (Rogers and Novitsky-Evans, 1977).

White and Robinson (1992) used sedimentological analysis of the Clarno Formation to determine that the Clarno arc was not a linear chain of stratocones, but instead a broad, diffuse arc of dominantly small, short-lived andesitic volcanoes with a few larger and longer-lived silicic centers. This accounts for the heterogeneous and spatially variable nature of the Clarno units.

White and Robinson (1992) also noted that the lack of compressional structures, the abundance of small volcanic centers in lowlands, and the thickness of the formation all suggest the Clarno was deposited in an extensional setting rather than a compressional setting. They attributed this to both intra-arc extension and regional block rotation due to the oblique subduction. This agrees with paleomagnetic work by Gromme et al. (1986) and Heller and Ryberg (1983), which show significant clockwise rotation took place both during and after the Clarno deposition. This rotation resulted in extension over much of the area that the Clarno now occupies.

Rogers and Novitsky-Evans (1977) held that the Clarno Formation mimicked a continental arc, but with a K_2O-SiO_2 relationship more intermediate between a continental arc and an island arc. Histograms of SiO_2 content for the Clarno rocks also indicate an intermediate character between island arcs and continental margins. Using the K_2O-SiO_2 relationship, they inferred that the Clarno was formed similarly to other continental arcs, but on a thinner (20-30 km thick) continental crust.

Noblett (1981) further distinguished between lower porphyritic and higher nonporphyritic units as resulting from small changes in depth to the subducting slab. Slab depths were calculated using the K-h diagrams of Nielson and Stoiber (1973) for both units. Since the upper nonporphyritic unit had slightly higher K values, a deeper depth is required for its formation. The lower unit resulted from hydrous melts originating on the slab and interacting with mantle peridotite, followed by fractionation. The presence of quartz in the upper unit requires a different explanation though. Marsh and Carmichael (1974) and Ringwood (1975) suggest that quartz is formed by

the partial melting of anhydrous quartz eclogite. The lack of hydrous phases in the source region could be attributed to the deeper slab. So the higher unit represents deeper melting of the slab under anhydrous conditions with little mantle interaction during assent and prior to differentiation. Due to the age of these studies, both used mostly major-element chemistry and petrology, with few trace elements, to reach these conclusions.

Rogers and Ragland (1980) conducted the first significant trace-element study on the Clarno Formation. They found that the trace elements support magmatism on a thin continental margin, intermediate between an Andean-style continental margin and an island arc. The lithophile elements (Na, K, Rb, Ba) were slightly higher than island arcs, but lower than most continental arcs. They modeled the Clarno by both Rayleigh and Nornst fractionation for Rb, Y, Zr, and Cr and concluded that the mostly likely explanation is a series of partial melts originating in the mantle.

More recent work by Suayah and Rodgers that also included some trace-element work (1991) suggested that crystal fractionation played only a minor role and that magma mixing and assimilation was the dominant process in the formation of the Clarno volcanics. The lack of clear trends on compatible-incompatible trace-element diagrams (ex. Ni-Rb), along with the failure of Rayleigh and least-square modeling for crystal fractionation are cited as evidence against widespread evolution by this process. In many samples, mixing or assimilation was immediately evident in the petrography. Disequilibrium textures such as resorbed phenocrysts, spongy textures on many phenocrysts, and xenoliths are common. Mixing is also consistent with linear trends of elemental variation diagrams (ex. CaO-FeO, MgO-Na_2O) and scatter on the Sr isotopic diagram. Sr isotope values also indicate both the magma generation and most of the subsequent mixing took place in the mantle with only minor amounts of young crust being assimilated. Therefore, they conclude that the Clarno's petrogenesis is dominated by mixing of mantle melts and minor assimilation, with some fractionation involved in the formation of some evolved suites.

Alkaline and Peraluminous Suites of the Clarno Formation

This study will encompass four main suites of rocks from the Clarno. Each of the units had been previously mapped or mentioned in other work, but none have been thoroughly studied. All of the units are either volumetrically or spatially significant, or are lithologically distinct from other Clarno rocks. Because of this, these suites are not likely to be related to minor interactions between the magmas and the surrounding crust.

Marshall Butte, about 4 km east-northeast of the town of Mitchell, is believed to be a large plug-like intrusion into the Clarno Formation (Figure 2.2). Whereas most of the Clarno lavas and intrusives are andesitic in nature, the suite from Marshall Butte is much more mafic in composition. The most conspicuous difference between this and other mafic suites in the area is the abundance of nepheline and lack of plagioclase, indicating a significant silica undersaturation. Corporate Butte, just over 1 kilometer north of the city of Mitchell, is another small intrusive plug (Figure 2.2). While this butte is not officially named, the presence of the word "corporate" over the butte on older topographic maps led to the unofficial name of Corporate Butte. This terminology will be used for the remainder of the study. While it is distinct from Marshall Butte, similarities in mineralogy and chemistry suggest a possible genetic relationship. Both intrusions seem to cross-cut the surrounding Clarno mudflows and lavas, and Cretaceous conglomerates.

The Hudspeth Mill (or Hudmill) suite is named for the old Hudspeth saw mill located about 8 km northwest of Mitchell (Figure 2.2). Here a large intrusion is cut by US 26, just south of the old mill. The intrusion is sill-like is some spots, but appears to cross-cut the strata in others. Again this suite is more mafic than the Clarno Formation tuffs that surround it. While not as mafic as Marshall and Corporate Buttes, it has higher concentrations of alkalis (Na & K) than most mafic rocks in the area.

A series of small mica-rich lamprophyric dikes crop out in the Black Butte and Spetch Rim area, about 10 km due west of Mitchell (Figure 2.2). Most of the dikes lie within a 2 km radius of the butte and along Spetch Rim to the south. These dikes are

lithologically, minerologically, and chemically distinct from other basalt dikes in the Mitchell area. Related to the Black Butte and Spetch Rim dikes are the Mud Creek dikes. These dikes lie 4 km due west of Mitchell along Mud Creek (Figure 2.2). While their mineralogy differs from the other lamprophyric dikes, they do contain abundant phenocrysts of mica. Both groups of dikes intrude the Cretaceous mudstone and conglomerate.

About 20 km northeast of Mitchell a dike invades the surrounding Cretaceous and pre-Cretaceous rocks near Scott Butte (Figure 2.2). This is a garnet and biotite-bearing rhyolite dike. The presence of garnet distinguishes this rhyolite from other silicic rocks in the area. Previous K/Ar dating shows this intrusion to be ~ 42 Ma (Brittain Hill, personal communication), during the period of late Clarno activity.

Each suite has unique characteristics that separate it from the dominant intrusive and volcanic activity of the Clarno. The goal of this investigation is to determine the petrogenesis of these suites and their relation to the dominant Clarno activity. This is done using bulk-rock and phase compositions, along with radioactive age determinations. This work is significant since many of these suites are either absent or briefly treated in the Clarno literature. Due to their unique characteristics, documentation and study of these suites can have significant ramifications on discussions of Clarno Formation tectonics, as well as significant implications for the broader belt of Eocene magmatic activity.

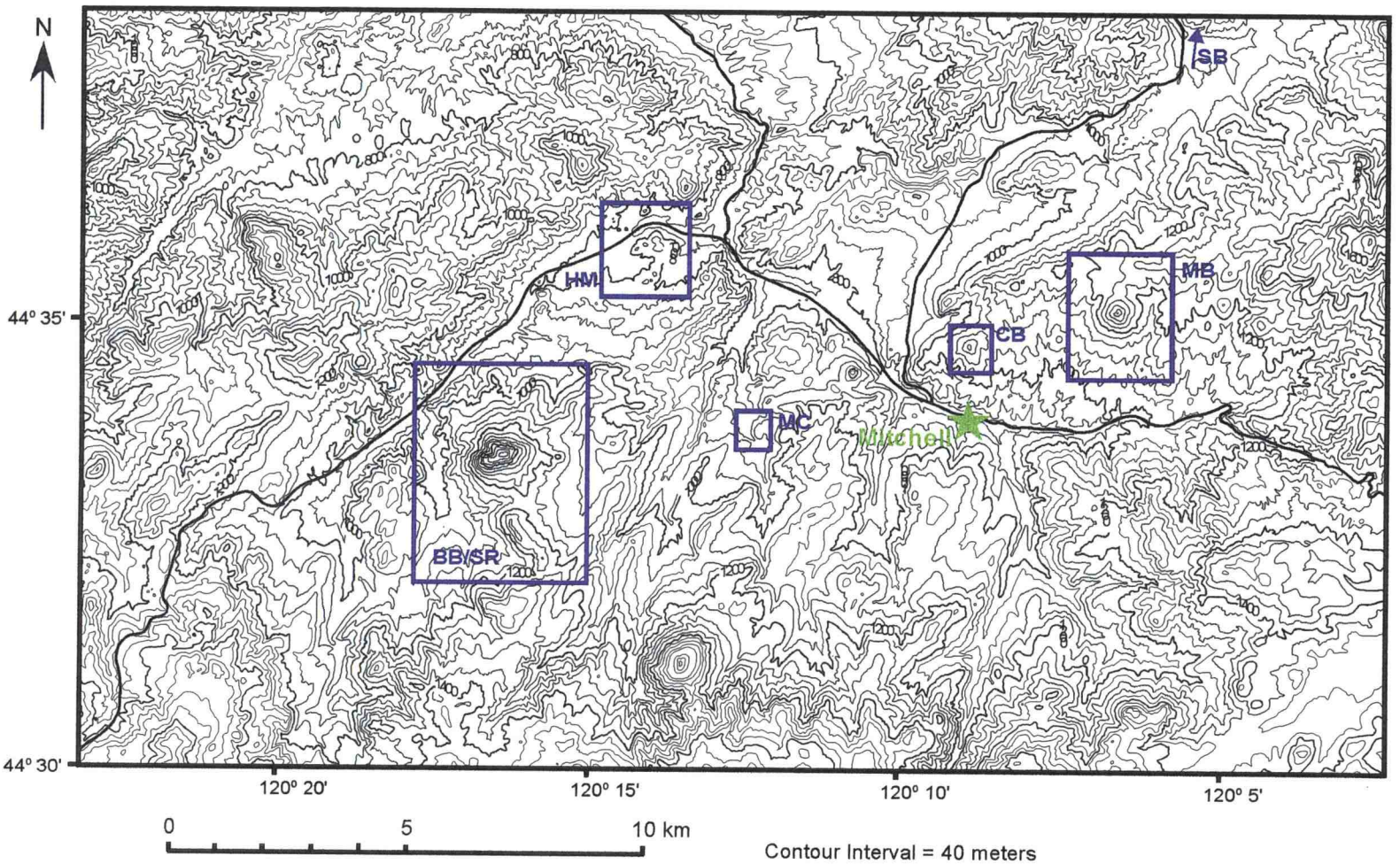

Figure 2.2: Topographic map of the study area with the locations of the four main groups of intrusives. MB: Marshall Butte, CB: Corporate Butte, HM: Hudspeth Mill Intrusion, BB/SR: Black Butte and Spetch Rim Lamprophyres, MC: Mudcreek Lamprophyres, SB: Scott Butte rhyolite dike

Chapter 3: Analytical Methods

The first step in classifying the rocks from these intrusive suites is to conduct a comprehensive geochemical study of them. Several hundred samples have already been collected by Dr. E. Taylor, Dr. H. Enlows, and Dr. K. Oles, and analyzed using X-ray fluorescence by Dr. Taylor and neutron activation analysis by Dr. Scott Hughes. This work has provided major, minor, and trace-element data on both these intrusives, and the other Clarno units as well. Further sampling of the alkaline and peraluminous suites was conducted by myself during the summer of 1999 for additional geochemical analysis.

Major-element bulk data were determined using Inductively Coupled Plasma - Atomic Emission Spectrometry (ICP-AES) at Oregon State University, and by X-Ray Fluorescence analysis conducted at Washington State University's Department of Geology. Major-element compositions for specific phases were analyzed by electron microprobe at the Oregon State University Microprobe Laboratory. Finally, trace- element compositions were determined by Inductively Coupled Plasma Mass Spectrometry (ICP-MS) at Oregon State. Both the ICP-AES and the ICP-MS analysis were conducted at the W.M. Keck Collaboratory for Plasma Spectrometry in the College of Oceanic and Atmospheric Sciences.

Dating of samples from both the intrusives and other Clarno rocks was done using a $^{40}Ar/^{39}Ar$ step-heating technique. This dating was accomplished at the United States Geological Survey's Denver facility under the supervision of Dr. Larry Snee.

Finally, in addition to geochemical and isotopic analyses, a petrographic analysis was conducted on the samples to determine both mineralogical and textural information for the suites.

Bulk Major-element Analysis

Two methods of bulk analysis were used to obtain major-element compositions of the samples. Samples from Marshall and Corporate Buttes, along with the Scott Butte rhyolite dike and Hudspeth Mill intrusion were analyzed at Washington State University using XRF analysis. Several of the above samples, older samples from the same suites, and the Black Butte, Mud Creek, and Spetch Rim area lamprophyres were analyzed at Oregon State using an ICP-AES. Additionally, data previously obtained by XRF at Oregon State by Dr. Edward Taylor, that remained unpublished until now, is also presented.

All of the above samples for bulk-rock major-element analysis were initially prepared the same way. First, samples were trimmed of weathering rinds with a rock saw. The remaining pieces were then broken using a rock hammer and chisel. These chunks were crushed in a tungsten carbide jaw crusher. The resulting chips were hand-picked under a binocular microscope to eliminate chips exhibiting contamination by the saw, chisel or any remaining weathering.

The samples analyzed by XRF were sent to Washington State where picked chips were prepared according to the procedures set forth in Johnson et al. (1999). This involved first powdering the rock chips in a tungsten carbide swing mill. The resulting powder was mixed with a dilithium tetraborate flux for several minutes to ensure both proper mixing and homogeneity. The powders were fused in a carbon crucible for 5 minutes at 1000°C. After the bead cooled, it was reground and refused to ensure homogeneity. The resulting bead was polished on a 600-grit wheel and cleaned repeatedly to remove contamination. The beads were analyzed with a Rigaku automated X-ray fluorescence spectrometer.

The samples analyzed by ICP-AES at Oregon State were powdered using an agate or alumina ceramic ball mill, and sieved to remove larger particles. Approximately two grams of sample was then ignited in a porcelain crucible for an hour to drive off the volitiles and to convert FeO to Fe_2O_3. Four-tenths of a gram of lithium

tetraborate flux was mixed with one-tenth of a gram of the ignited sample and fused at 1050°C for 15 minutes.

The fused bead was first dissolved in nitric acid to create a 1000-fold dilution factor. This dilution factor was used to run the trace elements and potassium and phosphorus. For the rest of the major elements, the solution was further diluted in nitric acid to an 8330-fold dilution before analysis. The nitric solution was spiked with 5 ppm Ge to monitor machine drift over the length of the analytical run. Five USGS standards and a drift corrector standard, also a USGS standard, were run with the samples. The raw counts were then manually reduced and each element was corrected using the drift corrector standard to adjust for machine drift and matrix effects between elements during the run. Finally, the five standards and the drift corrector were used to create a calibration curve relating the corrected counts to weight percent oxides.

Trace-element Analysis

Some trace-element data were obtained from the above runs. Additionally, samples from Marshall and Corporate Buttes, the Hudspeth Mill intrusion, and the Scott Butte rhyolite dike were analyzed on an ICP-MS. These samples were initially processed the same way as the ICP-AES samples. The chips left from crushing were hand-picked and powdered in an agate ball mill. In addition to regular cleaning of the ball mill, crushed glass was used to remove ground-in particles from the container every few samples. This glass was then tested as an unknown to determine if it contributed any contamination.

Since the abundances of the trace elements ranged over several orders of magnitude, two different dilutions were used for all of the samples including the standards. Initially, both 40 mg and 80 mg splits of the samples were measured into Teflon beakers. Then 500 µl of HF and 1.5 ml of 16N HNO_3 were added and the samples were heated in an oven at 65°C overnight to dissolve the samples. The beakers were then heated on a hotplate at about 85°C to evaporate the acid-silica complexes. Once

the samples were almost dry, 500 µl of 6N HCl was added and again evaporated to remove the remaining fluorine. Once the samples were dry, 500 µl of 8N HNO_3 was added and evaporated three times. This removed any remaining chlorine and helped to breakdown the samples for the final dissolution. Lastly, 10 ml of 2 mol HNO_3 is added to completely dissolve the remaining solid. This procedure results in complete dissolution of all types of igneous rocks and helps to remove the silicon that would overload the ICP-MS detectors.

The solutions were diluted one more time to create the final samples that were analyzed. This was done by combining 150 µl of the sample solution with 100 µl of an internal standard mix, and with 5 ml of 1% HNO_3. This resulted in approximately an 8000x dilution factor.

Major-element Analysis of Mineral Phases

Major-element analyses of specific phases were conducted at Oregon State University using a Cameca SX-50 Electron Microprobe on polished thin sections made at the University of Oregon. In the more mafic rocks, olivine, pyroxene, feldspar, and Fe-Ti oxides were analyzed. In the more hydrous rocks, pyroxene, feldspar, Fe-Ti oxides, and micas were analyzed. Additional data on the mica and garnet in the rhyolite was collected to bolster previous data collected by Brittian Hill at Oregon State University.

Olivine, garnet, Fe-Ti oxides, and pyroxene were analyzed at 15 kV, 50 nA accelerating voltage with a focused 1 micron beam. Feldspar and mica were analyzed using a 15 kV, 30 nA accelerating voltage with a 5 micron defocused beam. Count rates were converted to weight percent using calibrations from various mineral standards (Table 3.1). The data was then processes with the "F1" analysis program to calculate oxidation states for iron when appropriate, and to calculate the water content of the micas according to the equation of Deer et al. (1992).

Table 3.1: Reference Mineral Standards used in Electron Microprobe Analysis

Mineral	Element	Standard Name	Reference Number
Olivine	Al	Labradorite	USNM 115900
	Ca	Augite	USNM 122142
	Cr	Chromite	USNM 117075
	Fe	Olivine (Fo83)	USNM 2566
	Mg	Olivine (Fo83)	USNM 2566
	Mn	Pyroxmangite	ENGI #245
	Na	Anorthoclase	USNM 133868
	Ni	Ni_2Si	Asstimaz Scientific
	Si	Olivine (Fo83)	USNM 2566
	Ti	Basaltic Glass	USNM 113498/1
Pyroxene	Al	Augite	USNM 122142
	Ca	Augite	USNM 122142
	Cr	Chromite	USNM 117075
	Fe	Augite	USNM 122142
	Mg	Augite	USNM 122142
	Mn	Pyroxmangite	ENGI #245
	Na	Anorthoclase	USNM 133868
	Si	Augite	USNM 122142
	Ti	Basaltic Glass	USNM 113498/1
Garnet	Al	Garnet	USNM 87375
	Ca	Garnet	USNM 87375
	Cr	Chromite	USNM 117075
	Fe	Garnet	USNM 87375
	Mg	Augite	USNM 122142
	Mn	Pyroxmangite	ENGI #245
	Si	Garnet	USNM 87375
	Ti	Basaltic Glass	USNM 113498/1
Feldspar	Al	Labradorite	USNM 115900
	Ba	Sanidine	Asstimaz Scientific
	Ca	Labradorite	USNM 115900
	Fe	Augite	USNM 122142
	K	Sanidine	Asstimaz Scientific
	Mg	Augite	USNM 122142
	Na	Anorthoclase	USNM 133868
	Si	Anorthoclase	USNM 133868
	Sr	Strontianite	USNM R10065

Table 3.1 (cont): Reference Mineral Standards used in Electron Microprobe Analysis

Mineral	Element	Standard Name	Reference Number
Mica	Al	Labradorite	USNM 115900
	Ca	Augite	USNM 122142
	Cl	Tugtupite	Asstimaz Scientific
	F	Fluorophlogopite	M-6 (J.Rice)
	Fe	Augite	USNM 122142
	K	Fluorophlogopite	M-6 (J.Rice)
	Mg	Fluorophlogopite	M-6 (J.Rice)
	Mn	Pyroxmangite	ENGI #245
	Na	Anorthoclase	USNM 133868
	Si	Fluorophlogopite	M-6 (J.Rice)
	Ti	Basaltic Glass	USNM 113498/1
Fe-Ti Oxides	Al	Synthetic Corundum	USNM 675S
	Cr	Chromite	USNM 117075
	Fe	Magnetite	USNM 114887
	Mg	Chromite	USNM 117075
	Mn	Pyroxmangite	ENGI #245
	Si	Quartz	USNM R 17701
	Ti	Rutile	Asstimaz Scientific
	V	Vandadium Metal	Asstimaz Scientific
	Zn	Gahnite	USNM 145883

Isotopic Age Estimates

Age estimates for many of the samples were obtained using $^{40}Ar/^{39}Ar$ isotopic geochronology at the United States Geological Survey's facility in Denver, CO under the direction of Dr. Larry Snee.

Samples were trimmed of weathered areas using a rock saw. The remaining samples were then crushed in a standard steel crusher and pulverized using a tungsten-carbide shatterbox. This work took place at Oregon State University.

Samples were then washed and sieved for a size fraction between 40 and 60 mesh. Most of the samples were run through a magnetic separator to isolate specific

phases. In the lamprophyres and rhyolite dikes, mica was separated and analyzed. In the rest of the samples, phenocrysts were removed by magnetic separation so that whole-rock analysis could be done on the groundmass. In a couple of cases, heavy liquids were also used with mixed results. Whole-rock samples were soaked in 10% HCl to remove carbonate. All samples were washed in acetone and methanol to remove any residue and contamination. This work was done at the U.S.G.S. preparatory facility in Denver during September of 1999.

Fractions were encapsulated in aluminum and bombarded with neutrons at the TRIGA reactor in Denver to convert all ^{39}K back to ^{39}Ar prior to analysis. Each sample was then step-heated to release successive gas fractions allowing multiple analyses of each sample. Most samples were run from 500° to 1300°C at increments of 100°C. Each gas fraction was filtered several times to remove impurities prior to analysis.

In addition to the previously mentioned suites of rocks, several other samples from the Mitchell area were analyzed. Most of these were Clarno andesite flows near boundaries and unconformities. These were chosen to better establish an absolute timeline for the Clarno Formation. Several other intrusive bodies of undetermined age were also analyzed. These samples were prepared and analyzed in the same manner as described above.

Chapter 4: Marshall and Corporate Buttes

Setting

Marshall Butte, located about 4 km east-northeast of the town of Mitchell, is a large mafic-ultramafic plug intruded into the Clarno Formation (Figure 4.1). The butte is located on the east side of the Mitchell Anticline and the north side of the Mitchell Fault. It is surrounded by Clarno mudflows on the west, and Cretaceous sediments on the east, but is covered almost entirely by collovium and vegetation obscuring the contact in most places. Since the contact is not readily discernable, an intrusive relationship with the surrounding material is hard to define. However, the entire upper 2/3 of the butte is mantled by the mafic talus. South of the intrusion there are two weathered outcrops of similar mafic material. While the outcrops are in direct contact with cretaceous conglomerate, the contact appears to be a fault with slickensides showing a dip-slip motion. While the outcrop may be another exposed finger of the intrusion, movement along the fault may have resulted in displacement of the outcrop to a level lower than the main butte. While the basalt looks similar to Marshall Butte, there is no physical evidence suggesting it is connected, other than its proximity.

Results

Petrology and Phase Chemistry

Sampling from the summit down (MB-1 at summit to MB-4 down the southern slope, Figure 4.1), the upper outcrops display sub-rounded weathering with random fracturing. A fresh surface is dark gray to light black. The samples are generally porphyritic with small (< 2 mm) green to reddish-brown phenocrysts of pyroxene and olivine. The lower two outcrops both exhibit good columnar jointing (Figure 4.2).

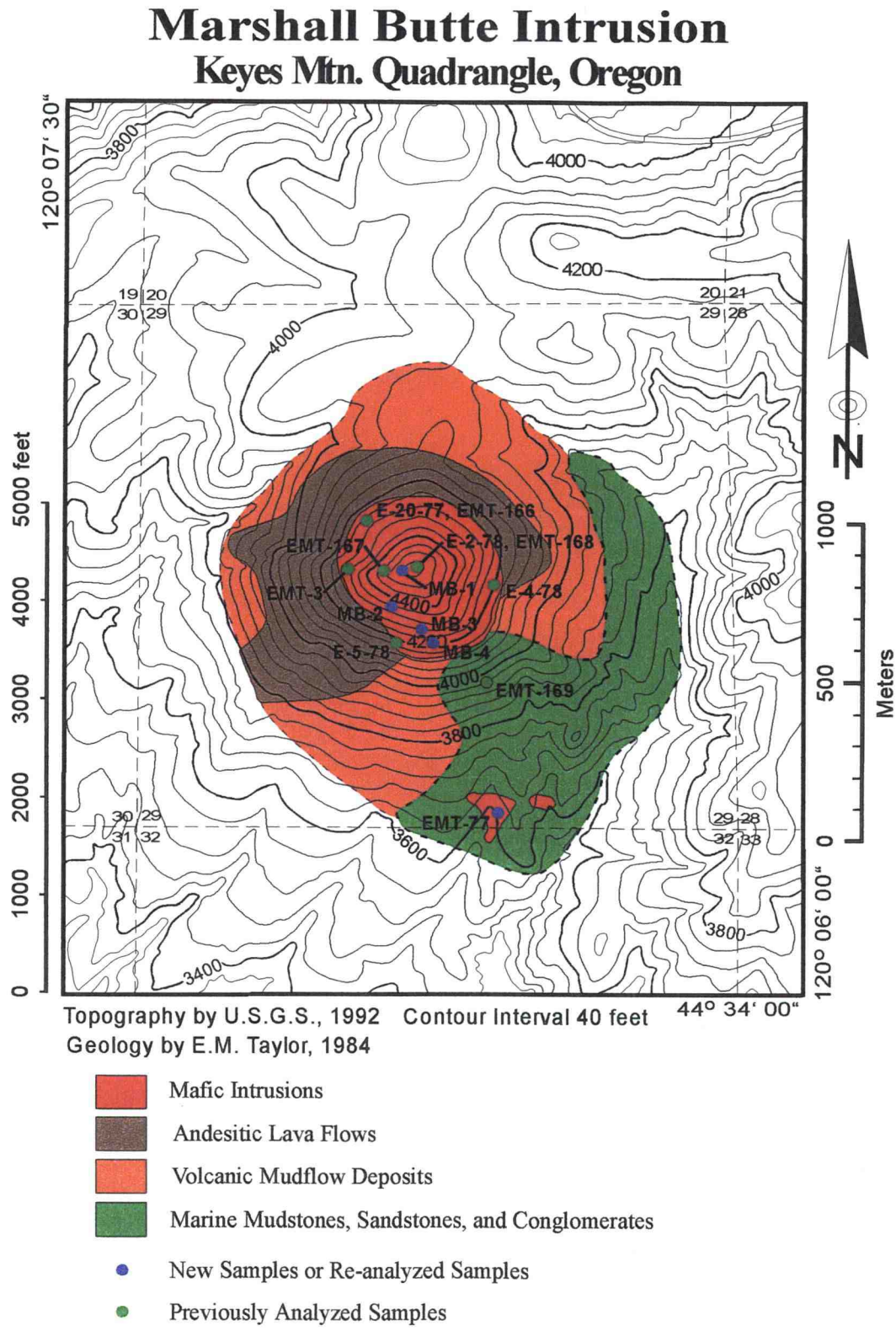

Figure 4.1: Geologic map of Marshall Butte and the surrounding sedimentary and volcanic rock units with sample locations.

MB-3 has larger columns 9-10 inches across, and smaller 4-5 inch columns filling the gaps between the larger ones, while MB-4 has all smaller columns 2-5 inches across. The columns trend NNW to NW, with shallow dips toward the north and into the hill.

Samples EMT-169 and EMT-77 are also from Marshall Butte, but were previously collected by Dr. Ed Taylor. EMT-169 was collected near MB-4, but slightly further downslope (Figure 4.1). Sample EMT-77 was collected at the southern outcrop that was mentioned above. Even though only small parts of the intrusion are accessible, the similarity of the samples suggests that zonation is absent from the intrusion.

Located just north of the town of Mitchell, Corporate Butte is another large mafic intrusion similar to Marshall Butte in mineralogy and composition. The area surrounding the intrusion is largely pediments underlain by andesite flows and mudflows of the Clarno Formation (Figure 4.3). On the western side, there are also Cretaceous sediments present, but these do not come into contact with the intrusion. The butte also lies north of the Mitchell Fault and east of the Mitchell Anticline.

The best outcrops are around the summit of Corporate Butte and exhibit columnar jointing. While the largest outcrop of columns is on the southeast flank of the summit, it is more highly weathered. The sample (CB-1) locale was an outcrop of medium-sized (3-6 inches) columns at the northern side of the summit that appeared both fresh and

Figure 4.2: Photograph of the bimodal columnar jointing from the MB-3 sampling site.

in situ (Figure 4.2). The columns are black and porphyritic with a very fine-grained groundmass. Euhedral to subhedral green clinopyroxene phenocrysts and subhedral olivines (both < 3mm) make up about 20-30% of the rock. There are several smaller outcrops most of the way down the flanks, but it is not possible to determine if they are in situ. The summit and flanks are covered by pieces of these columns that have broken into subangular blocks. As with Marshall Butte, samples EMT-149 and EMT-25 were previously collected by Dr. Ed Taylor.

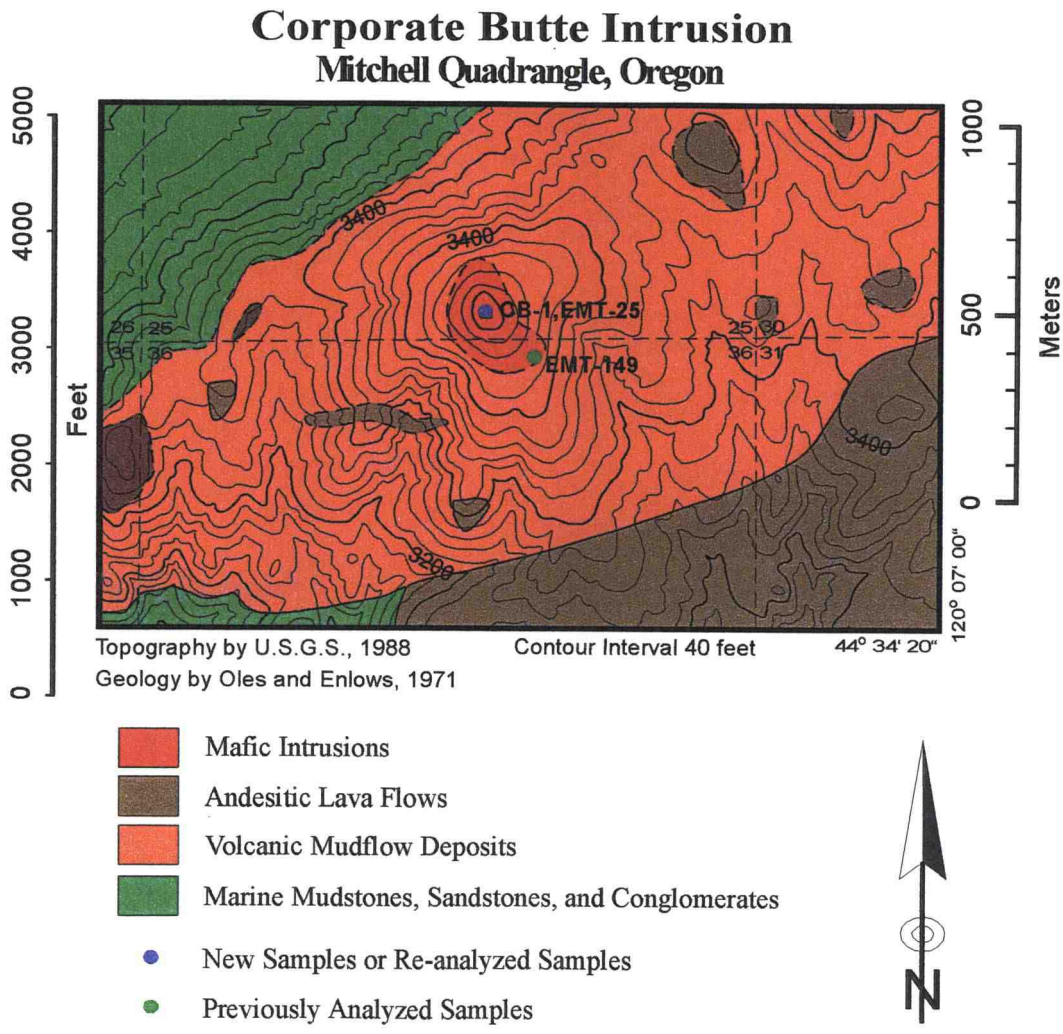

Figure 4.3: Geologic map of Corporate Butte and the surrounding rock units with sample locations.

In thin section, the Marshall Butte samples display porphyritic texture with euhedral phenocrysts of olivine up to 2 mm in size and clinopyroxene ranging from 0.25 to 1 mm in size. In several samples, the olivine and titanomagnetite form glomerocrysts. Almost all of the clinopyroxene appears to be both sector and oscillatory zoned, and polysynthetic twinned (Figure 4.4). Additionally, many of the olivine, and a few of the pyroxene phenocrysts contain inclusions of chromite. Phenocrysts account for 10-15% of the rock, of which over 75% are olivine. The groundmass contains abundant clinopyroxene laths, titanomagnetite, poikolitic nepheline, and minor glass. While the modes vary slightly (Table 4.1), on average olivine accounts for 13% of the rock by volume, clinopyroxene 59%, titanomagnetite 10%, and nepheline 18%. Plagioclase is noticeably absent in these samples, but Oles and Enlows (1971) have previously reported samples with 5-10% of An_{60}.

Overall, the petrography of the Corporate Butte samples is very similar to the Marshall Butte samples. Both the phenocrysts and groundmass phases are the same,

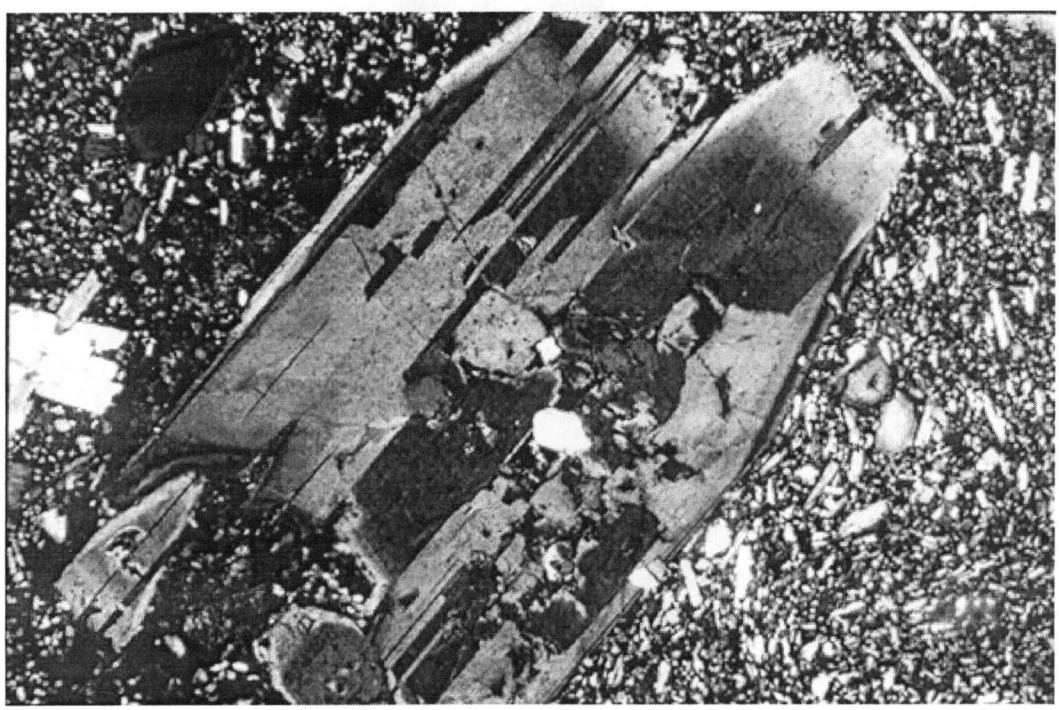

Figure 4.4: Photomicrograph of a Marshall Butte pyroxene. Note the complex sector and oscillatory zoning present. Photo taken at 10x power with polars crossed.

Table 4.1: Modal Estimate of samples from Marshall and Corporate Buttes

	MB-2	MB-3	EMT-168	CB-1	EMT-149
Phenocrysts	12 %	13%	14%	27%	24%
Olivine	9	14	11	9	7
Cpx	61	61	57	66	70
Fe-Ti Oxides	14	8	7	11	12
Nepheline	16	17	24	14	8
Apatite	--	--	--	Tr	Tr
Glass	Tr	Tr	Tr	<1	2

but with different modes (Table 4.1). In addition, traces of apatite are present in the groundmass of Corporate Butte samples. Corporate Butte samples also show significant evidence of disequilibrium not apparent in the Marshall Butte samples. Some of the olivine, and many of the pyroxene crystals exhibit spongy cores, indicating resorbtion has taken place. In the clinopyroxene, the complex sector zoning

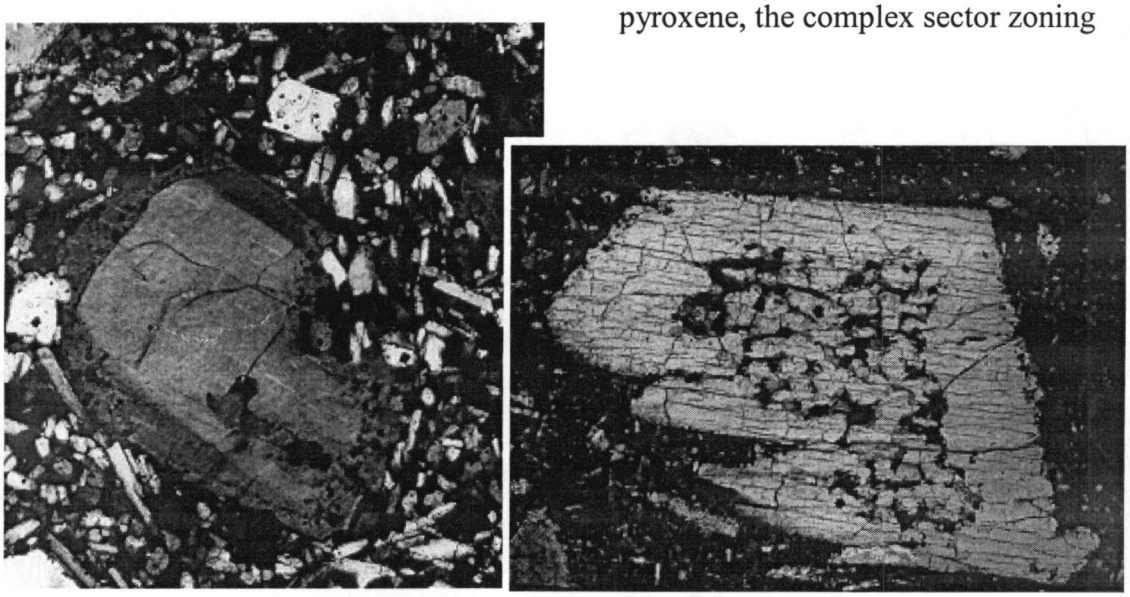

Figure 4.5: Photomicrographs of Corporate Butte pyroxenes. Note the spongy, rounded cores bounded by the dissolution surfaces, and oxide inclusion near the rims. Photos taken at 10x power with polars-crossed.

is often truncated by a dissolution surface. Bands of opaque inclusions often highlight this dissolution surface (Figure 4.5). Renewed growth covered the rounded cores and opaque bands, restoring the subhedral-euhedral outlines to many of the phenocrysts and sometimes resulting in hopper textures. Some of the Marshall Butte pyroxenes are more inclusion-rich near the rims, but dissolution boundaries and spongy cores are not evident.

For both buttes, the olivine ranges from ~Fo_{90} cores to ~Fo_{75} rims. In Figure 4.6a, microprobe traverses across several olivine grains have been normalized and plotted

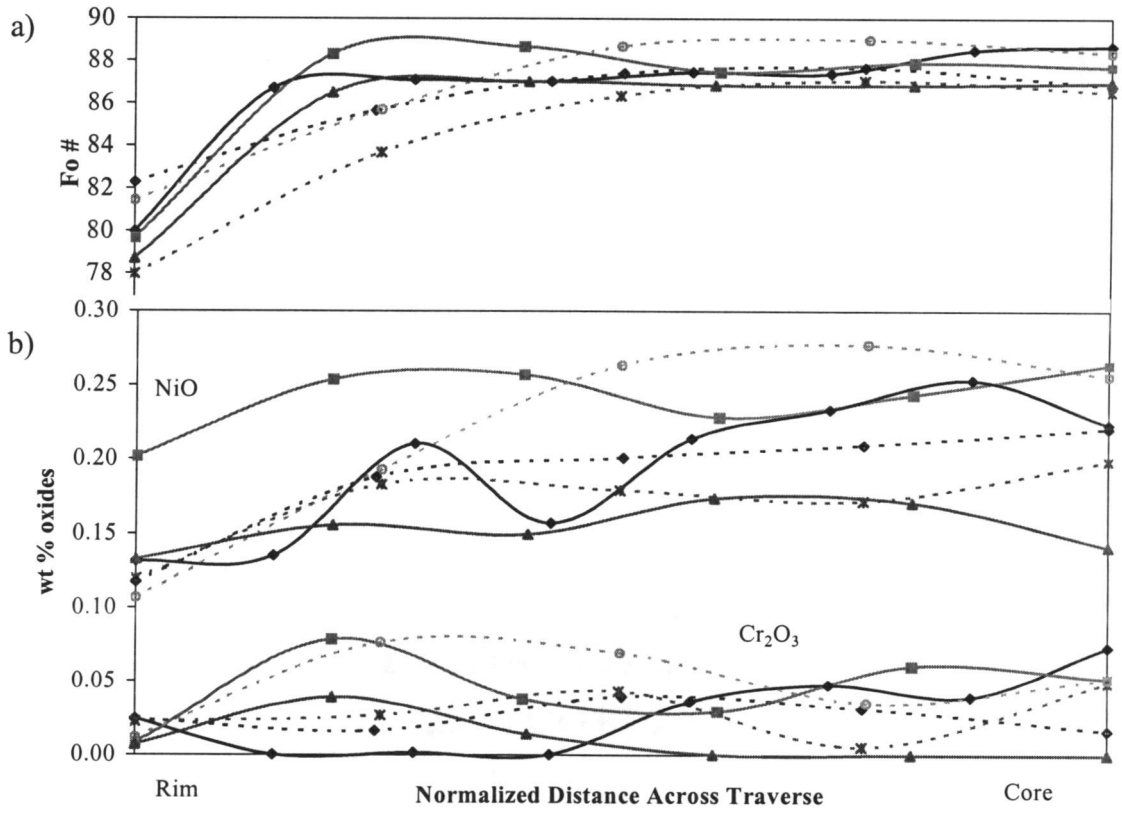

Figure 4.6: Microprobe traverses from select olivine grains for both buttes. Dashed- Marshall Butte, Solid- Corporate Butte. a) Fosterite content of the grains exhibits normal zoning. The more detailed traverses from Corporate Butte show that the Fo content is nearly constant over much of the crystal. The normal zonation is restricted to the outer third of the crystal. b) Minor elements show less distinctive trends with larger fluctuations. NiO shows a slight decrease toward the rims, but Cr_2O_3 appears to fluctuate independent of the Fo content.

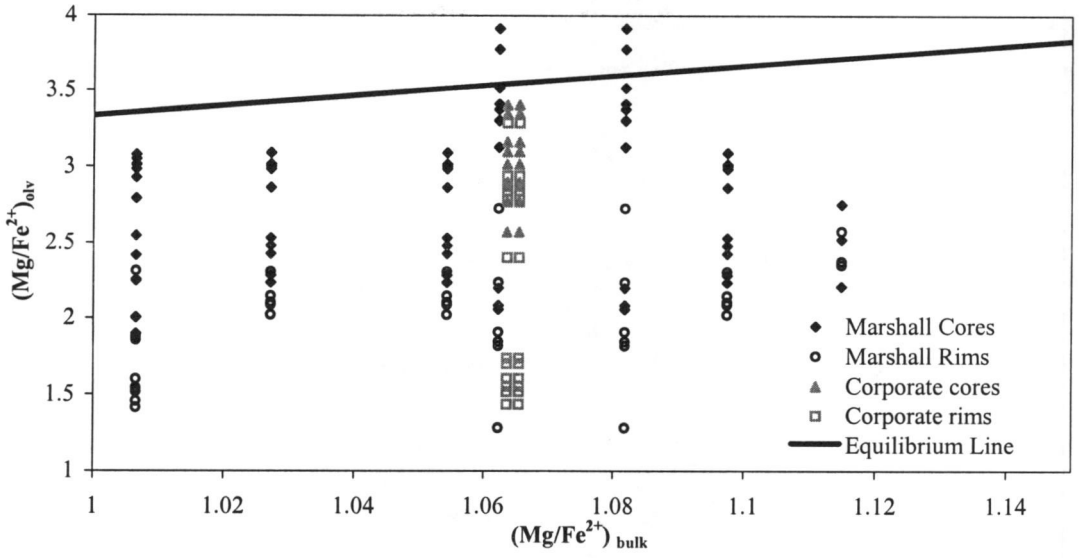

Figure 4.7: Mg/Fe^{2+} ratios for the olivine and bulk-rock compositions of the Marshall Butte (black) and Corporate Butte (gray) rocks. The equilibrium line is for olivine in a liquid according to Roeder and Emsley (1970). Cores below the line are not magnesian enough to be in equilibrium with the bulk rock. Cores above the line are too magnesian for the bulk rock. With the exception of two core analyses from a Marshall Butte sample, all of the analyses are not in equilibrium with the bulk rock composition and indicate that the olivine was in equilibrium with a liquid less magnesian than the bulk rock.

together for both buttes. A complete listing of the microprobe data for all phases is available in Appendix 2. The traverses show that most of an olivine crystal is $Fo_{85\text{-}90}$, with a drop in fosterite content near the rim. In the larger phenocrysts, the drop is quite abrupt and usually occurs in the outer 40-50 microns. In Corporate Butte, there is an increase in Fo# near the middle of the crystal, just inside of the rims. While a drop in NiO_2 accompanies the drop in fosterite, MnO and Cr_2O_3 appear to fluctuate independent of Fo# (Figure 4.6b). Many of the olivine crystals also contain chromite inclusions indicating early crystallization of oxides.

The relationship between the Mg/Fe^{2+} of the olivine and its host rock can be used to evaluate the degree of equilibrium between the olivine phenocrysts and the bulk rock. If the bulk-rock composition represents the liquid composition of the magma,

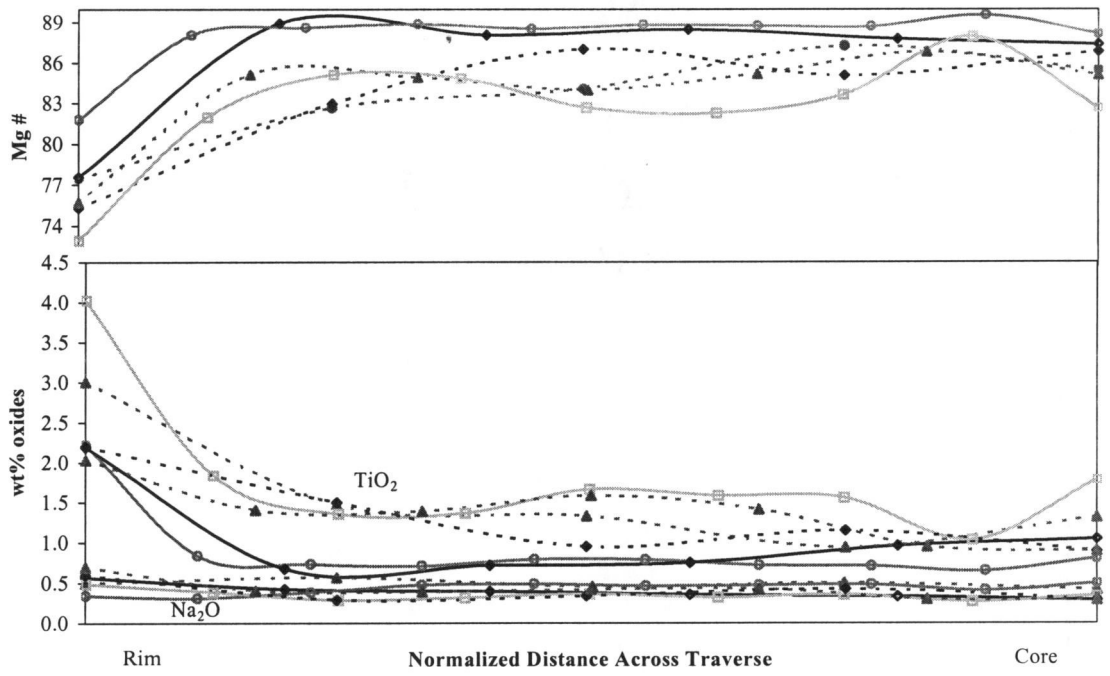

Figure 4.8: Microprobe traverses from select pyroxene grains. Dashed- Marshall Butte, Solid- Corporate Butte. a) Magnesium number (En/En+Fs) displays both normal zonation and some oscillatory zonation that is impossible to quantify due to large point spacing in the traverses. b) TiO_2 shows a similar, but opposite, pattern to Mg#. Na_2O fluctuates across the traverse, showing a slight increase toward the rims.

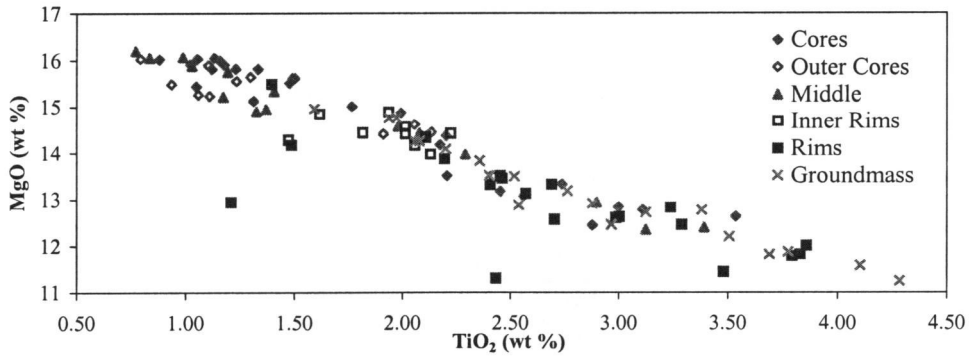

Figure 4.9: MgO vs. TiO_2 for Marshall Butte pyroxenes separated by crystal zones. A linear trend toward lower Mg and higher TiO_2 is consistent with fractional crystallization as the dominant factor controlling the compositions of the clinopyroxene. The composition of the rims and the groundmass is similar, indicating coeval crystallization.

the core analyses should lie on the equilibrium line of Roeder and Emsley (1970). With the exception of two core analyses from Marshall Butte, the most primitive olivine analyses from both buttes plot below the equilibrium line (Figure 4.7). This means the olivine would be in equilibrium with a less magnesian liquid. Therefore, the bulk-rock compositions are too magnesian to represent a liquid composition from which the olivine would crystallize.

The pyroxene phenocrysts range from $En_{47}Wo_{44.5}Fs_{8.5}$ cores to $En_{34.5}Wo_{51.5}Fs_{14}$ rims in Marshall Butte. Corporate Butte covers a similar range in composition, but with slightly more magnesian ($En_{48}Wo_{46}Fs_{6}$) cores. Microprobe traverses across the phenocrysts suggest some minor oscillatory zoning, with normally zoned rims for both buttes (Figure 4.8). However, the microprobe traverses were not detailed enough to quantify the minor oscillatory zoning. Additionally, Corporate Butte and some Marshall butte crystals show a small band of reverse zoning (higher Mg#) just inside the rims. The cores of the Marshall Butte pyroxene phenocrysts are magnesian and contain low TiO_2 while the rims have higher TiO_2, and lower Mg# (Figure 4.9). Groundmass pyroxenes are similar in composition to the rims of the phenocrysts. The same pattern occurs in the Corporate Butte sample (Figure 4.10).

The groundmass mineralogy also includes abundant (~ 10%) titanomagnetite (Figure 4.11) and (~ 18%) nepheline ($Ne_{80}Ka_{20}$ to $Ne_{85}Ka_{15}$).

The samples vary in degree of alteration from fresh to severely altered. In addition to groundmass alteration, many samples show some alteration of the phenocrysts, ranging from rims of iddingsite on the olivine to complete serpentinization of all phenocrysts by deuteric alteration. However, the more altered crystals were ignored since their source characteristics would be destroyed by the alteration.

Bulk Geochemistry

While previous works classified these rocks as trachybasalts and alkali basalts, the new data indicate lower silica values, resulting in a tephrite-basanite classification (Figure 4.12, Appendix 1). The basanites are more alkaline than most of the Clarno

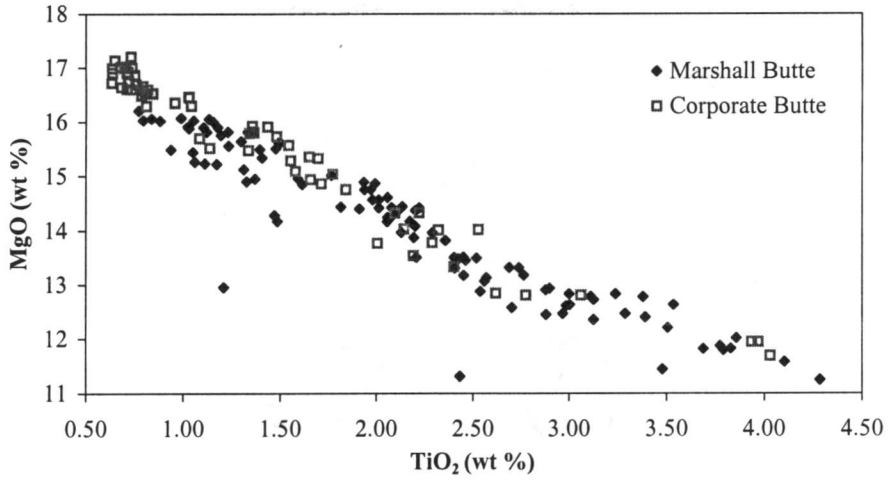

Figure 4.10: MgO vs. TiO_2 for pyroxenes from both buttes. While many of the Corporate Butte pyroxenes are more Mg-rich than Marshall Butte pyroxenes, they cover a similar range in compositions along a common trend.

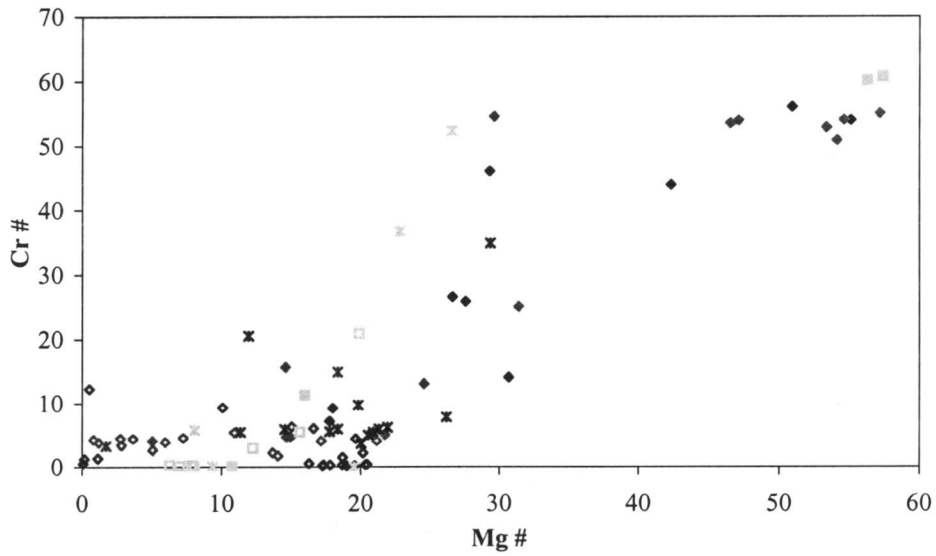

Figure 4.11: Cr# (Cr/Cr+Al) vs. Mg# ($Mg/Mg+Fe^{2+}$) for the Fe-Ti oxides from both buttes. Inclusions are filled symbols while hollow symbols are groundmass crystals. Boundary crystals fall along the edges or holes in crystals, which make determination of crystal type difficult. Diamonds represent Marshall Butte samples while squares represent Corporate Butte samples. Each color is a different sample. The trend from higher Cr and Mg numbers (chromites) to lower Cr and Mg numbers (titanomagnetites) is consistent with a fractionation-dominated system.

Formation, but form a sodic series (Na_2O/K_2O = 2.8-4.6). The volcanics from the Clarno Formation plot in the tholeiitic to calc-alkaline fields, while the Marshall and Corporate Butte rocks plot in the high-K calc-alkaline to alkaline fields (Figure 4.13). CIPW norms for the samples are strongly nepheline and olivine normative (Appendix 4).

One of the most altered samples was Marshall Butte sample MB-4. Bulk compositional data for the sample have much lower alkalis and higher silica values. With the exception of higher Sr, the trace-element concentrations are similar to other Marshall Butte samples. Since the trace elements are similar, and only the easily mobilized alkalis are significantly affected, the difference is consistent with increased weathering in the MB-4 sample.

EMT-77, sampled from the small outcrop south of the main butte, shows significant differences in many of the elements from the other Marshall Butte samples. It has higher Al, Si and Mg, but lower alkalis, Ti and P. In addition, compatible trace elements like Ni and Cr are much higher (~ 2x), while incompatible ones like Ba, Sr, Y, Zn, and Zr are lower. Yet its Mg# (72) is higher than the other Marshall Butte samples.

Marshall and Corporate Buttes are enriched in alkalis when compared to the Clarno Formation (Figure 4.12). Since magnesium numbers for the bulk rocks are ~ 68, and both Cr (430-480 ppm) and Ni (190-210 ppm) concentrations are high, these rocks can be treated as primitive. However, the bulk composition is not representative of a primary mantle melt since that would require an Mg# of ~ 72 to be in equilibrium with Fo_{90} cores of the olivine.

Trace-element and REE patterns are identical for both Marshall and Corporate Buttes. The trace elements display an overall convex upward trend that peaks at Nb and negative anomalies at Pb and P when normalized to condritic values (Figure 4.14a). The samples show a HFSE enrichment compared to both LREE (La/Nb ~ 0.58) and LILE (Ba/Nb ~ 6). The rare earth elements display a strong light-REE enrichment with La/Lu_n= 30-34. However, Rb/Sr values of 0.01-0.015 are much lower than for typical subduction zones. Normalizing the trace elements against MORB shows that the HREE's are actually depleted compared to N-MORB (Figure 4.14b). Cs shows a positive anomaly compared to other large-ion lithophile elements only when normalized to MORB.

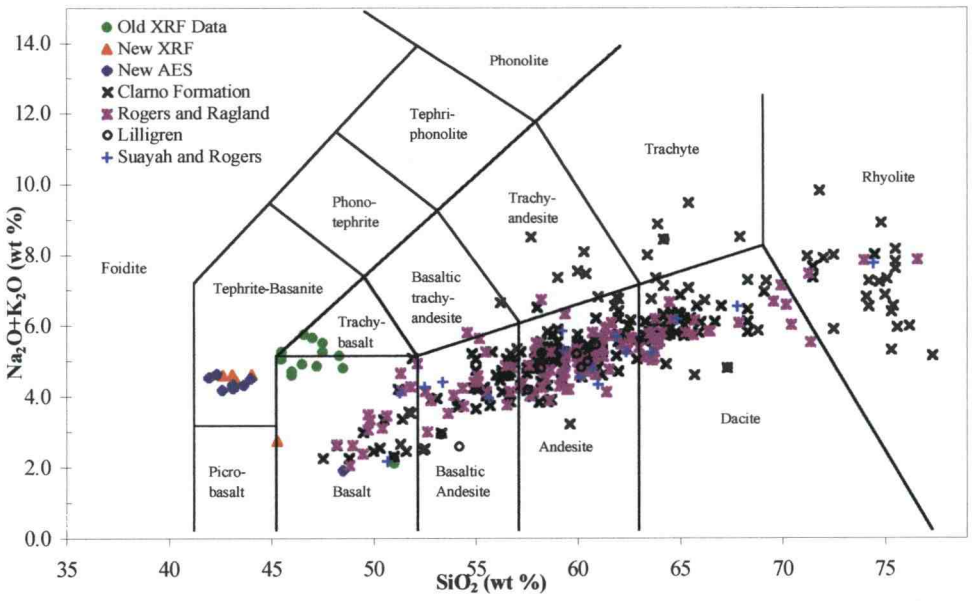

Figure 4.12: Classification of Marshall and Corporate Butte and other Clarno Formation rocks according to total alkali content (Le Maitre et al., 1989).

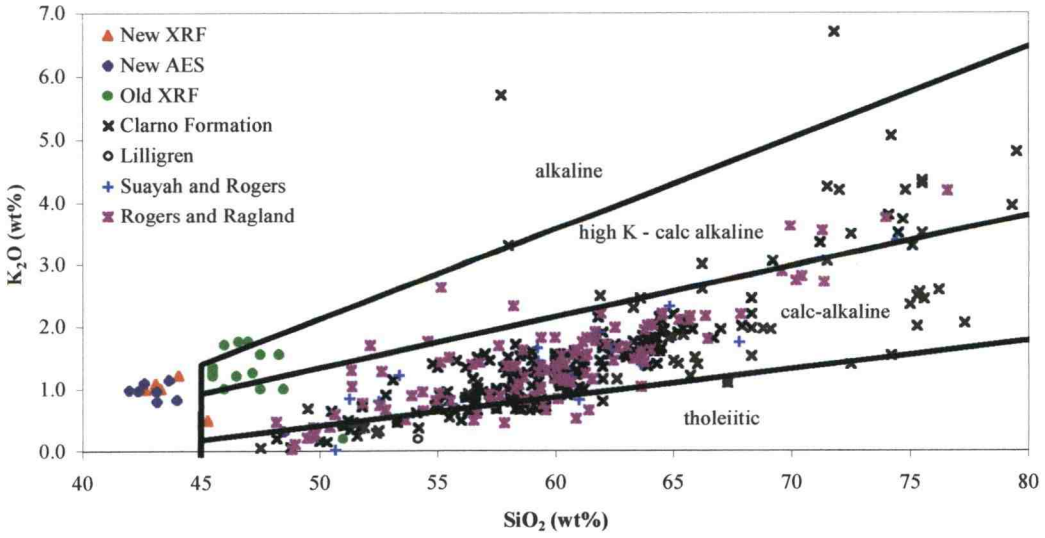

Figure 4.13: Alkalinity classification for Marshall and Corporate Butte. The rocks are high-K calc-alkaline to alkaline, while most of the Clarno Formation is tholeiitic to calc-alkaline using the divisions of Gill (1981).

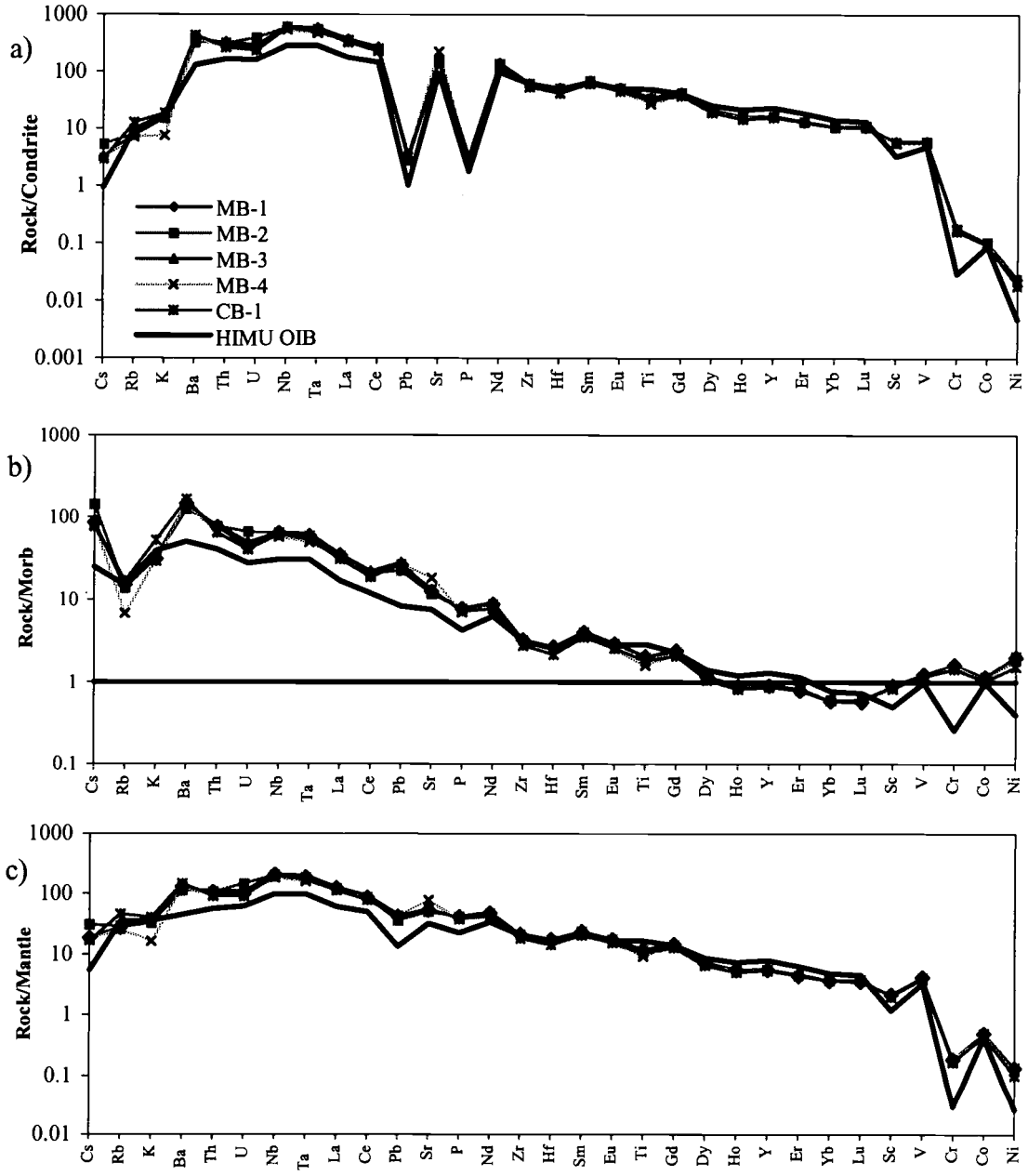

Figure 4.14: Spiderdiagrams for both buttes. a) Trace element patterns for both buttes normalized to condritic abundances of Sun and McDonough (1989). Also plotted is a HIMU-type OIB from Mangaia, Polynesia (Woodhead, 1996) to show the similarities between the buttes and HIMU OIB. b) Trace element abundances normalized to N-morb (Sun and McDonough, 1989). With the exception of the HREE, all elements are enriched relative to N-morb. c) Trace element abundances normalized to primitive mantle values (Sun and McDonough, 1989). The pattern is very similar to HIMU OIB, and lacks the HFSE depletion normally associated with subduction zones.

Primitive mantle normalized values again show a convex up pattern with a peak at Nb (Figure 4.14c). This normalization removes both Pb and P anomalies.

Geochronology

Age estimates were conducted on samples from both buttes. Since most of the K in the samples is locked up in the nepheline, bulk analysis of the groundmass was the only option for $^{40}Ar/^{39}Ar$ dating. Two samples from Marshall Butte (MB-1 and MB-3) and one sample from Corporate Butte (CB-1) were analyzed. All of the samples suffered from "argon recoil". This occurs during neutron bombardment of the samples when the Ar is redistributed, and even lost, as it recoils from the neutron capture. This leads to an inverse stair-step pattern with older ages in the lower T step and younger ages in the higher T steps. In addition, the first heating step of a sample is usually contaminated and results in a younger age. Due to the argon recoil, there was not a significant plateau in the data to allow an accurate date. Instead, isocron plots of $^{40}Ar/^{36}Ar$ vs. $^{39}Ar/^{36}Ar$ were used and two different York regression analyses were preformed on the data. CB-1 gave an age of 52 ± 3.9 Ma, MB-3 resulted in a 49 ± 0.49 Ma age, while MB-1 resulted in the youngest age, 46 ±1.2 Ma (Appendix 3).

Early work by Enlows and Parker (1972) was done using K-Ar dating and suggested that the Clarno Formation ranged from 46-30 Ma. Other dates in the 30 Ma range were also published in the seventies, however more recent work reports ages from 40-60 Ma (Suayah, 1990; Bestland et al., 1999). It is likely that the earlier dates are too young due to pervasive weathering in the samples, and the greater degree of error involved in the K-Ar method due to the need for multiple splits of sample and a single gas step instead of multiple steps used here.

Enlows and Parker (1972) published dates of 44.8 and 45.0 Ma for Marshall Butte. Since their measurements of Clarno Lava flows were significantly younger, this ended up resulting in Marshall Butte being older than most Clarno lava flows. A date in the upper 40's of millions of years ago places the buttes in the earlier stage of the Clarno activity, during or just after the largest flux of activity at 49 Ma.

Discussion

Marshall and Corporate Buttes Petrogenesis

The normal compositional zoning observed in the olivines and pyroxenes, along with the linear trends on Mg vs. TiO_2 plots for the pyroxene, are consistent with crystal fractionation being one of the dominant processes involved in the petrogenesis of these magmas. The similarity in compositions between the rims and the groundmass pyroxenes, as well as the trend from more Cr-rich and Mg-rich chromite inclusions in the phenocrysts to Cr-poor and Fe-rich titano-magnetites in the groundmass are also consistent with a fractionation-dominated petrogenesis. Since nepheline was crystallized late in the sequence, it tells very little about the history of the magma. It does however, suggest that the suite was still alkali-rich, but undersaturated enough in silica to produce nepheline rather than plagioclase.

However, the complexity of the zoning in the pyroxenes suggests that crystal fractionation may have not been the sole process modifying the magma. The oscillatory zoning in the Marshall Butte pyroxene is similar to zoning often found in plagioclase. This type of zoning often results from small changes in crystallization conditions within the magma chamber, rather than recharge or mixing events (Tepley et al., 1999). While not as strongly developed in Marshall Butte, weak sector zoning and the presence of reversely zoned bands in some phenocrysts suggest a more complex history than simple crystal fractionation.

Sector zoning of pyroxene is common in alkaline systems, but less abundant in pyroxene phenocrysts from subduction zone related magmas (Brophy et al., 1999). Several methods have been suggested for the formation of sector zoning, all relating to rapid growth. In the Aleutians, Brophy et al. favor rapid crystallization due to decompression and vapor saturation, which decreases the pH_2O causing a rapid increase in the liquidus temperature. Other causes for sector zoning include rapid cooling (often under water), and magma mixing. Rapid cooling is also consistent with the hopper textures as seen in the Corporate Butte samples.

However, the Corporate Butte samples also have sieve-textured cores, dissolution surfaces and inclusion bands. The microprobe traverses also show both olivine and pyroxene cores increase in Fo# and Mg# just inside the normally zoned rims. In plagioclase crystals, these features are usually the result of injection of hotter, more mafic magma into the chamber resulting in the resorbtion of the plagioclase (Tepley et al., 1999). The hotter magma causes resorbtion of the edges of the phenocrysts resulting in rounded and sieve-textured cores. Clear overgrowth rims result from a re-equilibration with the magma and subsequent rapid growth that tends to restore the euhedral outlines of the crystals. Initially these rims have higher An content than the core area on the other side of the dissolution surface. This leads to a band of reverse zoning as you cross the dissolution surface from the older core into the clear overgrowth rim. The corresponding rim is then strongly normal zoned as crystallization becomes dominant again. Since these textural features are abundant in Corporate Butte, magma mixing rather than decompression and vapor saturation is favored as the cause of the sector zoning.

Dissolution surfaces may also be present in the Marshall Butte samples, but they are definitely less conspicuous than in Corporate Butte. Likewise, the sector zoning, while present, is more poorly defined. And while absent in the olivine, some of the pyroxene traverses also display an increase in Mg# just inside of the normally zoned rims. This suggests that Marshall Butte may have also undergone magma mixing. Since Corporate Butte is much smaller than Marshall Butte, it may have been more significantly affected by small mafic injections, leading to stronger disequilibrium textures.

Injection of hotter, mafic material is more consistent with the textural features observed in the phenocrysts than simple fractionation. Since there is little scatter in the linear trends, it is likely that the injected magma was similar in composition to the original magma. Rather than two different magmas mixing to form these intrusions, the systems were probably experiencing recharge events from the same source magma. Since Marshall Butte was larger, the injected magma was more widely dis-

tributed and had less effect on the crystals. This is why the disequilibrium features are poorly developed in Marshall Butte when compared to Corporate Butte.

Two reasons for the disequilibrium between the olivine and the bulk-rock compositions can be suggested. In a closed system, accumulation of olivine makes the bulk-rock more magnesian than the original liquid. As a result, while the olivine is in equilibrium with the liquid, the olivine is not magnesian enough for the cumulate bulk-rock composition. Accumulation is also consistent with other evidence of crystal fractionation. However, since the rocks appear to have undergone only small degrees of accumulation (< 15% for Marshall Butte), the overall effects on the composition is minor. So while accumulation may have caused disequilibrium between the olivine and the bulk-rock, the overall character of the rock is similar to the original magma. Most importantly, accumulation of olivine (with minor cpx) would not significantly alter the silica undersaturated and the alkaline character of the magma.

In an open system, injection of more magnesian magma would increase the Mg# of the magma, resulting in a disequilibrium between the new liquid composition and the olivine. In this case, the bulk-rock composition would be more representative of the new liquid, while the olivine would remain in equilibrium with the previous liquid. This results in the olivine appearing too low in Mg to be in equilibrium with the bulk rock. Textural features (sieve-texture, dissolution surfaces, etc.) would also accompany an injection of more magnesian magma indicating a change in the liquid composition. Since several of these features have already been shown to exist in the Corporate Butte samples, the disequilibria between the olivine and the bulk-rock may be due injection of hotter (higher Mg) magma. However, it has already been shown that both process likely occurred in the formation of these magmas. Therefore, the disequilibrium likely reflects both some minor accumulation and some effects from recharge.

It does raise the question of whether Marshall Butte was simply an intrusion, or rather a magma chamber for a volcano. The fine-grained nature of the groundmass indicates that it cooled quickly, suggesting a shallow location. Nevertheless, if there were eruptive products from Marshall Butte, they would be alkaline-rich basalts and

no such rocks currently exist in the Mitchell area. This may simply be the result of long-term erosion, or it might suggest a closed intrusion.

The smaller outcrops south of the main butte have significant chemical differences from that of the main butte. Yet, their petrography, overall geochemisty, and location suggest a genetic relation to Marshall Butte. The combination of lower incompatible elements, higher compatible elements, and a slightly higher Mg# suggests a common source, but from larger degrees of partial melting.

For the bulk-rock analyses, the large enrichment in incompatible trace elements (LILE, HFSE) and significant depletion in compatible elements (Cr, Ni), coupled with high Mg#'s, suggests that Marshall and Corporate Buttes resulted from low degrees of partial melting. Of special significance, these rocks do not display the HFSE depletion (especially Nb & Zr) normally associated with subduction zone magmatism. A slight Ti and K depletion in conjunction with the flattening of the normalized HREE abundances suggests a source containing residual amphibole (LaTourrette et al., 1995; Hilyard et al., 2000). However, the trace-element patterns are not conclusive as to the presence of amphibole in the source, and since garnet preferentially incorporates the heavy rare earth elements, high La/Lu_n ratios could instead suggest partial melting of a garnet-bearing source.

A depleted MORB source (asthenospheric mantle) that was subsequently metasomatised would result in amphibole formation. Low degrees of partial melting of this source could result in trace-element patterns similar to those observed in both buttes. This is further corroborated by the fact that in subduction zones, the sub-arc lithosphere is enriched in LILE and Pb relative to HFSE. This results in a relative depletion of HFSE in lithospheric melts. However, the samples from both buttes bear no evidence of the HFSE depletion. It seems likely that the lithospheric mantle under Mitchell would have been enriched in LILE by both the previous and the current subduction events. Therefore, the lack of the depletion further argues for an asthenospheric mantle source.

The overall convex-up trend with a peak at Nb and La is most commonly observed in HIMU-type ocean island basalts (OIB) and in rift-related continental ba-

salts (Woodhead, 1996; Baker et al., 1994; Hole, 1988). Some authors also refer to a negative K anomaly, but this can be a result of plotting procedures rather than a characteristic of the rock itself (Woodhead, 1996). Since the same pattern is found in both oceanic and continental settings, which usually have different lithospheric compositions, the signal is often attributed to an asthenospheric mantle source (Paslick et al., 1995; Sun and McDonough, 1989). However, the pattern is still enriched relative to normal depleted asthenosphere (DMM), which has lead to a long debate of what causes the HIMU pattern. The most widely accepted hypothesis is that the HIMU pattern represents melting of asthenospheric mantle previously enriched by recycled oceanic crust (Baker et al., 1994; Sun and McDonough, 1989; Hole, 1988; Woodhead, 1996).

This HIMU-like OIB pattern is well documented in three main settings. The first, ocean island hotspots, is the type locality for the pattern. But since there is no current evidence that the magmatism under study here took place above a plume, these will not be considered. The two remaining localities where rocks with these patterns are found are in areas of continental rifting and along continental margins as subduction ceases. Both localities are also associated with alkaline magmatism.

Southwestern Poland is part of the Central European Alkaline Province. Here, intra-plate rifting resulted in small volumes of melilitites, nephlenites, basanites, alkali basalts and more differentiated alkaline rocks (Alibert et al., 1987). REE fractionation calculations suggest that the nephelinites and basanites formed from partial melting of 0.2-0.4% of a garnet-bearing (with minor amphibole) source at 50-70 km depth (Alibert et al., 1987). This is consistent with an asthenospheric mantle source.

Both nephelinite and basanite suites are present along the continental shelf off Norway, in Greenland, and a few other locations dotting the rim of the northern Atlantic Ocean (Prestvik et al., 1999). These alkaline rocks are associated with the rifting and opening of the Atlantic Ocean. Off of Norway, both the potassic basanite (Na_2O/K_2O = .82) and the sodic nephelinites (Na_2O/K_2O = 2.0-2.6), are strongly enriched in LREE (La_N = 210-475), and highly REE fractionated (Ce/Y = 4.1-8.3). While the basanites in Norway show the typical OIB pattern, the nephelinite shows a

slight positive Ba anomaly. While the REE fractionation could be attributed to residual garnet in the source, negative K, Rb, and Ti anomalies suggest residual amphibole/phlogopite in the source. The nephelinites represent a direct melt of the asthenospheric mantle (plume related). However, the basanite represents partial re-melting of a phlogopite-bearing peridotite (lithospheric mantle) that had been previously metasomatized. While the metasomatizing agent was not specified, subduction had not occurred in the area in over 100 Ma, and was not involved. The more likely cause is fluids derived from earlier extensional activity. Both magmas took advantage of pre-existing deep-seated faults (from earlier rifting) to migrate upward.

Isotopic and trace-element studies from northern Tanzania, part of the East African Rift, suggest another possible source of intraplate basalts (Paslick et al., 1995). They note that since basaltic magmas from areas of greatest extension within continental rifts, have trace-element and isotopic signatures similar to some ocean islands, previous work had identified the source region as being in the asthenosphere. However, they suggest an alternative location for the source of these melts. OIB melts intrude into the lithospheric mantle, where they cool and metasomatize surrounding lithosphere. Now part of the lithosphere, they would remain unaltered until a new heat source is introduced to the area. Small degrees of melting would mobilize the enriched lithosphere first. These melts would retain their original OIB signature, unless mixed with depleted lithospheric melts. Mixing of larger amounts of the non-OIB lithosphere would cause the melts to take on the dominant lithospheric signature and loose the original OIB signature. The larger amounts of mixing could be associated with a number of factors including higher-degree melting of the lithosphere and thicker lithosphere. This would explain why some melts have a slight subduction signature, while others have a depleted MORB signature. Of particular interest in this model is that it doesn't concern itself with the origin of the OIB signal, since it is the product of earlier activity that has little bearing on the volcanic event. However, this model fails to explain how an area that is first intruded by these asthenospheric melts and subsequently exposed to metasomatism by subduction, can retain its original OIB pattern while the rest of the lithosphere gains this subduction signature.

The Calatrava Volcanic Province in Spain is located in an area of intracontinental extension. While the Cebriá and Lopez-Ruiz (1995) classified the rocks on the basis of mineralogy, they include foidites, basanites, trachybasalts, and alkali basalts when classified with an alkali-silica scheme. The rocks are dominantly olivine, clinopyroxene and Fe-Ti oxide phyric, with feldspathoids, plagioclase, biotite, and apatite in minor amounts. Three of the four suites show enrichments in incompatible trace elements similar to HIMU-like OIB. Modeling suggests that these are related by differing degrees of partial melting of the HIMU-like source. The last suite (leucitites) is enriched in LILE compared to HFSE though. Both source areas appear to have phlogopite, with apatite also present in the leucitite's source. A simple two-source model of an asthenospheric diapir was used to explain the province. Early heating by a small asthenospheric diapir lead to the melting of ancient enriched blobs of lithospheric mantle resulting in the leucitites. Subsequently, the diapir itself (HIMU-like) would start to melt and reach the surface through lithosphere that was depleted by the previous melting. Geophysical data appear to be in agreement with such a model. They indicate the area has slightly thinner crust (30-35 km) and a shallower (~80 km) asthenosphere.

Basanite, trachybasalt, and shoshonite dikes make up part of the Tapuaenuku Igneous Complex in New Zeland (Baker et al., 1994). The complex is a large area of igneous activity that formed on the margin of Gondwana during or after the cessation of subduction in the mid-Cretaceous. During this time, a period of extension related to the fragmentation of Gondwanaland began. While Hole et al. (1991) have shown that a relationship existed between the cessation of subduction and alkaline volcanism surrounding the Pacific, the authors suggest the activity may instead relate to the extension. The dikes are the earliest stage of the igneous activity, and represent small degrees of partial melting. The dikes are similar to Marshall Butte in mineralogy, with Ca-rich pyroxene, and olivine, but with feldspar instead of nepheline. These dikes are followed by a series of alkaline intrusives that appear to have formed by fractionation of a source similar to the dikes. The dikes all display the convex upward trace-element pattern that peaks at Nb and Ta, the same as other intraplate volcanics

in New Zealand. Since parental magma was similar to HIMU-type OIB, a similar source region was postulated.

Alkaline magmas (basanites, tephrites, and alkali basalts) are also associated with the end of subduction along the Antarctic Peninsula (Hole, 1988). The basanites (Na_2O/K_2O= 1.6-1.8) are less sodic than Marshall Butte, but have similar Cr (>150 ppm) and Ni (>120 ppm). All the suites have trace-element patterns that are convex-upward with peaks at Nb and Ta and strongly fractionated REEs suggest a garnet-bearing source of ~80 km depth (Hole et al., 1993). Isotopic and trace-element characteristics for the rocks suggest an asthenospheric mantle source. A series of ridge crest-trench collisions resulted in the separation of the trailing plate from the down-going plate with the continued subduction of the down-going plate. This left a void into which asthenospheric mantle upwelled and partially melted due to decompression. Similar alkaline activity in conjunction with slab windows has been noted elsewhere (Baja Claifornia, British Columbia). Small melts of ne-normative alkali basalts, tephrites, and basanites are the common products of this interaction. However, occurrences are usually limited to areas of unusually thin, or previously thinned lithosphere.

The western Anatolia region of Turkey experienced two periods of igneous activity following the collision of continental lithosphere with the arc (Aldanmaz et al., 2000). While the cause of the earliest activity is not well constrained, the source region for the mafic-intermediate rocks was in the subduction-modified lithosphere. The two most likely causes of the lithospheric melting are delimitation and sinking of the thermal boundary layer or by detachment of the subducting slab. This is evident by the strong subduction signature in the suites. The second period exhibited more alkaline volcanism, resulting in olivine-rich basalt, trachybasalt and basanite lavas that extruded from along faults in extensional basins. While the earlier magmatic activity's cause is unclear, the cause of the second event has been successfully modeled. In response to regional extension, upwelling asthenophere resulted in decompression melting. The trace-element and REE patterns are similar to Marshall Butte (and HIMU OIB), with enrichments in all the incompatible elements with respect to

MORB except the HREE. None of the alkaline rocks contain HFSE depletions, suggesting the source was not the metasomatized lithospheric mantle. Results from a batch-melting model argue against simple one-stage melting of a depleted asthenospheric mantle. Instead, a two-stage model of asthenopheric mantle is favored. In this model, LILE-enriched fluids (or melts) are given off by the asthenopheric mantle as it approaches the solidus. These fluids migrate into the surrounding mantle causing metasomatism and greater degrees of melting.

In both of the above tectonic settings, extension took place and resulted in both asthenospheric melting, and preferential pathways for deepseated magma to reach the surface with little assimilation of lithospheric rocks. This appears to be the case in Mitchell also. Previous workers (Gromme et al., 1986; White and Robinson, 1992) have already suggested that extension was taking place during the eruption of the Clarno Formation. When combined with the lack of a "subduction-signature", it is plausible for the Marshall and Corporate Butte magmas to have originated as small-degree melts of enriched asthenospheric mantle with little subduction influence.

Marshall and Corporate Buttes and the Clarno Formation

Both buttes clearly represent a more alkaline magma than is common in the Clarno Formation. While they have long been associated with the Clarno, the relationship between them and the Clarno is poorly understood. This has been complicated by the fact that the geochronology has been inconclusive as to when they formed relative to the main Clarno activity. While it is possible that Marshall and Corporate Buttes were emplaced at different times, the similarities in chemistry and petrography would require these small-degree melts of asthenosphere to have existed for long periods of time. Yet the lack of other similar rocks could be used to argue against this. And it has already been stated that the Corporate Butte age was of lower quality. Instead, it is likely that that the Corporate Butte date is too old, and that its true age is at the younger end of the error. This would be consistent with the new 49 Ma date for Marshall Butte. It would also mean that they formed during the most ac-

tive period of Clarno volcanism. However, if the new 46 Ma age for Marshall is correct, then it were intruded up to 3 million years after the main pulse of Clarno activity. If this date is correct however, then the Corporate Butte age of 52 could suggest bracketing of the main pulse by alkaline lavas. Due to the strong similarities in geochemistry, mineralogy, and close location to one another, one pulse of magma resulting in two intrusions is favored here. Yet, regardless of how the Marshall and Corporate Buttes magmas relate to the main pulse of activity, calc-alkaline lavas were erupted from 54 Ma to 42 Ma (see chapter 8), suggesting possible contemporaneous alkaline and calc-alkaline activity.

Since the possibility exists coeval calc-alkaline and alkaline suites in the Clarno, an attempt to understand how the alkaline magma of Marshall Butte may be related to the rest of the Clarno is desirable. Even if Marshall and Corporate Buttes date from after the main pulse of activity, this does not preclude the existence of similar alkaline magmas during the main pulse of activity. It also does not preclude them from being parental magmas to later calc-alkaline lavas.

Mass balance calculations (Stormer and Nicholls, 1978) were used with major-element data to explore the possibility of Marshall Butte being a parental magma to other Clarno Formation rocks, especially the more primitive Clarno basalts. Average compositions from olivine, clinopyroxene, titano-magnetite and nepheline microprobe data were used in the calculations (Table 4.2). The average of the Marshall Butte bulk compositions was used as a starting magma and two different Clarno basalts (PH-16 from Suayah and Rogers, 1991 and JN-156 from Rogers and Ragland, 1980) were selected as daughter products. The calculations showed that a reasonable match ($r^2 \sim .2$) was possible with ~ 10% fractional crystallization of olivine, clinopyroxene, nepheline, titano-magnetite, and apatite (Table 4.2).

While these results based on major-element mass balance suggest that a relationship by fractional crystallization is possible, several problems exist. First, while the results fit the data well for most elements, P_2O_5 could only be modeled if apatite was included as a crystallizing phase. While apatite is located in the groundmass of a couple of samples in trace amounts, is does not appear to have played a significant role.

Table 4.2: Mass Balance Modeling of Marshall Butte Fractionation

	Initial	**Final 1**	**Final 2**	**Phases**				
	MB aveg	PH-16	JN-156	cpx	neph	apatite	magt	olv
SiO_2	43.54	50.78	49.91	49.4	44.6	0	0.4	40.2
TiO_2	2.60	0.99	0.97	2.0	0	0	15.2	0.1
Al_2O_3	11.37	14.72	13.50	4.9	32.8	0	7.5	0.2
FeO*	10.55	9.42	10.02	5.8	1.4	0.2	71.4	14.1
MgO	12.45	10.72	12.68	14.3	0.4	0.1	5.5	44.4
CaO	13.99	10.82	10.74	23.2	0.5	53.0	0	1.1
Na_2O	3.56	2.20	2.05	0.5	15.3	0.1	0	0.4
K_2O	1.03	0.14	0.03	0	5.0	0	0	0
P_2O_5	0.91	0.21	0.10	0	0	46.6	0	0
	Final 1	**(R^2)**	**% Frac**	**Phase %**				
		0.20	11.66	50.34	19.98	1.70	7.24	7.72
	Final 2	0.22	9.50	49.89	20.06	1.71	7.15	6.98

Second, the phase proportions calculated by the model need to be removed from the system, resulting in a residual liquid of basaltic composition. If the phases were removed by fractional crystallization, the phases and proportions in the results would represent only the phenocrystic phases of the Marshall Butte samples. Unfortunately, the only phenocrystic phases are clinopyroxene, olivine, and possibly titano-magnetite, not apatite or nepheline. Additionally, the proportions calculated also bear no resemblance to the actual phenocrystic proportions observed in the rocks. Simulations run using only olivine, clinopyroxene, and titano-magnetite resulted in r^2 values of 20. For these reasons, it seems unlikely that simple fractionation can link the Marshall Butte to the primitive Clarno Basalts.

The COMAGMAT model (Ariskin et al., 1993) was used to run several simulations with the average compositions for the Marshall Butte rocks in order to investigate whether Marshall Butte magmas could have fractionated into other Clarno rocks. The simulations were run at 1, 5, 10 and 15 kbars with 1%, 2%, and 2.5% water up to 80% crystallization or water saturation. Additional simulations were run using two basalts (same two basalts used in the mass balance model) to determine if they could

fractionate into other Clarno rocks. The resulting trends were complicated by the fact that Marshall Butte contains nepheline, a phase that the model did not account for.

Fractionation trends on the MgO-SiO_2 plot from the Marshall Butte simulation fail to match the observed trend in the actual data (Figure 4.15a). The trends lie completely outside of the Clarno field of data. Conversely, trends for the basalts lie completely within the field of Clarno rocks at 5 kbars, while at higher and lower pressures, the fractionation trends lie near the edges of the field of Clarno rocks. Due to the role of clinopyroxene, fractionating a Marshall Butte magma will draw the bulk liquid down in MgO with little change in SiO_2. This moves the composition of the liquid away from the basalts rather than towards them. Even with some nepheline fractionation (not accounted for in the model), the Marshall Butte liquid can't evolve in the direction of the basalts by fractionation alone.

Liquid trends for Marshall Butte fall along only the high Mg# side of the field of Clarno data, with higher pressures closer to the data (Figure 4.15b). The majority of Clarno rocks have significantly lower Mg# than the fractionation trends will allow. Fractionation first leads to a decrease in Mg#, with little change in the K/Ti ratio. While this moves the liquid composition toward the Clarno data field, the onset of oxides results in a rapid increase in the K/Ti ratio, while stabilizing the Mg#. Even at 10 kbars, fractionation is not able to produce most of the rocks below an Mg# of 50.

Again, the 5 kbars trend for basalts lies toward the middle of the Clarno field, with the higher and lower pressure trends lying toward the opposite edges of the field. However, the large scatter in the data suggests that simple isobaric crystallization cannot account for all the Clarno rocks. Rather, the scatter suggests that multiple processes may be simultaneously working to create the wider variety of rocks. Simple fractionation also cannot produce the primitive basalts from the Marshall Butte magma since the earliest residual liquids have lower Mg# and constant K/Ti ratios, while the basalts have Mg#'s comparable to Marshall Butte with much lower K/Ti ratios.

Fractionation modeling produced similar results for the trace elements. Initial Sr concentrations are much higher in Marshall Butte than in other Clarno rocks (Figure 4.16a). Fractional crystallization of olivine and clinopyroxene leads to an increase in

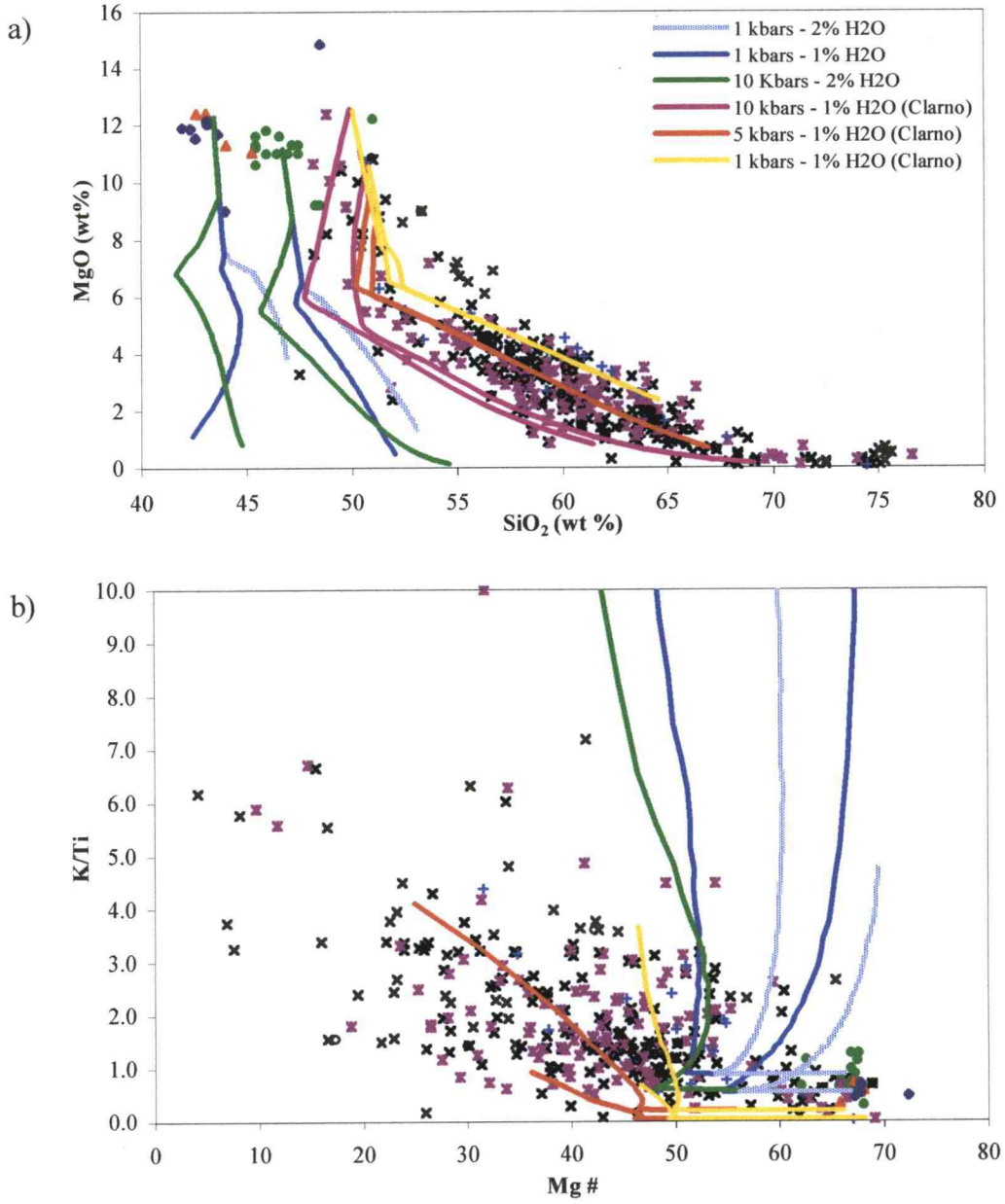

Figure 4.15: Simulations of the major-element compositions of the liquid lines of descent caused by fractional crystallization created using the COMAGMAT model. Symbols are same as in Figure 4.12. a) Simulation trends on the MgO vs. SiO_2 diagram show no relation to actual Clarno compositions if either old or new Marshall Butte data is used as a starting point. Trends for simulations using a primitive Clarno basalt as a starting point lie within the field of actual compositions. b) Trends on the K/Ti vs. Mg# plots are similar, with the simulations using a Marshall Butte starting point failing to explain the Clarno rocks. Trends for Clarno primitive basalts are within the field of actual rock compositions.

Sr concentrations in the melt, thereby driving the liquid away from the field of Clarno rocks. Likewise, fractionation immediately lowers the Mg#, making it impossible to fractionate Marshall Butte into the primitive basalts. While the fractionation trends for the basalts at 1 and 5 kbars lie within the Clarno field, even 80% crystallization fails to explain the more evolved compositions.

The modeling shows an initial increase in Ti and V, followed by a decrease in both elements as oxides begin to crystallize (Figure 4.16b). Once again, fractionation trends for the Marshall Butte magma lie significantly outside the field of data for the Clarno Formation. The trends also show no link between Marshall Butte and the Clarno basalts. Fractionation trends for the basalts again lie within the Clarno field of data, but fail to account for large degree of scatter.

The most significant failure of fractionation models is apparent by plotting trace-element ratios (Figure 4.17). Even when the simulations were run up to 80% crystallization, the resulting span of compositions for the liquid was almost negligible (at all pressures and water contents) for both the Marshall Butte magma and one of the basalts. The range in values for the Clarno rocks is at least 4 times greater than the modeling could produce. While the model for the other basaltic starting composition covers a larger range, fractionation moves the liquid in the opposite direction of the Clarno rocks.

Even though the phase equilibria modeling fails to account for the nepheline present in the Marshall Butte samples, simple fractionation of a Marshall Butte magma can not account for the rest of the Clarno Formation. While not conclusive, simple fractionation of the Clarno basalts does not reproduce the entire spectrum of rocks found in the Clarno Formation. Both K/Ti vs. Mg# and K/Ba vs. Rb/Sr strongly suggest that additional processes were also active, and that the parent magma for the Clarno formation was less alkaline than the Marshall Butte magmas.

Simple binary mixing of various Clarno magmas has been used to explain linear trends observed on Harker diagrams (Suayah and Rogers, 1991). However, some of the trends on Harker diagrams, along with trace element vs. trace element trends, are more parabolic than linear. Still, the authors cite significant petrologic evidence (spongy textures, xenocrysts, etc.) that suggests mixing is taking place. While they do admit that

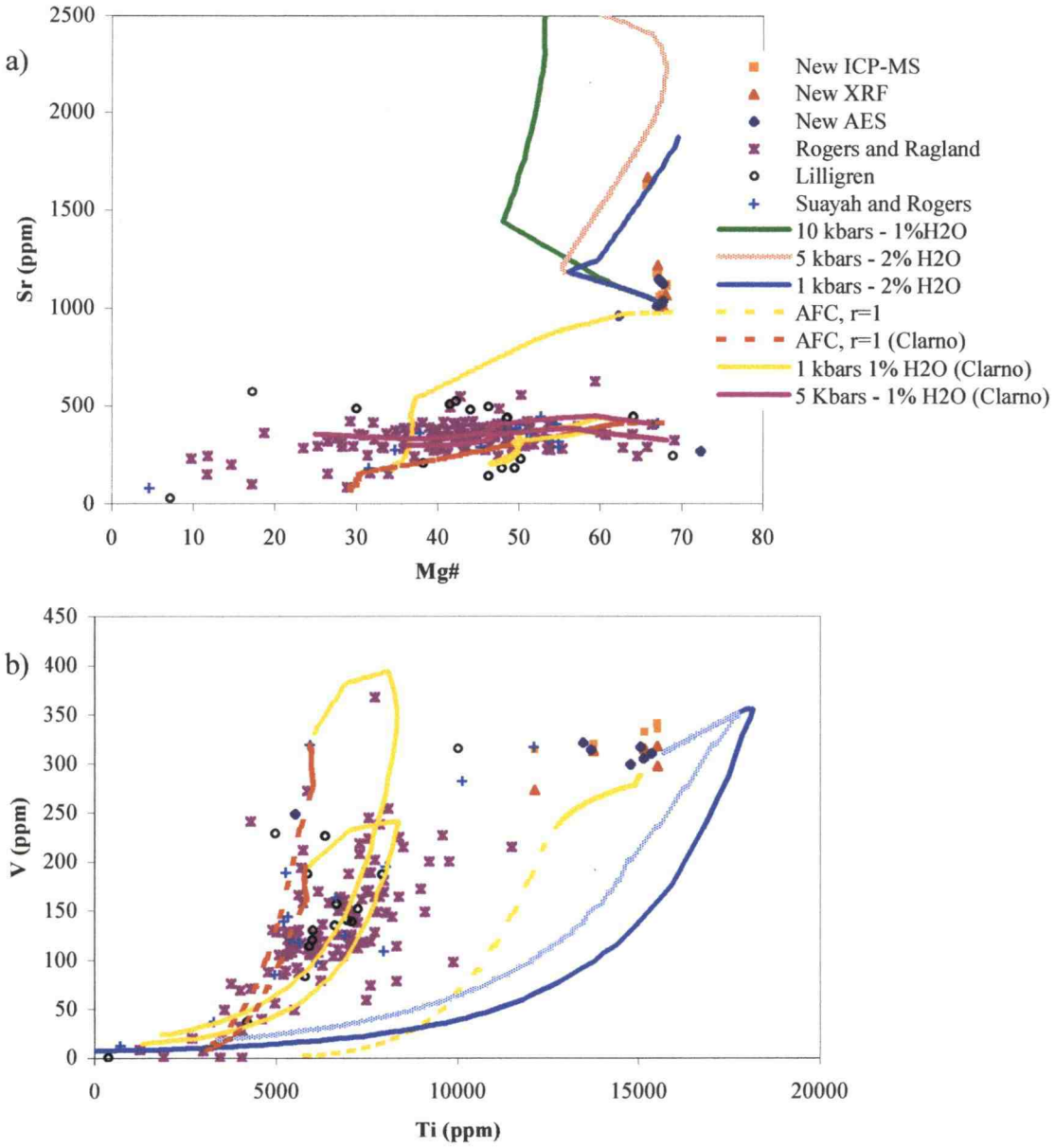

Figure 4.16: Simulation results for the trace-element compositions of liquid lines of descent caused by fractional crystallization and AFC created using the COMAGMAT and MIXFRAC models. a) Sr vs. Mg# shows that Marshall and Corporate Butte rocks have initial Sr concentration too high to evolve into any of the Clarno rocks. Trends from primitive Clarno basalts follow the trend of the actual data, but fail to explain the most evolved compositions. b) On V vs. Ti plots, fractionation trends for the Marshall Butte simulation show no relation to any of the Clarno rocks. Trends for the primitive basalts again lie within the actual data, but may have trouble accounting for the lower Ti rocks.

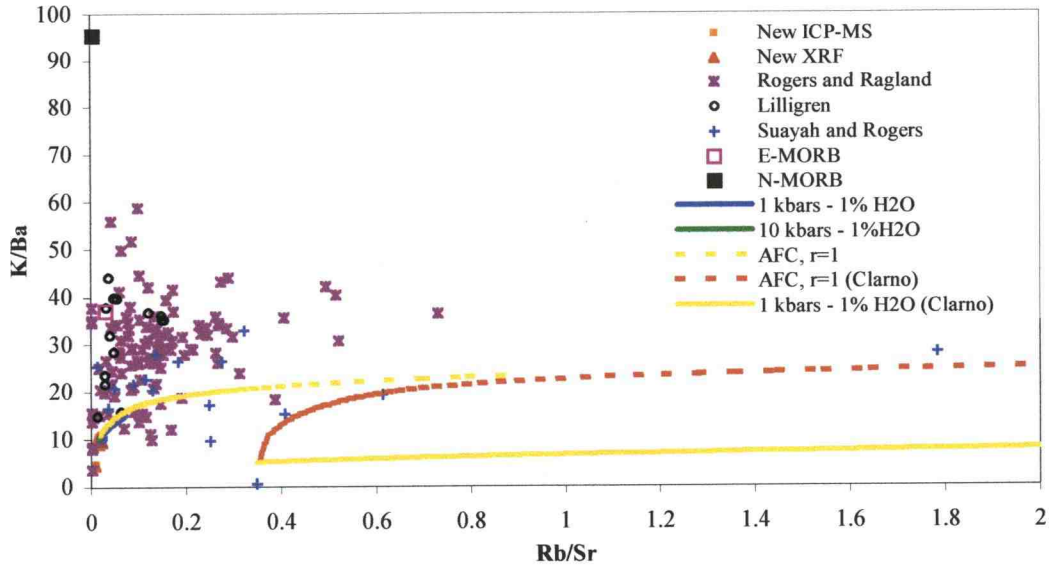

Figure 4.17: AFC and fractional crystallization simulations for both the Marshall Butte and Clarno primitive basalt result in only minor changes in K/Ba and Rb/Sr. Even 80% crystallization can only account for <10% of the Clarno rocks. Fractionation trends for the other Clarno basalts rapidly increase in Rb/Sr, in the opposite direction as the Clarno rocks.

some crystal fractionation appears to have also taken place, their model fails to take this into account.

AFC (assimilation and fractional crystallization) modeling combines both the fractionation modeling done earlier, with assimilation of a second source. Unlike fractional crystallization, AFC modeling is quite complex in that the liquid is not only affected by previous crystallization, but also by assimilation of new material. As a result, the starting composition for an increment of crystallization is not the same as the ending composition of the previous increment, as in the fractionation model used earlier. Currently, most modeling programs available are not able to model both major and trace elements at higher pressures and water contents. So AFC simulations were run at low pressure and low water content using the existing MIXFRAC program (Nielsen, 1992). While the results may not be accurate for the Clarno, the general trends should be similar for most elements. Additionally, the effect of high-

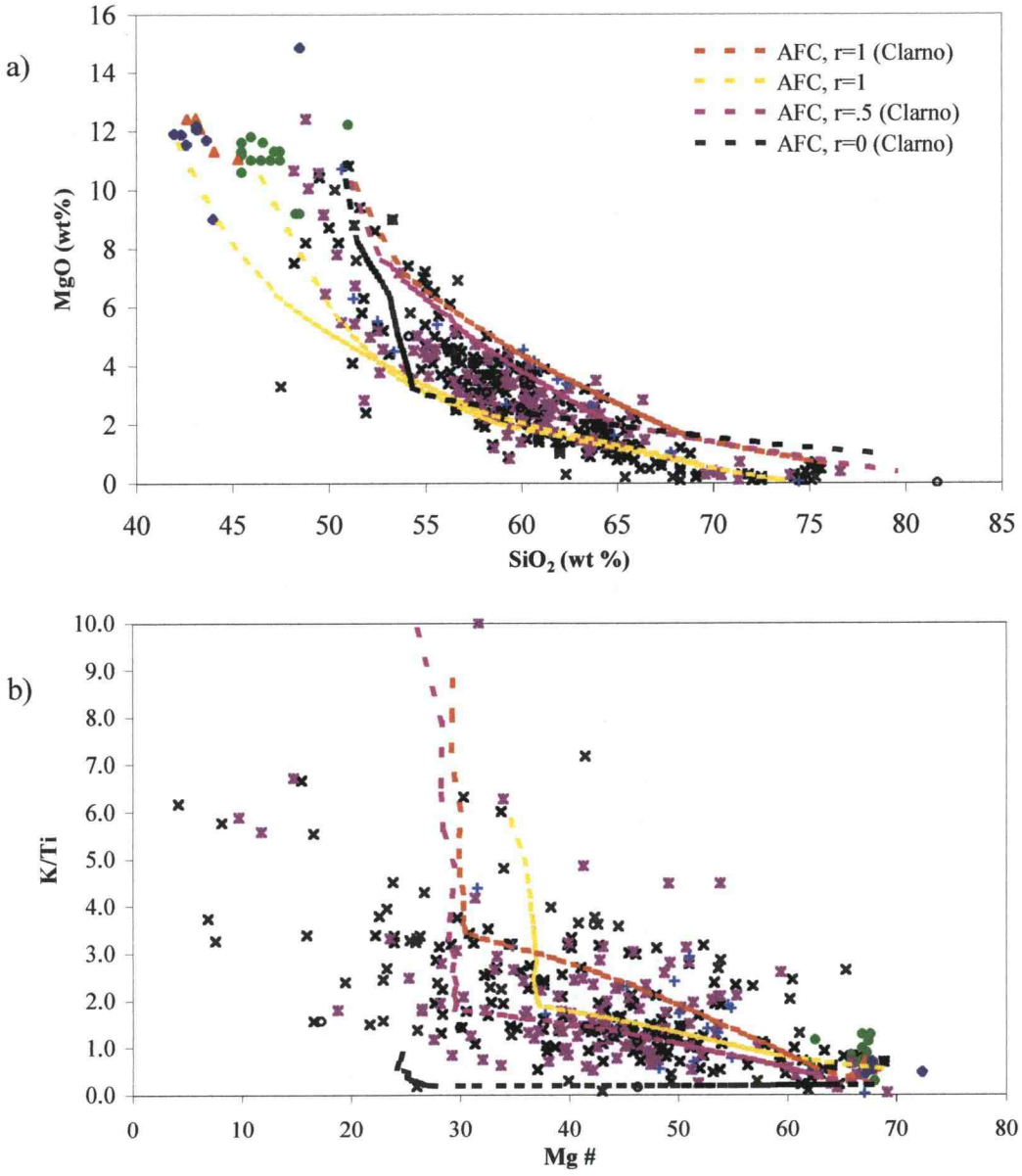

Figure 4.18: AFC simulations created using the MIXFRAC model plotted again Marshall, Corporate, and Clarno rocks for major elements. Symbols are same as Figure 4.15. a) AFC trends on the MgO vs. SiO_2 plot are more parabolic, similar to the actual trend of the data. AFC trends from Marshall Butte result are lower in MgO than most of the Clarno rocks. AFC trends using a primitive basalt from the Clarno as the starting composition lie along the higher silica and magnesia side of the data when r=1 is used. By lower r, the trends are closer to the middle of the field of data. b) AFC trend for all starting compositions lie within the field of Clarno rocks, but the large degree of scatter suggests other processes may also be occurring.

pressure crystallization on the resulting trends can be anticipated from the earlier fractionation simulations. The most significant effects of higher water contents would be the suppression of plagioclase till later in the sequence, so care was taken when examining the trends for the effects of plagioclase fractionation. As with the COMAGMAT model, MIXFRAC is not able to calculate the phase equilibria of nepheline.

Two different sources representing the primitive end member (Marshall Butte and the PH-16 basalt sample from Suayah and Rogers, 1991) were mixed with an evolved source (BC-16, a rhyolite from Suayah and Rogers, 1991) using the MIXFRAC model. The basalt represents alkali values more typical of Clarno mafic rocks, in contrast to the more alkaline Marshall Butte suite. Simulations were done using a constant r (mass of assimilant/mass of fractionated crystals) of 0, 0.5, 1, and 4. This ranges from ideal crystal fractionation to near binary mixing.

The results of the major-element simulations (Fig 4.18a) show a parabolic trend more similar to the actual data than simple fractionation alone. The generated trends for Marshall Butte still lie outside the field of data for the less evolved Clarno rocks, while demonstrating that the more evolved Clarno rocks could be related. Trends for the primitive basalts lie within the upper part of the Clarno field for all but the most evolved rocks. Fractionation at higher pressures would drop these trends more toward the center of the field of data. Unlike simple fractionation, AFC is able to produce the highly evolved Clarno rocks from a basaltic parent. Just like simple fractionation, AFC is not able to produce the primitive basalts from a Marshall Butte composition.

For both major-element ratios and some trace elements, the trends are similar to simple fractionation, but over large ranges (Figure 4.18b, 4.16a). However, with assimilation of an evolved composition, the lower Mg# rocks may be accounted for. AFC models of a Marshall Butte source produce liquid compositions that are closer to, but still not within, the Clarno field of data (Figure 4.16b). A larger degree of assimilation (r=1) of an evolved source reduces the early Ti enrichment. For the primitive basalts, the resulting trends lie along the edge of the field of data. A lower degree of assimilation (r=0.5) is very close to the original simple fractionation trends rather than intermediate between the r=1 trend and the fractionation trend. Adjusting the pressure and water con-

tent can shift the trends within the data field, but still does not explain the scatter of the data.

Finally, trace-element ratios show that assimilating an evolved material pulls the crystallization trends to higher Rb/Sr values, away from most of the Clarno rocks (Figure 4.17). Since both fractionation and AFC lead to much higher Rb/Sr values with only small increases in K/Ba, another process is needed prior to crystallization to explain the variety of K/Ba values. Mixing with a MORB-like source, followed by AFC, could produce the variety of compositions observed in the Clarno.

Both Sr and K/Ti suggest that Marshall Butte and the Clarno basalts may be related by differing degrees of partial melting. In both cases additional melting of the Marshall Butte magma source would further lower Sr concentrations and K/Ti values without significantly altering the Mg#. The same is true for V vs. Ti, where increased melting would result in lower Ti and V concentrations, moving the liquid in the direction of the basalts. However, additional melting would also drive the liquid toward higher MgO, while most Clarno basalts have less MgO.

Mass balance, fractionation, and AFC all fail to illustrate a clear connection between Marshall Butte and the Clarno rocks. However, while larger degrees of partial melting could result in primitive basalts, a link is not conclusive. Binary mixing of a Marshall Butte-like magma with a second (more tholeiitic) source prior to fractionation could be used to explain the Clarno. This is best seen on the K/Ba vs. Rb/Sr plot. Mixing of a typical N-MORB (Sun and McDonough, 1989) and Marshall Butte would result in intermediate compositions characteristic of some mafic Clarno rocks.

At the same time, the trends produced by phase equilibria and AFC modeling of the primitive basalts fell within the field of Clarno data. However, some of the plots (K/Ti vs. Mg#) show a large degree of scatter, while others (like Sr vs. Mg#) show clear trends with a few outliers. The orientation of process vectors relative to one another can be one reason for the scatter on the diagrams. The largest amount of scatter occurs when the process vectors are at large angles to one another (Nielsen, 1990). This causes the differing processes to shift the compositions in different directions. When the process vectors are subparallel, the processes move the compositions in the same directions, reducing

scatter. The large degree of scatter suggests that there are several processes occurring together, not just one or two.

A more complex system of RAFC (recharge-assimilation-fractional crystallization) may be needed to explain the genesis of the Clarno Formation. It does appear that the Marshall Butte magma was derived from a distinct source, unrelated to the majority of the Clarno rocks. The more alkaline magma of Marshall and Corporate Buttes represents melting of enriched asthenospheric mantle without input from subduction fluids or melts, as opposed to the calc-alkaline magmas of the Clarno Formation that are thought to have formed by melting of depleted asthenosphere due to subduction fluid fluxing. The exact cause of melting for the alkaline magma is not clear, but may be related to shifting subduction parameters and extension in the region.

Chapter 5: Hudspeth Mill Intrusion

Setting

Located about 8 km northwest of Mitchell, the Hudspeth Mill Intrusion is named for the nearby old Hudspeth Sawmill. The intrusion is actually a series of several small basaltic bodies, including one body that is cut by US 26 (Figure 5.1). The intrusion is largely surrounded by Clarno tuffs and volcanic mudflows, with small, interspersed outcrops of ash-flow tuff.

This intrusion is of interest because of its alkalic character. The contact between the intrusion and the tuffs near the highway appear to parallel the bedding of the tuffs, so it is often called a sill. However, in other locations the intrusions cross-cut the strata like a dike. It is likely that the intrusion "wormed" its way throughout the soft Clarno rocks.

Results

Petrology and Phase Chemistry

Along the road-cut on US 26 (HM-1), the basalt is porphyritic and light gray. While the exposure is recent (due to road construction), the outcrop has undergone both extensive alteration and weathering. There are large veins of zeolites that suggest dueteric alteration, and removal of some of the alkalis. The second sample (HM-2) was taken from the lower contact of a sill-like part of the intrusion (Figure 5.1). This contact is parallel with the bedding of the underlying Clarno tuffs. Here the basalt is much more fine grained and shows no significant alteration or weathering. While still porphyritic, the phenocrysts appear less abundant and much smaller. Samples EMT-172 and EMT-43 were reanalyzed along with the above samples.

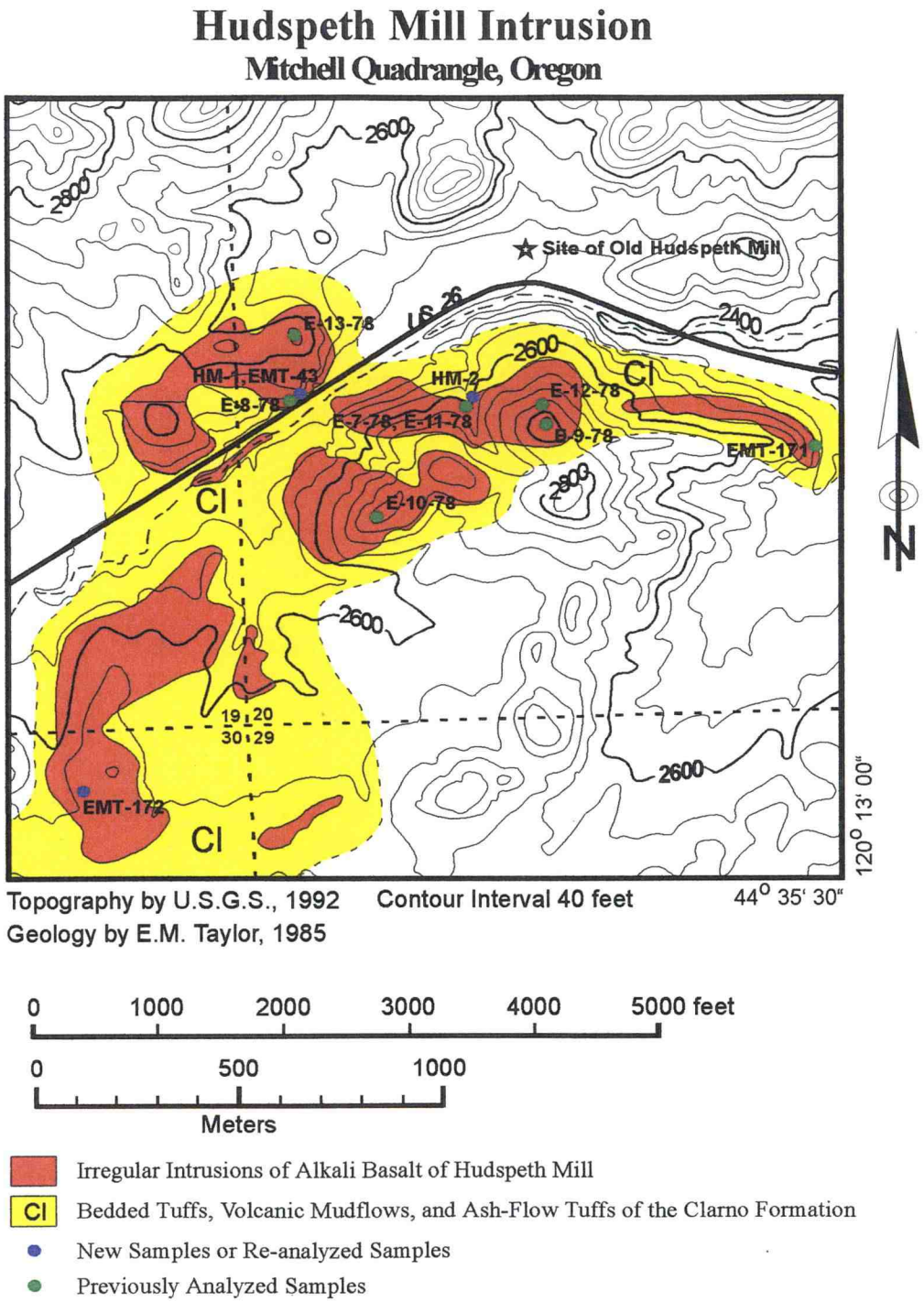

Figure 5.1: Geologic map of the Hudspeth Mill intrusion and surrounding Clarno tuffs and mudlfows. Also marked are the sample locales for the intrusion.

The texture and mineralogy of the samples varies both between bodies and within them. Samples from the base and top of the intrusion are much finer-grained and display a porphyritic texture, while near the middle of the bodies the samples are more seriate. Phenocrysts make up 10-25% of the samples, always consisting of olivine and clinopyroxene. The olivine ranges from subhedral to euhedral depending on the sample, with almost all containing inclusions of Fe-Ti oxides. Many of the olivines display resorbtion features such as embayments and rounded edges. Most of the olivine from the roadcut is serpentinized, further indicating dueteric alteration. While the phenocrysts cover a spectrum of sizes and shapes, two endmembers can be defined. The larger phenocrysts, ~ 1mm across, are more euhedral with large embayments and some rounded corners. The smaller olivine, around 0.5 mm across, are more subhedral with less resorption features and the occasional small (20 micron) clinopyroxene inclusion. While in some samples the two endmembers seem to define two populations, in others there seems to be a spectrum of crystals between the two endmembers. Olivine is not found as a groundmass phase.

Clinopyroxene is the dominant phenocryst phase in all of the samples, and is also present as microphenocrysts and in the groundmass. Phenocrysts of clinopyroxene range from euhedral, sieve-textured samples (~ 0.5 mm) to subhedral, clear micro-

Table 5.1: Modal Estimates of Hudspeth Mill by location within the bodies.

Part of Intrusion	Base	Base	Middle	Middle	Top
Phenocrysts	9 %	10 %	18 %	23 %	12 %
Olivine	10	9	9	13	6
Cpx	66	61	40	47	69
Plagioclase	18	17	11	8	22
Alkali Feldspar	Tr	Tr	23	22	Tr
Biotite	Tr	Tr	9	4	Tr
Oxides	5	3	7	4	1
Glass	Tr	Tr	Tr	2	2

phenocrysts (0.025 mm) that display zoning and some twinning. Glomerophyres of the larger sieve-textured clinopyroxene are also present. Additionally, in many of the samples small granular clusters of clinopyroxene and feldspar are present. While the small clusters retain relict phenocrystic texture and may therefore represent amphibole breakdown, the lack of significant opaques in the clusters makes this a tenuous conclusion. Pyroxene laths are also abundant around many of the small quartz inclusions, which appear to be xenocrysts. The pyroxene laths and clay minerals form radial coronas on the quartz grains.

A variety of feldspars are found in the groundmass of samples. The most noticeable in the thin-sections are the polysynthetic-twinned plagioclase (200-300 microns), but alkali feldspars are also abundant. The textures displayed by the feldspars vary as much as the composition. Many of the subhedral plagioclase laths are spherilitic to variolitic, while the rest are interstital. The alkali feldspars range from intersitial to poikolitic, with some plagioclases crystals displaying sanidine rims.

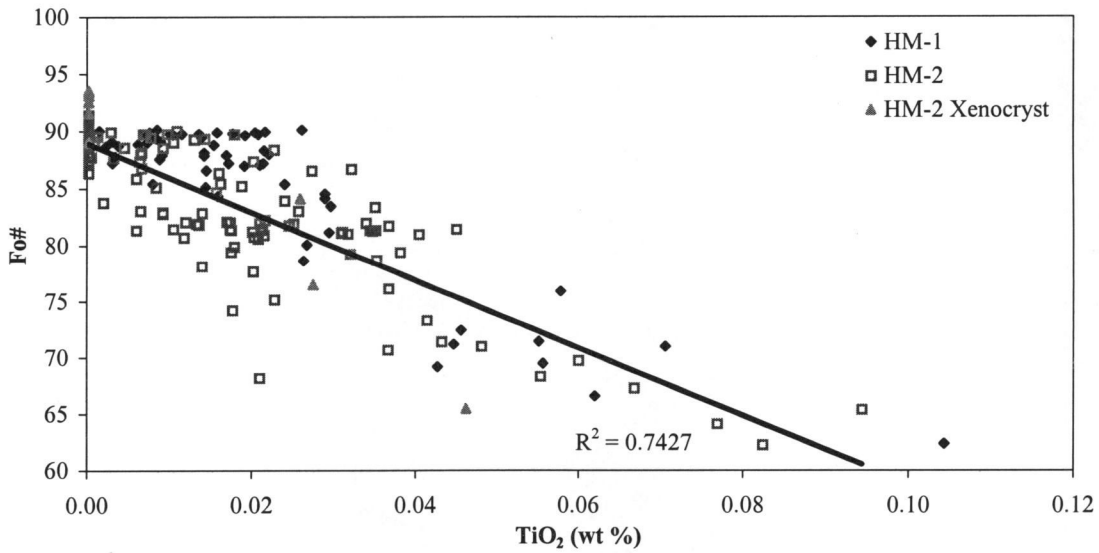

Figure 5.2: Olivine phenocrysts display a linear correlation between fosterite and Ti, consistent with crystal fractionation. The scatter is due mainly to uncertainties in the data.

Biotite is common in the groundmass as anhedral laths. Their late development, small size (<100 microns) and minor amounts (< 5%) suggest it was stable near the end of crystallization, as the pH_2O increased. Fe-Ti oxides and glass are also present in the groundmass to varying degrees. The oxides are usually <150 microns in size and are anhedral-subhedral granules. However, in a few samples with higher glass contents (now devitrified) the oxides are more abundant (~ 10%) and are small laths instead of granular in shape.

Olivine composition varies from $Fo_{91.5}$ to Fo_{62} in the samples analyzed by microprobe (Appendix 2). Overall, the olivine shows a general linear relationship between fosterite content and TiO_2 (r^2= 0.74) (Figure 5.2). The sample from the contact (HM-2) also contains a xenocryst of olivine (~$Fo_{93.5}$) not apparent in samples from the middle (HM-1) of the intrusion. While the xenocryst's core is more magnesian than other olivines, the rim composition is similar to the other phenocryst in the sample. This indicates that the outer part of the xenocryst had a shared history with the other olivine.

Major-element traverses of the olivine indicate the crystals are normally zoned overall (Figure 5.3). The traverses display a core of near constant Fo, and a 30-50 micron thick rim that is normally-zoned. Minor-element traverses display an oscillatory behavior in both NiO and MnO over much of the crystal, with the ~40 micron thick rim displaying behavior typical of normal zonation (Figure 5.3). However, while much of this oscillation is within the error of the analysis, there is enough variation to suggest some zonation of the crystal cores.

A comparison of bulk-rock and the olivine Mg/Fe^{2+} ratios indicates a disequilibrium exists between the two (Figure 5.4). The olivine plots lower than the equilibrium line of Rhoeder and Emslie (1970) for the middle of the intrusion (HM-1), meaning it is not magnesian enough for the bulk-rock composition. The sample near the contact (HM-2) displays cores closer to the equilibrium line, but still below it. However, one of the crystals in this sample clearly plots above the line, and so has been termed a xenocryst. The xenocryst's core appears to display weak reverse-

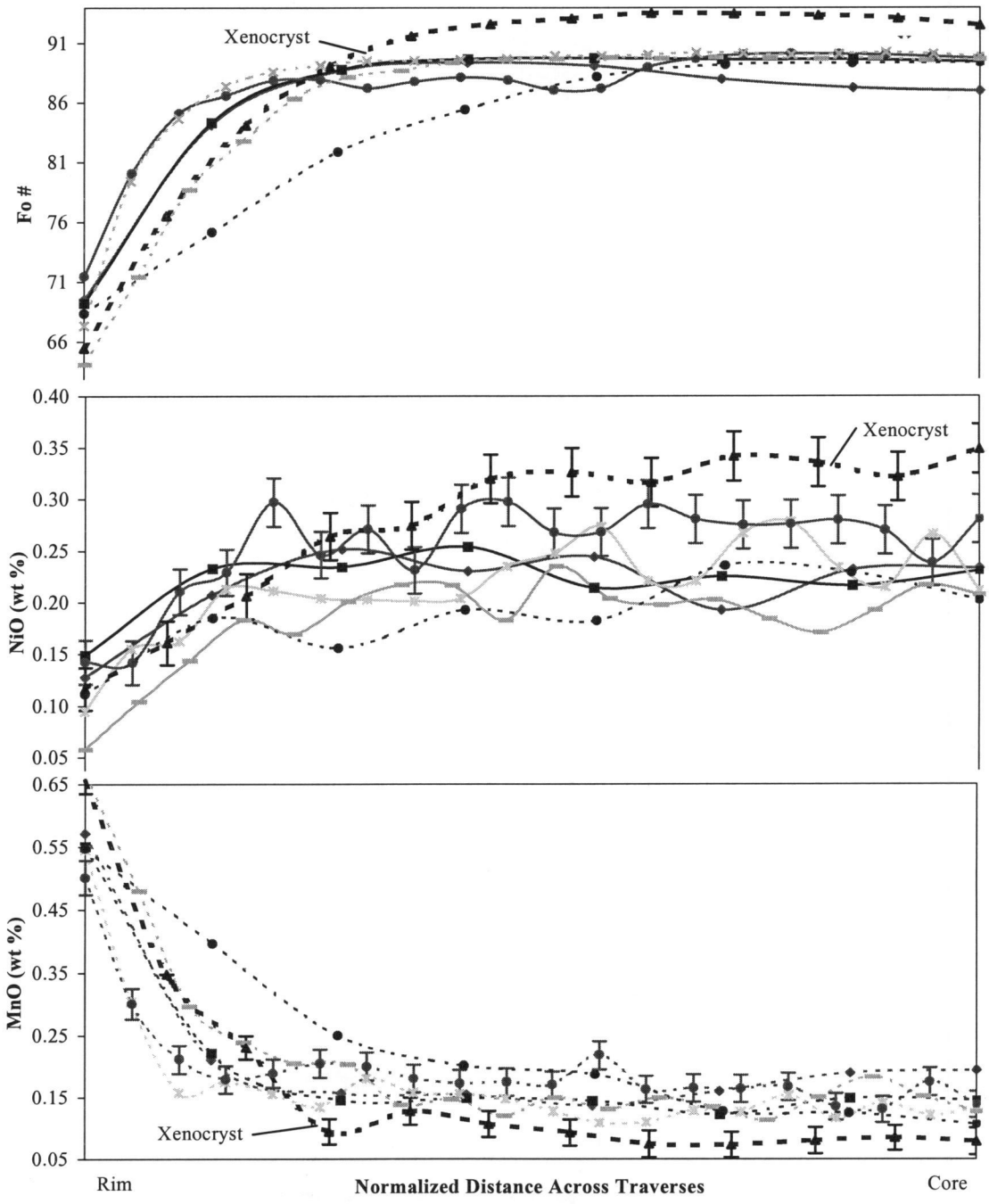

Figure 5.3: Microprobe traverses from select olivine phenocrysts. Solid lines– HM-1, near the middle of the intrusion; Dashed lines– HM-2, near the margin of the intrusion. The grains are nearly constant across much of the grain, with normally zoned rims. The oscillations in the minor elements are within the error of the analyses. Error bars have been plotted based on the counting statistics for the analyses.

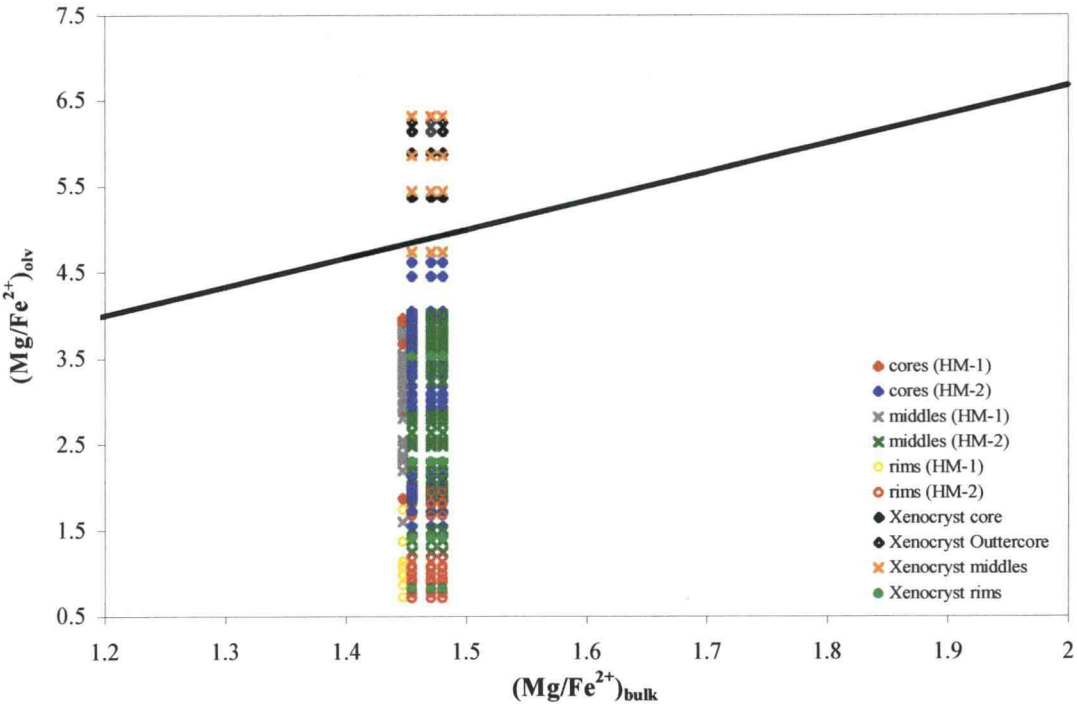

Figure 5.4: Mg/Fe^{2+} ratios for the olivine and bulk-rock with the equilibrium line of Rhoeder and Emslie (1970). With the exception of a xenocryst, all of the olivines plot below the line, indicating some degree of disequilibrium.

zoning, resulting in higher Mg/Fe^{2+} values for the outer core and inner middle analyses than either the cores or the rims.

Pyroxenes from the intrusion fall along the diopside-augite dividing line and range from $En_{51}Wo_{43}Fs_6$ to $En_{36}Wo_{50}Fs_{14}$. Overall, the crystals display a linear trend consistent with a fractionation-dominated petrogenesis (Figure 5.5). In both samples, most of the larger phenocryst core and middle analyses have higher MgO and lower TiO_2, while the microphenocrysts and groundmass pyroxenes have lower MgO and higher TiO_2. However, many of the rims in the larger phenocrysts are lower in MgO and higher in TiO_2 than both the microphenocrysts and the groundmass. While this pattern is present in both samples, it appears better defined in the sample from the contact (HM-2). In the HM-1 sample, what appears to be an inclusion of clinopyrox-

ene was found in one of the smaller olivines. It plotted with the higher MgO groundmass and microphenocrysts.

Traverses across the larger pyroxenes show significant (~ 3-7% change) oscillatory zoning over much of the crystal and strong (> 15%) normal zonation at the rims (Figure 5.6). The less detailed traverses display an overall normal zonation also, with near-constant core and middle composition. However, the lack of oscillatory zoning in these traverses may reflect the less detailed nature of the traverses rather than an unzoned crystal. TiO_2 displays similar behavior to the Mg#, with oscillatory or near-constant profiles over much of the crystals, with a strong enrichment in the rims (Figure 5.6). Cr_2O_3 values show the same type of pattern oscillation for the more detailed phenocrysts, with the others showing a large initial increase in Cr_2O_3, followed by an exponential decrease moving toward the rim. A large change in composition

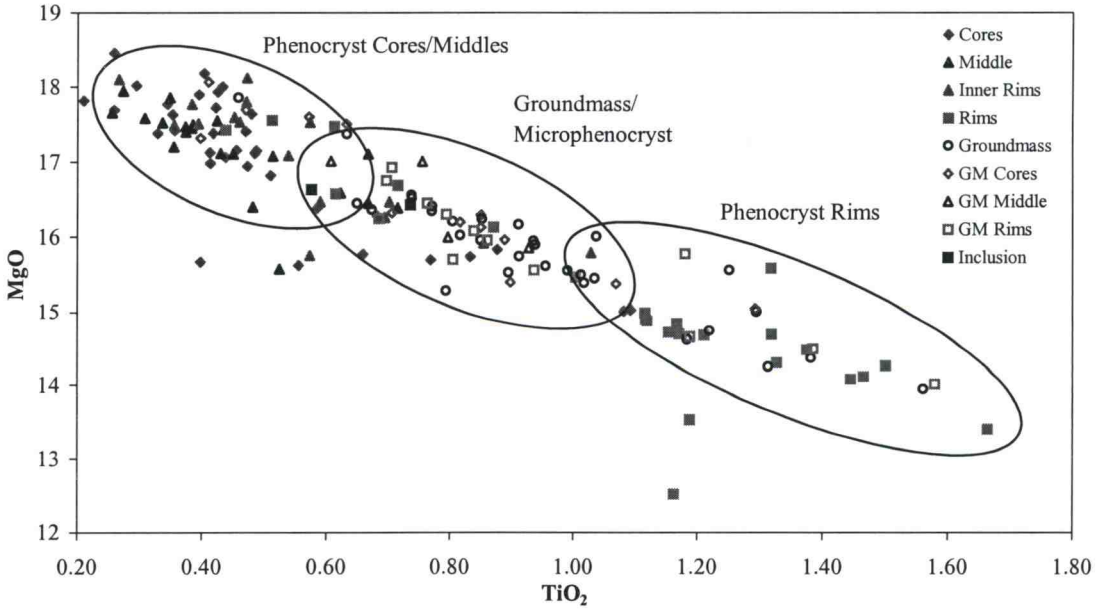

Figure 5.5: The pyroxenes exhibit an overall linear trend of decreasing MgO with increasing TiO_2. However, many of the groundmass crystals are more Mg-rich than the rims of the phenocrysts.

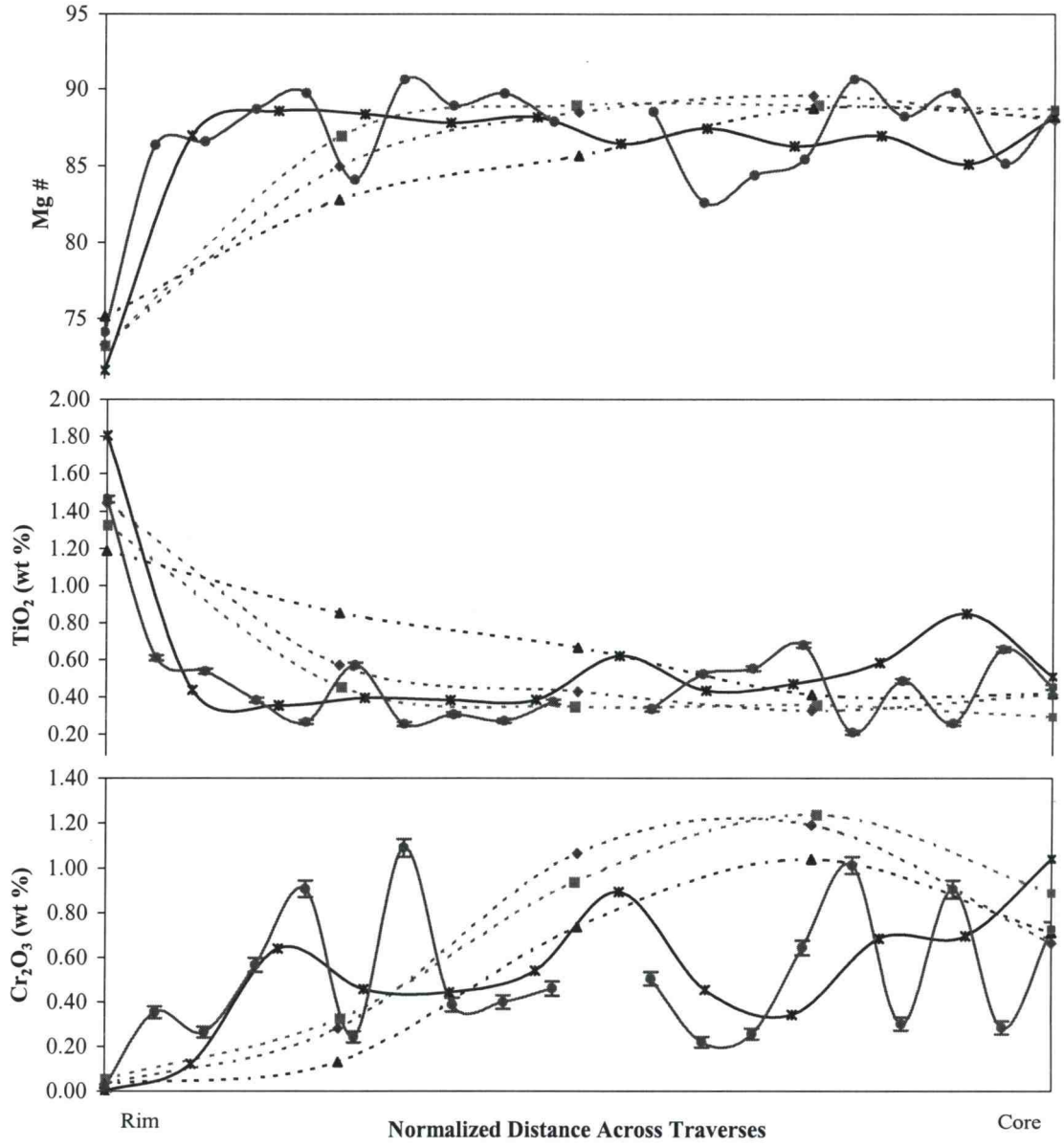

Figure 5.6: Microprobe traverses of select pyroxene grains. Solid– Phenocrysts; Dashed– Microphenocrysts. The phenocryst display oscillatory zoning over much of the crystal, with normally zoned rims, while the microphenocryst traverses were not detailed enough to determine this.

between the rim and cores is not present, possibly due to faster diffusion of Cr than Ti.

Both plagioclase and alkali feldspar are present in the groundmass of the samples. And while proportion and textures vary between the samples, the compositions are similar. The plagioclase ranges from An_{67} to An_{51}, while the alkali feldspars range from $Ab_{47}Or_{48}An_5$ to $Ab_{32}Or_{64}An_4$ (Figure 5.7).

Fe-Ti oxides decrease in Cr# and Mg# and increase in Fe content moving from the chromite inclusions to the titano-magnetites in the groundmass (Figure 5.8). However, some of the groundmass crystals in the HM-1 sample (middle of the intrusion) are also chromites. Comparison of the chromite inclusions to the fosterite of the olivine near the inclusion resulted in good correlations (r^2= 0.88-0.96) between the

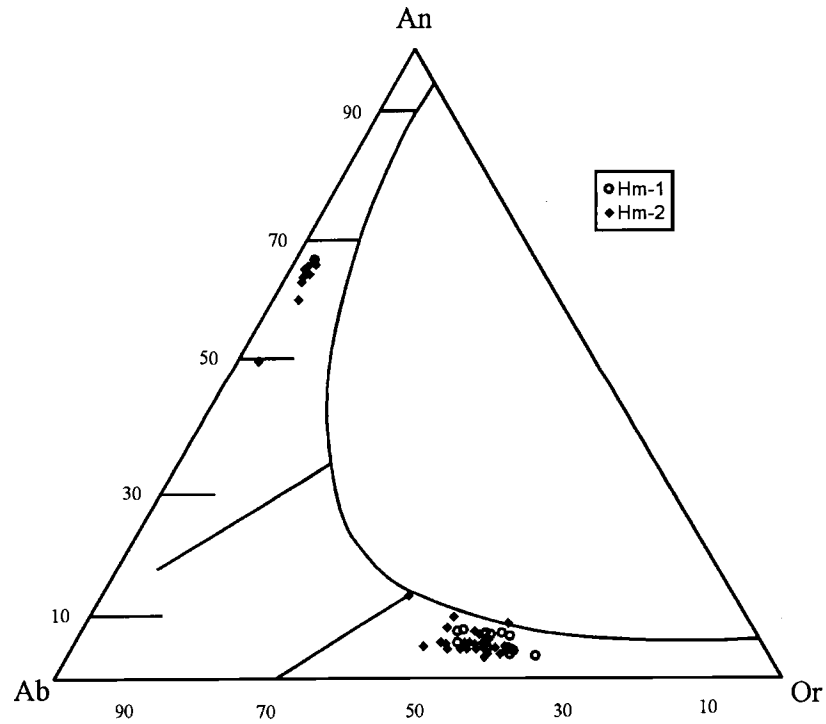

Figure 5.7: Plotting the feldspars on the classification ternary (after Deer et al., 1992) shows that both plagioclase and alkali feldspar are present in the intrusion.

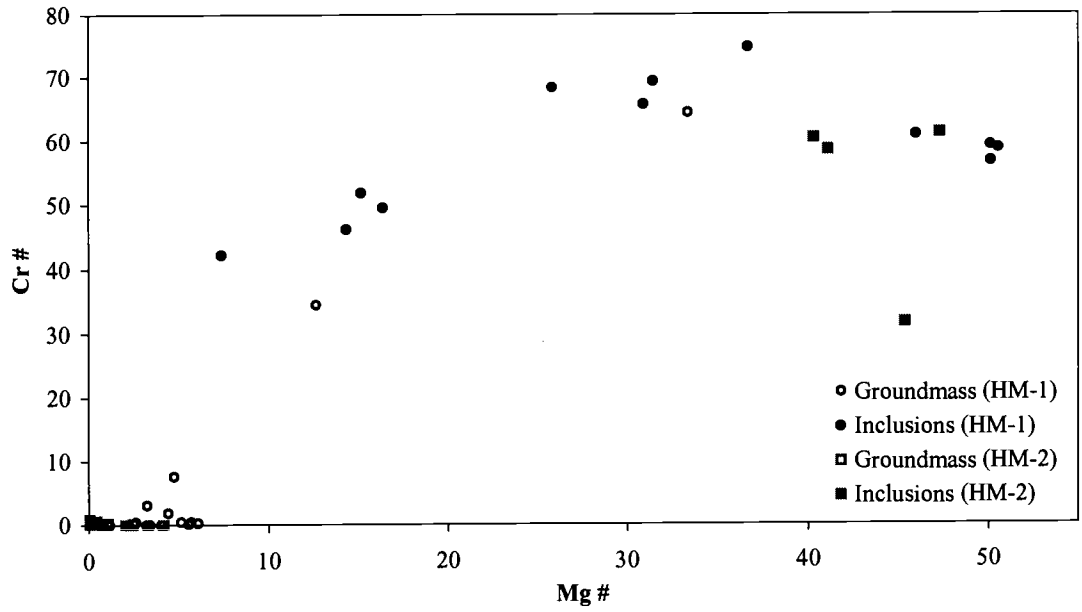

Figure 5.8: Fe-Ti oxides change in composition from chromite in the inclusions (filled) to titano-magnetites in the groundmass (hollow). They exhibit little variation from the margin (squares) to the interior (circles) of the intrusion.

fosterite content and the Cr and Mg numbers of the inclusions. This suggests that some of the chromites may have experienced diffusion and reequilibration with the magma, post entrapment.

Bulk Geochemistry

While older chemical data classifies the intrusion as basalt, basaltic andesite, trachy-basalt, or basaltic trachy-andesite when using a total alkali-silica scheme (Figure 5.9), the new data all falls within the basalt field of LeMaitre et al. (1989). Both older and new data fall within the alkaline field (Figure 5.10). Due to the higher quality of the new data, the intrusion will be classified as an alkali basalt. The intrusion has similar SiO_2, Na_2O, CaO, and TiO_2 values to other Clarno basalts, but has higher MgO and K_2O, and lower Al_2O_3.

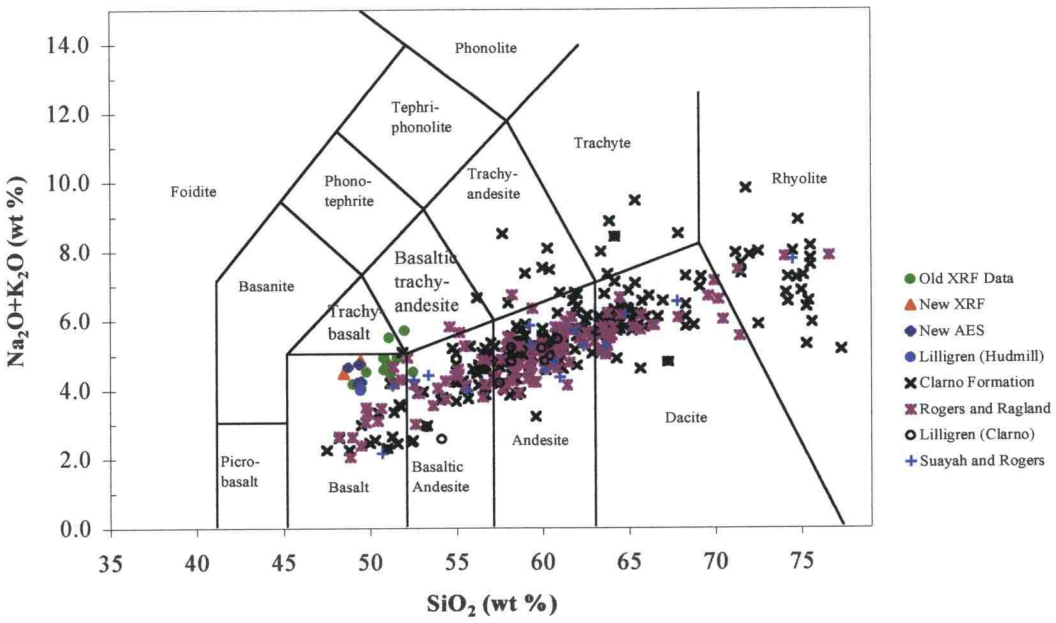

Figure 5.9: Classification of the Hudspeth Mill intrusion samples and other Clarno Formation rocks according to total alkali content. (Le Maitre et al., 1989).

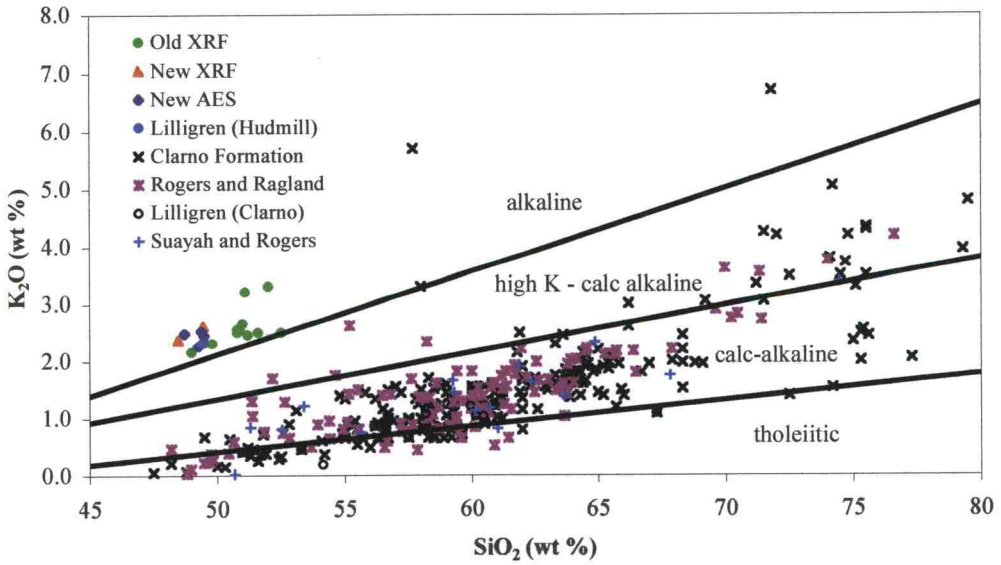

Figure 5.10: Alkalinity classification for the Hudspeth Mill intrusion. It is classified as alkaline, while most of the Clarno Formation is tholeiitic to calc-alkaline according to the subdivisions of Gill (1981).

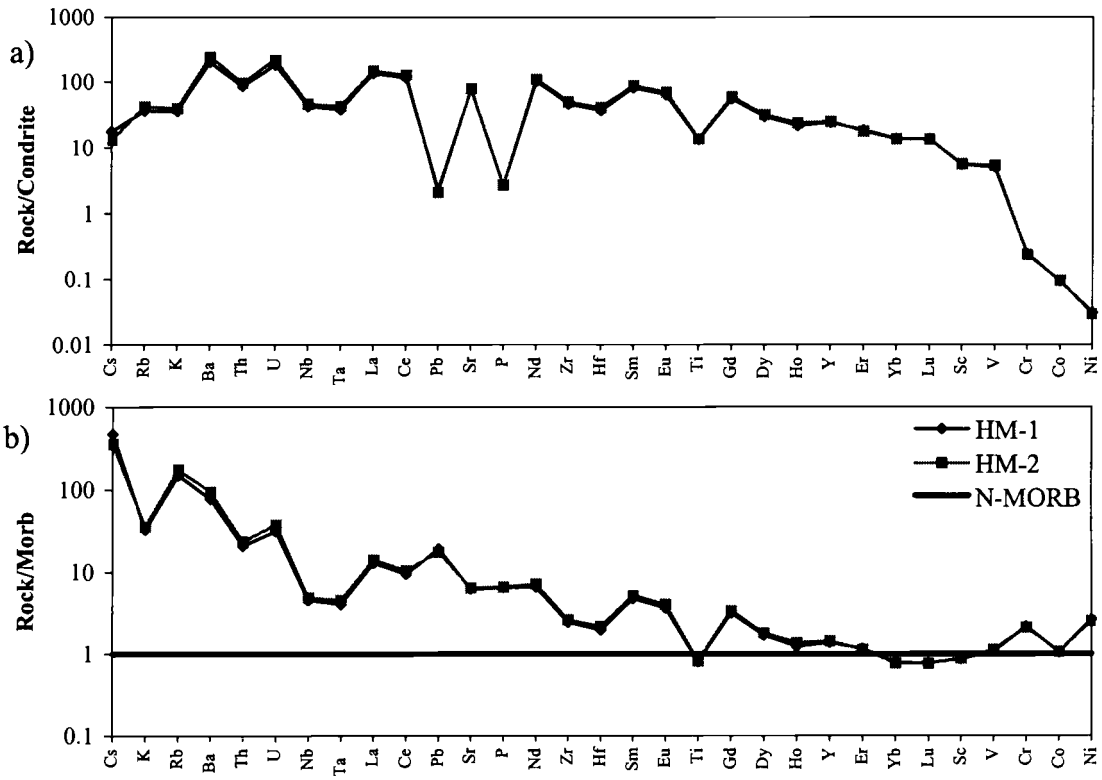

Figure 5.11: Trace-element diagrams for the intrusion normalized to a) condrite and b) N-MORB of Sun and McDonough (1989). The rocks are in enriched in all but the heavy REE's when compared to MORB. They display a HFSE depletion compared to LILE's, a characteristic common to subduction zone magmatism.

The intrusion is a potassic series with Na_2O/K_2O values ranging from 0.72 to 0.89. All of the samples have high Mg# (> 71), high Cr (> 780 ppm) and high Ni (236-340 ppm). This is consistent with the intrusion being a primitive magma. The rocks are slightly silica undersaturated to silica saturated with most samples nepheline normative (< 2%) and one sample hypersthene normative (6.5%) (Appendix 4).

Trace-element spiderdiagrams indicate the Hudspeth Mill intrusion is enriched in most of the incompatible trace elements. When normalized to condrite, the intrusion has large negative anomalies at Pb, P, and Ti (Figure 5.11a). However, Pb shows a

positive anomaly when normalized to MORB, and K instead shows a large negative anomaly (Figure 5.11b). Smaller negative anomalies also exist for the HFSE elements in both normalizations. The intrusion shows enrichments in almost all of the elements except Ti and the heaviest REEs compared to a typical MORB of Sun and McDonough (1989). The rare earth elements are all strongly enriched (13-136x relative to condrite), and fractionated ($La/Lu_n = \sim 10$).

Geochronology

Age determinations were conducted on the Hudspeth Mill Intrusion using the sample near the contact (HM-2). While the samples are high in K_2O, most of this is in groundmass minerals rather than the phenocrystic phases. Therefore, a whole rock groundmass sample was analyzed using $^{40}Ar/^{39}Ar$ step heating. With the exception of the first gas fraction, which is often contaminated, the remaining age steps ranged from 45.24 Ma to 43.94 Ma (Appendix 3). The ages show a progressive decrease with increasing temperature, the results of "argon recoil". This resulted in a total gas age of 44.40 ± .08 Ma. However, a more accurate method, isocron regressions of $^{40}Ar/^{36}Ar$ vs. $^{40}Ar/^{36}Ar$, yield an age of 45.26 ± .31 Ma.

Early work by Enlows and Parker (1972) was done using K-Ar dating and suggested that the Clarno Formation ranged from 46-30 Ma. Other dates in the 30 Ma range were also published in the seventies. However, more recent work reports ages from ~40-60 Ma (Suayah, 1990; Bestland et al., 1999). They also identify the most active period of Clarno activity around 49 Ma. It is likely that the earlier dates are too young due to pervasive weathering in the samples, and the greater degree of error involved in the K-Ar method due to the need for multiple splits of sample and a single gas step instead of multiple steps used here.

No previous age determination had been conducted on the Hudspeth Mill Intrusion. Therefore, due to the lack of comparable data, and the low degree of error in the results, the age of ~ 45 Ma seems appropriate for the intrusion. This would mean that

the more alkaline magmatism post-dates the major calc-alkaline magmatism by ~ 4 million years.

Discussion

Hudspeth Mill Intrusion Petrogenesis

The linear trends observed on olivine element-element diagrams, along with normally zoned crystals, are consistent with a system dominated by crystal fractionation. While the traverses suggest some oscillation in composition may be present in the olivine, such fluctuations are within the error of the analyses. This could reflect diffusion of elements across the olivine, rather than the original scale of differences in the crystal.

Fractional crystalization is further reinforced by the change from chromite inclusions to titano-magnetites in the groundmass. Hill and Roeder (1974) noted that a gap between chromites and titano-magnetites results from the onset of clinopyroxene crystallization. Clinopyroxene crystallization causes Cr content of the magma to drop rapidly and any chromites in the liquid to become unstable. This causes a hiatus in oxide formation and resorbtion of chromites in the liquid. The abundance of chromite in the olivine indicates that olivine crystallization occurred mainly before the onset of clinopyroxene crystallization.

When comparing the Mg/Fe^{2+} ratios of the olivine to the bulk-rock, the sample from near the margin of the intrusion plots just below the equilibrium line, within the error of the data. This suggests that the bulk rock may indeed reflect the actual liquid composition from which the olivine crystallized. Additionally, the smooth pattern of cores to lower Mg/Fe^{2+} value rims is consistent with crystal fractionation. The sample from near the middle of the intrusion plots significantly lower than the line. This indicates it was in equilibrium with a more evolved (higher Fe) bulk liquid. This is consistent with the middle of the intrusion experiencing recharge events that resulted in a more magnesian magma. Additionally, the xenocrystic olivine crystal plots much

higher than the equilibrium line. This suggests that it was in equilibrium with a more magnesian melt. The crystal also displays reverse zoning near the middle with outer cores/inner middles having higher Mg. While this crystal has been termed xenocrystic due to it chemistry, no clear textural evidence is present to further support this conclusion. Yet, it is clearly not like the other olivine crystals in the samples.

Clinopyroxene compositions also display an overall normal zonation consistent with fractionation. However, due to slower diffusion, the original zonation has been better preserved in the crystals. And while the major-element traverses have some oscillatory zoning, the minor elements show this in detail. There were clearly fluctuations in magma chemistry that suggest a more complex history than simple fractionation. This is further supported by the fact that rim compositions on the phenocrysts are more evolved than the pyroxene groundmass and microphenocryst compositions. These observations suggest that magma mixing, possibly as simple as a series of recharge events from the same source, was also occurring during fractionation.

The relegation of plagioclase and alkali feldspar to the groundmass, along with biotite in the groundmass, indicates that the magma was hydrous. The water resulted in suppression of plagioclase crystallization until the final stages of cooling. At this point, water content had increased due to crystallization, and biotite was stabilized. This may be further substantiated by the relict textures thought to represent amphibole. Partial melting of a source region rich in hydrous phase would result in a hydrous magma. Such a hypothesis is also strengthen by the Ti depletion and flattening of the REE pattern at the heaviest elements. Both of these reflect the presence of amphibole as a residual phase in the source region (LaTourrette et al., 1995; Hilyard et al., 2000). The intrusion is also depleted in HFSE relative to LILE, a pattern typically referred to as a "subduction signature" (Plank and Langmuir, 1998). This signature is thought to originate from fluids derived from the subducting slab as it undergoes dehydration reactions (Pearce, 1982; Sun and McDonough, 1989). The lack of the subduction signature in the Marshall Butte samples suggests that the asthenosphere under the area does not contain the HFSE depletion. However, melts of the asthenosphere mixed with the fluids derived from the slab may contain the signature also.

Additionally, areas of the lithospheric mantle that have been metasomatized by these fluids, and then melted at a later time, would also contain the signature. Due to the significant contribution of amphibole partial melting to the magma's trace-element characteristic, a lithospheric mantle source region is favored here.

The Hudmill intrusion is similar to other mafic alkaline rocks found in many of the other Eocene suites from the western U.S. (Chapter 2). While the Hudmill rocks fall into the basalt classification of Le Maitre et al. (1989), they are very similar to the mafic absarokites of the Yellowstone area (Hiza, 1999). Dudas noted that in the Crazy Horse Mountains, most of the basaltic rocks in his subalkalic series are actually absarokites. His subalkalic classification was based on the fact that they are all at or near silica-saturation, rather than strictly on K_2O content. However, most of the alkaline suites reported from the Eocene magmatic areas are actually lamprophyres. The overall compositions are very similar to alkali basalts and absarokites, but a much higher volatile content resulted in a hydrous mineralogy and a lamprophyric classification. For a more complete discussion of lamprophyres, and the occurrences throughout the western U.S., see Chapter 6.

In the previous chapter (Marshall and Corporate Buttes), it was noted that in many of the same locales that contain basanites and other silica-undersaturated alkaline suites, alkalic basalts are also present. However, many of the alkali and olivine basalts discussed in Chapter 4 are fundamentally different than the Hudspeth Mill Intrusion.

However, it must be noted that the presence of the subduction signature can be misleading. Previous authors have noted that in some locales (e.g. East African Rift, Antarctica) the formation of alkaline suites may be very complex (Paslick et al., 1995; Hole et al., 1993). Paslick et al. (1995) noted that in areas of lesser extension in Tanzania, asthenospheric melts are contaminated as they rise through the lithosphere. This problem has also been noted in the Basin and Range province (Hart and Carlson, 1987), where asthenospheric melts take on the trace-element patterns of the previously altered lithosphere. So caution must be used in relating the existence of subduction signatures to the source region and enrichment event timing.

Take for example the Antarctica alkali basalts (Hole, 1988). Major-element compositions immediately look different than the Hudmill basalts. They are much more evolved (Mg# ~ 45), more sodic (Na_2O/K_2O = 2.1-2.4), and have very little Cr (< 120 ppm). This nearly opposite of the Hudmill rocks, which are primitive (Mg# ~ 72), potassic (Na_2O/K_2O = 0.72-0.9), and rich in Cr (~ 800 ppm). Alkali basalts are also common in both the middle and late stages of the post-collision volcanism in western Anantolia, Turkey (Aldanmaz et al., 2000). However, the late stage alkali basalts and basanites have more in common with those found in Antarctica than the Hudmill rocks. They are also too differentiated and too sodic. While the middle stage of volcanism resulted in alkali basalts, they were again too evolved. They were the result of AFC processes acting on melts of subduction-altered lithosphere at it passed through metamorphic basement rocks. Of particular interest is that the metamorphic basement rock was similar to that thought to exist in the Mitchell area. Isotopic analyses were used to determine the AFC trends, data not available for the Hudmill rocks. However, the original magma or the Turkey alkali basalts, prior to AFC, may have been similar to the Hudmill magma. Their postulated origin within the metasomatized lithosphere is consistent with the likely source region for the Hudmill rocks.

The Hudspeth Mill Intrusion's petrogenesis is dominated by crystal fractionation (olivine and clinopyroxene), interspersed with recharge events. The alkaline nature and trace-element characteristics reflect partial melting of metasomatized lithospheric mantle, with residual amphibole. The intrusion bears a general resemblance to other mafic alkaline magmatism active across the western U.S. during the Eocene, but has some fundamental differences that set it apart. While the magma was hydrous, the volatile contents were low enough to crystallize anhydrous phases. This is contrary to many other alkaline lithospheric melts from the western U.S., where abundant volatiles resulted in the formation of lamprophyres instead. These rocks also bear little resemblance to alkali basalts mentioned in the previous chapter. They are more primitive and more potassic.

Hudspeth Mill and the Clarno Formation

The Hudspeth Mill Intrusion is clearly more alkaline, mostly more potassic, than the rest of the Clarno Formation. However, the similarity in trace-element patterns, particularly the strong enrichment in LILE compared to HFSE, to typical subduction zones suggests that the intrusion may be related to the Clarno lavas. The age of 45 million years suggests that it formed after the main pulse of activity. However, there is significant evidence, including new data (see Chapter 8), to suggest that traditional calc-alkaline activity was still occurring at this time.

Mass balance calculations (Stormer and Nicholls, 1978) were done using major-element data to explore the possibility of the Hudspeth Mill Intrusion being a parental magma to other Clarno Formation rocks, especially the more primitive Clarno basalts. Average compositions from olivine, clinopyroxene, and chromite microprobe analyses were used in the calculations. These phases were used since they are the only observed phases to have crystallized prior to the groundmass and to have possibly undergone fractionation. The average of Hudspeth Mill bulk compositions was used as a starting magma and two different Clarno basalts (PH-16 from Suayah and Rogers, 1991 and JN-156 from Rogers and Ragland, 1980) were selected as daughter products. The overall fit ($r^2 > 250$), along with negative amounts of crystals and high r^2 values for each oxide, indicate that it is not possible to simply fractionate these phases and create a primitive Clarno basalt.

Both phase equilibrium models and AFC models were used to simulate fractional crystallization liquid lines of decent under varying pressures, water contents, and assimilant amounts. Simple crystal fractionation was simulated at varying water contents (0.5-2.5%) and pressures (1,5,10,15 kbars) with the COMAGMAT model (Ariskin et al., 1993). AFC crystallization (r= 0-4) was simulated at low pressures and water content using the MIXFRAC program (Nielsen and DeLong, 1992). Average compositions for the intrusion, along with two tholeiitic basalts from the Clarno, PH-16 (Suayah and Rogers, 1991) and JN-156 (Rogers and Ragland, 1980), were

used as starting compositions for the simulations. For the AFC modeling, rhyolite PH-16 (Suayah and Rogers, 1991) was used as the assimilant.

Crystal fractionation simulations for the intrusion result in trends too low in MgO at a given silica value (Figure 5.12b). The closest trends suggest low pressure and high water content would be needed to create Clarno rocks from a Hudspeth Mill parental magma. Higher pressure fractionation further reduces the silica concentrations in the liquid, resulting in trends completely removed from the actual Clarno rocks. Fractionation of the Clarno basalts at low to medium pressures results in liquid compositions within the field of Clarno rocks.

While the fractionation trends for most of the other major elements are close to the Clarno rocks at lower pressures and higher water contents, K_2O presents the largest problem. The intrusion has about 2% more K_2O than the other most primitive basalts from the Clarno (Figure 5.12a). Crystal fractionation of common phases under all pressures and water contents only serves to increase the K_2O content with evolution of the magma. Therefore, the magma always contains too much potassium to have formed the Clarno rocks. In contrast, the primitive Clarno basalts actually have too low potassium. Their fractionation trends have lower K_2O than most of the Clarno rocks.

The conclusion that simple crystal fractionation cannot link the range of Clarno compositions is consistent with recent work on the formation. Both Rogers and Ragland (1980) and Suayah and Rogers (1991) argue against a common source that undergoes crystal fractionation to create the spectrum of Clarno compositions. The later paper argues that there is significant evidence within the Clarno for magma mixing. This evidence is both chemical (linear mixing trends) and textural (dissolution and resorbtion features). Therefore, in trying to relate the Hudspeth Mill Intrusion to the rest of the Clarno, AFC modeling provides a more realistic means of simulating the processes that generated the Clarno.

It needs mentioning that the model used, MIXFRAC, was developed for uses with MORB's and is designed for low pressure and anhydrous conditions. However, the trends will still provide a general idea of the descent lines for these magmas. By

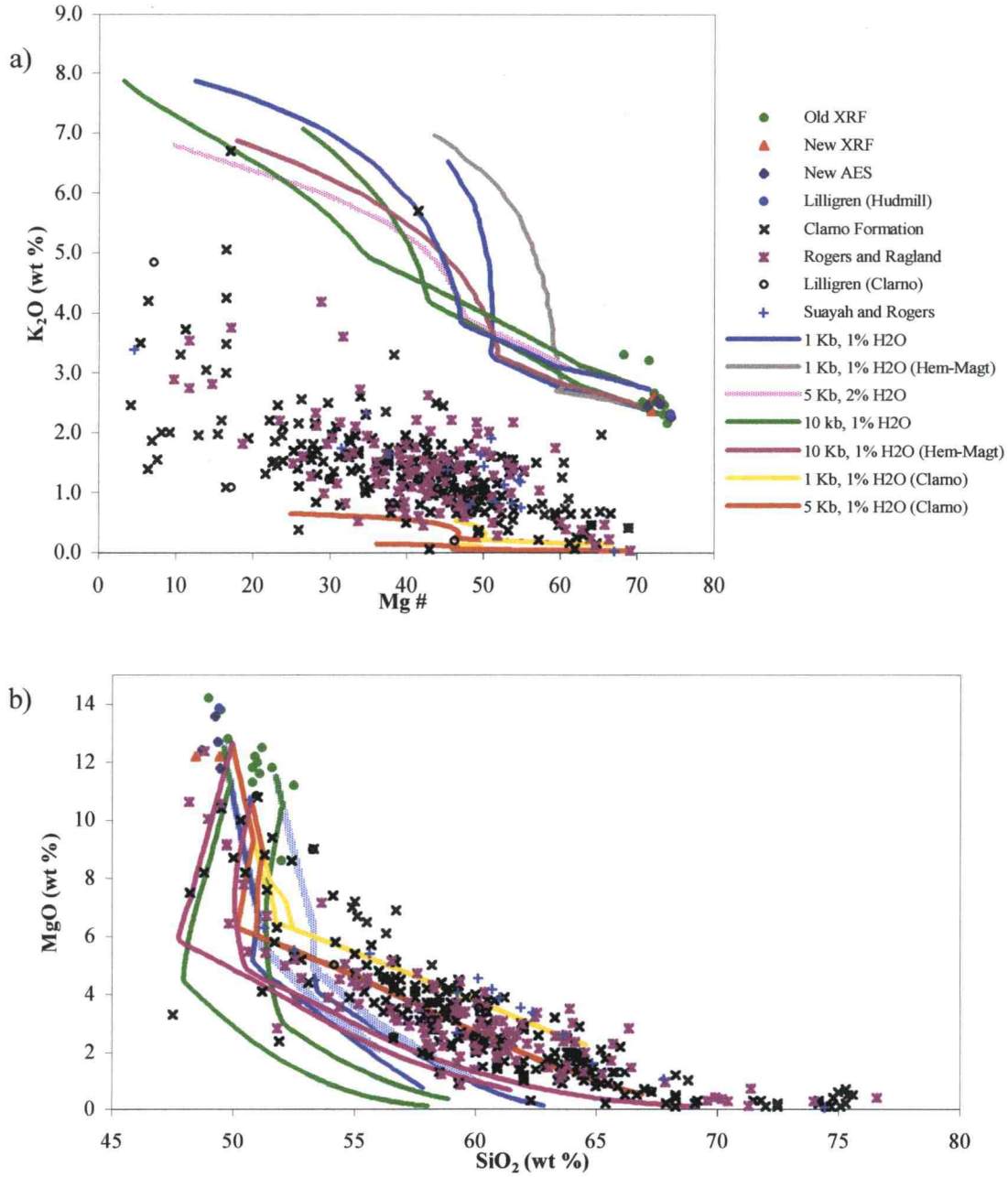

Figure 5.12: Crystal fractionation modeling of magma compositions using both a primitive Clarno basalt and the Hudmill samples as parents. a) K2O contents of the Hudmill magma are too high to fractionate into other Clarno rocks. b) Fractionation of the Hudmill parent reduces the Mg faster than the Si, resulting in liquid lines of descent along the bottom edge of the Clarno field of data.

comparing these results with the results from the previous modeling, where the effects of changing pressures and water content were already observed, a qualitative understanding of the AFC processes can be inferred at higher pressures and water contents.

The addition of small amounts of rhyolitic material to the melt as it evolves helps to increase the silica content of the magma (Figure 5.13a). At moderate mixing (r= 0.5-1), the liquid lines of descent for both the intrusion and the primitive Clarno basalts remain within the range of compositions defined by the actual Clarno rocks. It is only the extreme cases (r= 0 or r= 4) than seem to lie outside this field of data. This suggests that indeed a balance of mixing and fractionation could cover the spectrum of Clarno rocks. It also suggests that the endmembers of the processes, pure crystal fractionation or pure binary mixing, are too simple to have generated the Clarno rocks.

Once again, most major elements seem to agree with this conclusion. However, the problem of the high K_2O intrusion evolving into the much lower K_2O Clarno rocks is not solved using AFC either. These simulations used a rhyolite with a common potassium content of ~ 3.5%. The assimilation of this material only reinforced the trends of crystal fractionation toward higher K_2O content (Figure 5.13b). The trends from the intrusion still remain at higher potassium than that of Clarno rocks. AFC did help the Clarno basalt trends though. Assimilation of moderate amounts of rhyolite (r= ~ 0.5) by the basaltic magma as it evolves results in liquid lines of descent within the Clarno rocks.

Both phase equilibrium fractionation and AFC models were used to simulate the changing composition of several trace elements also. Sr concentrations are several hundred PPM's higher for the intrusion than for most of the sampled Clarno rocks (Figure 5.14). Fractionation trends result in enrichments in Sr in the liquid with crystallization. Only low pressure, lower water melts eventually decrease the Sr concentration of the magma as plagioclase begins to crystallize. Even under these conditions, the Sr concentrations of the magma under >50% crystallization is still greater than almost all Clarno rocks. Fractionation trends for the primitive Clarno basalts lie

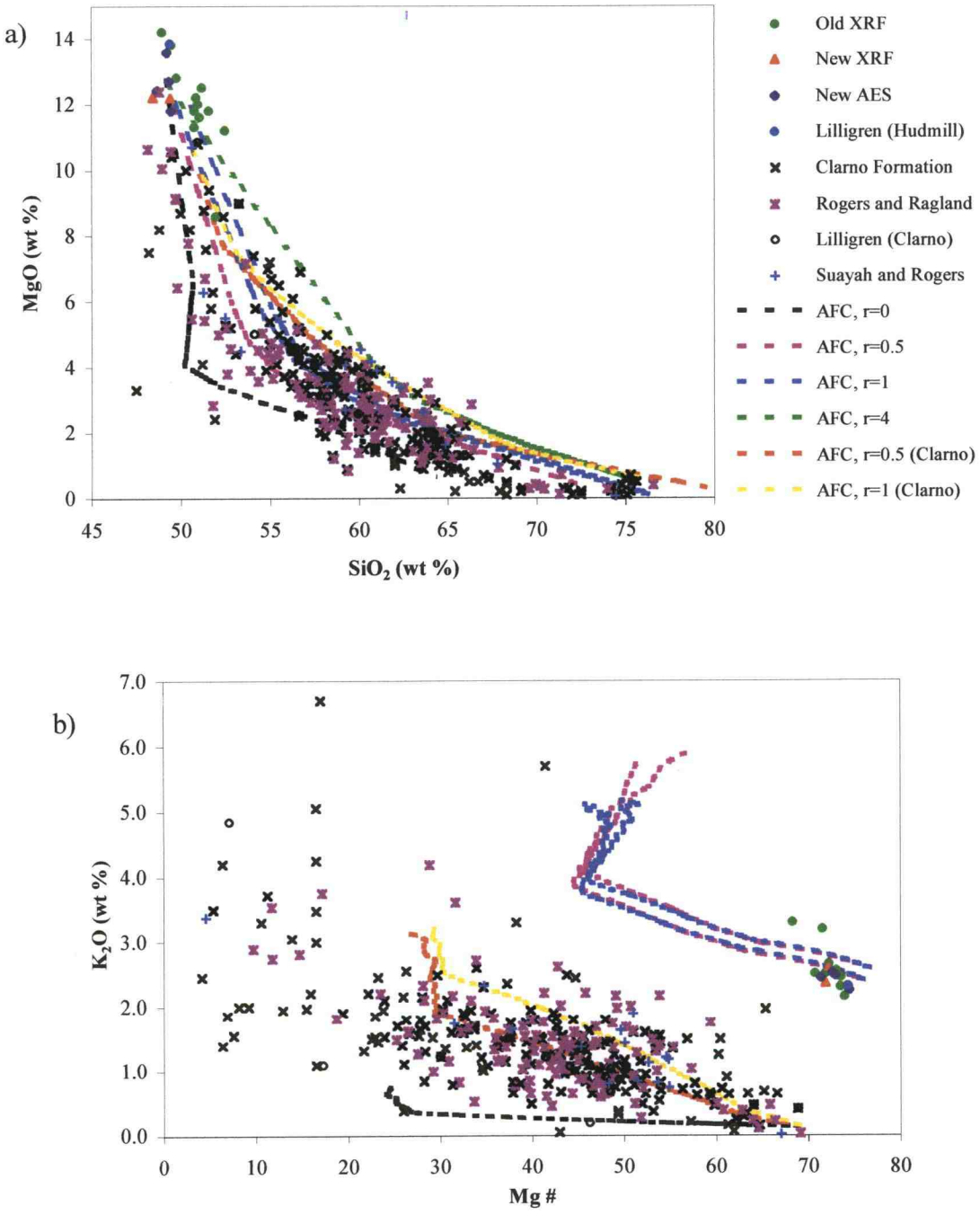

Figure 5.13: AFC simulation results for a Hudmill and primitive Clarno basalt parental composition. a) Si-Mg liquid lines of descent lie within the field of Clarno data for moderate amounts of assimilation for both parents. b) Even with assimilation, K_2O contents are too high to fractionate into other Clarno rocks for the Hudmill parent, but are reasonable for the primitive basalts.

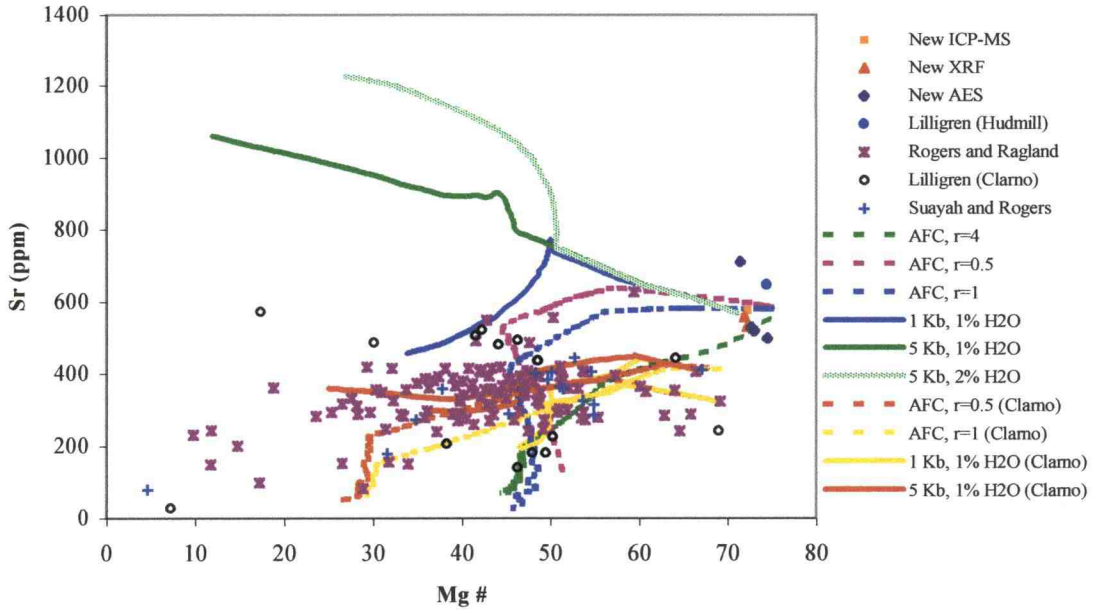

Figure 5.14: Fractional crystallization and AFC simulation results for Sr. Liquid lines of descent for both processes further reinforce that the Hudmill could not evolve into most Clarno rocks. Liquids derived from the primitive basalt follow within the field of Clarno Data.

within the observed Clarno concentrations, with the higher-pressure simulations covering a broader range of the actual rocks.

AFC simulations for the intrusion display trends that are initially too high in Sr, then drop off rapidly into the field of Clarno rocks with the onset of feldspar crystallization (Figure 5.14). These trends show no similarities to the overall trend of the actual rocks. AFC trends for the primitive Clarno basalts fall within the actual rocks and cover most of the range of compositions for mild to moderate assimilation rates (r= 0.5-1). Sr suggests that neither fractional crystallization nor AFC can adequately link the intrusion to the other Clarno rocks. However, the results of the modeling for the primitive basalts are consistent with the Clarno fractionating from the basalts with some assimilation of crystal material possible.

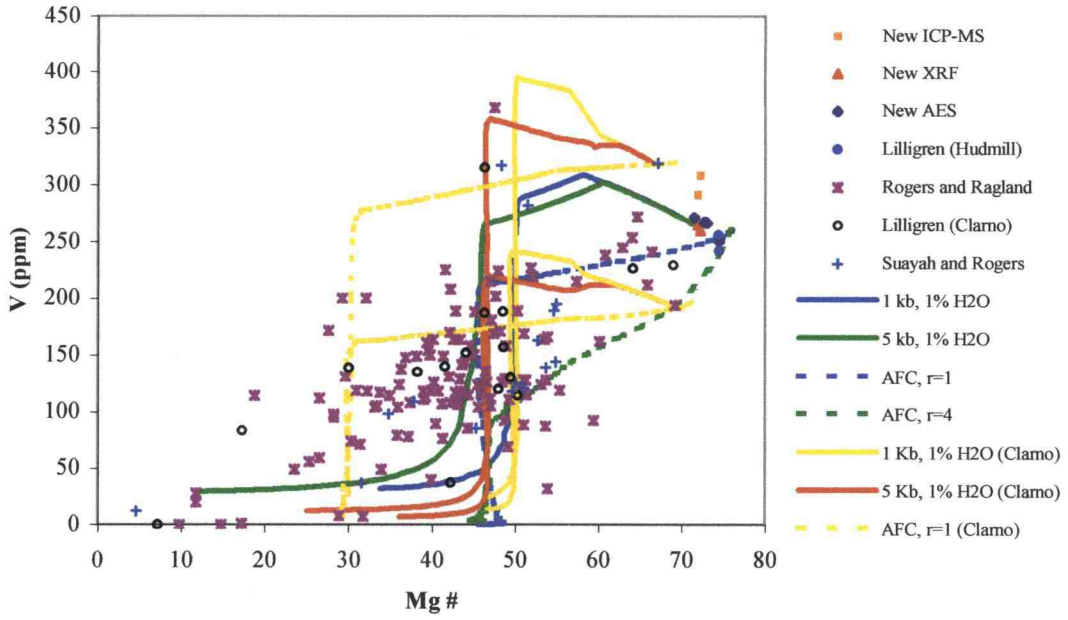

Figure 5.15: Results for fractional crystallization and AFC simulations for V. Magnetite crystallization causes a sharp drop in V content, while only a moderate decrease in V with decreasing Mg# is present in the Clarno rocks. The degree of scatter in the data argues against a single process such as fractionation or AFC.

The Clarno rocks show a general positive correlation between V and Mg# with the most differentiated silicics and the intrusion at opposite ends of the spectrum (Figure 5.15). Fractionation patterns show an initial increase in V, with a sharp drop with the onset of magnetite crystallization for all pressures, water contents, and starting compositions. The lack of a sharp break in the actual data suggests magnetite was not fractionated from the rocks. Even ignoring the effects of magnetite fractionation, the simulations show increasing V concentration, opposite of the actual trend of the data toward lower concentrations.

While AFC trends also display a sharp drop in V with the onset of magnetite crystallization, they indicate that V concentrations slowly decrease prior to this break if the amount of crystals fractionated is the same as the amount of assimilated material (Figure 5.15). Increasing the amount of assimilated material increases the slope

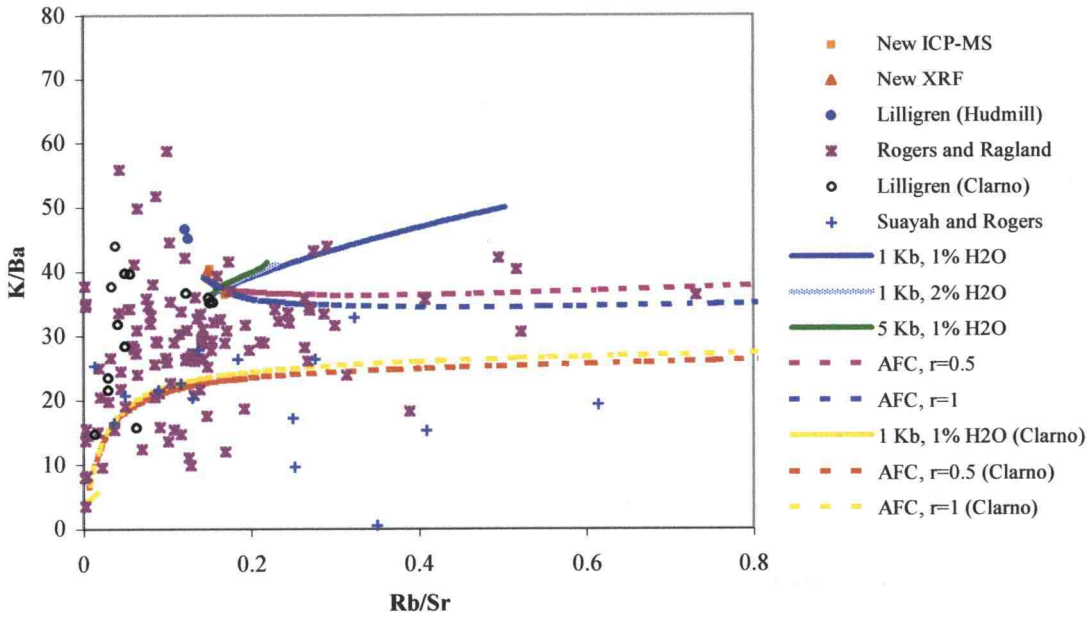

Figure 5.16: Fractionation modeling of trace-element ratios results in only minor changes in the magma. This is in contrast to a wide range of values observed in actual Clarno rocks. AFC modeling requires >30% crystallization and mixing to cover the range of Rb/Sr ratios, but fails to cover the large range in K/Ba.

of the liquid line of descent, resulting in trends similar to those observed in the real rocks. The breakdown of crystallization modeling for V, combined with the AFC trends suggests that the suites are better related by mixing than by fractionation.

Trace-element ratios can be more sensitive to processes like mixing, and so were used to test if mixing was more important than fractionation. Fractionation simulations were run up to 80% crystallization, and still often resulted in only minor changes in the trace-element ratios (Figure 5.16). The fractionation trends, even with assimilation included, indicate little change in K/Ba accompanied by increasing Rb/Sr values. Yet the actual Clarno rocks show only minor variations in Rb/Sr, while instead K/Ba varies over nearly two orders of magnitude. This large variation is much more consistent with primary mixing rather than fractionation. The Hudmill intrusion has higher Rb/Sr and K/Ba than much of the Clarno rocks. Neither fractionation nor

AFC can increase the K/Ba ratio to values seen in the intrusion using Clarno primitive basalts as a parent. Likewise, large degrees (> 30% at r= 1) of AFC are required for Rb/Sr values to approach intrusion values. Fractionation of over 30% would result in Mg#'s much lower than those observed in the Hudmill samples. On the basis of Rb/Sr and K/Ba ratios, a genetic relationship between the Clarno rocks and the Hudmill intrusion is unlikely.

The existence of coeval alkaline and calc-alkaline rocks within the Clarno Formation is significant in itself. Dickinson and Hatherton (1967) observed that in many subduction zones the K_2O content increased with distance from the trench. They inferred this to be related to the greater depth of the Benioff zone further from the trench. Therefore, they concluded that alkaline melts are usually formed behind the main axis of calc-alkaline volcanism or at a later time along the axis if the arc is migrating toward the trench. Later experimental work reaffirmed that deeper sources often result in more alkaline magmas (Meen, 1987). This idea lead previous worker to suggest that the Eocene magmatic activity across the western U.S. formed from either flat-slab subduction or a migration of the arc westward through the Eocene (Baker, 1987; Lipman, 1980; Dickenson, 1979). However, more recent work has shown that alkaline magmas were erupted coeval with calc-alkaline magmas in close proximity to one another (Dudas, 1991; O'Brien et al., 1988; Marvin et al., 1980). The alkaline lavas of the Hudspeth Mill intrusion, along with other alkaline suites such as Marshall Butte (see Chapter 4) and lamprophyric dikes from the Mitchell area (see Chapter 6), appear to have been emplaced during periods of active calc-alkaline activity. So as with many of the Eocene magmatic areas, the original suggestion of temporal and spatial variations in the alkalinity of magmatism is incorrect. Additionally, in the Andes were flat-slab subduction is known to occur, there is no magmatism associated with it. Since the distribution of these types of magmas was a fundamental piece of evidence for the flat-slab and migrating arc hypotheses, it seems that there is little strength left in them. However, while this holds great importance for the more eastern occurrence of magmatic activity, the most reasonable explanation for the Clarno Formation is still subduction.

In the previous chapter, Marshall and Corporate Butte were discussed. These suites are both more alkalic and more primitive than most of the Clarno rocks. Therefore, it would seem logical to attempt to establish a link between the Marshall/ Corporate suite and the Hudmill suite. As noted earlier in this chapter, many of these alkali basalts commonly found with basanites are quite different than the Hudmill rocks. So on the basis of those examples, an alkali basalt related to the Marshall/ Corporate Butte magma would be compositionally different than Hudmill. However, even more compelling evidence lies in the trace-element patterns for the suites. The trace-element patterns for the Hudspeth Mill Intrusion clearly display a typical subduction signature with HFSE depletions, while Marshall and Corporate Buttes lack this depletion. Since this depletion is thought to reflect the conditions in the source region rather than a later modification of the magma, it suggests two different sources. Marshall and Corporate Buttes are likely derived from an asthenospheric source, while the Hudspeth Mill Intrusion is more consistent with a lithospheric source. However, as noted above, caution must be taken to determine that the signature was not inherited through lithospheric contamination. The most accurate way to test this would be with isotopic analysis, but this data is not available for the Hudmill rocks. Nevertheless, a lithospheric source is the favored model for the Hudspeth Mill Intrusion. So while tempting, there is no sufficient evidence to link the two suites to each other at this time.

The Hudspeth Mill Intrusion represents a distinct magma with a petrogenesis different from other intrusions or lavas belonging to the Clarno Formation. The suite is distinct from the common calc-alkaline rocks of the Clarno by increased abundances of alkalis and trace elements. These enrichments make a genetic relationship between the two groups unlikely. Likewise, while there are other alkaline suites related to the Clarno (Marshall/Corporate Buttes, Lamprophyres), mineralogy and bulk-rock chemistry suggest different source regions and evolutionary paths. Since the intrusion likely postdated the major flux in calc-alkaline activity, it may suggest a shift in subduction parameters. However, without a more precise age determination, this will remain a mystery.

Chapter 6: Mitchell Area Lamprophyric Dikes

Setting

Black Butte and Spetch Rim Area Dikes

Black Butte, a large Clarno dacite intrusion, lies about 10 km due west of Mitchell. A series of small mica-rich lamprophyric dikes crop out in the areas surrounding Black Butte and Spetch Rim (Figure 6.1). These mafic dikes are distinguished from the other Clarno Formation basaltic dikes by the anomalous amounts of mica and apatite they contain. While the dikes intrude the Cretaceous mudstone and conglomerate that surrounds the butte, age determinations on the dikes indicate they are from the period of Clarno activity.

The best-preserved and unaltered dikes are on the northwest flank of the butte. The dikes lie on a ridge that radiates from the butte to the northwest, and range from highly crystalline basaltic rock to a breccia of sedimentary clasts in a matrix of igneous material. The crystalline dikes are porphyritic with large mica and pyroxene phenocrysts in a very fine-grained groundmass of igneous minerals. The breccia dikes contain mixed clasts of conglomeratic pebbles and mud rip-ups in an igneous matrix that contains abundant mica. All of the samples also appear to contain carbonate in differing amounts. Samples BB-1 and BB-2, EMT-68 were collected from two of these dikes on the northwest flank (Figure 6.1). Samples EMT-288, EMT-227, and EMT-102 were also collected from several other dikes located west of Black Butte.

South of Black Butte, there is a similar small dike on the northeast side of Spetch Rim. The dike consists of an igneous matrix rich in mica and containing abundant clasts of country rock. This dike appears to be moderately fresh, with less carbonate in it than many of the other dikes north of Black Butte. However, the dike is difficult to find, with only one small outcrop standing above the surrounding surface. Since the hill is mostly covered with colluvium, determination of the character of the surrounding rock was difficult. The scattered outcrops of conglomerate and large

KNOWN LOCATIONS OF MINETTE LAMPROPHYRES NEAR BLACK BUTTE AND SPETCH RIM

LAWSON MOUNTAIN QUADRANGLE, OREGON

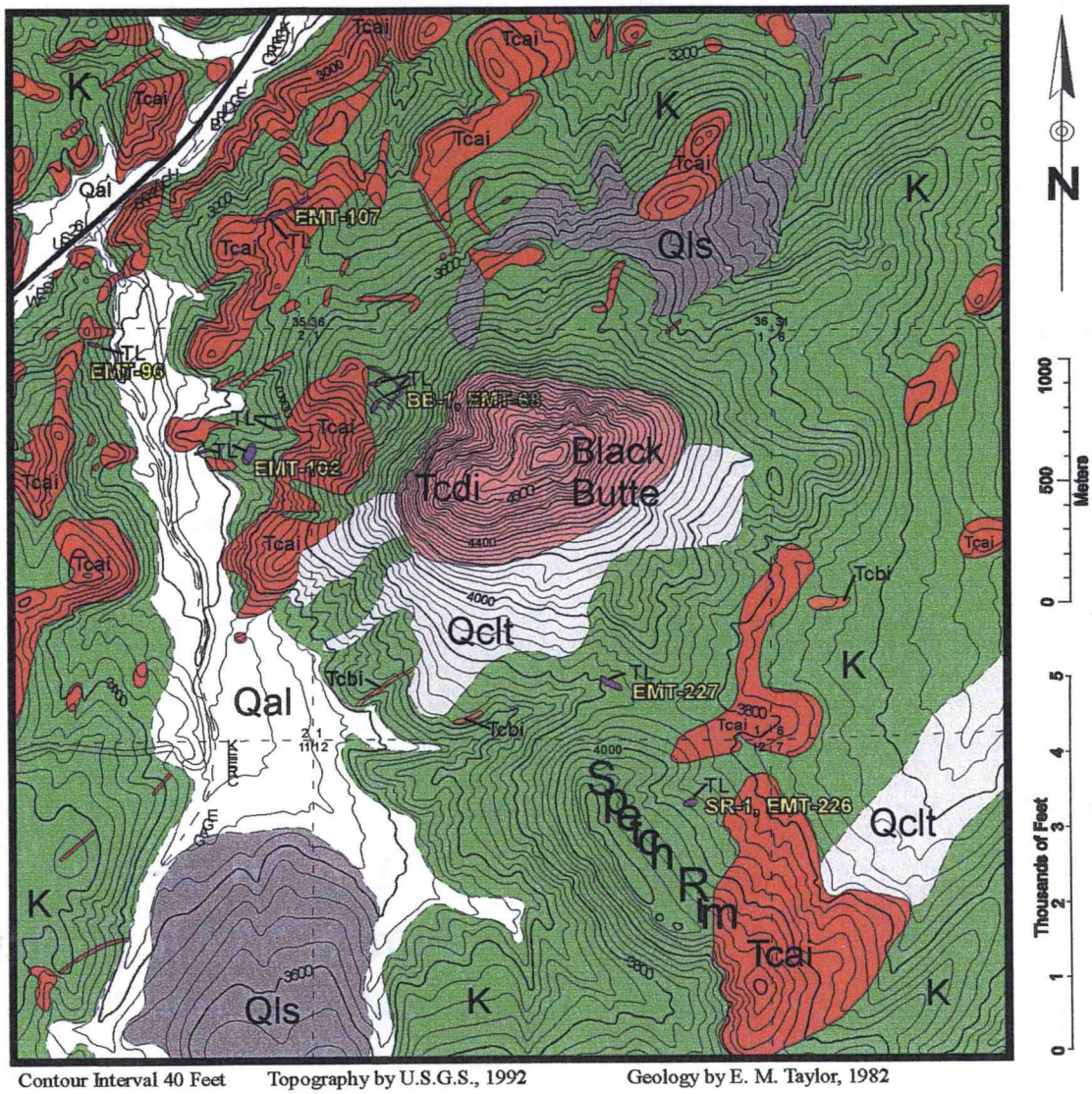

Contour Interval 40 Feet Topography by U.S.G.S., 1992 Geology by E. M. Taylor, 1982

TL Tertiary Minette Lamprophyre Intrusions (EMT-227- Sample Location)

Qal Quaternary Alluvium Qls Quaternary Landslide Deposits Qclt Quaternary Colluvium and Talus Deposits

Tcbi Tertiary Intrusive Basalt Tcai Tertiary Intrusive Andesite Tcdi Tertiary Intrusive Dacite

K Cretaceous Marine mudstones, pebbly mudstones, sandstones, and conglomerates of Hudspeth and Gable Creek Formations

Figure 6.1: Geologic map of the Black Butte and Spetch Rim area with dike sample locations.

amounts of conglomerate float in the colluvium suggest the dike is located in the conglomerates of Cretaceous sedimentary units. Due to the lack of good exposures of the dike, its exact size and orientation are difficult to determine, but a rough estimate places the strike at northeast-southwest with a near vertical dip.

The main outcrop (SR-1) looks more like a large boulder sitting on the side of the hill, but closer inspection reveals that the rock is still in situ. The outcrop has weathered purplish-brown with random fracturing. A sheen from the phlogopite is visible even in the weathered surface from several feet away, making the dike easily distinguishable. A fresh surface reveals that the groundmass is light brown-gray with a green-blue tint.

About 50 feet further downhill the dike crops out again (SR-2). Here it is level with the ground, and at first glance the area looks more like a conglomerate outcrop. Even though it is slightly lighter in color and contains much more of the conglomerate clasts, the mica suggests that this is actually a section of the dike. This lower outcrop is much wider than the more resistant outcrop further up the hill. It looks as if in this area the dike intruded not as a cohesive finger, but instead spread out and diffused into the country rock, incorporating much more of the conglomerate.

Mud Creek Dikes

Mud Creek, a main tributary of Gable Creek, cuts through many of the Cretaceous sedimentary units prior to joining Gable Creek. The Mud Creek area consists of alternating layers of Cretaceous mudstone and sandstone, that form the ravines, and conglomerates that form prominent questas here. In one small area just south of the Mitchell Fault, the creek has exposed several dikes similar to those around Black Butte and Spetch Rim. These dikes are basaltic, yet contain abundant phlogopite phenocrysts.

The northern dike (MC-1) strikes N27E across Mud Creek. Its dip is hard to determine, but is close to vertical. On the west side of the creek, it is located at the contact between the mudstone and a thick conglomerate bed. Here the dike is hard to

trace due to talus from the conglomerate. Yet the dike seems to follow the topographic lines closely, making it easy to pick-up again on the east side of the creek. Meanwhile, the contact between the mudstone and conglomerate trends slightly uphill, leaving the dike completely within the mudstone on the east side of the creek.

Figure 6.2: Photograph of the second dike at Mud Creek. The dike intrudes less resistant mudstone, forming a narrow spine and baking the mudstone where it is in contact with the

The outcrops of the dike show abundant blocky fracturing, with blocks ranging from a few inches to more than a foot across. A few outcrops were fractured even more, leaving only small pieces, less than an inch wide. Many of the outcrops show a greenish surficial weathering, with small cavities where phenocrysts have weathered away. A fresh face shows a medium gray groundmass with abundant (~ 10%) subhedral phenocrysts that appear to have been replaced by calcite. The samples also show abundant calcite veining and much less abundant (1-2%) euhedral phlogopite phenocrysts. One hand sample also has a single large (> 0.5 mm) apatite phenocryst in it.

The southern dike (MC-2) is also exposed on the east side of the creek, but further south than the first dike. This dike also appears to be completely within mudstone and is much smaller. The dike trends N18E with an approximate 70° dip to the east. The mudstone was much harder to orient, but is generally north-south with a 6 degree dip to the east. The contact between the dike and the mudstone is well exposed, and shows signs of baking for several inches into the mudstone. The dike itself appears continuous, forming a narrow spine pro-

truding anywhere from a foot to several feet above the ground (Figure 6.2). The dike is similar to the northern dike, with a couple of noticeable exceptions. First, there is much less calcite veining in this dike. Second, the light brown pyroxene phenocrysts are not weathered to calcite. Another sample from this dike (EMT-231), sampled by Dr. Ed Taylor, has also been reanalyzed.

Results

Petrology and Phase Chemistry

All of the Black Butte, Spetch Rim, and Mudcreek dikes have a common mineralogy, but can be separated by degree of alteration, phase abundance, and xenolith abundance. Due to the pervasive alteration of many of the samples (even with great care in sampling the freshest rocks), much of the original mineralogy must be inferred rather than directly observed. This is most significant in the modes, where the observed modes of some rocks reflect that the majority of minerals present are actually secondary alteration minerals like calcite, chlorite, and clays rather than primary phases. Attempts to reconstruct the original modes suggest that these rocks were dominantly pyroxene (~ 50%), mica (~ 15%), feldspar (~ 25%), and opaques (~ 10%). All of these dikes are porphyritic with between 10-20% phenocrysts of clinopyroxene and phlogopite. For the groundmass phases, some samples still retain some of their primary mineralogy (allowing the above estimation), while others contain only clay. So the above estimate is based on what could be reconstructed from the current mineralogy and the relict textures, and is certainly biased by differential alteration. Even these modal estimates are only possible on the fresher samples, leaving the true modal variability between dikes a mystery.

One of the dominant phenocrysts in all of the dikes is pyroxene. However, in some of the dikes, it has been completely replaced by calcite and clays. Pyroxene (augite in the unaltered samples) accounts for between 5-20% of the dike's original phenocryst mineralogy. The pyroxene phenocrysts are euhedral-subhedral and range

from just under a millimeter in the Spetch Rim dike to several millimeters in the Mudcreek dikes. Some samples show very few or no large phenocrystic pyroxene. However, all samples have microphenocrystic pyroxene that ranges from ~ 0.5 mm down to groundmass size.

Microprobe data was obtained for the pyroxenes from the less altered samples of the Mudcreek and Spetch Rims dikes. The pyroxene compositions display linear trends consistent with a fractionation-dominated petrogenesis for both dike groups (Figure 6.3). Due to the small amount of quality data from the Mudcreek samples, grouping of the crystal zones did not reveal clear trends (Figure 6.3a). However, data for the Spetch Rim dike indicate an increase in Ti coupled with a decrease in Mg from the core to the rim of the crystals (Figure 6.3b). This pattern of normal zonation is also present in the detailed crystal traverses (Figure 6.4), and is consistent with simple crystal fractionation. Traverses across the few remaining crystals in the Mudcreek dikes suggest they are normally zoned also (Figure 6. 4). While all of the traverses show additional zonation across the pyroxenes, the poorer quality of the crystals makes these small fluctuations suspect. One of the samples analyzed still has pyroxene remaining in the groundmass, but most samples have only relict crystal shapes that have been completely altered to calcite, clay, and opaques indicating that pyroxene was once abundant in the groundmass.

The other main phenocrystic phase in the dikes is phlogopite. While it is present in all of the dikes, its size and importance vary greatly between samples. In the Spetch Rim dike, the phlogopite phenocrysts are the largest phenocryst phase (~ 1.5 mm), while in one of the Mudcreek dikes (MC-1) it is relegated to the groundmass only. Nevertheless, it is abundant in all the dikes, usually as a phenocryst phase. The phlogopite phenocrysts are euhedral to subhedral, with some samples showing significant signs of chloritization. Phlogopite in the groundmass is generally subhedral and in a similar condition as the phenocrystic phlogopite. While it is spread throughout the groundmass as a primary phase, it is also often found rimming xenolithic inclusions as a reaction product.

Phlogopite compositional data suggest that the phenocrystic phlogopite is less

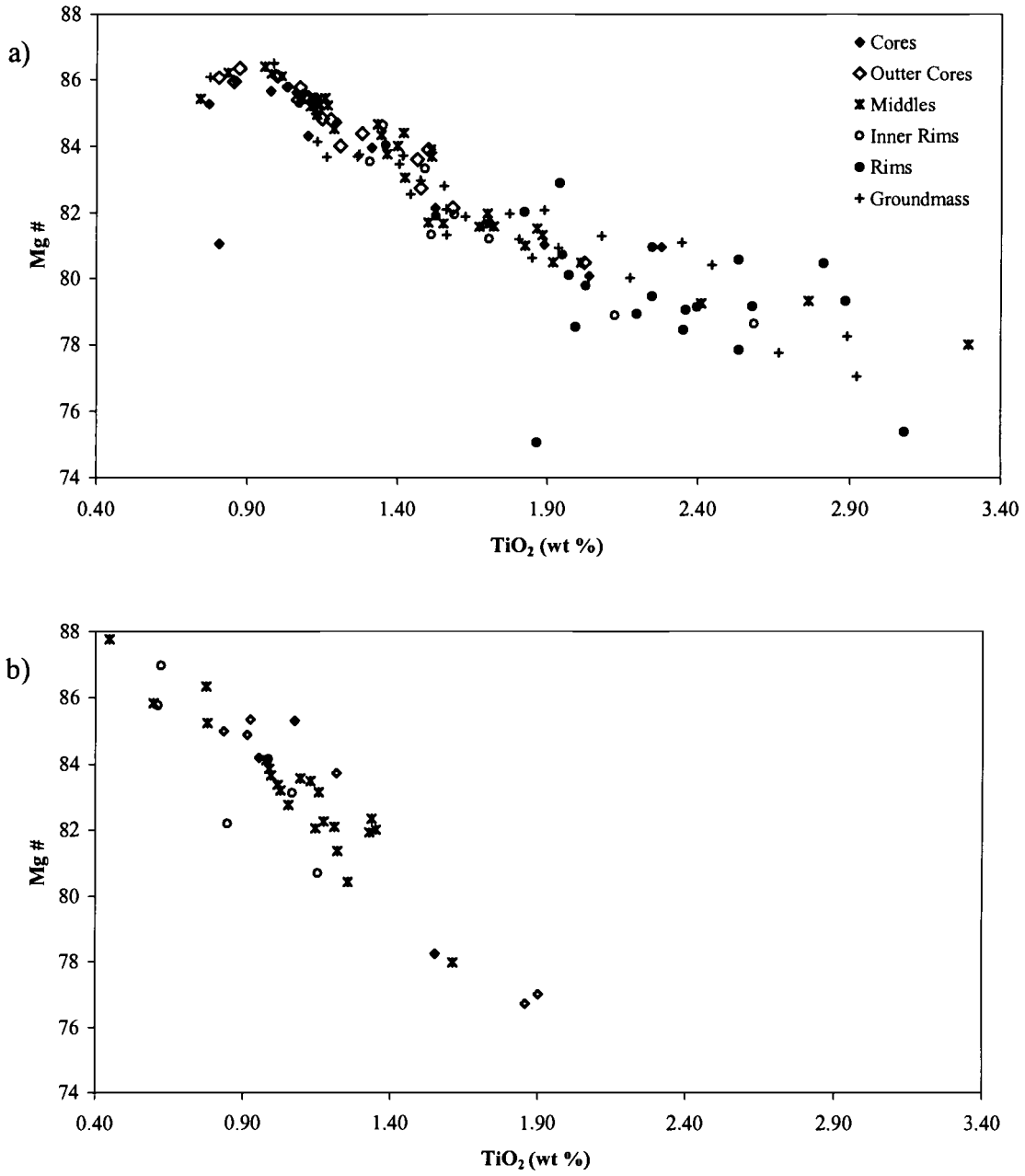

Figure 6.3: Major-element variations in the pyroxenes for a) Spetch Rim and b) Mudcreek. The Spetch Rim dike exhibits a linear trend with cores at higher Mg and lower Ti and rims at lower Mg and higher Ti. Due to weathering, few pyroxenes were unaltered in the Mudcreek samples, including no groundmass crystals. While the trend appears steeper, and suggests reverse zoning, the scarcity of data prohibits conclusive interpretation.

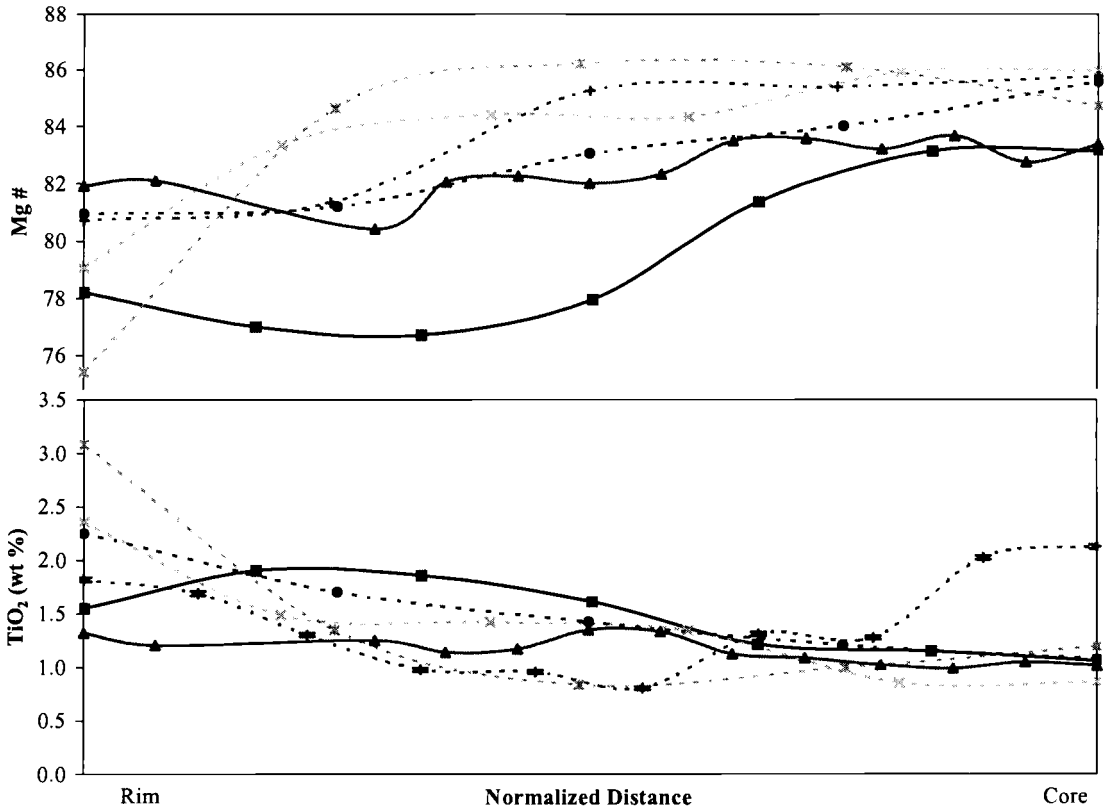

Figure 6.4: Microprobe traverses of select pyroxene phenocrysts. Solid– Mudcreek dike; Dashed– Spetch Rim dike. The Spetch Rim dike crystals are normally zoned, while the Mudcreek crystals appear weakly reverse zoned. The zoning in the Mudcreek sample is questionable due a limited selection of crystals and abundant alteration of the samples.

evolved, having higher MgO and K_2O, and lower TiO_2 than the groundmass crystals (Figure 6.5). Though microprobe traverses of phlogopite grains show an oscillatory pattern over much of the crystal, they are normally zoned at the rims, strongly in some cases (Figure 6.6). These trends are both consistent with crystal fractionation as a dominant processes in the petrogenesis of these magmas. Due to the fact that there are few phenocrysts of phlogopite in the Mudcreek dikes, only one good traverse was obtained. While it suggests lower K_2O concentrations than the Spetch Rim dike's

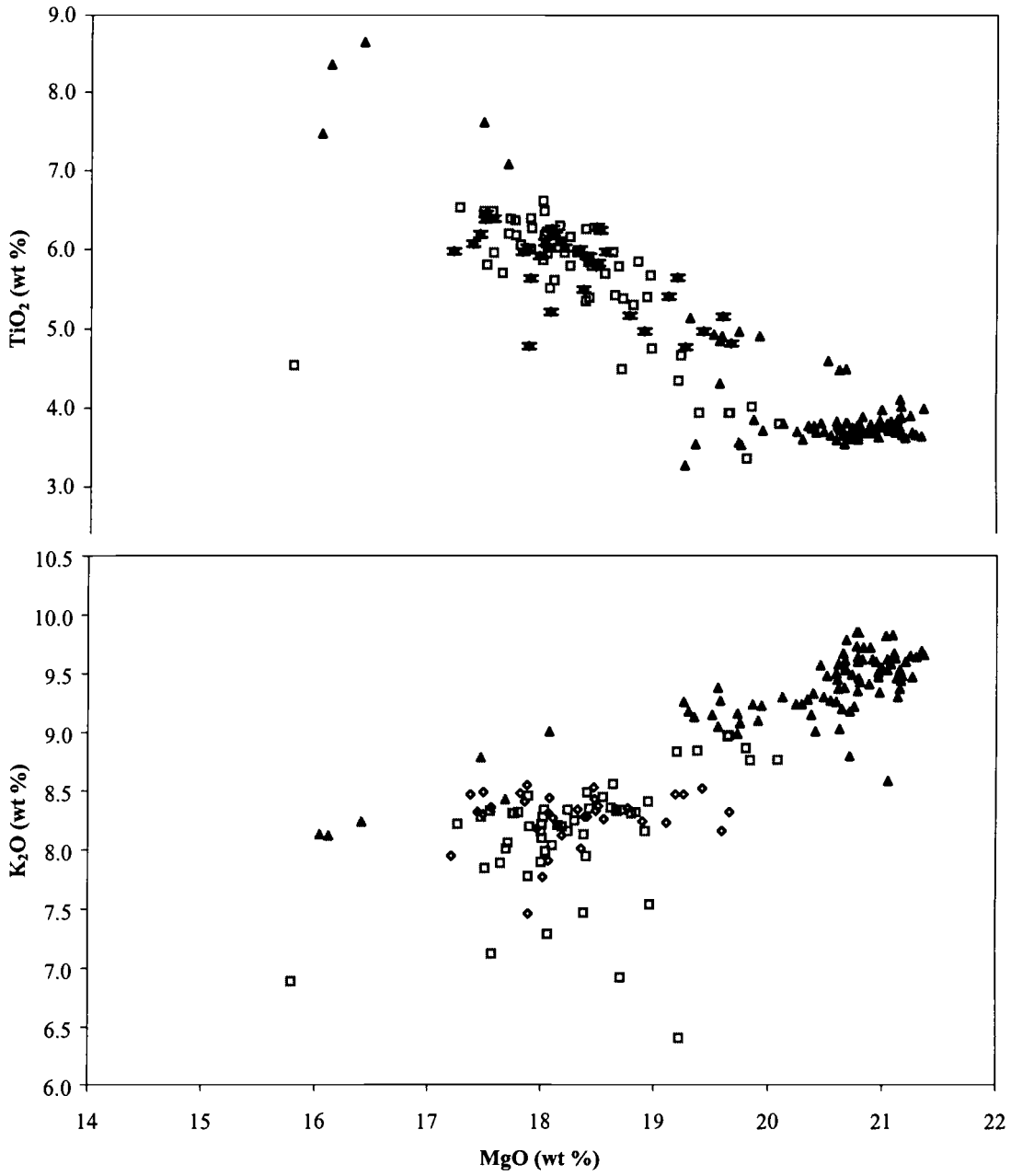

Figure 6.5: Phlogopite phenocrysts (filled) have higher K and Mg, and lower Ti than groundmass crystals (hollow). As with the pyroxene, the data exhibits a linear trend consistent with crystal fractionation.

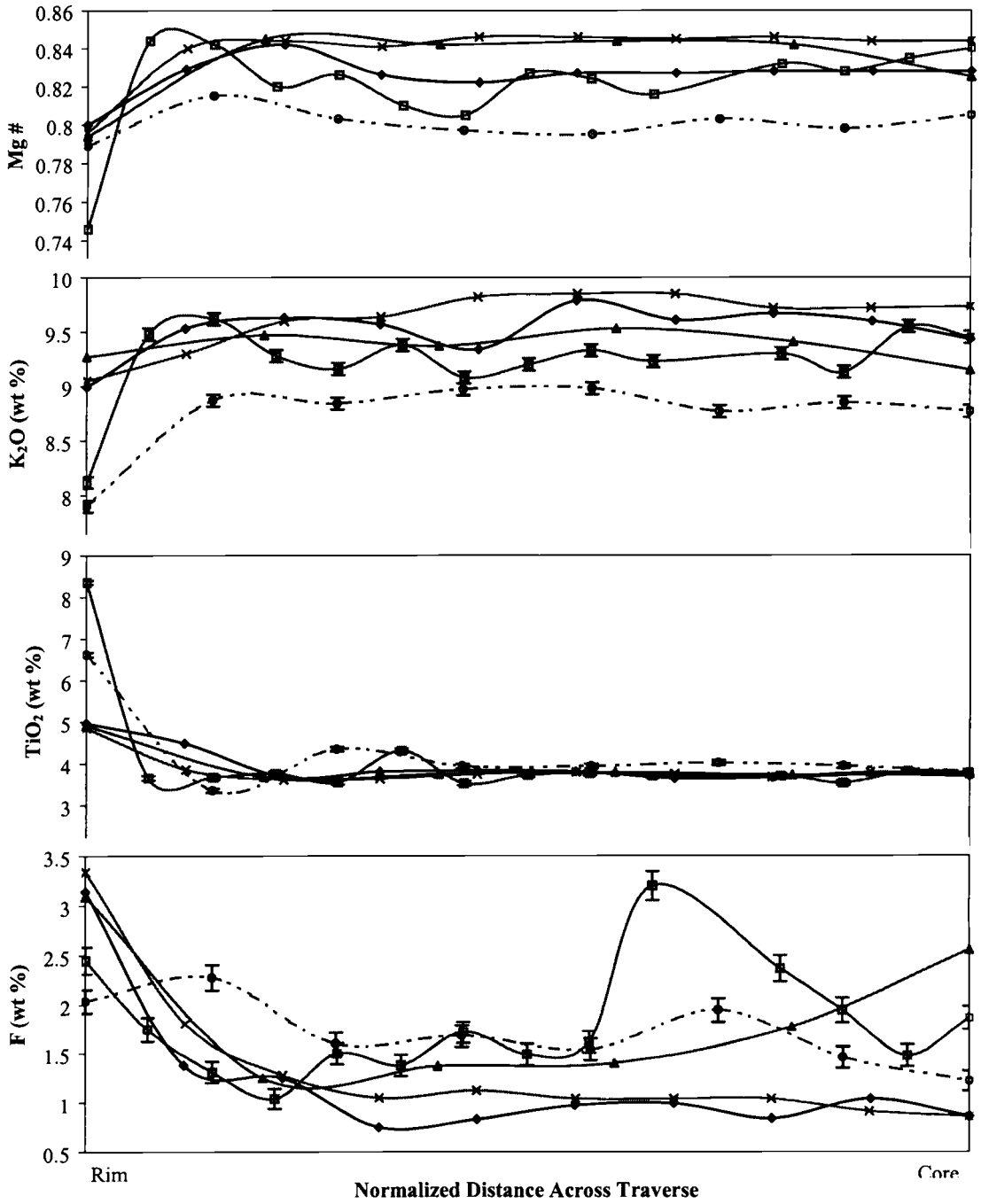

Figure 6.6: Microprobe traverses of select mica phenocrysts. Solid– Spetch Rim dike; Dashed– Mudcreek dike. The crystals are normally zoned, with some oscillatory zoning also present. The micas are also rich in titanium and fluorine.

phlogopite, this may be due to some minor chloritization of the crystal.

The most significant difference between the two groups of dikes is the groundmass feldspar. The Spetch Rim dike contains only alkali feldspar in the groundmass, while the Mudcreek dikes have both plagioclase and alkali feldspar in the groundmass (Figure 6.7). The alkali feldspar in the Spetch Rim dike ranges from $Ab_{59}Or_{35}An_7$ to $Ab_3Or_{96}An_1$. The Mudcreek dikes have a similar range in compositions, with a cluster of plagioclase (Labradorite to Oligoclase) from $An_{54}Ab_{42}Or_4$ to $An_{28}Ab_{60}Or_{11}$. They also contain a spread of anorthoclase and possibly sanidine with compositions ranging from $Ab_{60}Or_{22}An_{18}$ to $Ab_{51}Or_{48}An_2$.

Also abundant in the groundmass of the dikes is Fe-Ti oxide. In the Mudcreek samples, the oxides were ~20 microns in size, with some glomeropheres of crystals reaching 100 microns across. In the Spetch Rim dike, the oxides are generally less

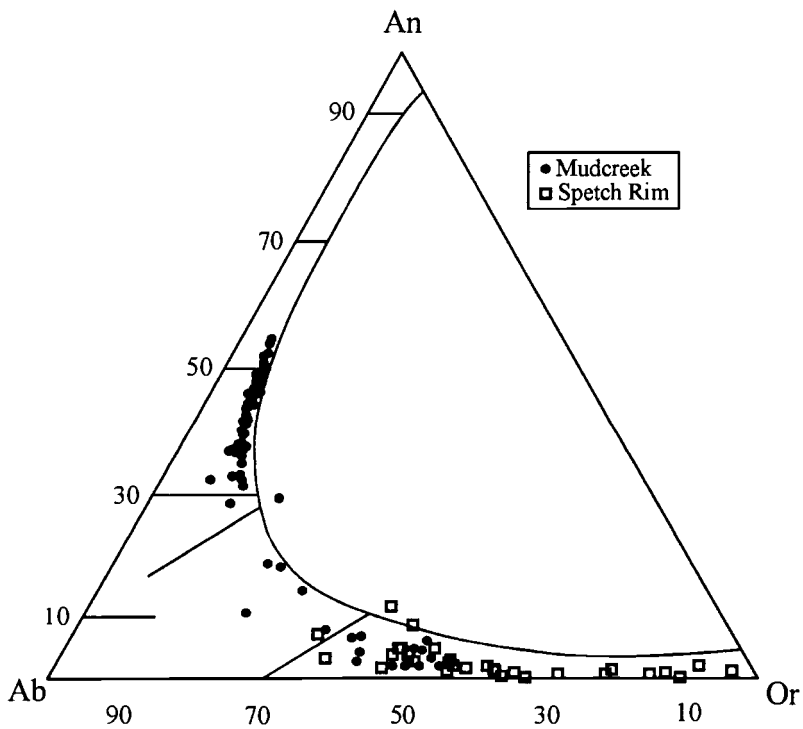

Figure 6.7: Ternary diagram for classification of groundmass feldspar. The two different classifications for the dikes is based on the fact that Spetch Rim has only alkali feldspar in the groundmass (minette), while Mudcreek has plagioclase (kersantite).

than 10 microns, with a few larger ones raching 20-25 microns. Oxides were also produced in the alteration of the pyroxene phenocrysts, both as oxidation rims of hematite, and as small opagues within the clay/calcite replacements of the pyroxene grains. The phlogopite phenocrysts contain only a few oxide inclusions, often near fractures making them suspect as primary inclusions. Fe-Ti oxides analyzed in the Mudcreek samples seem to be limited to titano-magnetites ($Cr < 0.1$ wt %) . Also abundant in the groundmass are rutile needles that were not analyzed due to their tiny size. Due to the smaller size and more weathered state of the oxides in the Spetch Rim dike, no good analyses were obtained from the sample.

The last identifiable primary groundmass phase is apatite. It is present in several of the dikes, including the Black Butte and Spetch Rim area dikes. While initially identified in the Mudcreek sample, none was found in several thin sections from the dike. Crystals in the Spetch Rim dike range up to 300 microns in size (making them microphenocrysts). While being distributed throughout the groundmass, many of the larger crystals are found next to the phlogopite. Even though it is a minor phase, in some samples it accounts for as much as 2.5% of the mode.

Due to the alteration of the samples, much of the groundmass is actually calcite, clays, and other alteration products. As already mentioned, these minerals replace many of the pyroxene and some of the phlogopite phenocrysts. They are also abundant in the groundmass, replacing both pyroxene crystals and other interstitial minerals. Calcite veins and irregular calcite masses rimmed by opaques are abundant in many of the samples as well. The alteration may also have completely removed a primary groundmass mineral, thereby masking its presence in the original rock. At the very least, this has occurred with the glass, making a determination of glass content virtually impossible for any of the dikes.

While not a result of the magmatic activity, the numerous xenoliths, or inclusion of country rock, reflect the mode of emplacement of the dikes. Most of the inclusions are pebbles or rip-ups from the Cretaceous sedimentary rocks through which the dikes intruded. These included quartz sandstone and mudstone clasts which have reacted with the liquid to produced complex halos. Several of the samples also have an-

other type of inclusion, one of igneous origin. These clasts are composed primarily of plagioclase, opaques, and a brownish-red alteration product. While the source of these clasts is not clear, the significant disequllibrium textures suggests they are indeed xenoliths. Two possibilities are that they are pebbles from the conglomeratic unit, or pieces from a lower magma chamber that had plated onto the side and were then incorporated into the lamprophyres as they passed through this chamber.

Bulk Geochemistry

Bulk-rock compositional data was obtained for the lamprophyres using ICP-AES. An initial set of data was thrown out due to calcite contamination. A second run was done after rinsing the picked chips in 2.5% HCl several times to remove the calcite. The lamprophyric dikes plot in the basanite, (alkali) basalt, trachy-basalt, and phonotephrite fields of Le Maitre et al. (1989). Two additional analyses plot in the foidite field, but this probably reflects incomplete removal of the calcite along with other alteration effects. Both the older XRF and the new AES data place most of the dikes above the alkaline dividing line of Gill (1981).

The dikes are slightly more potassic than sodic ($Na_2O/K_2O \sim 0.75$-0.90). The dikes range from Mg# 48-58, suggesting that they have undergone some differentiation; although the pervasive alteration of the mafic phases may also have contributed to these lower Mg numbers. The dikes all have several weight percent TiO_2 (2.2-4.8%) and P_2O_5 (1.0-2.8%), consistent with the abundant oxides and apatite observed in thin section. CIPW norms for the samples indicate the Mudcreek dikes are slightly silica undersaturated while most of the Black Butte area dikes are slightly silica oversaturated (Appendix 4). While both groups are apatite and illmenite normative, the Black Butte area dikes are significantly higher (2-4%) than the Mudcreek dikes.

While these dikes have compositions similar to absarokites and other mafic alkaline rocks, several characteristics distinguish them as lamprophyres. Rock (1977) identified several characteristics used to distinguish a lamprophyre from other rocks: 1) they are commonly the latest stage of igneous activity in a region; 2) they occur

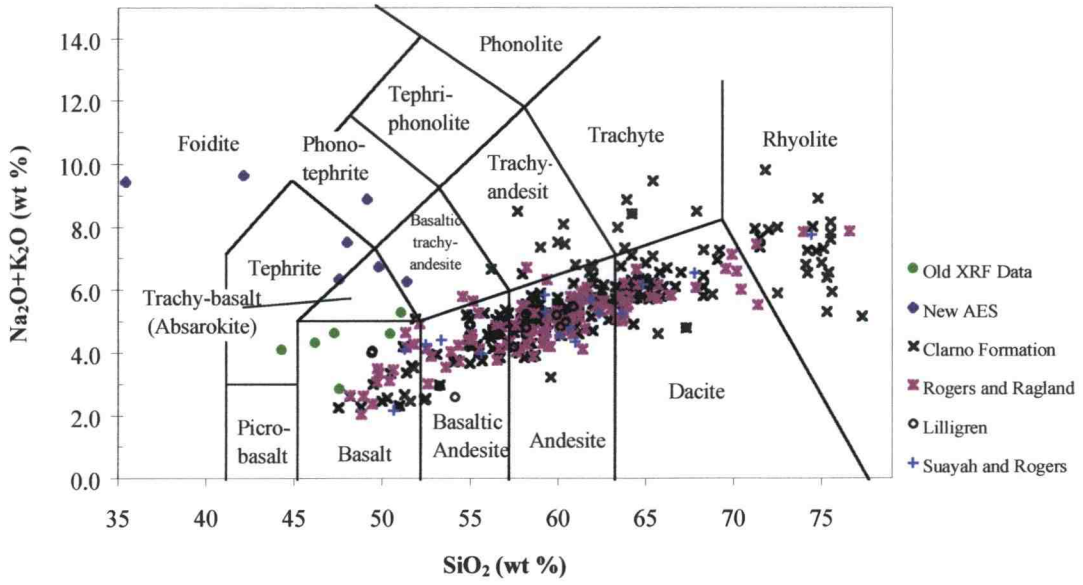

Figure 6.8: Classification of the lamprophyric dikes and other Clarno Formation rocks according to total alkali content. (Le Maitre et al., 1989)

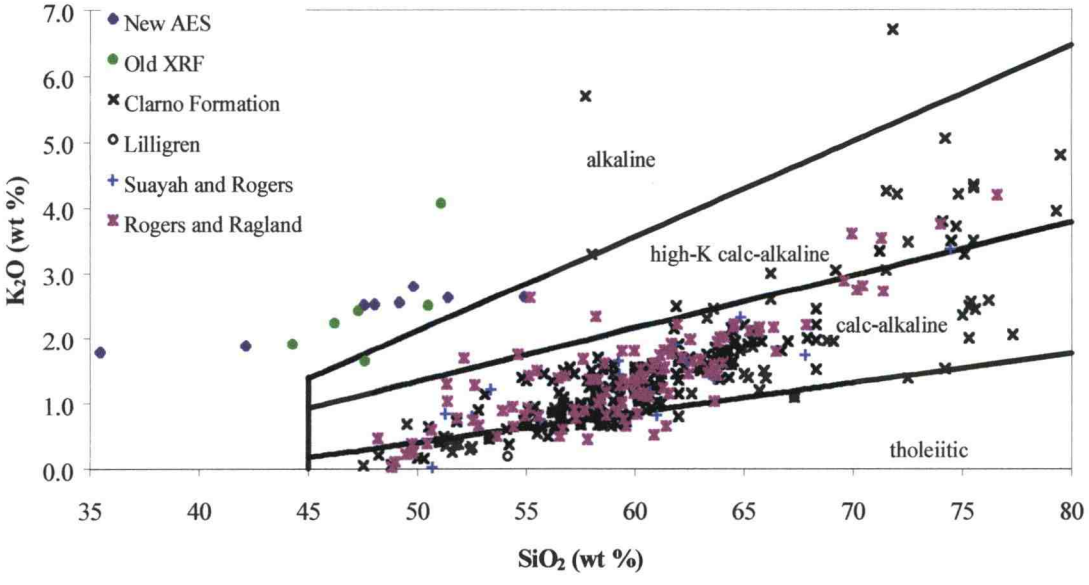

Figure 6.9: The lamprophyres are more alkalic than the rest of the Clarno Formation. They fall into the alkaline category (one exception in which it is high-K calc-alkaline), while the rest of the Clarno is tholeiitic to calc-alkaline.

primarily as dikes, lesser in plugs, and infrequently as sills and flows; 3) they frequently display evidence of explosive emplacement; 4) they are porphyritic and show a hydrous mineralogy with no felsic phenocrysts and no olivine in the groundmass; 5) they typically show a high degree of alteration and contain abundant inclusions; and 6) they contain a high alkali content for their silica content. In the case of the Black Butte and Mudcreek area dikes, they fit these characteristics quite well. Field examination shows they are small dikes with a hydrous phenocryst (phlogopite) that contain abundant inclusions of country rock and display significant alteration. The abundance of country rock fragments, including large mud rip-ups, suggests that these dikes were also emplaced violently. Petrographic work reinforces the abundance of a hydrous phenocrystic phase, the lack of olivine in the groundmass, the severe alteration, and the abundant inclusions. The only characteristic not consistent is that lamprophyres are commonly late-stage products. The geochronology (see below) indicates these dikes were emplaced during the height of regular calc-alkaline volcanism.

Rock (1977) divided lamprophyres into four main subgroups on the basis of mineralogy and bulk compositions. The Black Butte and Mud Creek area dikes are considered Shoshonitic lamprophyres since they are mildly potassic ($Na_2O<K_2O$). The type of the lamprophyre is further subdivided on the basis of phenocryst and groundmass mineralogy. While both have mica phenocrysts, the Mudcreek dikes have a plagioclase groundmass making them kersantites, and the Black Butte area dikes have an alkali feldspar groundmass and are therefore minettes.

Due to both the abundance of inclusions and the significant alteration of the samples, none of the dikes were analyzed using ICP-MS for trace elements. Some trace-element analyses were obtained during the ICP-AES runs.

Geochronology

Due to the abundance of phlogopite in the samples, it was separated out and dated using $^{40}Ar/^{39}Ar$ step-heating to determine the age of the dikes. Dates were obtained

for the southern Mudcreek dike (MC-2), one of the Black Butte area dikes (BB-1), and the Spetch Rim dike (SR-1). While argon recoil was not a problem as in several of the previously discussed suites (Marshall/Corporate Buttes, Hudspeth Mill), there was some scatter due to minor chloritization of the micas. Chloritization removes K from the micas and can alter the natural parent-daughter ratios resulting is erroneous dates. Nevertheless, plateaus were achieved on two of the three samples. The last sample (MC-2) did not plateau due to a smaller sample size resulting in gas fractions closer to background. A high-quality isocron age was calculated for this sample, however.

The Black Butte area sample and the Spetch Rim area sample yielded plateau ages of 48.97 ± 0.14 Ma and 48.65 ± 0.17 Ma respectively. The Mudcreek dike yielded an isocron age of 47.8 ± 0.24 Ma, slightly younger than the others. These ages clearly place them coeval with the Clarno Formation during its most active period of calc-alkaline activity around 49 Ma.

Discussion

Lamprophyre Petrogenesis

On the basis of mineralogy, geochemistry, and geochronology two different sets of dikes can be distinguished. The difference is classification between the two groups; Black Butte area dikes are minettes while the Mudcreek dikes are kersanitite, due to the presence of alkali feldspar and plagioclase in the groundmass, respectively. However, this classification is based on the hydrous phenocrysts and slight differences in feldspar mineralogy. Geochemically these dikes are potassic trachy-basalts similar to absarokites. Volatiles aside, these dikes have the same importance to a subduction system as other, more common, alkaline bodies. Likewise, they likely have a similar petrogenesis as other alkalkine bodies, but with more volatiles.

Mass balance modeling (XLFRAC; Stormer and Nichols, 1978) was used to test fractional crystallization relationships between the samples. For all cases, pyroxene +

phlogopite + apatite were used as the fractionating phases due to their phenocrystic abundance in the rocks. Phase compositions used in the modeling were average values calculated from microprobe data. Since no apatite phenocrysts were analyzed, an average value was used from Deer et al. (1992).

For the Mudcreek samples, using the EMT-231 sample as a parent, creating either of the MC samples (MC-1 and MC-2) results in a high (>15) r^2 value, suggesting they are not related. This is particularly disturbing for the MC-2 sample, which was from the same dike as EMT-231. This discrepancy may be due to incomplete removal of secondary minerals (carbonates) or differential weathering between the samples. The overall phase proportions calculated are reasonable for the rocks though. The two MC samples correlate well (r^2= 1.6) by comparison. The general proportions and small amount of mica present (as phenocrysts) also correlates with actual petrographic observations. While not conclusive, it appears that the two Mudcreek dikes may be related through simple crystal fractionation.

For the Black Butte and Spetch Rim area dikes, simulation results were mixed. What appears to be the most primitive sample, EMT-288, may actually be in error due to incomplete carbonate removal. If this is not the case, r^2 values in the high 80's suggest it is not related to the other dikes by fractionation of these phases. Other regressions, not as precise as the Mudcreek regression, displayed moderate r^2 values (6-10) that indicate a possible relationship between some of the samples from this suite. However, while the phase data is of excellent quality, the error in the bulk-rock analyses may account for some of the high r^2 values. As previously mentioned, all of the samples show signs of weathering, with some pervasively altered. Both alteration and incomplete removal of secondary phases can result in bulk-rock compositional error. Additionally, since TiO_2 and Al_2O_3 show high r values (1-4) in many of the samples, it is possible another phase (oxide?) may have been involved in fractionation. Still, based on the results generated, it seems likely that these various dikes are not related by just fractionation. Yet the similarities suggest a common shared history; even if the dikes resulted from separate parental magmas they must have undergone the same processes.

Due to the lack of trace-element data, the petrogenesis of these dikes remains unclear. However, lamprophyric dikes are quite common both in the western United States, and in subduction zones throughout the world (Fitton and Upton, 1985; O'Brien et al., 1991; Tingey et al., 1991; Carmichael et al., 1996; Davis et al., 1996; Dudás and Harlan, 1999; Wannamaker et al., 2000). Since the Black Butte and Mud Creek area dikes are so similar to those throughout the literature, speculation can be made as to the origin of these dikes based on other occurrences.

McKenzie (1989) proposed that remelting of small ultra-potassic bodies of magma within the lithosphere generates small alkaline bodies like lamprophyres. These bodies are created by small melts of convecting mantle that rise into the overlying lithosphere and solidify. The bodies then remain in place until the region is exposed to an increase in temperature or a decrease in pressure sufficient to cause melting of the ultra-potassic bodies and the surrounding metasomites. This means that these ultra-potassic bodies can remain in place for long periods of time before they are remelted and migrate toward the surface.

Thompson et al. (1989) compiled a series of references from different localities and tectonic settings in which such small alkaline bodies are common. While the tectonic regimes vary from rifting to subduction, all of the examples contain some degree of extension. This extension allows for both decompression melting and, in many cases, asthenospheric heating of the thinned lithosphere to occur. It also results in structural pathways that allow for rapid migration of these magmas with little crustal contamination.

A mixture of coeval calc-alkaline and alkaline rocks in a subduction arc is much more common that once thought. Examples from nearly all of the continents and throughout geologic history can be found. Some examples are the Sunda-Banda arc in Indonesia, southeastern Spain (Miocene), the Puerto Rican arc (Cretaceous), northern Turkey (Cretaceous), the Aegean arc (Miocene), the Mariana arc, the Japan arc, and the western United States (Eocene) (Lange and Carmichael, 1991). While a range of hypotheses has been given for the mixture of the two rock types, a common theme

in many of these locations is the existence of both convergence and extension within the arc.

An area of current subduction of particular interest is western Mexico, where two contrasting tectonic regimes are juxtaposed. The propagation of the East-Pacific rise spreading system to the north has resulted in its collision with an established subduction zone along the western coast of Mexico. This has resulted in both subduction related volcanic activity and rifting related extension through much of the area. In the Jalisco block, the Mexican volcanic belt (subduction arc) and the Tepic-Zacoalca rift zones intersect. While the area has a number of active large andesitic stratocones, it is also dotted by a series of smaller cinder cones that erupt ocean island type basaltic lavas due to the rifting (Carmichael et al., 1996). Mixed in with the subduction and rifting products is a variety of distinctive alkaline lavas like minettes. Due to interaction of the two different tectonic regimes, the lavas of western Mexico, including the alkaline suites, have been extensively studied.

Within the Jalisco block of western Mexico, a number of small potassic and hydrous eruptive centers occur about 70 km inland of the Mid-American Trench (Carmichael et al., 1996). In addition to the rift-related basalts, two main groups of subduction-related lavas occur throughout the area. These are the alkaline group, which includes absarokites and minettes, and the calc-alkaline group of andesites and basaltic andesites. There seems to be a continuum between the two series, with volatile content varying the most, suggesting a common genetic sequence. Yet no combination of fractionation and assimilation can reproduce the entire spectrum of rocks from a single parental source. Instead the variety in the observed rocks reflects the heterogeneity of the source region within the mantle wedge. Small-degree melts from both the typical mantle lherzolite and hydrous veins that contain phlogopite, amphibole, and apatite can be mixed in differing amounts to produce the wide range of rocks observed in the area. The minettes reflect the melting product of these veins at depth; with little mixing of less hydrous basaltic melts. Likewise, the calc-alkaline rocks contain very little of the vein melt component.

While melting of these mantle veins may be a common occurrence in subduction zones, a unique set of circumstances is needed for such mantle melts to reach the surface with little mixing or modification. In Mexico, the set of conditions responsible for this is hinted at by the restriction of these alkaline products to the extensional grabens of the forearc. This indicates that tectonically induced pathways play an important role in allowing such small volume magmas to move so high into the crust (or to the surface) with little modification. It also indicates that tectonics may be the trigger for the melting events, rather than the fluid fluxing typical of the main subduction arc. Lange and Carmichael (1991) further strengthen this point by noting that similar minettes and alkaline rocks can occur after the cessation of subduction, with no fluid fluxing present. Yet the magmas still contain strong subduction signatures in their trace-element patterns, suggesting that the veins can retain their subduction signature long after subduction has ceased. Melting can then be caused by a separate heating event, resulting in the alkaline magmatism observed at or near the surface with a subduction signature.

Alkalic suites, including lamprophyres, are common throughout the other Eocene age magmatic areas of the western United States. While previous workers have concentrated on the most abundant rocks throughout the Eocene areas, many of the newer studies have noted that coeval lamprophyres are also found in many of these areas (Dudas, 1991; O'Brien et al., 1991; Norman and Mertzman, 1991; MacDonald et al., 1992; O'Brien et al., 1995; Dudas and Harlan, 1999). O'Brien et al. (1991) concluded that in the Highwood Mountains, a parental olivine minette magma that underwent different modification processes (crystal fractionation, mixing, degassing, etc.) can account for the variety of dikes in the area. MacDonald et al. (1992) suggest a similar model of a parental minette magma that underwent fractional crystallization and some assimilation of crustal material to create the minettes and latites of the Bearpaw Mountains of Montana. These models are quite similar to those models proposed for Mexico. However, they suggest that normal fluxing of the mantle wedge resulted in the asthenospheric melting (instead of decompression melting) that mixed with anciently metasomatized lithosphere to form the lamprophyric melt.

The late Eocene Two Buttes intrusive complex in southeastern Colorado has been suggested to represent the late stages of the subduction-related Eocene magmatic belt previously mentioned (Davis et al., 1996). Two Buttes, and a number of other small intrusions that run parallel to the paleotrench, lie along the western edge of the cratonic lithosphere and the eastern edge of the area affected by the Laramide orogeny. These intrusions are all alkaline, ranging from trachybasalts to trachyandesites, but due to the abundance of hydrous phenocrysts they are instead classified as minettes. While the Two Buttes area dikes are ~ 36 Ma, the other intrusions become progressively older (up to 54 Ma) to the north. As with much of the magmatism in the western U.S. during the Eocene, it was originally attributed directly to subduction. This was further reinforced by the presence of a subduction signature (HFSE depletions) in the trace elements. However, isotopic evidence indicates the enrichment event was Proterozoic rather than Cenozoic. Instead of subduction related activity, upwelling asthenosphere heated previously metasomatized lithosphere and resulted in alkaline magmatism. The cause of the upwelling asthenosphere is not clear, but may have been due to slab-keel interactions or slab roll back.

Lamprophyres are not just confined to the early Cenozoic. While subduction influences clearly disappeared over most of the western United States during the Oligocene and Miocene, lamprophyres remained common magmatic products throughout the region. The Wasatch Plateau of central Utah is one of several plateaus that make up the stable Colorado Plateau. While crustal thickness measurements suggest that the stable Colorado Plateau has crust 1.5-2x thicker than the neighboring Basin and Range Province, magmatic activity on the plateau suggests that the region has also experienced some extension (Tingey et al., 1991). A series of alkaline dike swarms ranging from less hydrous melanephelinites to extremely hydrous minettes dot the Wasatch Plateau. These rocks range from 24 Ma for some of the melanephelinites to 7-8 Ma for the many of the minettes. Tingey et al. favor a two-stage model for the alkaline magmatism. It was triggered by the shift in subduction activity to the west in the Oligocene, which resulted in upwelling of hot asthenosphere as the plate rolled back. The early melanephelinites are a result of decompression-melting of this rising

asthenosphere. The later minettes are mixtures of these asthenospheric melts with small-degree melts of subduction-enriched lithosphere that was heated by the upwelled asthenosphere. The range in compositions between the two endmembers is due to the different amounts of interaction between the two melts. Isotopic signatures for the minettes suggest that the metasomatizing event for the lithosphere was related to the original crustal building event for the plateau back in the Proterozoic, ruling out a direct subduction relationship. However, these magmas can still be subduction related in the broadest sense, since slab rollback caused the asthenospheric upwelling. But the generated magmas had no chemical interaction with subduction fluids or melts. In this case the magmatism was triggered by other tectonic conditions (upwelling and extension) that favored melting. Generation of the small-volume alkaline melts was dependant on the existence of ultra-potassic veins in the lithosphere prior to the melting event, and pathways for the melts to reach the upper crust without significant modification.

However, alkaline and lamprophyric dikes are not just limited to the Wasatch portion of the Colorado Plateau; much of the plateau is sparsely covered by such bodies. An early Miocene lamproite dike system was recently discovered in southeastern Utah (Wannamaker et al., 2000). This is the first lamproite dike found on the Colorado plateau. Since this variety of lamprophyre is quite rare, only about 25 occurrences are documented worldwide; such a discovery is of significant importance. Lamproites are lamprophyres that are ultra-potassic, highly enriched in incompatible elements, and thought to originate from deeper in the lithosphere than most lamprophyres. While the source of lamproites has generally been interpreted to be depleted peridotite enriched in veins of phlogopite, K-Ti amphibole, clinopyroxene, apatite, and oxides melting incongruently, the depth of such activity is widely debated (ibid). Such a deep petrogenesis is further substantiated by the frequent inclusion of diamonds in the lamproites. However, depth estimates range from 100-200 km based on a variety of different dikes around the world (ibid). Depth calculations are hampered by the fact that magma genesis is polybaric, taking place over large columns of mantle. This results in mineral geobarometers suggesting a variety of depths for forma-

tion. Yet the general consensus is that they are formed in the lowermost lithosphere or upper asthenosphere. As with the lamprophyres of the Wasatch Plateau, the lamproite's trace and isotopic signatures suggest an anciently enriched lithosphere source mixed with a young asthenospheric component. And as with the previous example, the timing is consistent with shift from compression to extension throughout the region.

Similar lamprophyres are also found in areas surrounding the Colorado Plateau, including the 3400 km^2 of the Elkhead Mountains igneous province in northwest Colorado (Thompson et al., 1989). The province appears to have been active ~ 10 Ma during a late stage of Miocene post-Laramide extension. In addition to post-Laramide rebound, the area was affected by the sub-continental lithospheric thinning experienced by much of the western United States at this time. These dikes are augite and biotite-phyric, with amphibole and apatite also present. The trace-element patterns for the dikes contain a subduction pattern, despite a lack of such activity at the time. The dikes display a range of compositions from high-Mg, undifferentiated values to low-Mg evolved values. Simple fractionation models, binary mixing, and AFC models all fail to explain the range in compositions in the more primitive dikes. Instead, Thompson et al. favor mixing of basaltic and ultra-potassic melts in differing amounts to explain the range of compositions. Due to the lower melting temperatures of the potassic melts, they can be created coeval with basaltic melts that are formed at much deeper depths. In the case of the Elkhead lamprophyres, both extension and regional heating resulted in the partial melting of the asthenosphere (basalts), which migrated upward and mixed with melting ultra-potassic bodies within the lithospheric mantle to form the lamprophyres.

It seems logical that the lamprophyric dikes in the Mitchell area formed in a similar manner and in similar conditions as the above examples. They are likely small-degree melts of enriched lithosphere that was heated by (and possibly mixed with) asthenospheric melts. Since the area has experienced subduction several times, including the Eocene activity, it seems quite likely that there were ultra-potassic veins or bodies present in the lower lithosphere. White and Robinson (1992) have already

suggested that the Clarno area was under extension during the Eocene, as have many of the other workers on Eocene activity in the western U.S. (see chapter 2). The existence of these lamprophyric dikes at shallow levels of the crust seems to agree with such a conclusion. Whether this extension directly affected the asthenosphere is not clear, but since melting could just as easily be accomplished by volatile fluxing off the subducting slab, it is not necessary. Even if trace-element concentrations had been analyzed for the dikes, they would likely have subduction signatures. There would be little significance in this though, since such signatures can be established millions of years prior to the magma genesis according to isotopic evidence from the Colorado Plateau and the Highwood Mountains.

Alkaline Lamprophyres and the Clarno Formation

On the basis of geochronology, these dikes were emplaced at the height of Clarno volcanism. So in one aspect, these dikes must be related to the rest of the Clarno Formation. The fact that they are much more alkaline is not surprising, since several other alkaline features (Hudspeth Mill Intrusion, Marshall and Corporate Buttes) are also present in this area. What sets these dikes apart from both the Clarno and the other alkaline bodies discussed in this work is the apparent abundance of volatiles (especially water and CO_2) in these dikes.

Fractional crystallization and AFC modeling of the lamprophyres and the Clarno Formation in a manner similar to the previous chapters was inconclusive. This is to be expected if mixing of partial melts from metasomatized lithosphere and asthenosphere was important in the dikes' petrogeneses. Some major and trace-element diagrams (Si, K/Ti, Sr vs. Mg#) suggest a tenuous link between a couple of the lamprophyres and Marshall Butte by fractionation or AFC. Pyroxenes from the lamprophyres also exhibit chemical similarities to the other alkaline suites in many aspects (Figure 6.10 & 6.11). The Mudcreek pyroxenes are intermediate between Marshall Butte and the Hudspeth Mill intrusion in Ti, Na, and Ca in the most magnesian samples. However, in most cases the pyroxenes fall nearer to, or within, the zone of Hud-

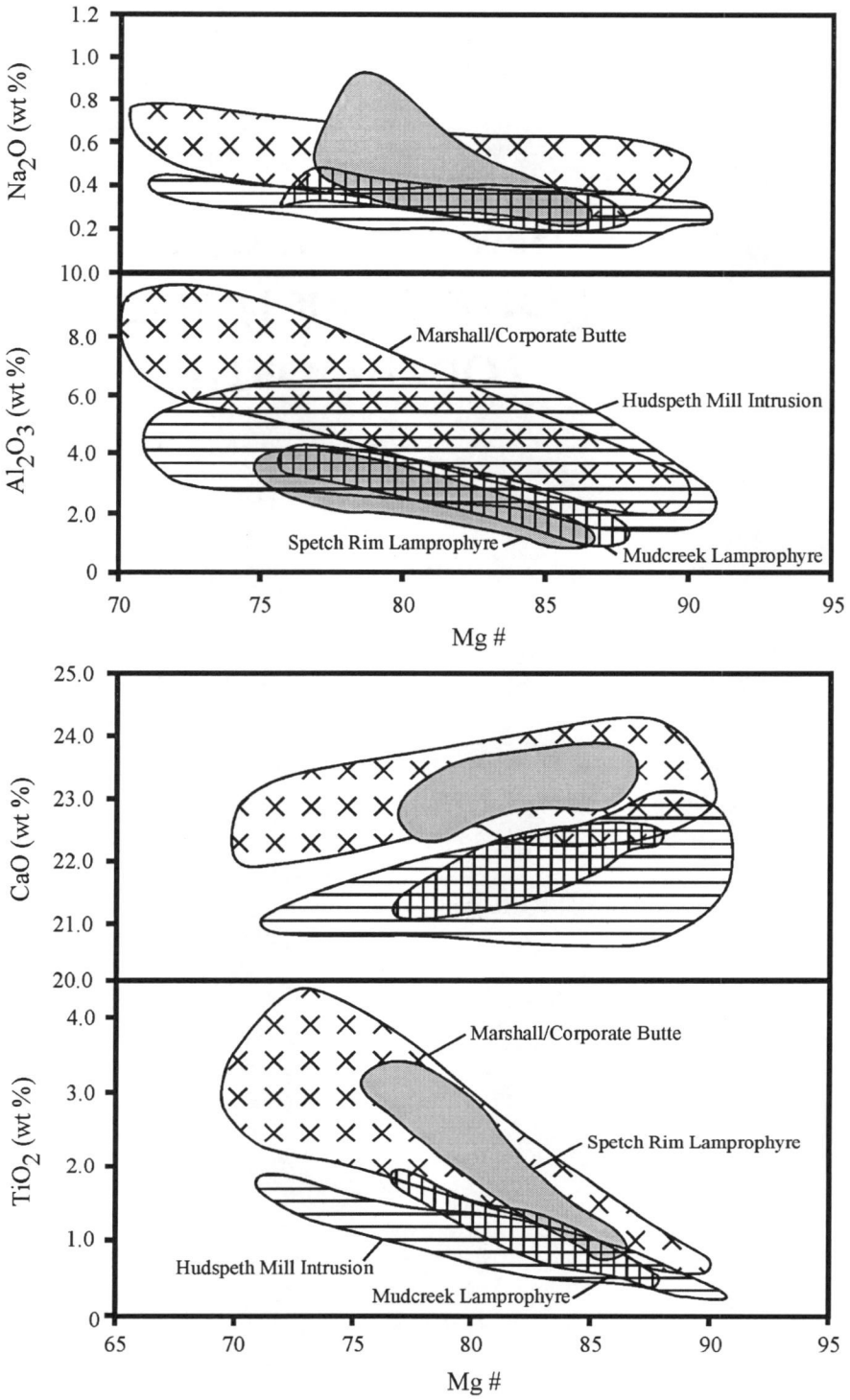

Figure 6.10: Pyroxene compositions for the four alkaline suites studied in this project. Overall the lamprophyres seem to fall intermediate to Marshall and Hudmill. The Mudcreek suite has more similarities with Hudmill, while Spetch Rim is more similar to Marshall Butte.

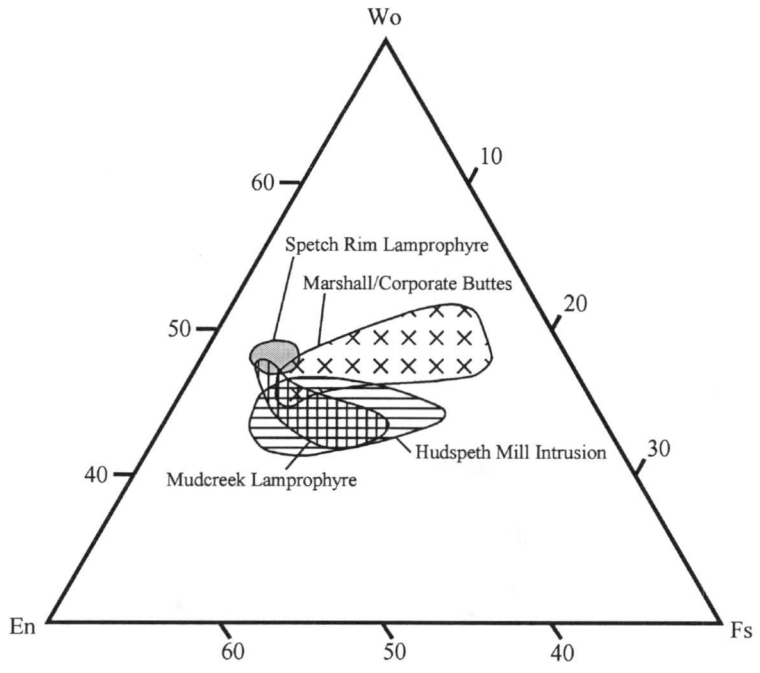

Figure 6.11: Pyroxene ternary with the four alkaline suites discussed in this project plotted. Note the similarity between the Mudcreek Lamprophyre and the Hudmill alkali basalt. The Spetch Rim Lamprophyre appears more similar to the Marshall Butte/Corporate Butte basanites.

mill pyroxenes. The Spetch Rim pyroxenes plot with the Marshall pyroxenes in Mg, Al, and Ca. In the case of Al, both lamprophyre suites have lower concentrations in their pyroxenes than either of the alkaline suites. Overall, it appears that the pyroxenes in the Mudcreek suite and Hudmill suite are similar, while the Spetch Rim dike's pyroxene is more similar to Marshall Butte pyroxenes. However, bulk-rock data for the lamprophyres exhibit less conclusive affinities for the other suites. Since pyroxene is the only mineral common to all the suites, other than oxides, caution must be used interpreting this information.

One possible scenario can be envisioned based on the literature presented over the last few chapters. Perhaps asthenospheric melts similar to the parental magmas of Marshall and Corporate Buttes are mixing with the lithospheric melts. The alkali ba-

salt might represent a primitive alkaline lithospheric melt with some minor asthenospheric input. Lastly, the lamprophyres could represent a mixture of these two also, but under slightly different conditions. Such a matter is made more complex by the fact that lithospheric melts are likely heterogeneous.

While not as precise as the ages on the dikes, the age determinations for Marshall Butte and Corporate Butte suggest coeval formation with the dikes. However, the age determination on the Hudmill intrusion indicates a younger age. With the quality and type of the data presented here, testing a hypothesis like the one above is not possible. As with many of the other suites studied here, and in other studies of related Eocene activity, more detailed age determinations and isotopic work would be of great value.

What can be concluded from this work is that alkaline rocks were emplaced coeval with calc-alkaline rocks during the height of Clarno volcanism. The alkaline magmatism formed at a variety of depths: Marshall/Corporate Buttes from the asthenosphere and the lamprophyres from the lithosphere. Neither suite needs direct chemical input (fluid fluxing) from subduction. Their existence does not require changing subduction parameters, but instead, the existence of heterogeneous mantle and differential sampling of it is probable. In agreement with White and Robinson (1992), the emplacement of these dikes, and the other alkaline suites, strongly suggests that the tectonics of the area were complex, and most likely included a strong component of extension.

Chapter 7: Scott Butte Rhyolite Dike

Setting

Scott Butte is a large Clarno basaltic andesite intrusion northeast of Mitchell. Cretaceous sediments, pre-Cretaceous metasediments, and Clarno lava flows and tuffs surround the butte (Figure 7.1). On the south flank of the butte, a large rhyolite dike has been exposed in a ravine due to erosion. The dike ranges from bright white to a light gray in color, and is easily distinguished from the browns of the intrusives and the grays of the metasediments. The dike can be directly observed only in the ravine, but in a few other places on the south side of the butte it is abundant in the float. While there are many felsic dikes and intrusions in the Clarno, this is the only known one which contains bright red, euhedral garnet phenocrysts.

Results

Petrology and Phase Chemistry

In the large stream-cut ravine, the dike's (SB-1) exposure is blocky to angularly fractured (Figure 7.2). The color ranges from the white to a light gray depending on the degree of weathering. The rock is fine-grained, with abundant large biotite, quartz, and plagioclase phenocrysts. Of particular interest are the euhedral garnet phenocrysts scattered throughout the dike. These are unique when compared with other Clarno silicic intrusions.

The second sample (SB-2) was taken from an area where there is no exposed outcrop, but the float is composed mainly of dike rocks (Figure 7.1). It was not possible to determine if the outcrop lies buried beneath the float, or if the area is actually a small landslide that carried a piece of the dike down slope and brecciated it. Much of the float has a pinkish-purple weathering rind on it, but otherwise the characteristics

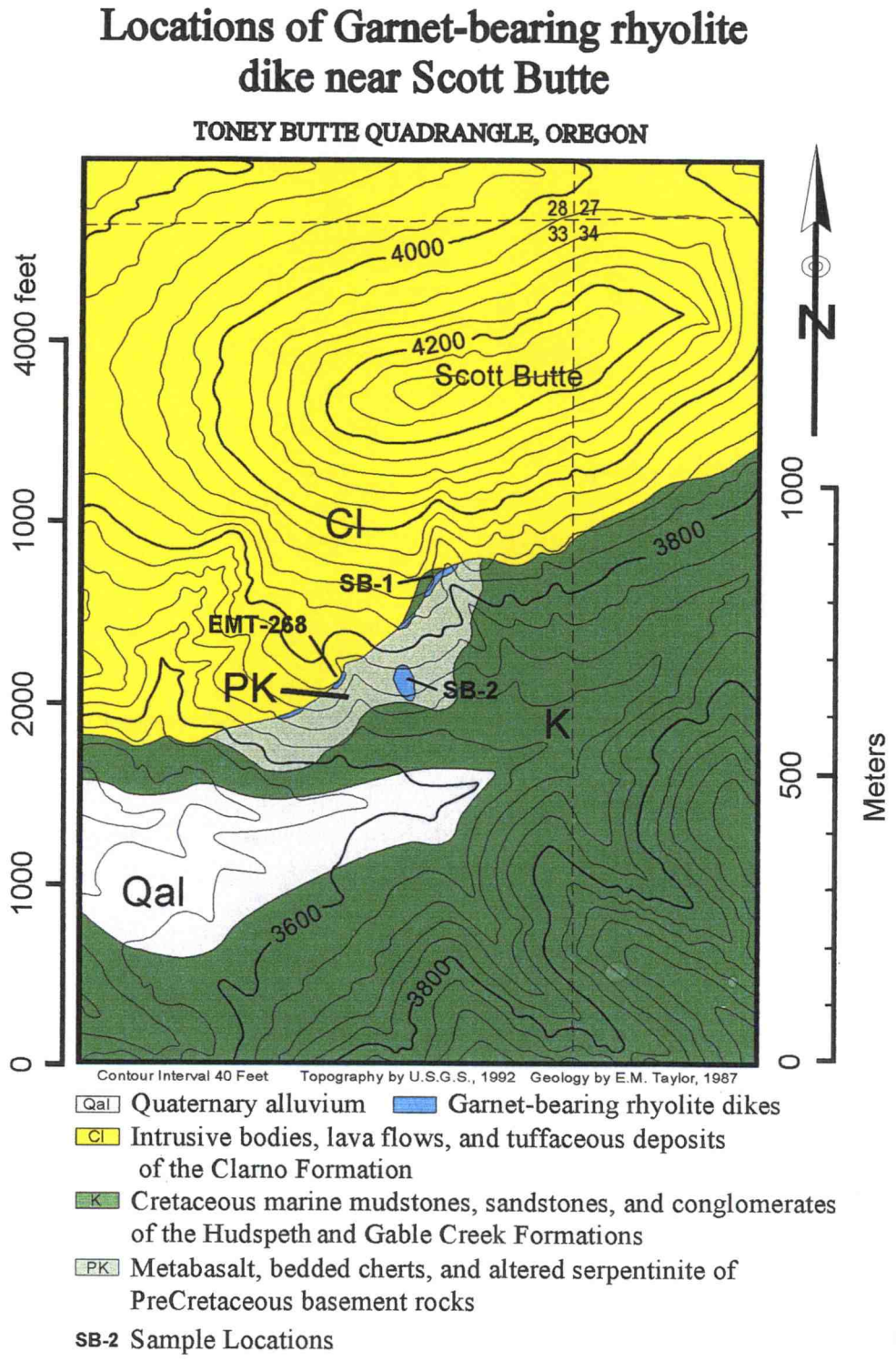

Figure 7.1: Geologic map of the Scott Butte Area with sample locations for the dike.

are the same as the outcrop in the ravine. Several additional samples, EMT-16, EMT-268, and GRD-1, were previously sampled by Dr. Ed Taylor and Dr. Brittian Hill.

The plagioclase phenocrysts are the most abundant of the phenocrysts, accounting for ~ 10% of the rock's mode (Table 7.1). They are subhedral, 1-2 mm in size, and exhibit abundant zoning with some also displaying Carlsbad twinning. Many of the plagioclase phenocrysts are moderately to severely altered to carbonate, typical of low temperature hydrothermal weathering. The quartz phenocrysts are roughly the same size as the plagioclase, ~ 1.5 mm, but despite embayments, are more euhdral. They are also much less abundant than the plagioclase, accounting for 2-5% of the rock. Often associated with the quartz phenocrysts are the euhedral, ruby-colored garnet phenocrysts (Figure 7.3). While they seem abundant in hand sample due to their bright color, they are present in trace amounts with only a crystal or two present per thin section. While some smaller crystals are around 150 microns, most garnets are ~ 1 mm in size and free of inclusions. The biotite phenocrysts range from less than 0.5 mm up to ~ 1 mm in size and make up 1-2% of the rock. Many of the biotites show some chloritization, suggesting low temperature weathering has occurred.

Figure 7.2: An exposure of the rhyolite dike where it is cut by a small stream ravine on the south side of Scott Butte (SB-1).

The groundmass makes up the majority of the rock, between 83-87% of the above samples. It consists of very fine-grained quartz, plagioclase feldspar, biotite, alkali feldspar, and possibly a few py-

Table 7.1: Modal Estimate of phenocrysts in the rhyolite dike.

	SB-1	SB-2
Plagioclase Phenocrysts	10 %	10 %
Quartz Phenocryst	2 %	5 %
Biotite Phenocryst	1 %	1.5 %
Garnet Phenocryst	< 1%	< 1%
Groundmass	87 %	83 %

roxenes. Due to the extremely fine-grained nature of the groundmass, exact modes could not be estimated. Nevertheless, survey work done with the electron microprobe suggests that the large majority of the groundmass is quartz. This work also failed to find any trace of cordierite or muscovite in the groundmass. The groundmass exhibits flow textures around many of the phenocrysts.

Due to the weathering of the feldspar phenocrysts, complete microprobe traverses were difficult to obtain. Partial traverses suggest that the crystals are normally zoned with some degree of oscillatory zoning also present (Figure 7.4). The phenocrysts are oligoclase and andesine (An_{35-24}) (Figure 7.5). The groundmass feldspars show a larger degree of variation ranging from $An_{28}Ab_{70}Or_2$ to $An_{0.5}Ab_{35.5}Or_{64}$.

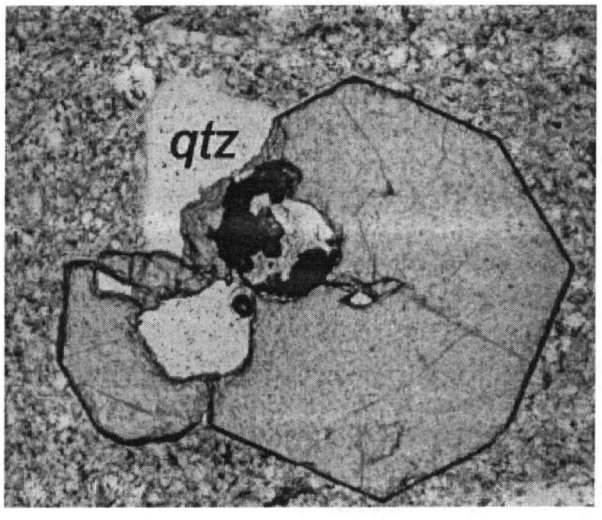

Figure 7.3: Photomicrograph of a garnet phenocryst from the dike. Note the euhedral shape, the associated quartz, and the lack of a reaction rim.

Biotite is found both as phenocrysts and in the groundmass. Due to their small size, no

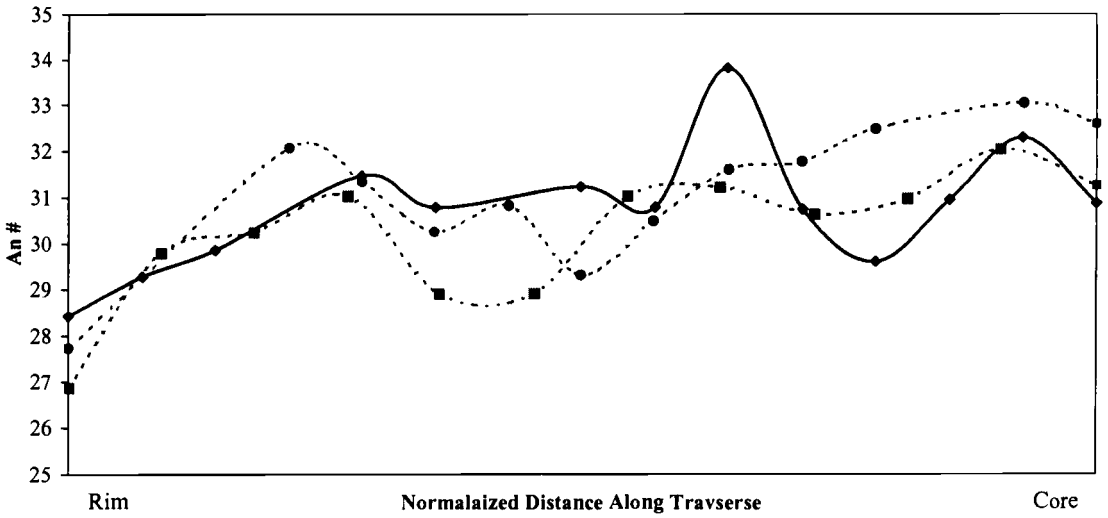

Figure 7.4: Microprobe traverses across sections of plagioclase phenocrysts. While the traverse do not completely cover the crystal, clear oscillatory zoning is present in partial traverses.

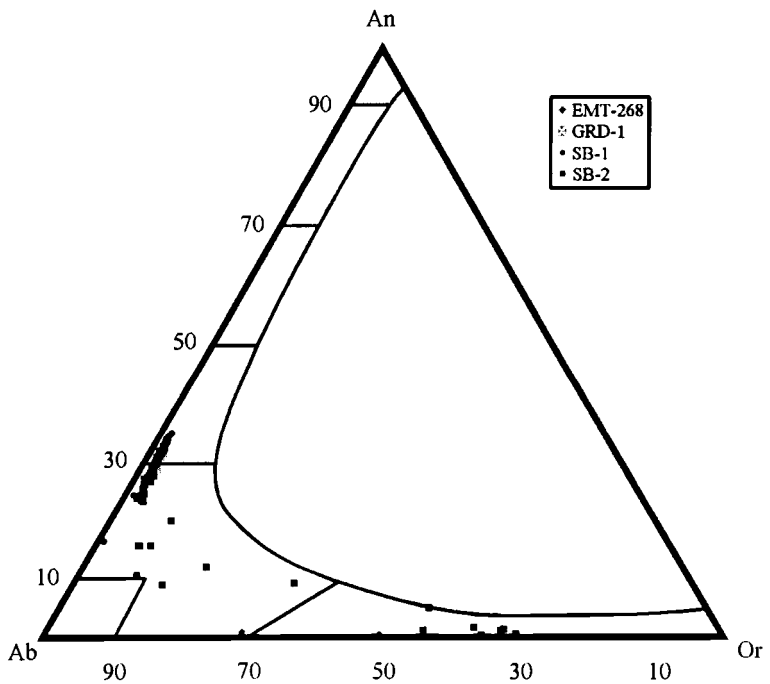

Figure 7.5: Feldspar classification diagram. The phenocrysts display a narrow range of plagioclase compositions, while the groundmass compositions cover a range of alkali feldspars.

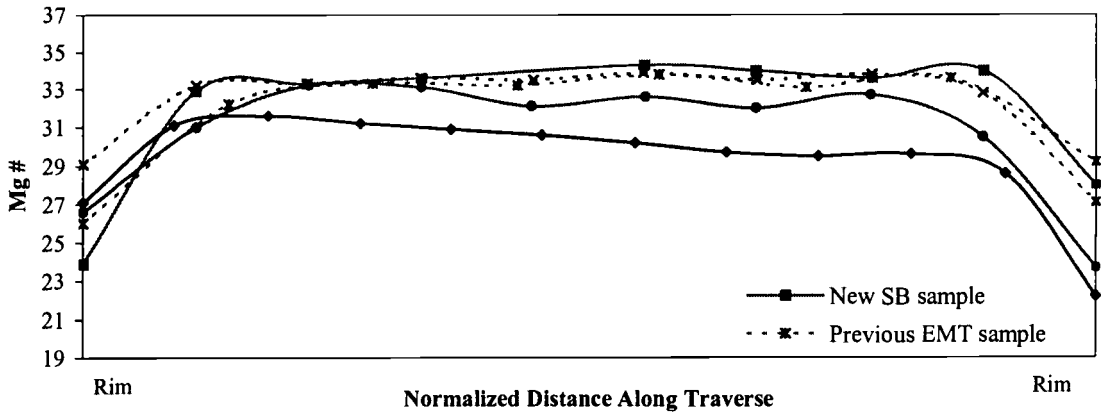

Figure 7.6: Microprobe traverses of biotite phenocrysts. The crystals show clear normal zonation near the rims.

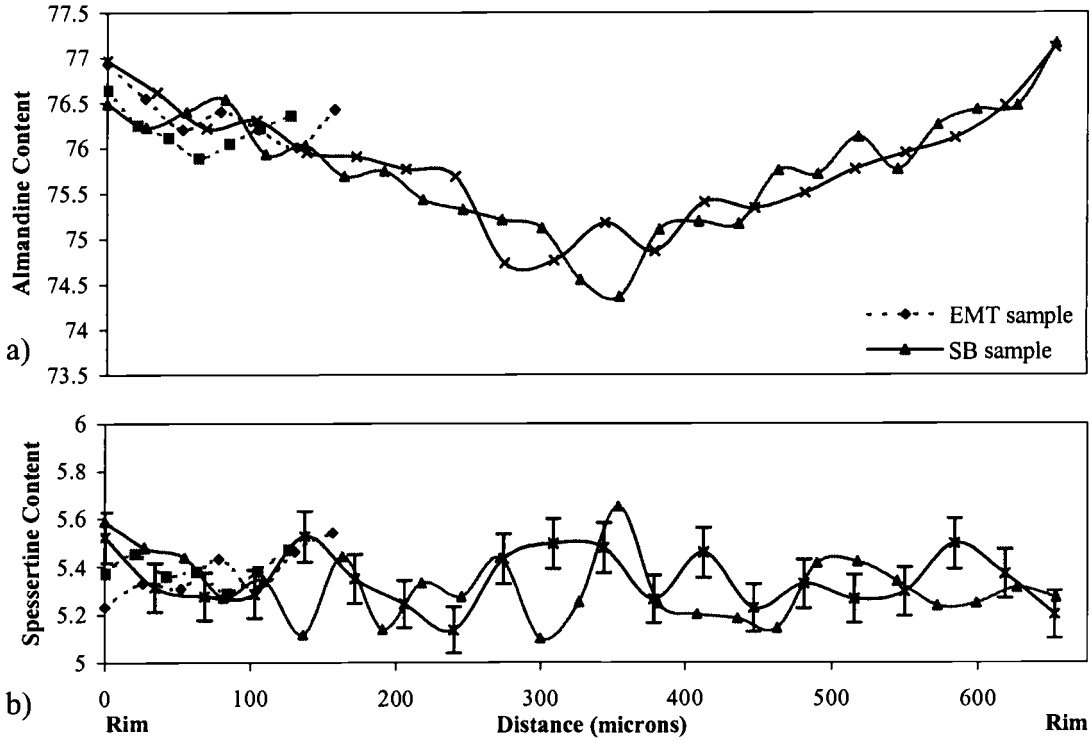

Figure 7.7: Microprobe traverses of two garnet phenocrysts from the dike. a) The crystals are dominantly almandine in compositions and display an overall normal zonation. b) Spessartine content remains nearly the same across the traverse, with most minor fluctuations within the analytical error.

chemical data were obtained on the groundmass biotite crystals, but several traverses were conducted across a variety of different sized phenocrysts. All of the crystals were similar in composition, and displayed normal zonation near the rims (Figure 7.6). Some of the crystals showed significant evidence of chloritization in the cores, with lower values for more mobile elements like K_2O.

Garnet traverses were conducted on two crystals, a small (150 micron) crystal and a larger (750 micron) one. Two traverses were conduced perpendicular to each other on each crystal. The garnet is dominantly almandine (~ 75%), with lesser pyrope (~ 11%), grossulaire (~ 7%), and spessertine (~ 5%). Both crystals displayed normal zoning, with increasing almandine content toward the rims (Figure 7.7a). Spessertine content remained nearly constant throughout the crystal (Figure 7.7b).

Bulk Geochemistry

The Scott Butte Dike is classified as a calc-alkaline rhyolite (Figures 7.8 & 7.9), similar in composition to other rhyolites from the Clarno Formation. However, the dike is slightly more sodic than potassic (Na_2O/K_2O= 1.3-1.6), resulting from lower K_2O values than most of the Clarno rhyolites. It is peraluminous (Na+K+2Ca/Al= 0.70-0.85) and high silica (~ 75% SiO_2). The normative compositions are typical for rhyolites, but also reflect the peraluminous nature of the dike with high normative corundum contents (4-6%).

The peraluminous nature is thought to reflect the original nature of the magma rather than a weathering effect. While weathering of the alkalis would result in the same classification, the samples analyzed were chosen from the freshest rocks and show only minor replacement of the phenocryst with calcite. Additionally, the rocks are less weathered than other Clarno rhyolites previously analyzed. These other rhyolites are still more alkaline-rich, suggesting that the Scott Butte rhyolite dike is fundamentally different than other Clarno rhyolites.

Spiderdiagrams indicate the rocks are enriched in most trace elements when compared to condrite or primitive mantle (Figure 7.10). However, Ti and Sc are depleted

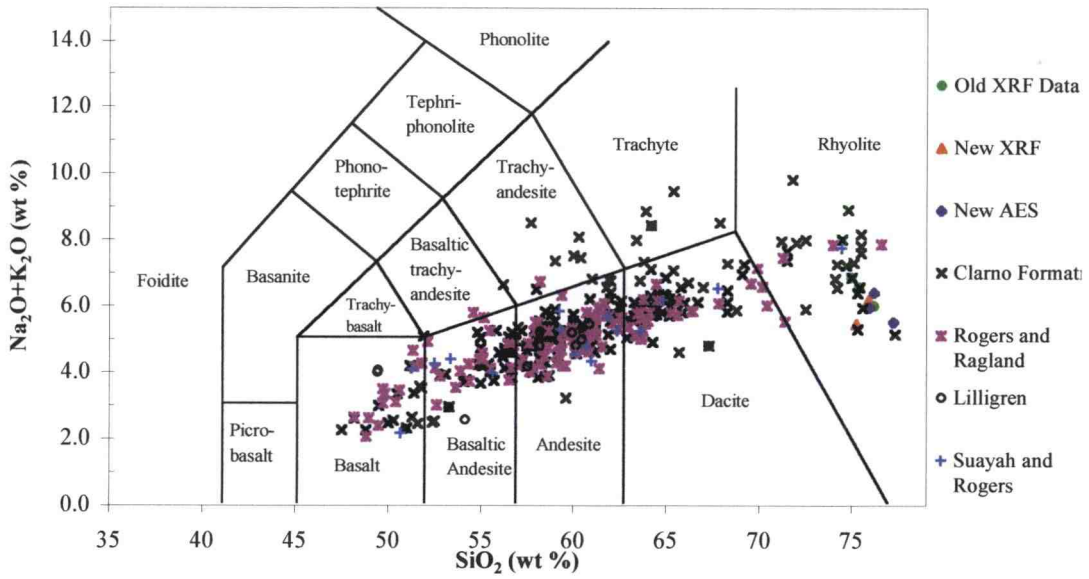

Figure 7.8: Classification of the Scott Butte Rhyolite Dike according to total alkali content. (La Maitre et al., 1989). The dike falls toward high-silica end of the rhyolite field.

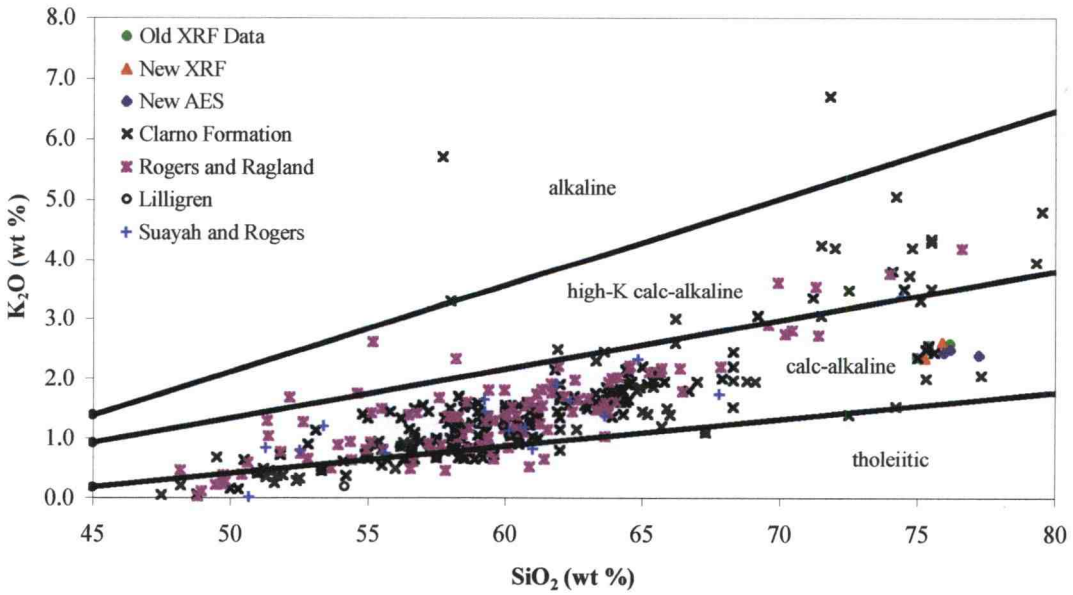

Figure 7.9: The Scott Butte Rhyolite Dike falls near the middle of the calc-alkaline field (Gill, 1981). Most other Clarno Formation rhyolites are high-K calc-alkaline.

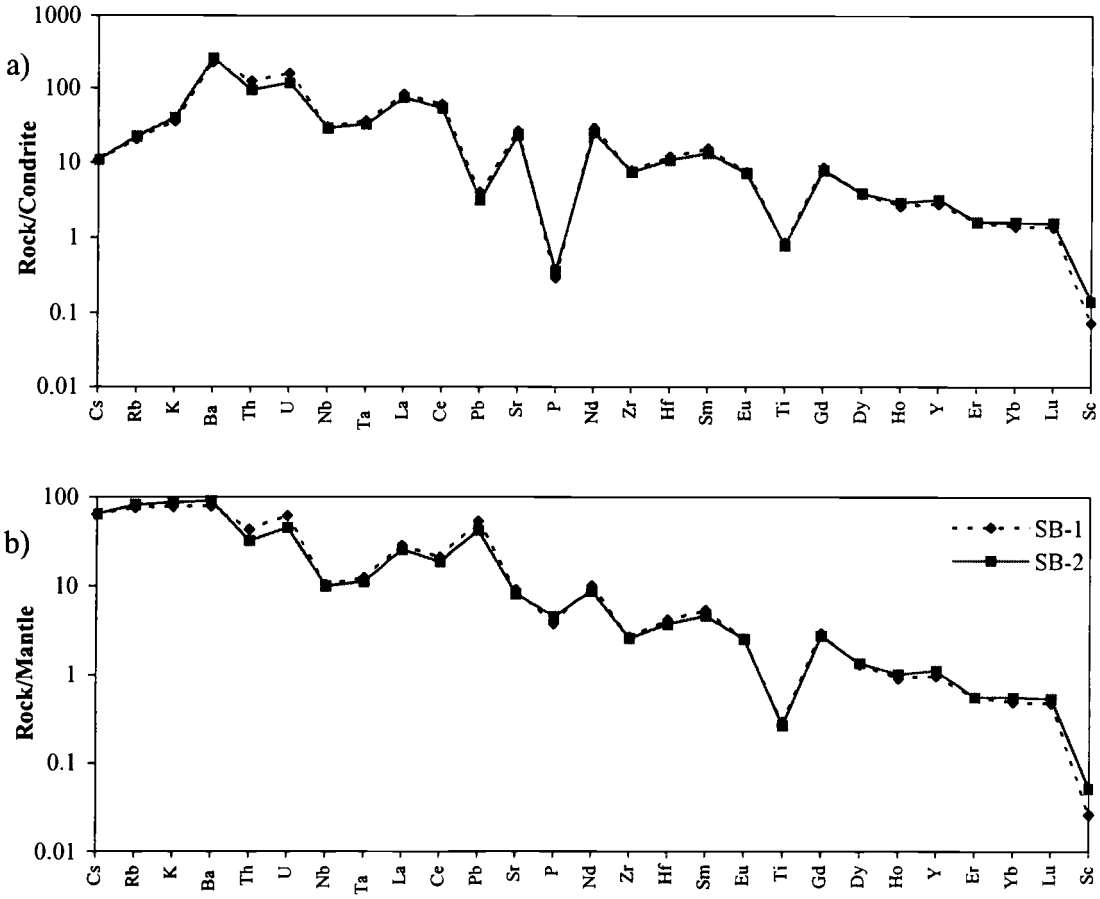

Figure 7.10: Trace-element patterns for the rhyolite dike normalized to a) condrite and b) primitive mantle using the values of Sun and McDonough (1989).

in both normalizations, along with the heavy rare-earth elements when normalized to primitive mantle. Large-ion lithophile elements show the largest enrichments, followed by the high field strength elements. In both normalizations though, the HFSE's display relative negative anomalies characteristic of subduction zones. REE's are highly fractionated ($La/Lu_N \sim 47\text{-}60$) and have negative anomalies at Eu ($Eu/Eu^* \sim 0.65$) and Er ($Er/Er^* \sim 0.7$) (Figure 7.11).

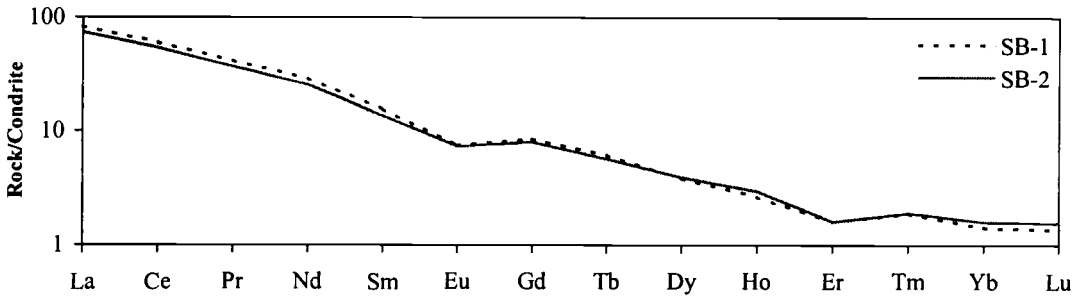

Figure 7.11: Rare Earth element concentrations normalized to condrite (Sun and McDonough, 1989). There are negative anomalies at Eu and Er.

Geochronology

Age analyses were conducted on both samples from the dike. Both samples have several percent biotite phenocrysts, and since the biotite has ~ 8% K_2O, it can be used to obtain precise $^{40}Ar/^{39}Ar$ age dates. The biotite was manually separated from the rest of the rock to reduce both possible sources of contamination and interferences caused by other minerals. Biotite from both samples was analyzed. For the in situ sample from the ravine (SB-1), 91% of the gas released resulted in a plateau of 50.93 ± 0.14 Ma (Appendix 3). For the sample from the float (SB-2), 96% of the total gas released resulted in a plateau at 50.97 ± 0.11 Ma.

A previous K/Ar analysis was conducted in 1991 by Brittian Hill at the College of Ocean and Atmospheric Sciences at Oregon State University. The resulting biotite separate gave at a date of 42.01 ± 0.45 Ma (person communication, 1999). However, this date is most likely incorrect due to chloritization of the biotite. Since K/Ar uses only one gas fraction, it is more susceptible to Ar loss due to low temperature alteration. The effect of chloritization is also seen in the lowest temperature step of the new analyses. However, the use of step-heating in these new analyses provides the ability to analyze several gas fractions from one sample. Since the low temperature alteration will only affect lowest temperature gas fractions, the remaining gas fractions will be accurate. With the use of a plateau test on the remaining fractions, an accurate

date can be obtained. This greatly reduces the possibility of simple weathering greatly affecting the final age. Therefore, the new dates are more accurate.

As noted in previous chapters, the more recent isotopic works report ages for the Clarno Formation from 40-60 Ma, with the largest flux around 49 Ma (Suayah, 1990; Bestland et al., 1999). A date of 51 Ma indicates the dike was emplaced during the Clarno activity, but prior to the largest fluxes of calc-alkaline and alkaline activity.

Discussion

Scott Butte Rhyolite Dike Petrogenesis

While there are other rhyolite lavas and intrusions throughout the Clarno, this dike is unique in its garnet phenocrysts. Rhyolitic melts are often thought of as upper crustal melts, but the presence of a high-pressure phase like garnet seems to contradict this. While such garnet rhyolites are rare in the Clarno, there are numerous occurrences of such rocks in other calc-alkaline suites.

The most important factor to be determined is if the garnets are magmatic in origin and if they are phenocrysts or actually xenocrysts. Works dating back to the 1950's and 60's identified that compositional variations, the euhedral crystal shapes, and the inclusion free nature of the crystals indicate crystallization directly from a silicic melt (Green and Ringwood, 1968; Fitton, 1972). This would indicate that the garnets in the dike are phenocrystic and reflect the petrogenesis of the dike's magma.

After comparing a number of suites containing magmatic garnet, it was determined that two main types of garnet are found in silicic rocks. The garnets are almandine-rich (Fe endmember), with one type also spessartine-rich (Mn endmember), and the other type spessartine-poor (Stone, 1988). Early experiments suggested that at moderate to high pressures (9-27 kb), quartz and garnet can be on the liquidus together in silicic magmas (Green and Ringwood, 1968). This work suggested that these magmas were formed by melting of deep crust/upper mantle at depth greater than 25 km. However, many of these rocks also contain cordierite, which is unstable at pressures higher than

10 kb. This lead Green (1976) to suggest that the higher Mn content of the pelitic protoliths could result in garnet stabilization at lower pressures. Green (1977) experimentally tested this and found that 20-25% spessartine would stabilize garnet at depths of 12 km or less. However, garnets that contain <10% spessartine are still likely to have crystallized at depths of 18 km or more. This lead to the conclusion that rocks with spessartine-rich garnet formed at lower pressures and higher water contents, while almandine-rich garnets with low spessartine content formed from deeper, less hydrous melts (Stone, 1988).

The garnets from the Scott Butte rhyolite dike are almandine-rich (~ 76%) with low spessartine contents (~ 5%). They are inclusion-free and often associated with quartz phenocrysts. While the garnet is euhedral, the associated quartz is often resorbed. This is consistent with high-pressure crystallization. The garnets are also normally zoned with almandine increasing toward the rims. This is consistent with simple crystal fractionation rather than a xenocrystic origin. The samples lack both muscovite and cordierite, common in shallower melts. This all suggests that the garnet crystallized with quartz at depths of 18-25 km from a silicic melt. Additionally, Stone (1988) points out that Mn enrichment toward the rims is often considered to indicate crystallization at falling temperatures. The garnets from the dike have near constant levels of Mn from rim to rim, suggesting near-constant temperatures. Finally, while the dike has biotite phenocrysts, the lack of hydrous minerals and the presence of feldspar in the groundmass, along with its very fine-grained nature is consistent with a low volatile content in the ascending magma. This would have allowed it to rise to its upper crustal location without significant crystallization. Migration through the crust may also have been facilitated by faults and planes of weakness due to possible extension in the area. This characteristic appears to be common in Clarno rhyolites, where most intrusions are extremely fined-grained and, with the exception of some biotite phenocrysts, lacking hydrous phases.

The question of the dike's protolith is difficult to address. At depths of 18-25 km, the source region was located within the lowest portions of the crust. However, the crust during the Eocene consisted of accreted oceanic terrains. The metamorphic rocks of the Blue Mountains, the same material, are mélanges of ocean islands and oceanic crust. Constraining the lower crustal composition is further hindered by the fact that the

Clarno Formation is remarkably free of xenoliths. And when xenoliths are present, they are generally Cretaceous sediments from the upper parts of the crust. However, it is unlikely that peltic material existed at the appropriate depths to have been the source of the rhyolite dike.

Scott Butte Rhyolite Dike and the Clarno Formation

The age determination of 51 Ma places the dike within the Clarno activity, although the earlier stages. This relationship is further strengthened by trace-element profiles of the dike. The profiles have the typical subduction signature of enriched LILE and HFSE depleted relative to LILE and REE. The HREE depletions suggest that garnet, while some still being present in the dike, has also fractionated out of the magma. The source region for the magma, likely the lower crust, had been exposed to modification by subduction derived fluids prior to melting. However, the timing of this enrichment event is not clear. The simplest case would be enrichment due to the Clarno subduction. The character may be a result of metasomitization followed by an injection of magma that caused melting, or simply an exchange of fluids between the injected magma and the new partial melt. The presence of a hydrous phase in the residual is suggested by the trace elements. This, along with the anhydrous nature of the magma, suggests melting of previously modified crust. As I have previously noted, this area had experienced earlier subduction events. These may have imparted the signature on the lower crust at that time. The problem of timing cannot be addressed without isotopic work . Nevertheless, the simplest explanation for the enrichment in some trace elements is that the melt formed as a result of the Eocene (Clarno) subduction.

Geochemically, the rhyolite dike is similar to other Clarno rhyolites. Overall, the composition for most major and trace elements is quite similar. And like the other silicic intrusions, the dike is very fine grained with hydrous minerals nearly absent from the groundmass. This suggests that the Clarno rhyolitic melts were all anhydrous.

There are also several differences that set this dike apart from the other Clarno silicic rocks. The dike contains much less K_2O than most Clarno rocks. The other

Clarno rhyolites are high-K calc-alkaline, yet this dike falls near the middle of the potassium range for calc-alkaline rocks. This distinction is likely related to both the petrogenesis and possibly the timing of the suite, rather than any alteration effects. The presence of garnet is evidence of the most significant difference, which is the deep crustal source for the dike. While the other intrusions have not been studied in detail, there is nothing suggesting that their source is nearly as deep as the dike's source.

The most logical conclusion is that the dike formed as a result of partial melting of the deep crust (18-25 km down). This was likely in response to injection of fresh magma related to subduction. At this time (51 Ma), volcanic activity was still limited. It is likely that much of the magma was not reaching the surface, but instead cooling in the crust. This would provide an excellent heat source to melt the crust and form the silicic magma.

Chapter 8: Radiometric Dating of Other Mitchell Area Suites

In addition to the previously mentioned suites, several other samples were collected in the Mitchell area for ages by $^{40}Ar/^{39}Ar$ (Figure 8.1). The first group is a series of andesite lavas from the Clarno Formation. These were chosen specifically to help constrain the timing of the Clarno activity, as well as unconformities within the Clarno. The second group is composed of several intrusive bodies not necessarily related to the Clarno, but that have significance in the geologic history of the area. A complete listing of the analyses and data from each of the samples is contained in Appendix 3.

Clarno Andesite Flows

The absolute dates of the Clarno magmatism are not well defined. There are several reasons for this, one being the spatially heterogeneous nature of the units. In many places the stratigraphic relationship of the individual units is not clear. Another significant problem is the extensive low-temperature alteration of the rocks. Previous workers have solved the first problem by sorting out the stratigraphy, but both the lack of widespread correlatible units and the heterogeneous nature of the deposits makes this extremely difficult. The problem of low temperature alteration (weathering) is also a significant cause of error in the published radiometric dates. It is hoped that newer $^{40}Ar/^{39}Ar$ dating techniques can overcome the effects of this alteration that plagued older K/Ar dates.

The Clarno Formation has been separated by the Mitchell anticline over much of the study area. Today there are significant differences in which units are preserved on the two sides of the anticline. To better constrain the timing and which units are present, along with which units are missing, both sides of the anticline were selected for radiometric dating. On the eastern flank of the anticline, samples were collected from both the uppermost and lowermost units. However, on the west side of the anticline,

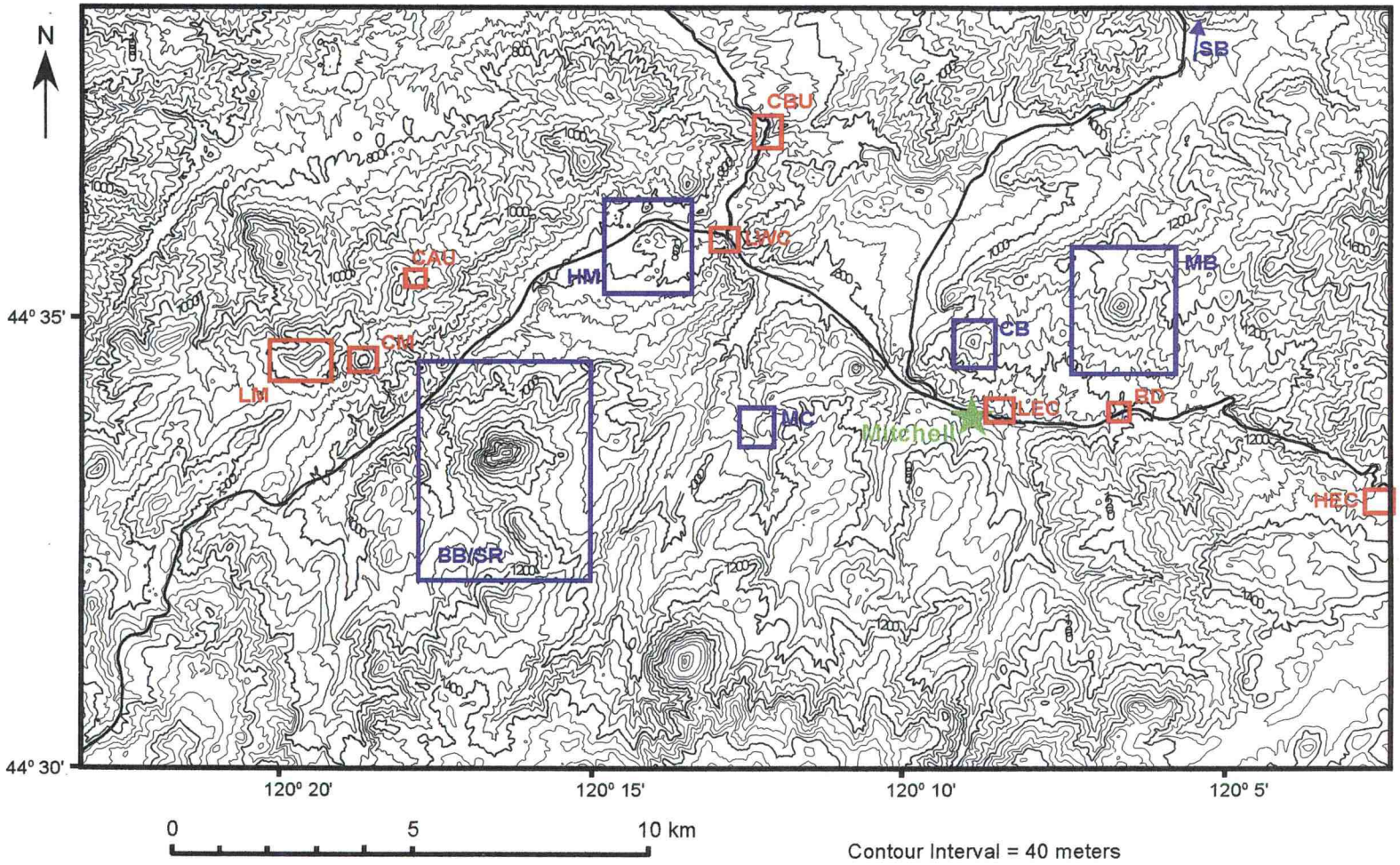

Figure 8.1: Topographic map of the Mitchell study area with all of the locations sampled for Ar/Ar dating. In addition to the previously mentioned intrusive groups, several Clarno andesite lavas and other Mitchell area intrusions.

stratigraphy and structure may be complicated by a possible unconformity in the upper Clarno. Since field observations suggest the presence of an angular unconformity, samples were taken from below and above the possible unconformity to help determine its timing.

Low East Clarno Andesite Lava Flow

Two andesite flows were sampled near the bottom of the Clarno Formation, just above the Cretaceous boundary on the east flank of the anticline. Although the exact number of flows lying between the sampled flows and the boundary was not determined, they are amongst the lowest on the east side of the Mitchell anticline. These flows belong to the quartz-bearing andesites previously described by Noblett (1981). Just up-section, above and below the lava flows there are abundant Clarno mudflows observed.

The first sample (LEC-1) was collected from the top of the cliff on the north side of US 26 at the intersection of Dollarhide Pond road. Here the andesite displays poorly developed platy jointing. The fresh surface is medium gray, with minor phenocrysts in hand sample. A stratigraphically higher flow in the canyon just to the east of the first sample locale was also sampled (LEC-2). While the platy jointing is much more distinct here, the dip of the plates to the west is not reflective of the flow's dip to the east. The overall character of the sample is the same as the previous flow.

The rocks are porphyritic with phenocrysts of quartz (< 1%), clinopyroxene (7-15%), and relict olivine textures (1-2%). Almost all of the phenocrysts exhibit reaction halos (usually pyroxene or opaques), probably due to magma mixing. Both plagioclase and opaques also form microphenocrysts. Many of these plagioclase crystals show significant evidence of weathering to clays. The groundmass exhibits flow textures around many of the phenocrysts, and is dominantly plagioclase laths and opaques, with some clinopyroxene also present.

Both samples were analyzed using groundmass separates since there were no abundant K-rich phenocrystic phases. However, using the groundmass rather than a specific phase resulted in significant argon recoil. This occurs during neutron bombardment of the samples when the Ar is redistributed, and even lost, as it recoils from the neutron capture. This leads to an inverse stair-step pattern with older ages in the lower-T step and younger ages in the higher-T steps. The samples yielded total gas ages of 48.8 Ma and 49.6 Ma, although due to the argon recoil there was not a significant plateau in the data. Instead, isocron plots of $^{40}Ar/^{36}Ar$ vs. $^{39}Ar/^{36}Ar$ were used and two different York regression analyses were preformed on the data to obtain a date. However, the LEC-1 sample suffered so heavily from argon recoil (ages dropped from 56 Ma to 39 Ma) that no usable date was obtained.

The lesser degree of argon recoil in the second sample (LEC-2) allowed for an isocron age of 49 ± 2 Ma to be determined. This places the lava within the time frame of the Clarno, but due to argon recoil, a more precise date was not possible.

High East Clarno Andesite Lava Flow

These samples are from a late-stage Clarno andesite flow taken from the east side of the anticline. The flows sampled are the uppermost flows, with the John Day Formation just above them. The sampling was done at a small quarry just south of US 26, at the top of Keyes Crest.

The lava is massive, with random large-scale fractures. Immediately noticeable is the abundant red banding present in all the samples. The bands range from criscrossing lines to concentric rings. They are even present in what appears to be a fresh surface. This is likely due to oxidation fronts due to weathering. The fresh surface is very fine-grained and light gray, with abundant phenocrysts.

The phenocrysts make up over 25% of the rock, and are mostly plagioclase. The plagioclase consists of two main populations, both exhibiting complex twinning (both albite and Carlsbad) and zoning patterns. The larger population, about a third of the total plagioclase phenocrysts, reaches sizes up to 2 mm and have resorbed cores.

As with many of the Clarno lavas, this is likely due to magma mixing. A Carlsbad-albite determination was done on the smaller population of plagioclase and indicates an anorthite content of ~ An_{50}. Clinopyroxene and olivine are also phenocrystic, but in smaller crystals and lesser amounts. They often form glomerophyres, and vary in degree of resorbtion. The groundmass is extremely fine grained and is mostly plagioclase and devitrified glass, with lesser opaques.

Two samples from the flow were dated using groundmass separates due to the lack of K-rich phenocrysts. Once again both samples suffered from argon recoil. The second sample (HEC-2) reported a total gas age of 49.0 Ma, but no regression was possible. Almost 80% of the ^{39}Ar released indicated an age between 49-51 Ma, with the higher temperature steps showing progressively younger ages due to the argon recoil. The first sample (HEC-1) reported a similar total gas age of 49.5 Ma, but resulted in an isocron age of 51.0 ± 0.8 Ma. This sample displayed a similar pattern to the previous sample, but with only ~ 60% of the ^{39}Ar indicating an age between 49 and 51 Ma.

Once again the lesser quality of the data hampers making firm conclusions about the stratigraphy. However, even with the significant error in this data, it does raise an important question about the duration of the events. Both the lowest flow and the highest flow appear to have near similar dates. Assuming that this is not a significant error in the analyses, then two possible reasons for this exist. First, the succession of activity on this side of the anticline occurred quite rapidly and in quite large volumes. Second, the stratigraphic assumptions made are incorrect. Either the flows do not lie in the sequence in the order in which we thought they did, or the sequence sampled represents one small part of the larger sequence in the area. To better address this problem, two things would be need. First, a more accurate determination of the stratigraphy between the two points would have to be completed. As previously mentioned, this is very difficult due to the heterogeneous nature of the formation, the post-emplacement deformation and faulting, and the significant erosion that has occurred in the last few million years. A second useful exercise would be to date more flows between the two units and determine if a smooth succession between the units

does exist. Before such work was undertaken, an attempt to obtain better quality age dates on the units should be addressed.

Low West Clarno Andesite Lava Flow

An andesite lava flow on the west side of the Mitchell anticline, and to the north of the Mitchell fault was sampled as the lowermost unit of the Clarno. The flow is the fourth above the Cretaceous/Clarno contact. Since this lava is much less weathered than the first three, it is a better selection to date. There is no significant paleosol between the lower flows, suggesting a short interval between their deposition. The samples were taken from the road cut along US 26 and were the freshest observed.

The sample contains about 15% plagioclase phenocrysts that are strongly oscillatory zoned and show significant resorbtion features. Many of the phenocrysts also look as if they are fragments of larger crystals that have been broken. These textures are interpreted to be due to magma mixing. There are a few (< 1%) clinopyroxene phenocrysts, but all are considerably altered. The groundmass has strong flow textures and is composed of mostly plagioclase and pyroxene, with abundant opaques and devitrified glass also present.

Only one sample from this flow was dated using a groundmass separate. As with the previous samples, this sample also suffered heavily from argon recoil. The sample yielded a total gas age of 52.3 Ma, with no isocron age. Over 75% of the ^{39}Ar released indicated an age between 54 and 52 Ma. While this age does not help to better define the onset of Clarno volcanism in the area, it does fit in with other ages from the Clarno that suggests volcanism began between 50-60 Ma.

Clarno Andesite Lava Flow Below the Unconformity

Two andesite flows from just below the possible unconformity were sampled on the west side of the anticline, and north of the Mitchell fault. While the lava flows

above the unconformity are not present in this area, the unconformity can be observed in the fact that the flows here dip much more steeply than the flows above the unconformity. Just up section, is the John Day Formation and the Painted Hills. The fact that the upper flows are missing here may just reflect post Clarno erosion, rather than the unconformity that lies within the Clarno itself.

The samples were taken adjacent to the Painted Hills Highway, 1.8 miles from its intersection with US 26. Bridge Creek, followed by highway construction, has cut deeply into the flows leaving good exposures that have weathered a reddish-brown color. The first flow (CBU-1) shows very good platy jointing, but joint orientations do not reflect the dip of the flow. A fresh face is light to medium gray and crystalline, with large white plagioclase phenocrysts. A second flow (CBU-2) was sampled up the road (south) about 100 feet. This flow is also platy jointed, but with the joint orientation similar to the flow orientation. All other characteristics are similar to the first flow.

Both samples are porphyritic, but with between 2 and 5% plagioclase phenocrysts. The plagioclase phenocrysts are strongly zoned (oscillatory) with many having both Carlsbad and albite twinning. As with all of the other magmas sampled, the textures observed strongly indicate magma mixing was significant in the petrogenesis of the lavas. Also present are opaque and clinopyroxene microphenocrysts that are completely altered. The groundmass of the first sample (CBU-1) is extremely fine-grained and appears to be mostly devitrified glass with some plagioclase crystals. Opaques and scattered clinopyroxene make up lesser amounts of the groundmass. The groundmass of the second sample (CBU-2) was much more crystalline, composed of primarily plagioclase and clinopyroxene, with lesser opaques and minor devitrified glass. As with the other flows, the plagioclase crystals are strongly aligned resulting in a well developed flow texture. Due to the more crystalline groundmass in the second sample, it was used for dating rather than the first sample.

A groundmass separate was again used due to the lack of significant K in the phenocrysts. While the sample did suffer from argon recoil, a plateau age was determined from three of the latter steps. The plateau age of 42.9 ± 0.2 Ma contained only

17.2% of the total ^{39}Ar gas released from the sample. While this is a low amount of gas, the lack of clustering of the other steps suggests that this may be a reliable date. Such a date clearly places this flow within the latter stages of the Clarno Formation. If the dates from the east side of the anticline are accurate, then the west side of the anticline has preserved rocks both much older and younger.

Clarno Andesite Lava Flow Above the Unconformity

Two flows that lie above the possible unconformity in the upper portion of the Clarno Formation on the west side of the Mitchell anticline, and north of the Mitchell fault were sampled. These flows are likely some of the highest, and therefore youngest, Clarno units in the area. The unconformity can be observed in the fact that the flows here dip much less steeply than the lower flows previously sampled.

The samples were taken from the ridge almost due north of Black Butte along Cougar Mountain Rd. The lava here (CAU-1) is a pinkish-purple brown with abundant red banding similar to the ones observed in the HEC samples. The outcrop is weakly platy-jointed, with the plates dipping at a steep angle into the hill. Once again, the dip of the jointing does not reflect the shallow dip of the flow. A fresh face is medium gray with both plagioclase phenocrysts and lesser greenish-brown clinopyroxene phenocrysts.

A second flow (CAU-2) was sampled from an outcrop further up the hill. It was not determined if this was the same flow, or a slightly younger one. Here the platy nature is replaced by a more blocky fracture. The rest of the sample characteristics are the same as the first sample.

Plagioclase and clinopyroxene are present as phenocrystic phases in both samples. In the first sample (CAU-1), almost all of the phenocrysts are plagioclase, with clinopyroxene only present in glomerophyres of clinopyroxene, plagioclase, and opaques. In the second flow, the majority of crystals are in glomerophyres, with less single crystals of plagioclase. This is also responsible for the phenocrystic modes rising from < 15% in the first flow to over 20% in the second flow. The phenocrysts

were unusually heavily resorbed. While all of the other lavas sampled had resorbtion features, none approached the high degree of reaction that all of the crystals exhibited in these samples. Both flows exhibit groundmass flow textures consisting of aligned plagioclase laths. Plagioclase is the most prominent groundmass phase, along with opaques and minor clinopyroxene and devitrified glass.

Both samples analyzed were groundmass separates and suffered argon recoil. The first sample (CAU-1) yielded a total gas age of 42.4 Ma, while the second sample (CAU-2) yielded a total gas age of 42.2 Ma. Isocron regression yielded ages of 42.0 ± 0.9 Ma and 42.9 ± 0.8 Ma respectively.

These ages fall within the age determined for the previous sample (CBU-2). With the lack of precision in these dates (due to argon recoil), the two sets of flows sampled seem to be coeval. This suggests either that any angular unconformity seen in the field represent very little time, or that there is no actual unconformity. However, there remains the possibility of sampling error once more. While the angle of dip of the beds was used as an indication of where the samples were located in the stratigraphy, this may instead have resulted in the sampling of similar units on the same side of the unconformity. If the later is the case, the orientation of the flows may have changed over the short sampling distance between the CBU and CAU samples.

Other Mitchell Area Intrusion

Several other intrusions in the Mitchell area were dated to better understand both their relation to the main volcanic formations, and their relation to the Mitchell Faulting event. Each one of the intrusions chosen has been previously studied, but no high-quality $^{40}Ar/^{39}Ar$ age date exists for them.

John Day Mafic Dike System

During the John Day period, volcanism shifted farther west to the western Cascades and the Smith Rock area. Yet in the Mitchell area, a series of basalt dikes was emplaced in echelon trending roughly east-west. A full description of the dike system, along with petrologic and geochemical data are available in Taylor's (1981) original paper.

Ed Taylor notes that that the dike system appears to have intruded into planes of weakness similar to the fault, but not the fault itself. Taylor also notes that the dikes do not show any signs of major offset, further indicating they were emplaced after the major faulting event. His interpretation is that the strike-slip faulting resulted in areas of tension that formed gash fractures. The dense basaltic magma was squeezed up into these fractures, forming the dike system. This would have had to occur shortly after faulting while the stress regime was still in place. This contradicts Oles and Enlows (1971) original hypothesis that one of the dikes was offset by the fault, indicating the faulting was younger than the dike system. However, field evidence suggests that instead the offset segments are two separate dikes rather than a single dike offset by the fault. To further refine the previous K/Ar ages on the dikes, several samples were collected to radiometrically date the dikes with the newer $^{40}Ar/^{39}Ar$ method.

Such a determination of the age of the Mitchell fault would be important. Through the Mitchell area, the entire Clarno and Cretaceous sections are cut by the fault. It appears that the older John Day units are also faulted, but that the younger John Day units are not. However, poor exposure of the fault in much of the John Day Formation leaves some question as to its exact timing. Therefore, these dikes offer an additional piece of evidence to further reinforce the field relations that suggest a middle-John Day movement.

One section of the dike system is easily accessible as it crosses Hwy 26 about 2 miles east of Mitchell (Keyes Creek Dike). The samples were taken just west of the cross-over, where the dike is just a few hundred feet north of the highway. Here the

dike is surrounded by Clarno mudflows that are much less resistant to erosion, resulting in the dike forming a sharp ridge.

The surface of the dike has weathered to a pinkish-reddish color, with random fractures that approach concoidal in nature. This is likely due to the fact that the dike is very glassy here. Despite its weathered appearance, the inside is still quite fresh, with a dark gray to black color. Two samples were taken here, about 50 feet apart, but there were no noticeable differences between the locales.

In thin section, the dike is extremely fine-grained with well-developed flow banding. While most of the rock is groundmass, about 3% of the rock is made up of small (< 0.5 mm) phenocrysts of plagioclase. These crystals are subhedral and display both polysynthetic twinning and zonation. There are a few trace clinopyroxene phenocrysts present, along with glomerophyres of tiny crystals in groundmass that suggest relict pyroxenes, but these account for much less than 1% of the rock. The groundmass is dominantly plagioclase (40%), magnetite (30%), and clinopyroxene (27%).

Due to the scarcity of phenocrysts, a groundmass separate was used to date the dike. The dike yielded a total gas age of 30.4 Ma (low due to argon recoil), and an isocron age of 34.1 ± 0.6 Ma. This age is consistent with previous work by Enlows and Parker (1972) on the Airport Dike, another section of the dike system, which reported ages of 33.3 ± 1.2 Ma and 33.5 ± 1.3 Ma. However, they report a younger age of 29.3 ± 0.5 Ma and 29.4 ± 0.6 Ma for the Nelson Creek section of the dike system. Both of these ages are whole rock analyses and were done using the older K/Ar method. Nonetheless, this clearly places the dikes within the John Day Formation and reinforces that magmatic activity continued in this area millions of years after the shift in the main volcanism further west. It also agrees with the conclusion of Taylor (1981) that the Mitchell faulting event took place around 34 Ma.

Lawson Mountain

Table 8.1: Bulk-rock analysis of Lawson Mountain

	EMT-73
SiO_2	68.8
Al_2O_3	16.0
FeO_T	4.1
CaO	3.7
MgO	1.0
K_2O	1.96
Na_2O	3.9
TiO_2	0.43
Total	99.9

Lawson Mountain is a large dacite intrusion or dome (Table 8.1) that trends northeast-southwest. The body is located either adjacent to, or within, the Mitchell fault. If the dome is adjacent to the fault rather than in it, then the fault runs along the north edge of the dome. This is just one of many silicic domes and intrusions that trend off to the west. It is likely that most of these silicic bodies are somehow related due to their alignment. One possibility is that they extend from a deeper large silicic batholith that runs the length of the intrusions. Another is that the fault has channeled the intrusions along it. To better understand the relation between the fault and Lawson Mountain, two samples were dated from it.

The samples (LM-1 and LM-2) were collected at the eastern edge of the summit. The samples are glassy dark gray dacite, with sparse feldspar phenocrysts. The outcrops exhibited columnar jointing, with columns of about 4-5 inches across. The columns had a light pinkish weathering rim a few millimeters thick on them.

The dacite contains between 3 and 5% subhedral alkali feldspar phenocrysts in a trachytic groundmass composed of opaques, amphiboles, feldspars, and quartz. The phenocrysts range from 1 to 3 mm in size and often exhibit Carlsbad twinning and zonation. Many of the phenocrysts also display microperthitic texture and have a spongy look from resorbtion. Additionally, many of the phenocrysts also show signs of alteration to calcite or clays. Amphibole is also present as a phenocrystic phase (< 1%), but many of the crystals show evidence of a breakdown reaction or resorbtion. One section even showed a glomerophyre of plagioclase and amphibole.

A groundmass separate from the sample was analyzed due to the questionable condition of the phenocrysts. The weakness of the glassy groundmass at retaining the K atoms during bombardment resulted in significant argon recoil once again. The sample yielded a total gas age of 18.6 Ma, although this was heavily weighted by the lowest temperature phase, which was clearly contaminated by atmospheric argon. The highest temperature steps allowed for a plateau age of 21.9 ± 0.1 Ma, with 20% of the ^{39}Ar gas.

It appears that the Lawson Mountain intrusion is younger than the fault. The difficulty in tracing the fault through the area may be due to the fact that the magma used the plane of weakness created by the fault to move through the crust and possibly erupt. This raises the question of whether the silicic intrusions/domes to the west are also John Day age and intruded along the fault. If this is the case, the line of silicic bodies may indicate the trace of the Mitchell fault along its poorly defined western extent.

Cougar Mountain

Located about 2 miles northwest of Black Butte and about a half of a mile east of Lawson Mountain, Cougar Mountain is a small hornblende-rich dacite intrusion (Table 8.2). It lies on the west side of the Mitchell anticline and just south of the Mitchell fault. It is the first in the line of silicic intrusions and domes mentioned above, indicating a possible relation between the butte and Lawson Mountain. As with Lawson Mountain, the age relation between the intrusion and the fault is not clear. However,

Table 8.2: Bulk-rock analysis of Cougar Mountain

	EMT-100
SiO_2	68.3
Al_2O_3	17.3
FeO_T	3.1
CaO	3.8
MgO	1.2
K_2O	1.52
Na_2O	4.3
TiO_2	0.58
Total	100.1

unlike Lawson Mountain, the fault appears to be traceable over the area running just north of the intrusion.

The sides of the butte are heavily vegetated with grass and small juniper, resulting in a few outcrops that are usually quite small and heavily weathered. The summit is covered by small outcrops and float. The weathered samples were bright pink with oxidized amphibole phenocrysts. The fresher samples are pinkish-gray, with about 15% amphibole phenocrysts and a few percent feldspar phenocrysts also present.

The abundant amphibole phenocrysts consist of heavily altered cores and coronas of opaque minerals. The altered cores are likely a result of weathering, while the opaque rims are a primary reaction reflecting depressurization of the magma as it ascends. The amphibole laths range in size from 2 to 3 mm. Due to the abundant alteration of the amphibole phenocrysts they were not usable for dating.

Alkali feldspar phenocrysts, probably anorthoclase, make up about 2% of the rock. These crystals are also 2 to 3 mm in size with euhedral facets. And similar to the amphibole, the feldspar has also undergone low-temperature alteration. Most crystals have clear, rounded cores, showing only Carlsbad twinning, surrounded by a zone of alteration, with mostly clear rims that restore the euhedral shape of the crystal. It is likely that the altered zone was chemically different than the rest of the crystal, causing a higher susceptibility to alteration. If this is the case, then the crystals display clear oscillatory zoning. The groundmass minerals range in size, but are all smaller than a millimeter. The most abundant phase is small subhedral feldspar laths that show abundant zonation. The rest of the groundmass is composed of anhedral quartz grains and opaques.

Due to the severe alteration of the amphibole phenocrysts, a date was obtained using a groundmass separate. This sample not only suffered from argon recoil, but also has evidence for ^{40}Ar loss also. The sample yielded a total gas age of 41.5 Ma, with no isocron age. The lower temperature steps yielded ages in the mid-30's Ma, while the majority of the steps yielded ages between 46-43 Ma. Since most of the data appear to be in the lower to middle 40's, it would appear that Cougar Mountain is related to the Clarno Formation. More importantly, it would appear the Cougar

Mountain and Lawson Mountain are not related. Its age also indicates that the intrusion predates the Mitchell Fault displacement by 10 Ma or more.

Discussion

Unfortunately even the $^{40}Ar/^{39}Ar$ method was not able to overcome all the problems and result in accurate and precise dates in the Mitchell area. All of the samples showed at least some weathering, which probably started soon after the lavas were deposited. Abundant mudflows and tropical paleosols from the period suggest it was a wet and warm climate into which these lavas were erupted. It is likely that abundant alteration seen throughout the Mitchell area began immediately in the Eocene and has continued ever since then.

Sadly, unlike many of the andesite intrusions, most of these lavas do not contain amphibole or other K-rich phases. This means that only whole rock dating of the groundmass is available. This resulted in massive argon recoil and a range of dates for a sample rather than a nice plateau. Therefore, while many of the sample dates can be used, none are of the precision and resolution needed to answer the persisting questions that plague not only the Clarno Formation, but also many of the other Eocene magmatic events throughout the western United States.

This does not preclude quality data from being assembled on the Clarno Formation. However, much effort will need to be spent determining better field relations and in finding better samples to date. One method may be to core samples from flows that are not exposed. If more recent weathering is significant in the samples previously collected, then cored samples would not as weathered, and would result in better dates. On the other hand, if most of the weathering took place during the Eocene, then even this would not provide better samples. Additionally, units with K-rich phenocrysts need to be sought out near the boundaries of the formation. Work done on this project using biotite and phlogopite separates were much more successful than any of the groundmass separates. Finally, higher quality equipment is becoming available that will allow an increased number of temperature steps (due to a need for

less gas in each step), and therefore a greater number of ages per sample. This will result in a greater number of usable steps making it easier to identify plateaus in the data. While useful information has been gained with the data presented here, better quality dates can still be quite valuable in understanding and defining the Clarno Formation.

Chapter 9: Conclusions

Marshall Butte and Corporate Butte are high-K calc-alkaline basanites emplaced between 52 and 46 Ma. They are distinguished by their lack of plagioclase and the abundance of groundmass nepheline. They are enriched in alkalis (Na, K) and incompatible trace elements. Normalized trace-element values indicate that the samples are enriched in HFSE compared to both LREE and LILE. This produces a convex-upward pattern with its peak at Nb in the spiderdiagrams. This pattern is commonly observed in ocean island basalts and is termed the HIMU-type OIB pattern. The pattern is also observed in silica-undersaturated rocks from active continental rift zones and in areas of post-subduction magmatism. Marshall and Corporate Buttes represent a partial melt of enriched asthenospheric mantle, with little or no lithospheric contamination or subduction input. Outside of ocean island plumes, the occurrence of this type of rock is most commonly linked to areas of extension. Extension results in lithospheric thinning and allows decompression melting of the asthenosphere. It also creates preferential pathways for deep-seated magma to reach the surface with little assimilation of lithospheric rocks.

Marshall and Corporate Buttes are not genetically related to the dominant calc-alkaline magmatism of the Clarno Formation. Crystal fractionation and AFC modeling using Marshall Butte as a parental melt, failed to account for either the most primitive basalts, or any of the more intermediate products. Likewise, primitive Clarno basalts reproduced the variety of Clarno rocks with only mild success. This agrees with both more recent work, and personal observation of the textures of the lavas, that favor formation by mixing and assimilation, with fractionation only significant in the most evolved suites.

The Hudspeth Mill Intrusion is group of alkali basalt bodies that intruded Clarno tuffs and mudflows 45.3 ± 0.31 million years ago. Its petrogenesis is dominated by crystal fractionation (olivine and clinopyroxene), interspersed with recharge events. The high Mg# (~72), high Cr (>780 ppm), and high Ni (235-340 ppm) indicate that

these are primitive magmas that have undergone little modification. The alkaline nature and trace-element characteristics (LILE, LREE enriched, HFSE depleted) reflect partial melting of metasomatized lithospheric mantle, with residual amphibole. While this melting may have been in response to subduction fluid-fluxing, it may also have resulted from progressive extension in the area that causes decompression melting of the lower lithosphere. The intrusion bears a general resemblance to other mafic alkaline magmatism active across the western U.S. during the Eocene, but is slightly less alkaline than absarokites and is less hydrous than the lamprophyres.

The Hudspeth Mill intrusion represents a distinct magma with a petrogenesis different from other intrusions or lavas belonging to the Clarno Formation. The suite is distinct from the common calc-alkaline rocks of the Clarno by increased abundances of alkalis and trace elements. These enrichments make a genetic relationship between the two groups unlikely. Likewise, while there are other alkaline suites related to the Clarno (Marshall/Corporate Buttes, lamprophyres), mineralogy and bulk-rock chemistry suggest different source regions and evolutionary paths. Since the intrusion likely postdated the major flux in calc-alkaline activity, it may suggest a shift in subduction parameters. However, calc-alkaline activity was present in the area until at least 43 Ma.

Two distinct sets of lamprophyric dikes, kersenatites and minettes, can be found associated with the Clarno Formation. These alkaline rocks were emplaced 50-48 Ma (49.0 ± 0.14– Black Butte area, 48.7 ± 0.17– Spetch Rim area, 47.8 ± 0.24– Mudcreek area), coeval with calc-alkaline rocks during the height of Clarno volcanism. These dikes are distinguished from other mafic dikes by the abundance of hydrous phenocryst phases (phlogopite), are divided on the basis of groundmass feldspar (alkali feldspar– minettes, plagioclase– kersantite). The dikes represent small-degree partial melts from within the lithosphere. The most commonly evoked lithospheric sources are ultra-potassic veins or bodies present in the lower lithosphere. The veins or bodies are augite and biotite-phyric with abundant amphibole and apatite also present. The existence of the lamprophyric dikes at shallow levels of the crust further indicates an extensional environment. Extension allows for both decompression melt-

ing of the alkaline bodies/veins and pathways for melt migration. The alkaline melts may have been further heated by (and possibly mixed with) asthenospheric melts similar to the basanite magma.

The alkaline magmas formed at a variety of locations: Marshall/Corporate Buttes from the asthenosphere and the lamprophyres and alkali basalt in the lithosphere (Figure 9.1). None of the suite needs direct chemical input (fluid fluxing) from subduction. This is most noticeable in Marshall Butte where there is no subduction signature, precluding a subduction input. In the case of the alkali basalt and the lamprophyres, a metasomatized source region is required. However, since the area had undergone previous subduction events, metasomatized lithosphere likely existed prior to Eocene subduction. So while alkaline rocks are often used as evidence of changing subduction parameters, these suites are instead related to the existence of heterogeneous mantle and differential sampling of it. In agreement with White and Robinson (1992), the emplacement of these alkaline suites is a further indication that the tectonics of the area were complex, and most likely included a strong component of extension.

The Scott Butte rhyolite dike is distinguished from other Clarno rhyolitic intrusions by the presence of euhedral garnet phenocrysts. The garnets are almandine-rich with low spessartine contents, inclusion-free, and often associated with quartz phenocrysts. The garnet crystallized with quartz at depths of 18-25 km from a silicic melt. Despite biotite phenocrysts, the mineralogy, textures, and shallow emplacement depth suggests a low volatile content in the ascending magma. This allowed it to rise to its upper crustal location without significant crystallization. Migration through the crust may also have been facilitated by extension, although the evidence from this study does not indicate whether extension was occurring this early. Due to garnet/quartz crystallization at depths of 18-25 km, the source region was located within the lowest portions of the crust. The Eocene crustal protolith would likely have been an accreted mélange of late Paleozoic and early Mesozoic ocean islands and oceanic crust. Due to the small volume of the dike, even the minor constituents of the metamorphic suites could have been the protolith. The most plausible explana-

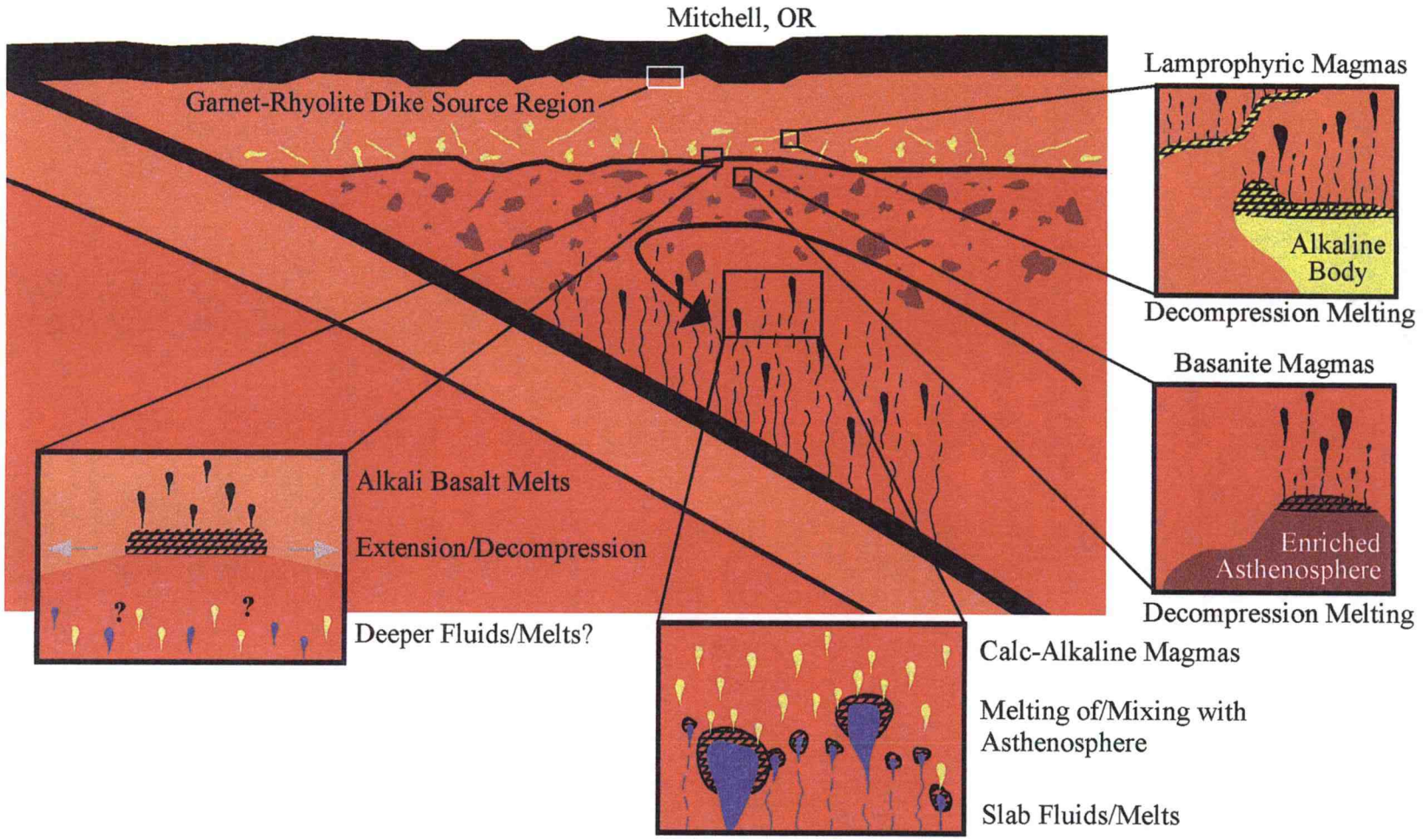

Figure 9.1: Simplified cross-section of the Mitchell area during the Eocene showing the source regions for the alkaline and calc-alkaline magmas.

tion for melting was in response to an injection of hot magma related to subduction. However, extension related decompression melting of previously metasomatized crust cannot be ruled out. This injection heated the surrounding crust, resulting in the silicic melt. The magma must have remained at depth, and hot, long enough for 1-2 mm garnet crystals to form.

New $^{40}Ar/^{39}Ar$ age determinations for the Clarno Formation were hampered by argon recoil and weathering of the samples. While the data were not precise enough for the detailed stratigraphic interpretations that they were originally intended, the data are still better than older K/Ar dates. It substantiates other data that indicate the Clarno was active ~ 60-40 Ma. In the Mitchell area, a flow from near the K-T boundary dates between 52-54 Ma, while samples from just below the contact with the John Day Formation indicate 42-43 Ma. Since sampling was done from stratigraphically low and high units on both sides of the Mitchell anticline, it was noted that the Mitchell anticline appears to have acted as a topographic high and separated the area. On the western side of the anticline, dates range from 54-42 Ma. On the eastern side, both the lowest and highest samples yielded age determinations between 49 and 51 Ma. While these dates are subject to imprecision, the fact that they are so similar indicates that only one sequence of eruptions may be represented in this area.

Other age determinations on Mitchell area intrusions have yielded important facts about the geologic history. The John Day mafic dike system is a series of basaltic dikes that cut across the Mitchell area. These dikes represent some of the youngest intrusive activity in the area, and are thought to be closely related in time and space to the Mitchell fault. The new age determination for the dike system (34.1 ± 0.6 Ma) agrees with older K/Ar determinations of ~ 33 ± 1 Ma, but is older than other ~ 29 Ma K/Ar dates of the dike system. If these dikes were emplaced shortly after the faulting, this indicates that the faulting occurred at about 34 Ma.

In the area of Lawson Mountain (a large dacite dome), the Mitchell fault is very difficult to trace. While the fault is well mapped east of the mountain, west of the mountain its trend is not clear. Since the dome seems to have extruded so near the fault, it is significant to determine if it predates the fault (causing the fault cut the

dome or to adjust its location) or postdates it (migrated upward along the fault's plane of weakness). Age determinations for the dome indicate that it was erupted ~ 22 Ma. This is considerably younger than the 34 Ma age of the fault. If the magma used the plane of the fault to migrate through the crust, it may explain why the fault trace disappears in the area of the mountain. It may also suggest that the line of silicic bodies trending off to the west may be John Day age and have intruded through the fault also. This would be significant since the fault has not been located through much of this area.

Cougar Mountain, a small hornblende-dacite intrusion, is located just east of Lawson Mountain. This is the first in a series of silicic intrusions (Lawson Mt. is the second) trending off to the west. Age determinations for Cougar Mountain were not conclusive, but seem to indicate an age in the lower 40's Ma. This places the intrusion into the Clarno Formation, and likely precludes any relation with Lawson Mountain.

While the focus of this study was to document and determine the petrogenesis of the alkaline and peraluminous suites, the findings have some significance to the tectonic interpretations of the Eocene in central Oregon. Both paleomagnetic and sedimentological analyses of the Clarno indicate that it was emplaced in an area undergoing extension. The presence of many of these alkaline suites, especially with asthenospheric sources not related to subduction-derived fluxing, is further evidence to support this conclusion.

The occurrence of coeval alkaline and calc-alkaline rocks in the Clarno Formation has not been documented previously. This work can be added to other recent publications that indicate that many of the magmatic provinces in the broader Eocene magmatic belt contain both alkaline and calc-alkaline rocks that are contemporaneous. This is of particular significance since the flat-slab or migrating arc theories commonly used to explain the magmatic belt are based primarily on alkalinity-slab depth relations, and temporal progressions of these rocks. With the help of more precise age determinations, the previously assumed spatial and temporal variations in alkalinity of the magmatism have become questionable. However, while in provinces

farther east recent works (Chapter 2) are suggesting the magmatism is not directly related to subduction, the Clarno as a whole is probably still subduction driven. Nevertheless, the tectonic setting and mechanics of magmatism are more complex than once thought.

References

Alibert, C., Leterrier, J., Panasiuk, M., Zimmermann, J.L., 1987, Trace and isotopic geochemistry of the alkaline Tertiary volcanism in southwestern Poland. Lithos, vol. 20, pp. 311-321.

Aldanmaz, E., Pearce, J.A., Thirlwall, M.F., Mitchell, J.G., 2000, Petrogenetic evolution of late Cenozoic, post-collision volcanism in western Anatolia, Turkey. Journal of Volcanology and Geothermal Research, vol. 102, pp. 67-95.

Ariskin, A.A., Frenkel, M.Y., Barmina, G.S., Nielsen, R.L., 1993, COMAGMAT; a Fortran program to model magma differentiation processes. Computers and Geosciences, vol. 19, pp. 1155-1170.

Armstrong, R. L., 1988, Mesozoic and Cenozoic magmatic evolution of the Canadian Cordillera. In Clark, S.P., Burchfiel, B.C., Suppe, J., eds, Processes in Continental Lithospheric Deformation. GSA Special Paper 218, pp. 55-91.

Baker, D.W., 1987, Central Montana Alkalic Province: critical review of Laramide plate tectonic models that extract alkalic magmas from abnormally thick Precambrian lithospheric mantle. Northwest Geology, vol. 20, pp. 71-95.

Baker, J.A., Gamble, J.A., Graham, I.J., 1994, The age, geology, and geochemistry of the Tapuaenuku Igneous Complex, Marlborough, New Zealand. New Zealand Journal of Geology and Geophysics, vol. 37, pp. 249-268.

Bestland, E.A., Hammond, P.E., Blackwell, D.L.S., Kays, M.A., Retallack, G.J., Stimac, J., 1999, Geologic framework of the Clarno Unit, John Day Fossil Beds National Monument, central Oregon. Oregon Geology, vol. 61, pp. 3-19.

Brophy, J.G., Whittington, C.S., Park, Y-R., 1999, Sector-zoned augite megacrysts in Aleutian high alumina basalts: Implication for the conditions of basalt crystallization and the generation of calc-alkaline series magmas. Contributions to Mineralogy and Petrology, vol. 135, pp. 277-290.

Carlson, D.H., Fleck, R., Moye, F.J., Fox, K.F., 1991, Geology, geochemistry, and isotopic character of the Coville Igneous Complex, Northeastern Washington. Journal of Geophysical Research, vol. 96, pp. 13,313-13,333.

Carmichael, I.S.E., Lange, R.A., Luhr, J.F., 1996, Quaternary minettes and associated volcanic rocks of the Mascota, western Mexico: a consequence of plate extension above a subduction modified mantle wedge. Contributions to Mineralogy and Petrology, vol. 124, pp. 302-333.

Cebriá, J.M, López-Ruiz, J., 1995, Alkali basalts and leucitites in an extensional intracontinental plate setting: The late Cenozoic Calatrava Volcanic Province (central Spain). Lithos, vol. 35, pp. 27-46.

Davis, L.L., Smith, D., McDowell, F.W., Walker, N.W., Borg, L.E., 1996, Eocene potassic magmatism at Two Buttes, Colorado, with implications for Cenozoic tectonics and magma generation in the western United States. Geological Society of America Bulletin, vol. 108, pp. 1567-1579.

Deer, W.A, Howie, R.A., Zussman, J., 1992, The Rock-Forming Minerals. Addison Wesley Longman Ltd., 2nd Edition.

Dostal, J., Robichaud, D.A., Church, B.N., Reynolds, P.H., 1998, Eocene Challis-Kamloops volcanism in central British Columbia: an example from the Buck Creek basin. Canadian Journal of Earth Sciences, vol. 35, pp. 951-963.

Dudás, F.O., 1991, Geochemistry of igneous rocks from the Crazy Mountains, Montana, and tectonic models for the Montana Alkalic Province. Journal of Geophysical Research, vol. 96, pp. 13,261-13,277.

Dudás, F.O., Harlan, S.S., 1999, An ancient depleted mantle sample from a 42-Ma dike in Montana: constraints on persistence of the lithosphere during Eocene magmatism. Journal of Geology, vol. 107, pp 287-299.

Enlows, H.E., Parker, D.J., 1972, Geochronology of the Clarno igneous activity in the Mitchell quadrangle, Wheeler County, Oregon. The Ore Bin, vol. 34, pp. 104-110.

Fitton, J.G., Upton, B.G.J., 1985, Alkaline igneous rocks: a review symposium. Journal of Geologic Society of London, vol.142, pp.697-708.

Dickinson, W.R., 1979, Cenozoic plate tectonic setting of the Cordilleran region in the United States. in Armentrout, J.M., Cole,M.R., Terbest, eds, Cenozoic paleogeography of the western United States. Society of Economic Paleontology and Mineralogy, Pacific Section, pp. 1-13.

Dickinson, W.R., Hatherton, T., 1967, Andesitic volcanism and seismicity around the Pacific. Science, vol. 157, pp. 801-803.

Gill, J.B., 1981, Orogenic Andesites and Plate Tectonics. Springer-Verlag, Heidelberg-New York, pp. 385.

Green, T.H., 1976, Experimental generation of cordierite or garent-bearing grantic liquids from a pelitic composition. Geology, vol. 2, pp. 85-88.

Green, T.H., 1977, Garnet in silicic liquids and its possible use as a P-T indicator. Contributions to Mineralogy and Petrology, vol. 65, pp. 59-67.

Green, T.H., Ringwood, A.H., 1968, Origin of garnet phenocrysts in calc-alkaline rocks. Contributions to Mineralogy and Petrology, vol. 18, pp. 163-174.

Gromme, C.S., Beck Jr., M.E., Wells, R.E., Engebretson, D.C., 1986, Paleomagnetism of the Tertiary Clarno Formation of central Oregon and its significance for the tectonic history of the Pacific Northwest. Journal of Geophysical Research, vol. 91, pp. 14,089-14,103.

Hart, W.K., Carlson, R.W., 1987, Tectonic controls on magma genesis and evolution in the northwestern United States. Journal of Volcanology and Geothermal Research, vol. 32, pp. 119-135.

Heller, P.L., Ryburg, P.T., 1983, Sedimentary record of subduction to forearc transition in the rotated Eocene basin of western Oregon. Geology, vol. 11, pp. 380-383.

Hill, R., Roeder, P., 1974, The crystallization of spinel from basaltic liquid as a function of oxygen fugacity. Journal of Geology, vol. 82, pp. 709-729.

Hilyard, M., Nielsen, R.L., Beard, J.S., Patinõ-Douce, A., Blencoe, J., 2000, Experimental determination of partitioning behavior of rare earth and high field strength elements between pargasitic amphibole and natural systems. Geochimica et Cosmochimica Acta, vol. 64, pp. 1103-1120.

Hiza, M.M., 1999, The geochemistry and geochronology of the Eocene Absaroka Volcanic Province, northern Wyoming and southwestern Montana, USA. PhD Thesis, Oregon State University.

Hole, M.J., 1988, Post-subduction alkaline volcanism along the Antarctic Peninsula. Journal of the Geological Society, London, vol. 145, pp. 985-998.

Hole, M.J., Rogers, G., Saunders, A.D., Storey, M., 1991, The relationship between alkalic volcanism and slab-window formation. Geology, vol. 19, pp. 657-660.

Hole, M.J., Kempton, P.D., Millar, I.L., 1993, Trace-element and isotopic characteristics of small-degree melts of the asthenosphere: Evidence from the alkalic basalts of the Antarctic Peninsula. Chemical Geology, vol. 109, pp. 51-68.

Johnson, D. M., Hooper P. R, Conrey R. M., 1999, XRF analysis of rocks and minerals for major and trace elements on a single low dilution Li-tetraborate fused bead. Advances in X-ray Analysis, vol. 41, pp. 843-867.

Kleinhans, L.C., Balcells-Baldwin, E.A., Jones, R.E., 1984, A paleogeographic reinterpretation of some Middle Cretaceous units, north-central Oregon: Evidence for a submarine turbidite system. In Nelsen, T.H., ed, Geology of the Upper Cretaceous Hornbrook Formation, Oregon and California, Pacific Section, Soc. Econ. Paleo. Min., vol. 42, pp. 239-257.

Lange, R.A., Carmichael, I.S.E., 1991, A potassic volcanic front in western Mexico: the lamprophyric and related lavas of San Sebastian. Geological Society of America Bulletin, vol. 103, pp. 928-940.

LaTourrette, T., Hervig, R.L., Holloway, J.R., 1995, Trace element partitioning between amphibole, phlogopite, and basanite melt. Earth and Planetary Science Letters, vol. 135, pp. 13-30.

Le Maitre, R.W., Bateman, P., Dudek, A., Keller, J., Lameyre Le Bas, M.J., Sabine, P.A., Schmid R., Sorensen, H., Streckeisen, A., Woolley, A.R., Zanettin, B., 1989, A classification of igneous rocks and glossary of terms. Blackwell, Oxford.

Lewis, R.S., Kiilsgaard, T.H., 1991, Eocene plutonic rocks in south central Idaho. Journal of Geophysical Research, vol. 96, pp. 13,295-13,311.

Lipman, P.W., 1980, Cenozoic volcanism in the western United States: Implication for continental tectonics. In Continental Tectonics, Studies in Geophysics, U.S. National Academy of Sciences, pp. 161-174.

MacDonald, R., Upton, B.G.J., Collerson, K.D., Hearn Jr., B.C., James, D., 1992, Potassic mafic lavas of the Bearpaw Mountains, Montana: mineralogy, chemistry, and origin. Journal of Petrology, vol. 33, pp. 305-346.

Marsh, B.D., Carmichael, I.S.E., 1974, Benioff zone magmatism. Journal of Geophysical Research, vol. 79, pp. 1196-1206.

Marvin, R.F. Hearn Jr., B.C., Mehnert, H.H., Naeser, C.W., Zartman, R.E., Linsey, D.A., 1980, Late Cretaceous-Paleocene-Eocene igneous activity in north central Montana. Isocron West, vol. 29, pp. 5-25.

McKenzie, D., 1989, Some remarks on the movement of small melt fractions in the mantle. Earth and Planetary Science Letters, vol. 95, pp. 53-72.

Meen, J.K., 1987, Formation of shoshintes from calc-alkaline basalt magmas: geochemical and experimental constraints from the type locality. Contributions to Mineralogy and Petrology, vol. 97, pp. 333-351.

Nielsen, R.L., 1990, The use of simulated data sets for the evaluation of the sensitivity of Pearce element ratio analysis. in Russell, J.K. and Stanley, C.R., eds., Theory and application of Pearce Element Ratios to geochemical data analysis. vol. 8, pp. 157-178.

Nielsen, R.L., DeLong, S.E., 1992, A numerical approach to modeling boundary layer fractionation: Application to differentiation in natural open magma systems. Contributions to Mineralogy and Petrology, vol. 110, pp. 355-369.

Nielson, D.R., Stoiber, R.E., 1973, Relationship of potassium content of andesitic lavas and depth to the seismic zone. Journal of Geophysical Research, vol. 78, pp. 6887-6892.

Noblett, J.B., 1981, Subduction-related origin of the volcanic rocks of the Eocene Clarno Formation near Cherry Creek, Oregon. Oregon Geology, vol. 43, pp. 91-99.

Norman, M.D., Mertzman, S.A., 1991, Petrogenesis of challis volcanics from central and southwestern Idaho: trace element and Pb isotopic evidence. Journal of Geophysical Research, vol. 96, pp. 13,279-13,293.

O'Brien, H.E., Irving, A.J., McCallum, I.S., 1988, Complex zoning and resorption of phenocryst in mixed potassic mafic magmas of the Highwood Mountains, Montana. American Mineralogist, vol. 73, pp. 1007-1024.

O'Brien, H.E., Irving, A.J., McCallum, I.S., 1991, Eocene potassic magmatism in the Highwood Mountains, Montana: petrology, geochemistry, and tectonic implications. Journal of Geophysical Research, vol. 96, pp. 13,237-13,260.

O'Brien, H.E., Irving, A.J., McCallum, I.S., Thirlwall, M.F., 1995, Strontium, neodymium, and lead isotopic evidence for the interaction of post-subduction asthenospheric potassic mafic magmas of the Highwood Mountains, Montana, USA, with ancient Wyoming craton lithospheric mantle. Geochemica et Cosmochimica Acta, vol. 59, pp. 4539-4556.

Oles, K.F., 1973, Hudspeth and Gable Creek Formations, in: Geologic field trips in northern Oregon and southern Washington. Oregon Department of Geology and Mineral Industries, Bulletin 77, p. 2-14.

Oles, K.F., Enlows, H.E., 1971, Bedrock geology of the Mitchell Quadrangle, Wheeler County, Oregon. Department of Geology and Mineral Industries, State of Oregon, Bulletin 72.

Paslick, C., Halliday, A., James, D., Dawson, J.B., 1995, Enrichment of the continental lithosphere by OIB melts: Isotopic evidence from the volcanic province of northern Tanzania. Earth and Planetary Science Letters, vol. 130, pp. 109-126.

Pearce, J.A., 1982, Trace element characteristics of lavas from destructive plate boundaries. in Thorpe, R.S., eds, Andesites. John Wiley and Sons, New York, pp. 526-548.

Plank, T., Langmuir, C.H., 1998, The chemical composition of subducting sediment and its consequences for crust and mantle. Chemical Geology, vol. 145, pp. 325-394.

Prestvik, T., Torske, T., Sundvoll, B., Karlsson, H., 1999, Petrology of early Tertiary nephelinites off mid-Norway: Additional evidence for an enriched endmember of the ancestral Iceland plume. Lithos, vol. 46, pp. 317-330.

Ringwood, A.E., 1975, Composition and petrology of the earth's mantle. McGraw-Hill, New York, pp. 618.

Robinson, P.T., Brem, G.F., McKee, E.H., 1984, John Day Formation of Oregon: A distal record of early Cascade volcanism. Geology, vol. 12, pp. 229-232.

Rock, N.M.S., 1977, The nature and origin of lamprophyres: Some definitions, distinctions, and derivations. Earth Science Reviews, vol. 13, pp. 123-169.

Roeder, P.L., Emslie, R.F., 1970, Olivine-liquid equilibrium. Contributions to Mineralogy and Petrology, vol. 29, pp. 275-289.

Rogers, J.J.W., Novitsky-Evans, J.M., 1977, The Clarno Formation of central Oregon, USA: Volcanism on a thin continental margin. Earth and Planetary Science Letters, vol. 34, pp. 55-66.

Rogers, J.J.W., Ragland, P.C., 1980, Trace elements in continental-margin magmatism: 1. Trace elements in the Clarno Formation of central Oregon and the nature of the continental margin on which eruption occurred. Geological Society of America Bulletin, vol. 91, part 1: pp. 196-198, part 2: pp. 1217-1292.

Stone, M., 1988, The significance of almandine garnets in the Lundy and Dartmoore granites. Mineralogical Magazine, vol. 52, pp. 651-658.

Stormer, J.C, Nicholls, J., 1978, XLFRAC: A program for the interactive testing of magmatic differentiation models. Computers and Geosciences, vol. 4, pp. 143-159.

Suayah, I.B., 1990, Rb-Sr systematics in lava flows of the Clarno Formation in north-central Oregon: Chronologic and petrologic significance. Isochron/West, vol. 56, pp. 24-29.

Suayah, I.B., Rogers, J.J.W., 1991, Petrology of the lower Tertiary Clarno Formation in north-central Oregon: The importance of magma mixing. Journal of Geophysical Research, vol. 96, pp. 13,357-13,371.

Sun, S.s., McDonough, W.F., 1989, Chemical and isotopic systematics of oceanic basalts: implications for mantle compositions and processes. In Saunders,A.D. and Norry,M.J., eds, Magmatism in the Ocean Basins. Geological Society Special Publication 42, pp. 313-345.

Swanson, D.A., 1969, Lawsonite blueschist from north-central Oregon. U.S. Geol. Survey Prof. Paper 650, pp. 8-11.

Taylor, E.M, 1981, A mafic dike system in the vicinity of Mitchell, Oregon, and its bearing on the timing of Clarno-John Day volcanism and early Oligocene deformation in central Oregon. Oregon Geology, vol. 43, pp. 107-112.

Tepley III, F.J., Davidson, J.P., Clynne, M.A., 1999, Magmatic interactions as recorded in plagioclase phenocrysts of Chaos Crags, Lassen Volcanic Center, California. Journal of Petrology, vol. 40, pp. 787-806.

Tingey, D.G., Christiansen, E.H., Best, M.G., Ruiz, J., Lux, D.R., 1991, Tertiary minette and melanephelinite dikes, Wasatch Plateau, Utah: records of mantle heterogeneities and changing tectonics. Journal of Geophysical Research, vol. 96, pp. 13,529-13,544.

Thompson, R.N., Leat, P.T., Dickin, A.P., Morrison, M.A., Hendry, G.L., Gibson, S. A., 1989, Strongly potassic mafic magmas from lithospheric mantle sources during continental extension and heating: evidence from Miocene minettes of northwestern Colorado, USA. Earth and Planetary Science Letters, vol. 98, pp. 139-153.

Wannamaker, P.E., Hulen, J.B., Heizler, M.T., 2000, Early Miocene lamproite from the Colorado Plateau tectonic province, southeastern Utah, USA. Journal of Volcanology and Geothermal Research, vol. 96, pp. 175-190.

White, J.D.L., Robinson, P.T., 1992, Intra-arc sedimentation in a low-lying marginal arc, Eocene Clarno Formation, central Oregon. Sedimentary Geology, vol. 80, pp. 89-114.

Woodhead, J.D., 1996, Extreme HIMU in an oceanic setting: the geochemistry of Mangaia Island (Polynesia), and temporal evolution of the Cook-Austral hotspot. Journal of Volcanology and Geothermal Research, vol. 72, pp. 1-19.

Appendices

Appendix 1: Bulk Compositional Data by Suite

Marshall Butte

	E-20-77	E-2-78	E-3-78	E-4-78	E-5-78	KFO-1701b	KFO-1701a	EMT-3	EMT-77
(wt %)	Old XRF	Old XRF	Old XRF	Old XRF	Old XRF	Old XRF	Old XRF	Old XRF	Old XRF
SiO_2	45.5	45.5	45.5	47.5	48.3	46.6	47	45.5	51
Al_2O_3	11.8	11.6	11.1	12.1	13.2	12.5	12.6	12.6	13.4
TiO_2	2.25	2.45	2.45	1.9	1.85	1.9	1.9	2.45	0.95
Fe*	9.8	10	10	9.7	9.8	9.9	9.7	10	10.2
MnO									
CaO	13.2	13	13	11.4	11.6	11.3	11.8	13.5	10.4
MgO	10.6	11.2	11.3	11.3	9.2	11.6	11	11.6	12.2
K_2O	1.35	1.2	1.3	1.55	1.55	1.75	1.75	1.25	0.2
Na_2O	3.9	3.9	3.8	3.7	3.6	4	3.9	3.8	1.9
P_2O_5									
Total	98.4	98.85	98.45	99.15	99.1	99.55	99.65	100.7	100.25
(ppm)									
Li									
Sc									
V									
Cr									
Co									
Ni									
Cu									
Zn									
Ga									
Rb									
Sr									
Y									
Zr									
Nb									
Cs									
Ba									
La									
Ce									
Pr									
Nd									
Sm									
Eu									
Gd									
Tb									
Dy									
Ho									
Er									
Tm									
Yb									
Lu									
Hf									
Ta									
Pb									
Th									
U									

(Marshall Butte cont.)

	EMT-77	EMT-166	EMT-167	EMT-168	EMT-169	EMT-169	MB-1	MB-1	MB-2
(wt %)	ICP-AES	Old XRF	Old XRF	Old XRF	Old XRF	ICP-AES	New XRF	ICP-MS	New XRF
SiO_2	48.51	47.5	46	46.5	46	43.16	43.10		43.31
Al_2O_3	12.40	12.7	12.1	11.2	11.4	11.25	11.03		11.33
TiO_2	0.92	1.95	2.4	2.55	2.3	2.47	2.591		2.532
Fe*	11.22	9.4	9.7	10.2	10	11.64	10.37		10.39
MnO	0.18					0.19	0.185		0.216
CaO	10.15	11.8	13	13.2	13	13.85	13.94		13.54
MgO	14.85	11	11	11	11.8	12.05	12.42		12.07
K_2O	0.32	1	1.7	1.2	1	0.80	1.08		1.00
Na_2O	1.59	4.5	2.9	3.7	3.7	3.44	3.53		3.41
P_2O_5	0.14					0.84	0.898		0.899
Total	100.29	99.85	98.8	99.55	99.2	99.68	99.14		98.69
(ppm)		INAA							
Li								14	
Sc	38.9	32.2				31.9	31	34.5	29
V	249	295				299	318	341	315
Cr	938	510				468	438	483	443
Co								52	
Ni	349	180				208	192	257	201
Cu	97					108	97	111	90
Zn	83					90	94	112	92
Ga							17		18
Rb		19					18	17.3	18
Sr	268	1480				1148	1064	1115	1038
Y	16					24	24	25	23
Zr	68					221	224	238	225
Nb							†143	147	†147
Cs								0.59	
Ba	125	1130				954	893	906	939
La		88					92	85	81
Ce		161					139	152	145
Pr								16.6	
Nd								63.8	
Sm								10.4	
Eu								2.94	
Gd								8.7	
Tb								1.1	
Dy								5.3	
Ho								0.90	
Er								2.1	
Tm								0.30	
Yb								1.80	
Lu								0.26	
Hf								5.4	
Ta								7.7	
Pb							3	9	3
Th		8					10	9.0	7
U								2.04	

† - denotes values >120% of highest standard.

Fe* - total Fe expressed as FeO for XRF and Fe_2O_3 for ICP-AES.

(Marshall Butte cont.)

(wt %)	MB-2 ICP-AES	MB-2 ICP-MS	MB-3 New XRF	MB-3 ICP-AES	MB-3r ICP-AES	MB-3 ICP-MS	MB-4 New XRF	MB-4 ICP-MS
SiO_2	43.13		42.65	42.36	41.98		45.30	
Al_2O_3	11.37		11.32	11.30	11.35		12.19	
TiO_2	2.53		2.592	2.56	2.51		2.025	
Fe*	11.46		10.52	11.56	11.30		10.20	
MnO	0.23		0.195	0.20	0.20		0.181	
CaO	13.56		13.98	13.73	13.53		13.49	
MgO	12.16		12.40	11.87	11.91		11.03	
K_2O	0.96		0.99	0.97	0.98		0.49	
Na_2O	3.37		3.61	3.66	3.56		2.26	
P_2O_5	0.83		0.914	0.87	0.85		0.810	
Total	99.60		99.17	99.09	98.17		97.98	
(ppm)								
Li		16				12		9
Sc	33.3	32.7	30	33.1	34.7	33.1	31	31.7
V	305	332	297	310	317	335	273	314
Cr	484	464	438	449	452	452	478	471
Co		52				50		48
Ni	210	264	191	180	199	239	194	240
Cu	96	97	98	104	102	113	86	97
Zn	94	122	90	95	95	112	92	118
Ga			20				17	
Rb		18.4	17			17.7	17	16.4
Sr	1035	1054	1005	1008	1023	1063	†1669	1629
Y	24	26	24	25	25	26	24	25
Zr	221	237	225	232	230	240	203	203
Nb		149	†149			151	†135	133
Cs		0.99				0.61		0.56
Ba	926	907	769	747	756	782	921	872
La		84	97			88	76	81
Ce		154	164			165	134	144
Pr		16.5				17.3		15.1
Nd		63.4				66.6		56.9
Sm		10.5				10.7		9.2
Eu		2.96				3.03		2.60
Gd		8.5				8.8		7.8
Tb		1.0				1.1		0.9
Dy		5.3				5.4		5.0
Ho		0.92				0.91		0.88
Er		2.2				2.2		2.1
Tm		0.31				0.32		0.31
Yb		1.83				1.84		1.87
Lu		0.27				0.27		0.28
Hf		5.3				5.5		4.4
Ta		7.7				8.3		6.5
Pb		7	5			9	10	9
Th		9.1	11			9.6	6	7.9
U		3.08				2.30		1.93

† - denotes values >120% of highest standard.

Fe* - total Fe expressed as FeO for XRF and Fe_2O_3 for ICP-AES.

Corporate Butte

	EMT-25	EMT-25	EMT-149	EMT-149	CB-1	CB-1	CB-1
(wt %)	Old XRF	ICP-AES	Old XRF	ICP-AES	New XRF	ICP-AES	ICP-MS
SiO_2	47.2	42.61	48.5	43.99	44.06	43.66	
Al_2O_3	12.3	11.26	11.8	15.06	11.35	11.05	
TiO_2	1.95	2.26	2.1	2.29	2.297	2.25	
Fe*	9.8	10.83	10	10.80	9.87	11.00	
MnO		0.19		0.17	0.189	0.19	
CaO	12.8	14.36	13.9	14.50	14.67	14.57	
MgO	11.3	11.54	9.2	9.01	11.30	11.68	
K_2O	1.25	1.10	1	0.83	1.21	1.14	
Na_2O	3.6	3.09	3.8	3.68	3.40	3.19	
P_2O_5		0.78		0.82	0.836	0.76	
Total	100.2	98.01	100.3	101.13	99.19	99.49	
(ppm)	INAA						
Li							9
Sc	29.9	35.9		37.0	29	36.3	33.4
V	268	321		314	313	321	320
Cr	331	461		485	423	459	434
Co							46
Ni	110	150		136	152	150	198
Cu		121		130	120	117	115
Zn		91		88	83	91	100
Ga					15		
Rb	39				30		29.2
Sr	1120	1663		959	1218	1123	1180
Y		24		25	23	24	24
Zr	170	195		199	194	198	203
Nb					†140		143
Cs							0.54
Ba	980	904		839	1079	950	1030
La	72.7				84		77
Ce	138				145		140
Pr							15.3
Nd							55.8
Sm							9.1
Eu							2.58
Gd							7.6
Tb							1.0
Dy							4.8
Ho							0.82
Er							2.1
Tm							0.32
Yb							1.83
Lu							0.28
Hf							4.4
Ta							7.0
Pb					4		8
Th	8				7		7.7
U							1.87

† - denotes values >120% of highest standard.

Fe* - total Fe expressed as FeO for XRF and Fe_2O_3 for ICP-AES.

Hudspeth Mill Intrusion

(wt %)	E-7-78 Old XRF	E-8-78 Old XRF	E-9-78 Old XRF	E-10-78 Old XRF	E-11-78 Old XRF	E-12-78 Old XRF	E-13-78 Old XRF	EMT-43 INAA	EMT-43 ICP-AES
SiO_2	50.8	52	51.1	50.9	51	49.8	51.2		49.26
Al_2O_3	12.7	14.9	12.8	12.8	12.6	12.2	12.7	12.1	11.55
TiO_2	0.9	1.05	0.95	0.9	0.9	0.85	0.9	1.23	0.97
Fe*	8.3	7.1	8.2	8	8.2	8.2	8	8.54	9.21
MnO								0.168	0.15
CaO	9.7	9.5	9.8	9.9	9.4	9.8	9.8	8.5	10.66
MgO	11.3	8.6	11.6	12.2	12	12.8	12.5	10.8	13.58
K_2O	2.5	3.3	3.2	2.55	2.65	2.3	2.45		2.26
Na_2O	2.4	2.4	2.3	2	2.1	2.2	2	2.19	1.92
P_2O_5									0.65
Total	98.6	98.85	99.95	99.25	98.85	98.15	99.55		100.21
(ppm)									
Li									
Sc								32.9	32.8
V								263	251
Cr								710	870
Co									
Ni								220	259
Cu									83
Zn									86
Ga									
Rb								83	
Sr								470	498
Y									36
Zr								210	169
Nb									
Cs									
Ba								460	446
La								31.8	
Ce								69	
Pr									
Nd									
Sm									
Eu									
Gd									
Tb									
Dy									
Ho									
Er									
Tm									
Yb									
Lu									
Hf									
Ta									
Pb									
Th								3	
U									

† - denotes values >120% of highest standard.
Fe* - total Fe expressed as FeO for XRF and Fe_2O_3 for ICP-AES.

(Hudspeth Mill Intrusion cont)

	EMT-171	EMT-172	EMT-172	HM-1	HM-1	HM-2	HM-2	HM-2r	HM-2
(wt %)	Old XRF	Old XRF	ICP-AES	New XRF	ICP-MS	New XRF	ICP-AES	ICP-AES	ICP-MS
SiO_2	50.8	52.5	49.47	48.46		49.44	49.37	48.71	
Al_2O_3	12.8	12.9	12.64	12.13		12.38	12.33	12.28	
TiO_2	0.95	0.95	1.03	1.015		1.032	1.04	1.01	
Fe*	8	7.8	9.35	8.50		8.36	9.47	9.09	
MnO			0.16	0.154		0.154	0.16	0.15	
CaO	9.6	10	10.14	10.02		10.16	10.11	10.15	
MgO	11.8	11.2	11.80	12.20		12.19	12.71	12.42	
K_2O	2.55	2.5	2.44	2.36		2.60	2.52	2.47	
Na_2O	2	2	1.77	2.09		2.23	2.21	2.17	
P_2O_5			0.76	0.760		0.770	0.71	0.70	
Total	98.5	99.85	99.56	97.69		99.31	100.61	99.17	
(ppm)									
Li					12				13
Sc			34.7	35	32.8	34	32.4	32.9	33.7
V			271	265	291	260	267	267	308
Cr			864	841	644	788	810	813	629
Co					47				48
Ni			249	273	340	245	236	241	325
Cu			87	84	87	86	88	82	93
Zn			91	86	97	85	88	88	103
Ga				15		16			
Rb				83	84.1	91			97.3
Sr			711	557	558	531	529	518	577
Y			39	37	38	37	39	38	40
Zr			189	173	180	179	184	182	192
Nb				9.2	11	10.4			11
Cs					3.30				2.49
Ba			546	489	485	583	583	583	594
La				35	32	42			35
Ce				79	71	66			78
Pr					10.1				10.5
Nd					48.0				52.0
Sm					12.4				13.6
Eu					3.72				4.08
Gd					11.5				12.3
Tb					1.6				1.7
Dy					7.6				8.1
Ho					1.24				1.38
Er					3.1				3.0
Tm					0.41				0.39
Yb					2.37				2.34
Lu					0.35				0.35
Hf					4.0				4.4
Ta					0.5				0.6
Pb				0	6	4			6
Th				4	2.5	2			2.8
U					1.47				1.77

† - denotes values >120% of highest standard.

Scott Butte Rhyolite Dike

	GRD-1	EMT-16	EMT-16	EMT-1600	EMT-268	SB-1	SB-1
	Old XRF	Old XRF	ICP-AES	Old XRF	ICP-AES	New XRF	ICP-AES
SiO_2	76.2	75	76.20	75.4	75.96	75.26	77.23
Al_2O_3	15	14.4	14.65	14.1	14.61	14.95	15.31
TiO_2	0.07	0.05	0.07	0.05	0.06	0.063	0.08
Fe*	1.07	1.8	1.76	2.5	1.25	0.62	0.74
MnO	0.01		0.01		0.01	0.006	0.00
CaO	1.07	1	0.93	0.9	1.14	0.90	0.82
MgO	0.56	0.6	0.64	0.5	0.49	0.77	0.74
K_2O	2.58	2.35	2.48	2.55	2.44	2.34	2.39
Na_2O	3.42	4.5	3.91	4	3.52	3.11	3.12
P_2O_5	0.06		0.06		0.05	0.082	0.05
Total	99.98	99.7	100.71	100	99.52	98.10	100.49
(ppm)	INAA						
Li							
Sc	0.96		1.1		0.6	2	0.7
V	7		4		6	0	4
Cr	1.4		9		9	0	14
Co							
Ni	20		0		0	8	0
Cu			0		13	2	2
Zn	33		34		18	37	27
Ga	16					15	
Rb	66					52	
Sr	182		171		203	210	213
Y	6		7		4	6	6
Zr	57		63		58	57	65
Nb	7.9					8.5	
Cs							
Ba	606		746		625	570	555
La	16.6					19	
Ce	37.9					44	
Pr							
Nd							
Sm							
Eu							
Gd							
Tb							
Dy							
Ho							
Er							
Tm							
Yb							
Lu							
Hf							
Ta							
Pb						6	
Th	4					2	
U							

† - denotes values >120% of highest standard.

Fe* - total Fe expressed as FeO for XRF and Fe_2O_3 for ICP-AES.

(Scott Butte Rhyolite Dike cont)

	SB-1	SB-2	SB-2
(wt %)	ICP-MS	New XRF	ICP-MS
SiO_2		75.91	
Al_2O_3		14.49	
TiO_2		0.058	
Fe*		0.72	
MnO		0.010	
CaO		1.14	
MgO		0.48	
K_2O		2.61	
Na_2O		3.56	
P_2O_5		0.099	
Total		99.07	
(ppm)			
Li	17		18
Sc	0.4	0	0.8
V	0	0	0
Cr	3	0	3
Co	0		0
Ni	0	9	0
Cu	3	6	5
Zn	35	21	25
Ga		17	
Rb	48.3	58	51.9
Sr	190	179	172
Y	4	5	5
Zr	30	52	29
Nb	7	7.5	7
Cs	2.03		2.06
Ba	554	653	632
La	20	18	17
Ce	36	43	33
Pr	3.9		3.5
Nd	13.4		11.9
Sm	2.4		2.1
Eu	0.43		0.42
Gd	1.7		1.6
Tb	0.2		0.2
Dy	1.0		1.0
Ho	0.15		0.17
Er	0.3		0.3
Tm	0.05		0.05
Yb	0.24		0.27
Lu	0.03		0.04
Hf	1.3		1.2
Ta	0.5		0.5
Pb	11	1	9
Th	3.7	2	2.7
U	1.29		0.95

† - denotes values >120% of highest standard.
Fe* - total Fe expressed as FeO for XRF and Fe_2O_3 for ICP-AES.

Black Butte and Spetch Rim Area Lamprophyres

	EMT-64	EMT-107	EMT-96	EMT-102	EMT-226	BB-1A	EMT-288	EMT-227	EMT-102
(wt %)	Old XRF	Old XRF	Old XRF	Old XRF	Old XRF	ICP-AES	ICP-AES	ICP-AES	ICP-AES
SiO_2	44.3	46.2	47.6	50.5	51.1	49.82	35.48	42.15	49.17
Al_2O_3	10.6	9.5	10.4	10.4	9.5	10.96	10.08	9.82	10.84
TiO_2	3.75	4.1	4.1	4.2	2.72	4.37	4.96	4.78	4.13
Fe*	10.4	5.1	8.4	6.9	8.26	12.29	13.44	15.27	12.41
MnO						0.13	0.74	0.55	0.13
CaO	12.2	14.2	14.2	8.6	11.43	8.63	18.23	11.84	7.53
MgO	7.6	5.8	4.9	8.5	8.7	6.72	9.43	9.64	8.88
K_2O	1.9	2.22	1.65	2.5	4.07	2.80	1.78	1.88	2.55
Na_2O	2.2	2.1	1.2	2.1	1.2	2.05	2.02	1.43	2.25
P_2O_5						1.53	2.79	2.22	1.45
Total	92.95	89.22	92.45	93.7	96.98	99.30	98.95	99.58	99.33
(ppm)									
Li									
Sc						23	32	29	24
V						389	497	467	363
Cr						552	358	340	449
Co									
Ni						554	581	511	419
Cu						586	803	772	494
Zn						215	267	333	188
Ga									
Rb									
Sr						1995	2756	2354	1973
Y						24	50	45	25
Zr						955	1238	1168	926
Nb									
Cs									
Ba						1467	1974	1936	1201
La									
Ce									
Pr									
Nd									
Sm									
Eu									
Gd									
Tb									
Dy									
Ho									
Er									
Tm									
Yb									
Lu									
Hf									
Ta									
Pb									
Th									
U									

† - denotes values >120% of highest standard.

Fe* - total Fe expressed as FeO for XRF and Fe_2O_3 for ICP-AES.

(Black Butte Lamprophyres cont)

	EMT-68
(wt %)	ICP-AES
SiO_2	48.04
Al_2O_3	11.87
TiO_2	4.67
Fe*	13.07
MnO	0.10
CaO	7.30
MgO	7.50
K_2O	2.51
Na_2O	2.26
P_2O_5	1.38
Total	98.72
(ppm)	
Li	
Sc	22
V	397
Cr	544
Co	
Ni	510
Cu	614
Zn	226
Ga	
Rb	
Sr	1880
Y	28
Zr	1045
Nb	
Cs	
Ba	1496
La	
Ce	
Pr	
Nd	
Sm	
Eu	
Gd	
Tb	
Dy	
Ho	
Er	
Tm	
Yb	
Lu	
Hf	
Ta	
Pb	
Th	
U	

Mudcreek Area Lamprophyres

	EMT-245	MC-1	MC-2	EMT-231
(wt %)	Old XRF	ICP-AES	ICP-AES	ICP-AES
SiO_2	47.3	54.91	51.41	47.55
Al_2O_3	12.3	12.57	11.93	13.25
TiO_2	1.89	2.23	2.21	2.51
Fe*	8.2	11.18	11.32	13.18
MnO		0.23	0.28	0.36
CaO	14.33	7.56	11.78	11.46
MgO	5.3	5.21	6.26	6.34
K_2O	2.42	2.63	2.63	2.51
Na_2O	2.2	2.27	2.32	2.30
P_2O_5		0.99	1.07	0.97
Total	93.94	99.79	101.21	100.44
(ppm)				
Li				
Sc		20	22	20
V		302	283	339
Cr		517	404	530
Co				
Ni		423	393	505
Cu		330	297	293
Zn		160	154	201
Ga				
Rb				
Sr		1789	1942	1648
Y		24	27	26
Zr		554	489	585
Nb				
Cs				
Ba		1083	1107	1157
La				
Ce				
Pr				
Nd				
Sm				
Eu				
Gd				
Tb				
Dy				
Ho				
Er				
Tm				
Yb				
Lu				
Hf				
Ta				
Pb				
Th				
U				

† - denotes values >120% of highest standard.

Fe* - total Fe expressed as FeO for XRF and Fe_2O_3 for ICP-AES.

Appendix 2: Microprobe Data for Specific Phases

Marshall Butte

Pryoxene

Label	Na_2O	MgO	Al_2O_3	SiO_2	CaO	TiO_2	Cr_2O_3	MnO	FeO	Total	En	Wo	Fs
MB-1.1_1	0.64	12.95	1.08	51.89	22.55	1.21	0.00	0.34	8.83	99.49	37.8	47.2	15.0
MB-1.1_2	0.51	14.17	4.08	49.68	23.48	2.06	0.00	0.16	6.10	100.24	41.0	48.8	10.2
MB-1.1_3	0.39	14.44	4.32	48.92	23.47	2.13	0.09	0.11	5.82	99.69	41.7	48.7	9.6
MB-1.1_4	0.36	15.61	3.21	50.65	23.32	1.50	0.56	0.15	4.55	99.91	44.6	47.9	7.5
MB-1.2_1	0.49	13.97	3.97	49.75	23.27	2.13	0.00	0.18	6.36	100.13	40.7	48.7	10.7
MB-1.2_2	0.38	13.96	5.03	48.14	23.44	2.29	0.05	0.12	6.08	99.51	40.7	49.1	10.1
MB-1.2_3	0.32	15.62	3.22	50.59	23.47	1.49	0.45	0.12	4.58	99.87	44.5	48.0	7.5
MB-1.2_4	0.30	16.00	2.58	51.76	23.53	1.15	0.70	0.11	4.03	100.15	45.4	48.0	6.6
MB-1.2_5	0.36	16.05	2.69	51.38	23.33	1.13	0.64	0.11	4.05	99.74	45.7	47.7	6.6
MB-1.3	0.60	12.35	7.47	44.39	22.91	3.13	0.00	0.15	7.83	98.82	37.1	49.5	13.4
MB-1.4	0.61	12.20	7.75	45.00	22.91	3.51	0.00	0.19	7.27	99.43	37.1	50.1	12.7
MB-1.5_1	0.51	12.46	7.60	45.58	23.13	3.29	0.00	0.14	6.82	99.53	37.8	50.4	11.8
MB-1.5_2	0.39	14.42	5.45	47.87	23.02	2.22	0.71	0.09	5.27	99.44	42.4	48.7	8.8
MB-1.5_4	0.31	15.81	2.80	51.51	23.38	1.33	0.31	0.10	4.40	99.96	45.0	47.8	7.2
MB-1.6	0.34	14.61	4.32	48.73	23.23	2.06	0.18	0.15	5.67	99.28	42.3	48.3	9.4
MB-1.7	0.34	15.82	2.65	51.90	23.67	1.23	0.54	0.12	4.16	100.42	44.9	48.3	6.8
MB-1.8_1	0.52	12.83	7.29	45.33	23.22	3.24	0.04	0.12	6.71	99.30	38.5	50.0	11.5
MB-1.8_2	0.39	14.85	4.55	49.17	23.47	1.62	0.64	0.11	4.76	99.54	43.1	49.0	7.9
MB-1.8_3	0.52	16.05	2.96	51.88	22.64	0.83	1.07	0.11	3.73	99.81	46.6	47.2	6.2
MB-1.8_4	0.62	15.22	4.11	50.54	22.27	1.17	0.94	0.11	4.37	99.35	45.1	47.4	7.5
MB-1.8_5	0.61	16.03	2.54	52.43	22.62	0.79	0.26	0.12	4.33	99.74	46.1	46.7	7.2
MB-1.8_6	0.49	13.51	5.66	47.86	23.48	2.21	0.24	0.12	5.93	99.48	40.0	50.0	10.1
MB-1.9	0.45	14.86	4.05	48.87	22.94	1.99	0.27	0.12	5.58	99.14	43.0	47.7	9.3
MB-1.10	0.61	13.18	5.57	47.08	22.50	2.76	0.03	0.19	7.58	99.50	39.1	48.0	12.9
MB-1.11_1	0.44	15.49	3.19	51.05	23.47	1.39	0.16	0.08	4.67	99.94	44.2	48.2	7.6
MB-1.11_2	0.49	12.83	7.02	46.46	23.19	3.00	0.03	0.12	6.48	99.62	38.7	50.2	11.1
MB-1.11_3	0.51	12.40	7.63	45.43	23.08	3.39	0.02	0.16	6.94	99.55	37.6	50.3	12.1
MB-1.12	0.53	11.58	9.10	42.91	22.95	4.10	0.04	0.13	7.75	99.08	35.6	50.8	13.6
MB-1.13	0.49	13.82	5.16	48.12	23.47	2.36	0.01	0.09	6.24	99.76	40.4	49.3	10.4
MB-1.14	0.48	12.78	7.24	45.71	23.24	3.11	0.00	0.13	6.77	99.47	38.3	50.1	11.6
MB-2.1_1	0.65	14.17	2.44	50.50	22.97	1.49	0.02	0.21	6.12	98.57	41.4	48.2	10.4
MB-2.1_2	0.32	14.42	4.24	49.01	23.41	2.01	0.06	0.10	5.58	99.16	41.9	48.9	9.3
MB-2.1_3	0.31	15.34	3.07	50.54	23.57	1.41	0.46	0.07	4.33	99.10	44.1	48.7	7.1
MB-2.1_4	0.35	15.90	2.61	51.41	23.45	1.10	0.62	0.06	3.85	99.34	45.5	48.2	6.3
MB-2.1_5	0.42	16.02	2.42	52.06	23.53	0.88	0.73	0.07	3.52	99.65	45.8	48.4	5.8
MB-2.2	0.53	12.91	6.54	47.01	22.53	2.88	0.17	0.14	6.33	99.04	39.4	49.5	11.1
MB-2.3	0.32	14.75	4.06	49.13	23.19	1.94	0.32	0.10	5.55	99.35	42.6	48.2	9.2
MB-2.4	0.57	13.17	4.89	48.35	23.01	2.45	0.04	0.16	6.26	98.90	39.5	49.6	10.8
MB-2.5	0.57	13.13	5.32	48.19	22.85	2.57	0.01	0.14	6.13	98.92	39.7	49.7	10.6
MB-2.6_1	0.52	12.01	8.73	44.12	23.17	3.86	0.02	0.10	6.58	99.10	37.1	51.4	11.6
MB-2.6_2	0.38	16.07	2.46	52.23	23.44	0.99	0.73	0.07	3.75	100.11	45.8	48.0	6.1
MB-2.6_3	0.28	15.82	2.76	51.61	23.52	1.12	0.69	0.08	3.93	99.81	45.2	48.3	6.4
MB-2.7	0.35	15.51	3.28	50.74	23.25	1.48	0.52	0.09	4.65	99.89	44.5	47.9	7.6
MB-2.8	0.45	14.25	4.32	48.94	23.24	2.08	0.03	0.09	5.70	99.11	41.7	48.8	9.5
MB-2.9	0.37	14.76	4.14	49.18	22.99	1.97	0.20	0.11	5.54	99.25	42.8	48.0	9.2
MB-2.10	0.38	14.25	4.36	49.27	23.22	2.06	0.04	0.06	5.57	99.20	41.8	48.9	9.3
MB-2.11_1	0.57	13.51	4.98	48.50	23.15	2.45	0.02	0.13	5.97	99.27	40.3	49.6	10.2
MB-2.11_2	0.45	14.89	4.00	49.56	23.16	1.94	0.17	0.06	5.36	99.57	43.1	48.1	8.8

Label	Na_2O	MgO	Al_2O_3	SiO_2	CaO	TiO_2	Cr_2O_3	MnO	FeO	Total	En	Wo	Fs
MB-2.11_3	0.36	15.88	2.52	52.10	23.36	1.03	0.72	0.09	3.85	99.91	45.5	48.1	6.3
MB-2.11_4	0.53	15.26	3.97	50.92	22.82	1.06	1.22	0.09	3.73	99.60	45.1	48.5	6.3
MB-2.11_5	0.57	15.44	3.74	51.24	23.02	1.05	1.17	0.08	3.83	100.12	45.2	48.4	6.4
MB-2.12_1	0.37	16.02	2.47	51.88	23.54	1.05	0.74	0.07	3.77	99.93	45.6	48.2	6.1
MB-2.12_2	0.51	14.95	4.02	50.14	23.24	1.37	1.07	0.06	4.24	99.60	43.9	49.0	7.1
MB-2.12_3	0.61	13.32	5.57	47.91	23.05	2.69	0.02	0.12	6.22	99.51	39.8	49.5	10.6
MB-2.13_1	0.58	13.88	4.24	49.10	23.17	2.20	0.01	0.14	6.00	99.31	40.8	49.0	10.1
MB-2.13_2	0.37	14.56	4.37	49.24	23.19	2.01	0.13	0.09	5.49	99.44	42.4	48.5	9.1
MB-2.13_3	0.33	15.75	2.76	51.37	23.52	1.19	0.73	0.09	3.96	99.72	45.1	48.4	6.5
MB-2.13_4	0.41	16.20	2.45	52.36	23.02	0.77	0.84	0.10	3.49	99.64	46.6	47.6	5.8
MB-2.13_5	0.54	15.23	4.01	50.77	22.81	1.11	1.25	0.09	3.79	99.60	45.1	48.5	6.4
MB-2.13_7	0.45	13.07	6.72	46.57	23.37	2.56	0.21	0.10	6.31	99.37	39.1	50.2	10.7
MB-2.14_1	0.61	11.44	8.88	44.21	22.93	3.48	0.00	0.11	7.25	98.90	35.7	51.4	12.9
MB-2.14_2	0.43	14.40	4.88	49.11	23.14	1.91	0.91	0.08	4.73	99.59	42.7	49.3	8.0
MB-2.14_3	0.30	15.91	2.46	52.13	23.50	1.02	0.67	0.09	3.79	99.87	45.5	48.3	6.2
MB-2.14_4	0.50	11.79	8.35	44.56	23.09	3.79	0.00	0.08	6.84	99.00	36.5	51.4	12.0
MB-2.15	0.45	14.95	3.56	50.07	23.48	1.59	0.47	0.09	5.00	99.66	43.1	48.7	8.2
MB-2.16	0.46	12.78	7.20	46.12	23.30	3.38	0.33	0.08	6.21	99.84	38.7	50.7	10.7
MB-2.17	0.51	12.72	7.33	46.22	23.05	3.13	0.64	0.08	5.99	99.67	38.9	50.7	10.4
MB-2.18_1	0.50	13.32	6.34	47.21	23.12	2.74	0.15	0.10	6.00	99.48	39.9	49.8	10.3
MB-2.18_2	0.37	14.57	4.34	49.49	23.44	1.98	0.06	0.11	5.48	99.84	42.2	48.8	9.1
MB-2.18_3	0.62	12.58	5.90	47.63	22.80	2.70	0.03	0.14	7.12	99.51	38.1	49.6	12.3
MB-2.19	0.45	12.63	7.69	45.52	23.01	3.54	0.12	0.08	6.47	99.50	38.5	50.4	11.2
MB-2.20	0.36	14.34	4.51	49.35	23.33	2.11	0.00	0.14	5.75	99.88	41.7	48.7	9.6
MB-2.21	0.42	13.49	5.80	48.08	23.43	2.52	0.02	0.10	6.00	99.86	40.0	49.9	10.1
MB-3.1_1	0.54	11.82	8.46	43.86	22.13	3.83	0.02	0.14	7.36	98.17	37.0	49.8	13.2
MB-3.1_2	0.48	12.45	7.19	45.86	22.45	2.88	0.05	0.14	7.05	98.53	38.2	49.5	12.4
MB-3.1_3	0.50	13.31	5.33	47.40	22.86	2.41	0.00	0.15	6.54	98.51	39.7	49.0	11.2
MB-3.2_1	0.74	11.31	3.21	48.62	21.68	2.43	0.00	0.31	9.63	97.93	34.8	48.0	17.2
MB-3.2_2	0.34	14.17	4.99	47.96	23.01	2.17	0.09	0.13	5.77	98.63	41.7	48.6	9.7
MB-3.2_3	0.41	12.94	6.89	45.89	22.56	2.90	0.02	0.10	6.26	97.96	39.5	49.6	10.9
MB-3.3_1	0.44	13.45	5.67	47.46	22.81	2.46	0.00	0.12	6.24	98.65	40.3	49.1	10.7
MB-3.3_2	0.40	13.48	6.10	47.42	22.83	2.43	0.05	0.10	6.00	98.80	40.5	49.3	10.3
MB-3.3_3	0.37	14.42	4.63	48.89	22.96	2.08	0.13	0.09	5.35	98.94	42.4	48.6	9.0
MB-3.3_4	0.33	15.64	2.96	50.93	23.05	1.30	0.46	0.11	4.39	99.17	45.0	47.7	7.3
MB-3.3_5	0.31	15.90	2.58	51.32	23.13	1.18	0.62	0.10	4.08	99.20	45.6	47.7	6.7
MB-3.4_1	0.51	12.46	6.73	46.04	22.94	2.97	0.04	0.14	6.87	98.69	37.9	50.1	12.0
MB-3.4_2	0.41	14.37	4.68	48.22	22.93	2.20	0.33	0.12	5.61	98.86	42.2	48.4	9.4
MB-3.4_3	0.52	11.87	8.14	44.11	22.50	3.78	0.01	0.13	7.31	98.37	36.8	50.2	13.0
MB-3.5_1	0.50	12.63	7.12	45.95	22.54	3.00	0.05	0.12	6.55	98.46	38.8	49.7	11.5
MB-3.5_2	0.57	14.28	4.70	48.87	22.21	1.47	0.48	0.10	5.35	98.05	42.9	47.9	9.2
MB-3.5_3	0.45	14.90	4.19	49.75	22.44	1.33	0.59	0.12	5.04	98.81	43.9	47.5	8.5
MB-3.5_4	0.50	15.49	3.42	50.60	22.62	0.94	1.31	0.10	4.04	99.01	45.5	47.7	6.8
MB-3.5_5	0.41	15.12	3.90	49.86	22.69	1.31	0.75	0.11	4.60	98.75	44.4	47.9	7.7
MB-3.6_1	0.50	12.61	7.13	45.32	22.70	2.99	0.01	0.16	6.48	97.90	38.6	50.0	11.4
MB-3.6_2	0.39	14.43	4.63	48.23	22.88	1.82	0.84	0.09	4.50	97.80	43.2	49.2	7.7
MB-3.6_3	0.28	15.56	2.64	50.50	23.15	1.23	0.51	0.10	4.10	98.07	45.0	48.1	6.8
MB-3.6_4	0.32	15.01	3.62	49.18	22.85	1.77	0.35	0.13	5.01	98.23	43.7	47.9	8.4
MB-3.7	0.43	14.09	4.66	48.89	23.26	2.20	0.03	0.12	5.91	99.60	41.2	48.9	9.9
MB-3.8	0.50	13.51	5.46	48.20	23.16	2.40	0.01	0.14	6.05	99.43	40.2	49.5	10.3
MB-3.9	0.62	11.25	9.07	43.12	22.68	4.28	0.01	0.15	7.52	98.69	35.3	51.2	13.5
MB-3.10	0.58	11.81	7.89	44.42	22.53	3.69	0.01	0.13	7.41	98.46	36.7	50.2	13.1
MB-3.11	0.55	12.88	5.98	46.59	22.63	2.54	0.00	0.15	6.66	97.98	39.1	49.3	11.6
MB-4.1_1	0.75	12.16	6.38	47.41	22.26	2.37	0.03	0.16	7.79	99.32	37.3	49.0	13.7

Label	Na_2O	MgO	Al_2O_3	SiO_2	CaO	TiO_2	Cr_2O_3	MnO	FeO	Total	En	Wo	Fs
MB-4.1_2	0.40	15.05	4.33	50.44	23.32	1.42	0.89	0.12	4.76	100.72	43.6	48.5	7.9
MB-4.1_3	0.41	14.89	4.74	49.95	23.23	1.56	0.74	0.10	5.09	100.71	43.2	48.4	8.4
MB-4.2	0.48	14.60	0.11	54.72	22.93	0.18	0.00	0.26	7.39	100.67	41.3	46.6	12.1
MB-4.3	0.64	11.52	9.04	45.05	22.36	3.20	0.00	0.15	8.28	100.25	35.7	49.7	14.6
MB-4.4	0.28	16.24	2.67	52.33	23.26	1.02	0.32	0.06	4.70	100.89	45.6	46.9	7.5
MB-4.5_1	0.60	12.84	5.86	47.27	22.98	2.20	0.00	0.17	7.51	99.43	38.2	49.0	12.8
MB-4.5_2	0.29	15.38	3.84	50.51	22.72	1.50	0.14	0.13	5.64	100.14	44.0	46.7	9.3
MB-4.5_3	0.34	16.43	2.38	52.64	23.08	0.95	0.65	0.08	4.37	100.92	46.3	46.7	7.0
MB-4.5_4	0.42	15.64	4.07	50.70	22.65	1.15	0.72	0.08	4.90	100.32	45.1	46.9	8.0
MB-4.5_5	0.29	16.27	2.38	52.77	23.32	0.89	0.36	0.08	4.40	100.77	45.8	47.1	7.1
MB-4.6	0.33	14.97	3.73	50.93	23.33	1.48	0.04	0.12	5.66	100.59	42.8	47.9	9.3
MB-4.7	0.53	12.47	7.35	46.35	22.22	2.77	0.02	0.17	8.49	100.35	37.5	48.0	14.6
MB-4.9_1	0.75	11.47	9.12	45.22	22.00	2.74	0.03	0.18	8.38	99.89	35.7	49.3	15.0
MB-4.9_2	0.48	14.39	5.32	49.59	22.84	1.70	0.25	0.08	5.77	100.41	42.2	48.2	9.6
MB-4.9_3	0.44	15.39	4.09	50.75	23.17	1.19	1.15	0.07	4.67	100.92	44.4	48.0	7.7
MB-4.9_4	0.49	16.25	3.09	52.32	22.93	0.82	1.03	0.10	3.86	100.89	46.5	47.2	6.3
MB-4.9_5	0.54	14.57	6.29	49.22	22.37	2.03	0.12	0.11	5.64	100.90	43.0	47.5	9.5
MB-4.10_1	0.46	13.33	7.20	47.06	22.74	2.78	0.06	0.12	6.51	100.27	39.9	48.9	11.1
MB-4.10_2	0.39	15.11	4.63	50.37	23.09	1.44	0.99	0.06	4.84	100.92	43.9	48.2	8.0
MB-4.10_3	0.33	16.43	2.31	52.93	23.26	0.85	0.77	0.08	4.18	101.12	46.2	47.0	6.7
MB-4.11	0.64	11.60	8.62	45.52	22.44	3.18	0.02	0.17	8.15	100.34	35.8	49.8	14.4
MB-4.12	0.35	15.42	3.48	51.36	22.80	1.34	0.03	0.10	5.74	100.63	43.9	46.7	9.3
MB-4.13	0.31	16.29	2.47	52.54	23.26	0.91	0.43	0.08	4.52	100.81	45.8	47.0	7.3
MB-4.14	0.68	11.52	8.47	45.63	22.79	2.97	0.04	0.17	7.86	100.11	35.6	50.5	13.9
MB-4.15	0.54	13.25	6.52	48.36	22.96	2.19	0.02	0.11	6.61	100.56	39.5	49.2	11.3
MB-4.16	0.61	11.94	8.36	45.69	22.52	3.17	0.00	0.15	7.89	100.33	36.6	49.6	13.8
MB-4.17_1	0.72	11.99	7.48	46.66	22.16	2.36	0.00	0.21	8.65	100.23	36.5	48.4	15.1
MB-4.17_2	0.46	15.70	3.37	51.75	23.14	0.90	1.14	0.08	4.11	100.65	45.3	48.0	6.8
MB-4.17_3	0.41	15.62	3.43	51.73	23.01	0.92	1.17	0.06	4.05	100.39	45.3	48.0	6.7
MB-4.17_4	0.45	15.90	3.33	51.85	23.02	0.86	1.09	0.07	3.90	100.46	45.9	47.7	6.4
MB-4.17_5	0.42	15.88	3.30	52.20	23.00	0.88	1.13	0.06	3.90	100.76	45.9	47.7	6.4
MB-4.17_6	0.48	15.48	3.51	51.58	22.70	0.87	1.15	0.07	3.98	99.81	45.4	47.9	6.7
MB-4.17_7	0.44	16.15	3.09	52.26	22.68	0.76	1.17	0.10	3.91	100.57	46.5	47.0	6.5
MB-4.17_8	0.33	16.28	2.28	53.04	23.11	0.84	0.66	0.07	4.03	100.64	46.3	47.2	6.5
MB-4.18	0.59	11.28	8.42	45.57	22.11	3.12	0.00	0.16	8.54	99.79	35.2	49.6	15.2
MB-4.19	0.62	11.04	8.56	44.52	23.04	3.28	0.00	0.11	8.04	99.22	34.3	51.5	14.2
MB-4.20	0.62	12.08	7.52	46.73	22.27	2.35	0.00	0.18	8.64	100.38	36.6	48.5	15.0
MB-4.21_1	0.70	12.48	6.23	48.39	22.50	2.03	0.01	0.18	7.14	99.67	38.1	49.4	12.5
MB-4.21_2	0.40	15.14	4.25	50.25	23.27	1.40	0.83	0.07	4.72	100.33	43.8	48.4	7.8
MB-4.21_3	0.39	15.01	4.05	50.62	23.49	1.39	0.60	0.10	4.76	100.41	43.4	48.8	7.9
MB-4.21_4	0.42	14.76	4.75	49.56	22.94	1.58	0.84	0.10	5.03	99.98	43.3	48.3	8.4
MB-4.21_5	0.43	15.18	4.49	50.59	23.03	1.41	0.95	0.10	4.71	100.90	44.1	48.1	7.8
MB-4.21_6	0.30	16.21	2.47	52.51	23.15	0.95	0.61	0.12	4.39	100.71	45.8	47.0	7.2
MB-4.21_7	0.29	16.12	3.59	51.44	21.15	0.89	0.52	0.08	5.05	99.13	47.1	44.4	8.4
MB-4.22_1	0.43	13.75	6.01	48.59	23.23	2.22	0.05	0.09	6.22	100.59	40.5	49.1	10.4
MB-4.22_2	0.31	16.19	2.28	52.84	23.46	0.89	0.50	0.11	4.21	100.79	45.6	47.5	6.8
MB-4.22_3	0.31	16.29	2.44	52.78	23.03	0.84	0.49	0.09	4.37	100.65	46.1	46.8	7.1
MB-4.22_4	0.31	16.30	2.33	52.79	23.45	0.88	0.50	0.08	4.16	100.80	45.9	47.4	6.7
MB-4.22_5	0.45	13.62	6.14	48.49	23.20	2.17	0.02	0.11	6.28	100.47	40.2	49.2	10.6
MB-4.23	0.59	12.51	6.20	47.90	22.30	2.27	0.00	0.19	8.26	100.22	37.6	48.2	14.3
MB-4.24	0.61	12.11	8.12	46.15	21.38	2.77	0.00	0.15	8.79	100.08	37.3	47.3	15.4
MB-4.25	0.40	14.79	5.22	49.11	21.00	1.74	0.08	0.17	7.25	99.75	43.5	44.3	12.2

Olivine

Label	Na_2O	MgO	Al_2O_3	SiO_2	CaO	TiO_2	Cr_2O_3	MnO	FeO	NiO	Total	Fo	Fa
MB-1.4	0.05	44.02	0.42	39.25	0.40	0.03	0.03	0.35	14.39	0.17	99.10	84.5	15.5
MB-1.5	0.03	44.04	0.04	38.92	0.39	0.01	0.04	0.37	15.25	0.16	99.24	83.7	16.3
MB-1.7	0.02	46.28	0.04	39.55	0.27	0.01	0.02	0.24	12.86	0.18	99.45	86.5	13.5
MB-1.8	0.02	46.90	0.03	39.73	0.26	0.00	0.02	0.18	12.13	0.22	99.50	87.3	12.7
MB-1.9	0.02	44.65	0.04	39.07	0.42	0.00	0.05	0.36	14.57	0.23	99.41	84.5	15.5
MB-1.10	0.02	46.24	0.05	39.56	0.33	0.00	0.02	0.24	13.03	0.21	99.71	86.3	13.7
MB-1.11	0.04	45.52	0.05	39.03	0.30	0.02	0.07	0.34	13.99	0.21	99.57	85.3	14.7
MB-1.12	0.05	44.92	0.03	39.66	0.25	0.01	0.10	0.31	13.86	0.21	99.40	85.2	14.8
MB-1.13	0.01	44.69	0.03	39.18	0.35	0.02	0.01	0.36	14.73	0.20	99.57	84.4	15.6
MB-1.14	0.05	45.43	0.03	39.22	0.31	0.01	0.04	0.30	13.68	0.24	99.30	85.5	14.5
MB-1.15	0.05	45.61	0.02	39.46	0.31	0.00	0.04	0.24	13.28	0.19	99.20	86.0	14.0
MB-1.16	0.02	43.87	0.03	38.83	0.41	0.01	0.04	0.41	15.40	0.16	99.19	83.5	16.5
MB-1.17	0.04	43.70	0.02	38.85	0.43	0.00	0.00	0.42	15.60	0.17	99.24	83.3	16.7
MB-2.3	0.03	45.08	0.02	38.91	0.32	0.03	0.03	0.32	13.75	0.17	98.65	85.4	14.6
MB-2.6_1	0.04	42.57	0.02	38.70	0.42	0.02	0.02	0.44	16.05	0.13	98.42	82.5	17.5
MB-2.6_2	0.04	43.35	0.01	38.89	0.34	0.02	0.01	0.38	15.30	0.16	98.49	83.5	16.5
MB-2.6_3	0.02	43.94	0.01	39.04	0.32	0.01	0.00	0.30	14.46	0.17	98.28	84.4	15.6
MB-2.6_4	0.03	40.91	0.47	38.21	0.84	0.05	0.00	0.47	17.44	0.09	98.52	80.7	19.3
MB-2.7_3	0.01	46.44	0.02	39.38	0.28	0.01	0.03	0.19	11.52	0.21	98.09	87.8	12.2
MB-2.7_4	0.03	45.90	0.13	39.19	0.32	0.01	0.04	0.19	12.32	0.20	98.32	86.9	13.1
MB-2.7_5	0.03	40.76	0.03	38.43	0.69	0.04	0.00	0.58	17.39	0.11	98.07	80.7	19.3
MB-2.8_2	0.04	46.21	0.04	39.54	0.34	0.01	0.04	0.22	12.10	0.25	98.79	87.2	12.8
MB-2.8_3	0.02	43.58	0.00	39.11	0.46	0.01	0.00	0.36	15.13	0.18	98.86	83.7	16.3
MB-2.8_4	0.57	15.13	3.70	49.71	22.86	1.05	1.22	0.07	3.72	0.02	98.06	87.9	12.1
MB-2.8_5	0.51	15.50	3.31	50.18	23.04	0.90	1.08	0.05	3.64	0.04	98.26	88.4	11.6
MB-2.8_6	0.66	11.50	7.85	43.69	23.03	3.72	0.06	0.13	6.95	0.07	97.66	74.7	25.3
MB-2.9_1	0.03	41.21	0.03	38.38	0.60	0.03	0.00	0.55	17.56	0.10	98.49	80.7	19.3
MB-2.9_2	0.03	42.88	0.03	38.78	0.29	0.02	0.02	0.43	15.94	0.21	98.62	82.7	17.3
MB-2.9_3	0.04	42.96	0.04	38.69	0.31	0.04	0.03	0.40	16.00	0.17	98.69	82.7	17.3
MB-2.10_2	0.04	47.53	0.03	40.21	0.31	0.00	0.05	0.21	11.17	0.26	99.81	88.4	11.6
MB-2.10_3	0.03	47.87	0.04	40.08	0.31	0.01	0.04	0.15	10.56	0.28	99.36	89.0	11.0
MB-2.10_4	0.06	47.51	0.05	39.83	0.30	0.02	0.07	0.16	10.83	0.26	99.08	88.7	11.3
MB-2.10_5	0.04	45.11	0.04	39.26	0.30	0.02	0.08	0.27	13.42	0.19	98.73	85.7	14.3
MB-2.10_6	0.03	42.02	0.03	38.45	0.55	0.01	0.01	0.48	17.08	0.11	98.77	81.4	18.6
MB-2.11_2	0.05	45.47	0.02	39.31	0.31	0.01	0.03	0.27	12.95	0.20	98.62	86.2	13.8
MB-2.11_3	0.04	47.52	0.02	39.92	0.31	0.01	0.10	0.16	10.32	0.27	98.66	89.1	10.9
MB-2.11_4	0.04	48.46	0.02	40.08	0.30	0.00	0.09	0.15	9.96	0.29	99.39	89.7	10.3
MB-2.11_5	0.03	47.69	0.02	39.98	0.31	0.00	0.03	0.15	10.85	0.23	99.29	88.7	11.3
MB-2.12_1	0.05	41.42	0.01	38.45	0.73	0.04	0.00	0.46	17.42	0.09	98.65	80.9	19.1
MB-2.12_2	0.02	45.16	0.04	39.39	0.33	0.01	0.11	0.29	13.40	0.19	98.92	85.7	14.3
MB-2.12_3	0.03	47.62	0.01	39.97	0.29	0.00	0.05	0.17	10.57	0.26	98.98	88.9	11.1
MB-2.12_4	0.05	48.43	0.04	39.95	0.30	0.00	0.02	0.12	9.60	0.26	98.77	90.0	10.0
MB-2.12_5	0.05	46.99	0.05	39.61	0.77	0.01	0.01	0.16	10.80	0.20	98.66	88.6	11.4
MB-3.1_1	0.02	42.72	0.04	38.64	0.72	0.09	0.02	0.44	16.40	0.12	99.21	82.3	17.7
MB-3.1_2	0.02	45.18	0.03	39.18	0.36	0.03	0.02	0.28	13.50	0.19	98.79	85.6	14.4
MB-3.1_3	0.04	46.50	0.03	39.54	0.28	0.00	0.04	0.23	11.95	0.20	98.82	87.4	12.6
MB-3.1_4	0.03	46.63	0.02	39.46	0.35	0.01	0.03	0.21	11.71	0.21	98.66	87.7	12.3
MB-3.1_5	0.02	45.90	0.03	39.38	0.48	0.01	0.02	0.29	12.45	0.22	98.81	86.8	13.2
MB-3.2_1	0.02	42.72	0.01	38.66	0.62	0.06	0.04	0.42	15.88	0.12	98.54	82.7	17.3
MB-3.2_2	0.02	43.64	0.17	38.93	0.38	0.00	0.01	0.32	14.82	0.14	98.44	84.0	16.0
MB-3.2_3	0.03	44.40	0.03	39.25	0.33	0.00	0.01	0.28	13.88	0.16	98.37	85.1	14.9
MB-3.2_4	0.01	44.53	0.01	39.01	0.32	0.01	0.02	0.33	14.23	0.18	98.65	84.8	15.2

Label	Na_2O	MgO	Al_2O_3	SiO_2	CaO	TiO_2	Cr_2O_3	MnO	FeO	NiO	Total	Fo	Fa
MB-3.3_1	0.04	43.53	0.02	38.85	0.65	0.03	0.02	0.38	15.12	0.16	98.80	83.7	16.3
MB-3.3_2	0.03	46.35	0.03	39.33	0.30	0.01	0.01	0.20	12.06	0.19	98.50	87.3	12.7
MB-3.3_3	0.01	46.97	0.04	39.53	0.28	0.01	0.13	0.19	11.27	0.19	98.63	88.1	11.9
MB-3.3_4	0.04	46.82	0.02	39.58	0.31	0.00	0.05	0.20	11.10	0.25	98.39	88.3	11.7
MB-3.3_5	0.04	46.45	0.02	39.35	0.29	0.00	0.05	0.23	11.88	0.20	98.52	87.5	12.5
MB-3.3_6	0.07	43.63	0.04	38.92	0.51	0.02	0.03	0.38	14.67	0.11	98.38	84.1	15.9
MB-3.4_1	0.02	44.78	0.02	39.30	0.43	0.01	0.03	0.30	13.72	0.15	98.77	85.3	14.7
MB-3.4_2	0.01	46.01	0.02	39.39	0.33	0.01	0.04	0.22	12.47	0.19	98.70	86.8	13.2
MB-3.4_3	0.03	45.24	0.01	39.32	0.31	0.01	0.04	0.28	13.16	0.15	98.55	86.0	14.0
MB-3.4_4	0.03	42.83	0.04	38.60	0.68	0.01	0.00	0.38	15.49	0.10	98.17	83.1	16.9
MB-3.5_1	0.04	42.51	0.02	38.62	0.69	0.02	0.00	0.40	15.68	0.12	98.10	82.9	17.1
MB-3.5_2	0.03	44.85	0.03	39.08	0.40	0.01	0.02	0.30	13.61	0.16	98.50	85.5	14.5
MB-3.5_3	0.07	45.85	0.03	39.09	0.31	0.00	0.05	0.25	12.45	0.17	98.29	86.8	13.2
MB-3.5_4	0.01	46.25	0.04	39.41	0.31	0.00	0.05	0.24	11.90	0.20	98.42	87.4	12.6
MB-3.5_5	0.02	46.19	0.00	39.36	0.31	0.03	0.00	0.24	11.94	0.21	98.31	87.3	12.7
MB-4.1_1	0.02	39.16	0.05	38.08	0.45	0.04	0.02	0.61	21.48	0.11	100.02	76.5	23.5
MB-4.1_2	0.04	39.24	0.06	39.66	0.39	0.01	0.00	0.43	18.40	0.10	98.33	79.2	20.8
MB-4.1_3	0.01	44.31	0.03	39.29	0.37	0.02	0.00	0.27	15.44	0.15	99.91	83.7	16.3
MB-4.1_5	0.02	47.00	0.02	40.13	0.25	0.01	0.02	0.19	12.10	0.17	99.90	87.4	12.6
MB-4.1_6	0.02	46.76	0.03	40.30	0.30	0.00	0.02	0.19	11.79	0.21	99.61	87.6	12.4
MB-4.1_7	0.02	44.94	0.03	39.56	0.29	0.01	0.04	0.28	14.43	0.18	99.78	84.7	15.3
MB-4.2_1	0.03	39.27	0.21	38.67	0.44	0.03	0.04	0.49	20.07	0.11	99.35	77.7	22.3
MB-4.2_2	0.01	42.99	0.02	39.03	0.33	0.02	0.02	0.33	16.63	0.17	99.54	82.2	17.8
MB-4.2_3	0.07	35.93	1.34	40.79	0.48	0.01	0.04	0.43	17.41	0.12	96.62	78.6	21.4
MB-4.2_4	0.00	42.91	0.02	38.94	0.29	0.02	0.07	0.38	16.75	0.15	99.54	82.0	18.0
MB-4.2_5	0.01	44.11	0.04	39.14	0.30	0.01	0.05	0.28	15.23	0.19	99.36	83.8	16.2
MB-4.2_6	0.01	42.11	0.05	38.99	0.30	0.02	0.01	0.37	17.60	0.17	99.63	81.0	19.0
MB-4.2_8	0.02	39.82	0.02	38.18	0.34	0.02	0.02	0.48	20.00	0.11	99.01	78.0	22.0
MB-4.3_2	0.01	44.48	0.09	39.77	0.32	0.00	0.07	0.30	14.92	0.16	100.13	84.2	15.8
MB-4.3_4	0.02	47.09	0.05	39.84	0.27	0.00	0.02	0.17	11.97	0.21	99.64	87.5	12.5
MB-4.3_5	0.01	47.22	0.03	39.90	0.27	0.01	0.06	0.19	11.92	0.21	99.82	87.6	12.4
MB-4.3_6	0.00	47.00	0.03	39.94	0.27	0.00	0.01	0.17	11.86	0.20	99.49	87.6	12.4
MB-4.3_7	0.02	47.10	0.04	40.59	0.28	0.00	0.03	0.18	11.99	0.20	100.44	87.5	12.5
MB-4.3_8	0.02	46.82	0.03	40.29	0.26	0.01	0.07	0.19	12.07	0.24	100.00	87.4	12.6
MB-4.3_9	0.01	46.87	0.02	39.72	0.27	0.00	0.04	0.18	12.20	0.21	99.52	87.3	12.7
MB-4.4_1	0.03	39.95	0.01	38.25	0.44	0.05	0.02	0.53	20.13	0.12	99.53	78.0	22.0
MB-4.4_2	0.01	44.13	0.02	39.39	0.32	0.00	0.03	0.28	15.35	0.18	99.72	83.7	16.3
MB-4.4_3	0.01	46.29	0.03	39.77	0.30	0.00	0.04	0.22	13.05	0.18	99.89	86.3	13.7
MB-4.4_4	0.01	46.65	0.03	39.86	0.28	0.00	0.01	0.22	12.37	0.17	99.59	87.1	12.9
MB-4.4_5	0.02	46.43	0.03	39.76	0.29	0.00	0.05	0.19	12.91	0.20	99.87	86.5	13.5
MB-4.5_1	0.01	39.01	0.02	37.93	0.45	0.03	0.01	0.52	20.78	0.10	98.87	77.0	23.0
MB-4.5_2	0.03	42.24	0.01	39.18	0.37	0.01	0.04	0.40	17.46	0.14	99.88	81.2	18.8
MB-4.5_3	0.00	45.27	0.02	39.57	0.29	0.00	0.00	0.22	14.14	0.18	99.71	85.1	14.9
MB-4.5_4	0.03	46.40	0.02	39.87	0.29	0.00	0.03	0.16	12.47	0.17	99.44	86.9	13.1
MB-4.5_5	0.02	47.17	0.04	40.03	0.28	0.00	0.03	0.15	11.93	0.25	99.91	87.6	12.4
MB-4.5_6	0.02	47.10	0.02	39.90	0.27	0.00	0.04	0.23	12.14	0.22	99.94	87.4	12.6
MB-4.5_7	0.00	45.40	0.02	39.60	0.29	0.00	0.04	0.28	13.84	0.20	99.67	85.4	14.6
MB-4.5_8	0.01	42.97	0.02	38.84	0.30	0.00	0.08	0.35	16.65	0.16	99.39	82.2	17.8
MB-4.5_9	0.01	42.44	0.02	38.87	0.33	0.00	0.02	0.36	17.34	0.21	99.61	81.4	18.6
MB-4.5_10	0.01	44.22	0.01	39.16	0.26	0.02	0.02	0.32	15.22	0.22	99.45	83.8	16.2

Nepheline

Label	Na_2O	MgO	Al_2O_3	SiO_2	K_2O	CaO	FeO	SrO	BaO	Total
Mb-1.4	13.00	3.00	30.75	43.01	4.97	0.52	2.49	0.06	0.01	97.81
Mb-1.5	15.09	0.12	33.31	42.36	5.60	0.69	0.95	0.12	0.03	98.27
Mb-1.6	15.52	0.16	32.36	43.79	5.64	0.21	1.06	0.13	0.04	98.92
Mb-1.11	15.35	0.43	32.97	43.19	5.88	0.26	1.19	0.13	0.04	99.44
Mb-1.14	14.54	0.70	31.96	44.16	5.08	0.40	1.29	0.12	0.05	98.30
Mb-1.17	14.50	1.22	31.89	43.32	5.25	0.26	1.67	0.04	0.02	98.17
MB-2.4	16.12	0.10	32.40	44.11	4.38	0.58	1.04	0.14	0.09	98.96
MB-2.5	16.13	0.06	34.01	42.78	4.88	0.56	0.99	0.28	0.02	99.71
MB-2.7	16.40	0.10	33.73	43.97	4.74	0.46	1.16	0.19	0.04	100.80
MB-2.8	16.21	0.08	33.73	43.44	4.54	0.82	1.08	0.18	0.01	100.09
MB-2.12	15.93	0.14	33.72	43.27	4.93	0.58	1.10	0.09	0.05	99.80
MB-2.13	16.39	0.07	33.56	42.97	4.69	0.59	1.15	0.15	0.08	99.65
MB-2.15	16.25	0.07	33.48	44.04	4.69	0.67	1.16	0.20	0.05	100.60
MB-2.17	16.12	0.06	33.29	43.30	4.73	0.56	1.10	0.31	0.04	99.51
MB-2.20	16.15	0.19	33.20	44.35	4.23	0.55	0.97	0.09	0.04	99.77
Mb-3.1	13.51	0.95	30.53	44.98	4.42	0.46	2.22	0.10	0.04	97.21
Mb-3.2	14.38	0.26	31.95	43.95	5.49	0.34	1.49	0.09	0.00	97.94
Mb-3.3	15.34	0.17	31.91	44.23	5.29	0.26	1.25	0.07	0.03	98.55
Mb-3.4	14.32	0.14	31.66	44.54	5.02	0.35	1.11	0.06	0.00	97.21
Mb-3.5	14.93	0.22	31.23	45.16	4.95	0.36	1.15	0.11	0.05	98.16
Mb-3.6	13.60	0.49	31.71	43.90	5.03	0.50	2.13	0.10	0.05	97.51
Mb-3.7	13.38	1.10	30.63	46.02	4.36	0.43	2.28	0.00	0.03	98.25
Mb-3.12	14.68	0.29	31.69	44.74	5.09	0.35	1.19	0.08	0.03	98.13
Mb-3.13	14.52	0.45	31.42	45.09	4.75	0.40	1.42	0.04	0.03	98.11
Mb-3.14	14.97	0.22	31.54	44.48	5.17	0.30	1.01	0.05	0.02	97.77
Mb-3.17	14.12	0.49	31.98	43.91	5.14	0.42	2.07	0.08	0.02	98.22

Titano-magnetites

Label	SiO_2	TiO_2	Al_2O_3	Cr_2O_3	Fe_2O_3(c)	FeO	V_2O_3	MnO	MgO	ZnO	Total
MB-1.1	0.38	16.16	5.71	0.86	27.65	39.21	0.42	0.89	3.89	0	95.18
MB-1.2	0.15	19.25	3.25	0.75	24.45	43.03	0.48	0.91	2.7	0.07	95.03
MB-1.3	9.66	13.14	11.45	0.18	8.11	47.11	0.46	0.61	6.19	0	96.9
MB-1.4	0.43	16.97	4.58	0.66	26.86	38.82	0.46	0.79	4.33	0.06	93.98
MB-1.5	0.54	4.34	11.38	19.96	29.13	22.64	0.13	0.4	9.31	0.11	97.94
MB-1.8	1.98	19.09	1.67	0.88	21.44	46.11	0.43	1.41	1.55	0.23	94.78
MB-1.9	0.11	18.22	3.72	0.85	26.03	38.65	0.49	0.78	4.75	0.11	93.7
MB-1.10	0.08	20.33	0.82	0.01	23.79	46.45	0.25	1.51	0.02	0.15	93.41
MB-1.12	0.29	21.82	0.7	0.22	20.73	47.92	0.31	1.69	0.14	0.13	93.95
MB-1.13	0.14	11.83	7.14	2.62	35.13	29.99	0.23	0.5	7.44	0.03	95.04
MB-1.14	0.08	14.34	6.11	3.53	26.92	38.14	0.39	0.92	2.89	0.02	93.35
MB-1.15	0.1	20.21	2.71	0.35	23.16	42.87	0.49	0.87	3.07	0.11	93.93
MB-1.16	0.15	20.79	1.4	0.04	21.38	46.97	0.27	1.37	0.04	0.08	92.48
MB-1.17	0.35	19.76	1.62	0.05	23.55	46.42	0.26	1.27	0.3	0.04	93.63
MB-1.18	0.06	16.57	5.62	0.97	28.37	38.24	0.43	0.8	4.63	0.05	95.74
MB-1.19	2.25	15.7	5.93	0.91	23.94	38.38	0.37	0.73	5.63	0	93.83
MB-1.20	0.07	17.27	5.06	0.52	28.3	38.03	0.47	0.68	5.21	0	95.61
MB-2.1	0.38	13.9	5.68	2.23	28.16	35.07	0.25	0.75	4.42	0.06	90.89
MB-2.2	51.75	0	1.4	2.97	0	16.29	0	0.06	26.78	0	99.25
MB-2.4	37.68	0.45	0.11	0	0	14.19	0	0.19	42.91	0	95.53
MB-2.7	20.45	11.08	5.58	0.13	0	44.35	0.27	0.83	7.46	0	90.15
MB-2.9	0.36	16.57	2.44	0.23	26.61	41.37	0.34	1.03	1.23	0	90.17
MB-2.10	0.29	17.45	2.35	0.18	25.35	43.06	0.35	1.5	0.42	0.07	91.02

Label	SiO_2	TiO_2	Al_2O_3	Cr_2O_3	Fe_2O_3 (c)	FeO	V_2O_3	MnO	MgO	ZnO	Total
MB-2.11	2.28	11.09	6.3	6.52	27.02	26.63	0.35	0.37	10.24	0	90.79
MB-2.12	0.03	2.49	13.47	35.32	14.86	19.54	0.11	0.45	9.76	0.1	96.1
MB-2.13	0.17	16.16	3.45	0.44	27.99	39.12	0.34	0.84	2.68	0.13	91.3
MB-2.14	0.5	6.4	7.77	20.92	24.49	27.14	0.14	0.55	6.4	0.06	94.38
MB-2.15	0.19	14.27	5.01	2.08	28.29	36.43	0.32	0.76	3.48	0.11	90.93
MB-2.16	0.79	2.61	13.93	34.97	15.52	18.46	0.2	0.34	11.84	0.11	98.77
MB-2.17	0.19	17.67	2.24	0.23	24.82	42.31	0.35	1.18	0.9	0.14	90.02
MB-2.19	0.08	17.22	2.4	0.25	27.21	42.91	0.4	1.12	0.68	0.15	92.43
MB-2.20	0.28	17.6	1.51	0.15	25.87	43.07	0.32	1.76	0.2	0.05	90.81
MB-2.21	0.31	17.52	2.29	0.18	26.01	43.08	0.32	1.32	0.7	0.16	91.91
MB-2.23	1.12	16.76	2.94	0.18	23.92	42.61	0.33	1.02	1.27	0	90.16
MB-2.24	0.07	2.45	14.13	37.22	13.07	17.18	0.15	0.22	11.59	0.04	96.13
MB-2.25	0.35	17.66	1.8	0.16	25.97	43.52	0.3	1.65	0.29	0.08	91.79
MB-2.26	0.19	6.36	9.1	3.07	40.49	28.44	0.14	0.31	5.2	0.02	93.33
MB-2.27	0.41	16.93	1.78	0.19	27.81	41.06	0.27	1.03	1.8	0.09	91.37
MB-2.28	0.12	17.3	2.55	0.23	26.62	41.64	0.33	1.1	1.48	0.07	91.44
MB-3.1	0.09	13.29	6.68	0.99	33.29	34.18	0.3	0.62	5.39	0	94.83
MB-3.2	0.08	13.49	6.59	0.93	33.36	34.68	0.29	0.61	5.27	0	95.31
MB-3.3	0.06	15.42	6.06	0.85	28.28	38.23	0.4	0.72	3.64	0.01	93.66
MB-3.4	0.06	13.88	6.37	0.9	32.56	36.08	0.4	0.67	4.55	0	95.48
MB-3.6	0.09	15.61	5.82	0.3	29.48	38.9	0.45	0.81	3.45	0.19	95.1
MB-3.7	0.1	14.14	6.45	0.71	31.29	37.27	0.4	0.81	3.67	0.2	95.04
MB-3.8	0.07	12.65	6.53	1.58	35.66	34.91	0.33	0.71	4.84	0.25	97.54
MB-3.9	0.82	13.87	6.81	0.8	30.15	35.74	0.38	0.7	5.18	0.16	94.59
MB-3.10	0.26	2.85	15.57	36.09	12.21	17.9	0.17	0.27	11.83	0.13	97.28
MB-3.11	0.18	14.46	6.36	0.7	31.08	38	0.41	0.79	3.65	0.14	95.78
MB-3.12	0.24	10.18	7.54	5.65	36.32	29.24	0.31	0.56	7.5	0.21	97.76
MB-3.14	0.26	14.55	6.59	0.87	30.39	36.85	0.43	0.73	4.46	0.21	95.35
MB-3.15	0.05	12.33	6.74	1.28	37.33	32.51	0.28	0.52	6.47	0.01	97.51
MB-3.16	4.46	11.1	6.6	1.29	34.65	29.55	0.24	0.52	12.08	0.01	100.51
MB-3.17	1.89	14.11	7.2	0.61	26.01	37.08	0.39	0.73	5.21	0.05	93.27
MB-3.18	0.07	14.25	6.36	0.6	32.35	36.81	0.39	0.76	4.27	0.12	95.98
MB-3.20	0.09	12.73	6.6	0.79	35.3	34.04	0.32	0.6	5.31	0.05	95.82
MB-3.21	0.05	2.56	14.1	38.67	12.08	16.36	0.1	0.26	12.24	0	96.42
MB-3.22	1.03	2.65	12.99	33.47	14.04	20.41	0.1	0.4	9.96	0	95.06
MB-3.23	0.37	17.02	5.56	0.22	24.29	39.36	0.52	0.87	3.6	0.06	91.87
MB-3.24	0.09	13.01	6.41	0.83	35.22	34.66	0.35	0.65	5.14	0.06	96.41
MB-3.25	0.08	13.15	6.54	0.62	34.87	34.62	0.35	0.65	5.21	0.05	96.14
MB-4.1	0.88	14.66	6.41	0.08	28.34	37.89	0.5	0.68	4.13	0.1	93.67
MB-4.2	0.08	14.22	6.26	0.04	33.04	36.73	0.44	0.57	4.46	0.03	95.88
MB-4.3	0.09	14.76	6.46	0.03	29.63	36.54	0.45	0.62	4.27	0.11	92.95
MB-4.4	0.07	9.82	10.23	8	30.24	30.48	0.41	0.48	6.5	0.08	96.3
MB-4.5	1.46	9.62	9.09	7.36	29.18	31.9	0.33	0.51	6.49	0	95.95
MB-4.6	0.34	6.24	9.99	19.11	25.78	27.8	0.35	0.47	6.46	0.1	96.64
MB-4.7	0.08	14.03	7.11	0.06	32.4	35.42	0.44	0.61	5.11	0.11	95.36
MB-4.8	0.89	12.97	6.96	0.24	29.18	35.15	0.46	0.56	4.53	0.05	90.99
MB-4.9	0.65	13.8	7.05	0.05	30.07	36.55	0.43	0.73	4.3	0.14	93.77
MB-4.10	0.09	13.83	7.17	0.36	32.07	35.33	0.45	0.62	5.01	0.07	95.01
MB-4.12	0.19	13.86	7.19	0.06	31.08	34.94	0.49	0.64	5.01	0.19	93.66
MB-4.13	0.16	2.02	14.87	39.11	11.34	17.03	0.21	0.2	11.72	0.1	96.78
MB-4.14	1.06	8.04	10.01	12.01	27.82	29.56	0.3	0.46	6.88	0.11	96.25

Label	SiO_2	TiO_2	Al_2O_3	Cr_2O_3	Fe_2O_3(c)	FeO	V_2O_3	MnO	MgO	ZnO	Total
MB-4.15	0.15	13.64	6.91	0.05	30.79	35.11	0.48	0.61	4.52	0.1	92.35
MB-4.16	2.55	12.95	7.56	0.03	26.56	37.21	0.35	0.53	5.08	0.06	92.86
MB-4.17	0.22	1.65	14.6	41.72	10.91	18.63	0.14	0.4	10.84	0.14	99.24
MB-4.18	0.16	13.71	7.1	0.03	32.27	35.74	0.44	0.58	4.7	0.12	94.85

Corporate Butte

Pyroxenes

Label	Na_2O	MgO	Al_2O_3	SiO_2	CaO	TiO_2	Cr_2O_3	MnO	FeO	Total	En	Wo	Fs
CB-1.1_1	0.40	14.86	4.61	49.49	23.74	1.71	0.55	0.07	5.15	100.57	42.7	48.9	8.4
CB-1.1_2	0.47	16.69	2.70	52.33	23.29	0.75	0.63	0.07	3.88	100.82	46.8	47.0	6.2
CB-1.1_3	0.55	15.70	3.78	50.93	23.15	1.08	0.99	0.09	4.39	100.66	45.0	47.7	7.2
CB-1.1_4	0.52	16.52	2.95	51.92	23.15	0.81	0.87	0.08	4.02	100.82	46.6	46.9	6.5
CB-1.1_5	0.48	16.92	2.44	52.66	22.71	0.64	0.20	0.08	4.36	100.48	47.3	45.7	7.0
CB-1.2_1	0.53	16.60	2.98	51.98	23.16	0.73	0.58	0.06	4.03	100.64	46.7	46.8	6.4
CB-1.2_2	0.50	16.73	2.98	52.44	23.14	0.72	0.59	0.06	3.91	101.07	47.0	46.7	6.3
CB-1.2_3	0.46	17.00	2.52	52.46	23.06	0.64	0.27	0.07	4.06	100.53	47.4	46.2	6.5
CB-1.2_4	0.43	17.03	2.56	52.49	23.28	0.71	0.58	0.08	3.72	100.87	47.4	46.6	5.9
CB-1.4_1	0.50	13.77	4.67	49.05	23.52	2.01	0.05	0.14	6.82	100.52	39.8	48.9	11.3
CB-1.4_2	0.32	15.36	3.76	49.89	23.51	1.65	0.10	0.12	5.65	100.36	43.3	47.6	9.1
CB-1.4_3	0.34	15.33	3.89	49.52	23.87	1.70	0.06	0.09	5.67	100.47	42.9	48.0	9.1
CB-1.5	0.40	13.79	6.15	47.24	23.51	2.29	0.11	0.09	6.35	99.94	40.2	49.3	10.5
CB-1.6	0.52	16.29	3.19	51.62	23.36	0.81	0.80	0.08	3.98	100.65	46.1	47.5	6.4
CB-1.7	0.28	15.92	3.28	50.32	23.85	1.43	0.21	0.11	5.21	100.61	44.2	47.6	8.3
CB-1.9_1	0.54	13.34	5.44	48.04	23.58	2.40	0.03	0.16	7.06	100.59	38.9	49.4	11.8
CB-1.9_2	0.34	15.04	4.38	49.65	23.93	1.77	0.04	0.10	5.55	100.80	42.5	48.6	9.0
CB-1.9_3	0.27	16.45	2.43	52.04	24.12	1.03	0.36	0.06	3.95	100.71	45.6	48.1	6.2
CB-1.9_4	0.35	15.29	3.97	50.10	23.92	1.55	0.10	0.10	5.25	100.64	43.1	48.4	8.5
CB-1.9_5	0.32	15.09	3.86	49.97	23.84	1.58	0.00	0.10	5.71	100.48	42.5	48.3	9.2
CB-1.9_6	0.36	14.94	4.35	49.60	23.80	1.66	0.03	0.08	5.51	100.33	42.5	48.6	8.9
CB-1.9_7	0.32	15.81	3.15	50.80	23.99	1.36	0.07	0.10	4.94	100.53	44.1	48.1	7.9
CB-1.9_8	0.29	15.93	3.25	50.67	24.11	1.36	0.12	0.09	4.87	100.68	44.2	48.1	7.7
CB-1.9_9	0.39	14.76	4.76	48.99	23.93	1.84	0.07	0.10	5.70	100.52	41.9	48.8	9.2
CB-1.9_10	0.49	11.69	9.51	43.22	23.36	4.03	0.02	0.08	7.66	100.05	35.6	51.1	13.2
CB-1.10_1	0.48	11.95	8.97	43.74	23.27	3.97	0.05	0.11	7.92	100.45	36.0	50.4	13.6
CB-1.10_2	0.39	14.02	6.12	47.21	23.84	2.53	0.44	0.10	5.88	100.52	40.6	49.6	9.7
CB-1.10_3	0.29	15.74	3.47	50.28	23.65	1.48	0.21	0.12	5.17	100.42	44.1	47.6	8.3
CB-1.10_4	0.29	15.79	3.26	51.11	24.02	1.34	0.09	0.07	4.91	100.88	44.1	48.2	7.8
CB-1.10_5	0.35	15.57	3.63	50.56	24.03	1.54	0.06	0.11	5.29	101.15	43.4	48.1	8.4
CB-1.10_6	0.37	14.33	5.01	48.53	23.67	2.10	0.01	0.09	6.29	100.41	41.0	48.7	10.3
CB-1.10_7	0.52	12.85	6.12	47.60	23.43	2.62	0.00	0.14	7.18	100.45	38.0	49.8	12.2
CB-1.10_8	0.44	12.81	6.69	46.06	23.27	3.06	0.00	0.12	7.89	100.35	37.6	49.1	13.2
CB-1.11_1	0.34	14.33	5.51	48.09	23.86	2.22	0.20	0.07	5.63	100.26	41.3	49.4	9.2
CB-1.11_2	0.31	16.52	2.27	52.47	23.84	0.84	0.36	0.06	3.94	100.61	46.0	47.7	6.2
CB-1.11_3	0.38	17.01	2.28	52.97	23.73	0.74	0.39	0.09	3.81	101.38	46.9	47.0	6.0
CB-1.11_4	0.48	16.91	2.47	52.75	23.42	0.71	0.50	0.07	3.71	101.00	47.2	46.9	5.9
CB-1.11_5	0.49	16.66	2.93	52.29	23.32	0.79	0.56	0.07	3.78	100.89	46.8	47.1	6.1
CB-1.11_6	0.47	16.58	2.77	52.12	23.49	0.79	0.60	0.08	3.65	100.53	46.6	47.5	5.9
CB-1.11_7	0.47	16.75	2.64	52.54	23.38	0.72	0.55	0.07	3.72	100.84	46.9	47.1	6.0
CB-1.11_8	0.48	16.61	2.74	52.55	23.42	0.71	0.50	0.08	3.70	100.79	46.7	47.3	6.0
CB-1.11_9	0.41	17.14	2.28	52.99	23.23	0.65	0.67	0.07	3.49	100.92	47.8	46.6	5.6
CB-1.11_10	0.50	16.52	3.32	52.09	23.15	0.80	0.60	0.09	3.87	100.94	46.7	47.0	6.3
CB-1.12_1	0.57	13.54	5.11	48.25	23.47	2.19	0.03	0.16	6.83	100.15	39.4	49.1	11.4
CB-1.12_2	0.42	17.03	2.19	52.76	23.14	0.68	0.66	0.08	3.70	100.66	47.6	46.5	5.9

Label	Na_2O	MgO	Al_2O_3	SiO_2	CaO	TiO_2	CrO	MnO	FeO	Total	En	Wo	Fs
CB-1.12_3	0.40	16.92	2.31	52.75	23.32	0.72	0.34	0.08	4.01	100.84	47.0	46.6	6.4
CB-1.12_4	0.36	16.87	2.22	52.83	23.72	0.75	0.42	0.08	3.84	101.08	46.7	47.2	6.1
CB-1.12_5	0.33	16.36	2.45	52.04	24.00	0.95	0.41	0.07	4.00	100.61	45.6	48.1	6.4
CB-1.12_6	0.29	16.30	2.54	51.72	24.09	1.04	0.23	0.08	4.12	100.41	45.3	48.1	6.6
CB-1.13_1	0.42	15.82	4.20	50.37	23.64	1.35	0.56	0.06	4.65	101.08	44.6	47.9	7.5
CB-1.13_2	0.58	15.52	4.32	50.81	22.66	1.14	0.72	0.08	4.79	100.62	44.9	47.1	7.9
CB-1.13_3	0.57	15.48	5.01	49.89	22.37	1.33	1.01	0.13	4.75	100.55	45.1	46.9	8.0
CB-1.13_4	0.48	16.46	3.42	51.55	22.48	1.03	0.95	0.08	4.38	100.82	46.9	46.0	7.1
CB-1.13_5	0.43	17.21	2.31	52.93	22.63	0.73	0.87	0.10	3.99	101.19	48.1	45.5	6.4
CB-1.13_6	0.60	12.81	6.45	47.05	23.27	2.77	0.03	0.13	7.29	100.42	38.0	49.6	12.4
CB-1.14_1	0.45	17.00	2.48	52.51	23.45	0.70	0.49	0.06	3.73	100.88	47.2	46.8	5.9
CB-1.14_2	0.46	16.60	2.91	51.99	23.06	0.81	0.77	0.11	3.81	100.51	46.9	46.9	6.2
CB-1.14_3	0.46	16.48	3.04	51.74	22.98	0.78	1.09	0.11	3.64	100.32	47.0	47.1	6.0
CB-1.14_4	0.53	16.64	2.88	52.18	23.01	0.68	1.17	0.06	3.28	100.43	47.5	47.2	5.4
CB-1.14_5	0.52	16.53	3.26	51.90	23.18	0.84	0.51	0.08	3.81	100.63	46.7	47.1	6.2
CB-1.14_6	0.51	16.72	2.64	52.37	23.17	0.63	0.92	0.08	3.36	100.39	47.4	47.2	5.5
CB-1.15	0.49	11.94	8.39	43.61	23.21	3.93	0.01	0.12	7.87	99.58	36.1	50.4	13.5
CB-1.16	0.38	14.02	5.12	47.56	23.24	2.32	0.00	0.11	7.24	99.98	40.2	47.9	11.8
CB-1.17	0.42	14.03	4.96	48.26	23.46	2.14	0.00	0.14	6.79	100.21	40.3	48.5	11.2

Olivines

Label	Na_2O	MgO	Al_2O_3	SiO_2	CaO	TiO_2	Cr_2O_3	MnO	FeO	NiO	Total	Fo	Fa
CB-1.1_1	0.00	41.86	0.02	38.24	0.58	0.08	0.02	0.46	18.67	0.13	100.09	80.0	20.0
CB-1.1_2	0.00	46.85	0.00	39.65	0.41	0.02	0.00	0.22	12.80	0.14	100.09	86.7	13.3
CB-1.1_3	0.01	47.03	0.04	39.74	0.32	0.03	0.00	0.23	12.41	0.21	100.02	87.1	12.9
CB-1.1_4	0.01	47.16	0.01	39.65	0.29	0.02	0.00	0.21	12.53	0.16	100.04	87.0	13.0
CB-1.1 5	0.01	47.27	0.02	39.87	0.31	0.01	0.04	0.22	12.09	0.21	100.05	87.5	12.5
CB-1.1_6	0.01	46.84	0.47	39.57	0.35	0.04	0.05	0.20	12.05	0.23	99.81	87.4	12.6
CB-1.1_7	0.01	47.87	0.03	40.16	0.30	0.01	0.04	0.18	11.10	0.25	99.97	88.5	11.5
CB-1.1_8	0.01	47.63	0.03	40.30	0.29	0.03	0.07	0.10	10.85	0.22	99.54	88.7	11.3
CB-1.2_1	0.02	47.43	0.03	39.68	0.32	0.03	0.05	0.20	11.88	0.26	99.89	87.7	12.3
CB-1.2_2	0.03	47.58	0.03	39.83	0.31	0.04	0.06	0.18	11.68	0.24	99.98	87.9	12.1
CB-1.2_3	0.01	47.30	0.01	39.72	0.42	0.02	0.03	0.20	12.09	0.23	100.03	87.5	12.5
CB-1.2_4	0.01	48.33	0.03	40.12	0.30	0.03	0.04	0.17	11.02	0.26	100.31	88.7	11.3
CB-1.2_5	0.02	48.05	0.03	39.80	0.32	0.04	0.08	0.15	11.34	0.25	100.08	88.3	11.7
CB-1.2_6	0.01	41.42	0.02	38.29	0.35	0.04	0.01	0.45	18.85	0.20	99.65	79.7	20.3
CB-1.3_1	0.01	40.01	0.14	38.18	0.65	0.06	0.00	0.52	19.93	0.14	99.63	78.2	21.8
CB-1.3_2	0.02	46.86	0.02	39.63	0.42	0.03	0.01	0.16	12.64	0.18	99.96	86.9	13.1
CB-1.3_5	0.02	46.67	0.02	39.74	0.35	0.02	0.01	0.18	12.44	0.16	99.60	87.0	13.0
CB-1.3_6	0.00	47.06	0.01	39.67	0.32	0.03	0.00	0.21	12.38	0.19	99.88	87.1	12.9
CB-1.3_7	0.00	46.81	0.01	39.59	0.40	0.02	0.03	0.23	12.60	0.21	99.90	86.9	13.1
CB-1.3_8	0.02	40.12	0.01	37.83	0.64	0.09	0.00	0.58	20.49	0.13	99.92	77.7	22.3
CB-1.4_1	0.03	40.32	0.01	38.17	0.63	0.08	0.01	0.47	19.48	0.13	99.35	78.7	21.3
CB-1.4_2	0.00	46.53	0.03	39.59	0.49	0.04	0.04	0.23	12.96	0.16	100.05	86.5	13.5
CB-1.4_3	0.01	46.79	0.04	39.62	0.44	0.02	0.01	0.25	12.45	0.15	99.79	87.0	13.0
CB-1.4_4	0.00	46.62	0.00	39.51	0.42	0.02	0.00	0.24	12.58	0.17	99.56	86.8	13.2
CB-1.4_5	0.03	46.87	0.01	39.70	0.41	0.03	0.00	0.20	12.66	0.17	100.09	86.8	13.2
CB-1.4_6	0.02	46.88	0.02	39.78	0.39	0.04	0.00	0.22	12.55	0.14	100.04	86.9	13.1
CB-1.6_1	0.00	39.14	0.05	37.71	0.72	0.08	0.03	0.62	21.12	0.09	99.56	76.8	23.2
CB-1.6_2	0.00	46.33	0.00	39.48	0.46	0.01	0.01	0.27	12.98	0.15	99.71	86.4	13.6
CB-1.6_3	0.01	45.28	0.04	39.50	0.52	0.03	0.01	0.25	13.67	0.19	99.51	85.5	14.5
CB-1.6_4	0.01	43.13	0.21	40.24	1.64	0.08	0.04	0.26	13.92	0.14	99.67	84.7	15.3

Nepheline

Label	Na_2O	MgO	Al_2O_3	SiO_2	K_2O	CaO	FeO	SrO	BaO	Total
CB-1.5	14.88	0.11	33.64	42.94	5.65	1.36	0.99	0.14	0.02	99.73
CB-1.9	14.83	0.16	32.84	43.48	5.03	1.56	1.30	0.17	0.03	99.41
CB-1.10	15.14	0.16	32.92	44.09	4.95	1.52	0.92	0.08	0.02	99.81
CB-1.11	12.92	0.41	31.85	44.47	4.25	1.48	2.78	0.12	0.06	98.34
CB-1.13	14.61	0.15	31.71	46.91	3.63	0.93	1.18	0.00	0.04	99.17
CB-1.14	14.57	0.75	32.32	43.26	5.25	2.53	1.41	0.15	0.02	100.27

Titano-magnetites

Label	SiO_2	TiO_2	Al_2O_3	Cr_2O_3	Fe_2O_3(C)	FeO	V_2O_3	MnO	MgO	ZnO	Total
CB-1.4	0.11	18.38	4.42	0.02	25.63	43.73	0.47	1.1	1.84	0.08	95.8
CB-1.5	0.26	16.25	5.13	0.71	28.94	42.36	0.48	0.87	2.08	0.14	97.21
CB-1.6	5	11.97	6.92	1.98	24.69	41.92	0.44	0.6	4.46	0.14	98.12
CB-1.7	0.15	16.77	5.13	0.01	29.14	41.66	0.49	0.73	2.8	0.11	96.99
CB-1.8	0.1	17.31	4.83	0.01	28.42	42.58	0.48	0.71	2.46	0.15	97.07
CB-1.9	0.13	17.9	4.63	0.03	26.76	43.34	0.54	0.97	2.06	0.1	96.46
CB-1.11	0.13	17.38	4.61	0.02	27.93	42.87	0.46	0.7	2.1	0.34	96.53
CB-1.12	0.03	11.67	6.46	8.39	32.69	33.74	0.49	0.54	5.59	0.32	99.91
CB-1.13	0.03	8.24	7.89	19.44	27.54	30.39	0.43	0.57	6.16	0.34	101.02
CB-1.14	0.12	2.03	12.87	43.46	11.02	16.7	0.17	0.23	12.04	0.22	98.87
CB-1.15	0.04	2.03	12.7	43.97	11.3	16.35	0.12	0.24	12.33	0.06	99.13
CB-1.16	0.06	15.55	5.32	0.7	32.29	38.89	0.48	0.72	4.03	0.18	98.22
CB-1.17	0.09	13.74	5.66	3.35	33.65	36.12	0.47	0.59	5.02	0.22	98.94
CB-1.18	0.19	18.72	4.08	0.03	24.82	44.15	0.52	1.1	1.65	0.25	95.52
CB-1.20	0.08	15.71	5.09	0.35	31.1	40.03	0.5	0.79	3.12	0.05	96.85
CB-1.21	0.2	14.92	5	0	33.13	36.45	0.48	0.59	4.96	0.1	95.83
CB-1.22	3.25	17.79	6.95	0	14.75	47.23	0.51	1.57	1.48	0.12	93.65
CB-1.23	0.16	19.09	3.95	0	23.45	44.28	0.45	1.15	1.5	0.16	94.2

Hudspeth Mill Intrusion

Pyroxenes

Label	Na_2O	MgO	Al_2O_3	SiO_2	CaO	TiO_2	Cr_2O_3	MnO	FeO	Total	En	Wo	Fs
HM-1.1	0.28	15.53	3.71	50.77	21.47	0.89	0.14	0.16	7.09	100.03	44.3	44.1	11.6
HM-1.2_1	0.29	14.99	4.29	50.01	21.93	1.12	0.13	0.13	7.36	100.24	42.9	45.1	12.0
HM-1.2_2	0.20	15.79	4.57	50.36	22.33	1.03	0.19	0.11	5.34	99.91	45.3	46.0	8.8
HM-1.2_3	0.21	17.08	2.77	52.18	22.48	0.51	1.13	0.08	4.11	100.55	48.0	45.4	6.6
HM-1.2_4	0.33	17.12	3.48	52.09	21.38	0.48	1.42	0.11	4.11	100.54	49.1	44.1	6.8
HM-1.2_5	0.34	15.74	5.16	50.59	22.70	0.83	1.06	0.08	4.20	100.70	45.7	47.3	7.0
HM-1.3	0.28	14.74	4.97	49.49	21.68	1.22	0.08	0.16	7.67	100.29	42.5	44.9	12.7
HM-1.4_1	0.31	12.52	3.16	43.78	24.56	1.16	0.03	0.25	8.66	94.44	35.6	50.2	14.2
HM-1.4_2	0.24	16.26	2.67	51.94	21.59	0.69	0.04	0.16	6.78	100.36	45.6	43.5	10.9
HM-1.4_3	0.26	15.01	4.97	49.44	21.16	1.08	0.06	0.14	7.73	99.85	43.3	43.9	12.8
HM-1.4_4	0.27	15.03	4.18	50.20	22.07	1.09	0.14	0.15	7.14	100.27	43.0	45.3	11.7
HM-1.5	0.24	15.96	4.04	50.95	22.31	0.86	0.10	0.13	5.51	100.11	45.4	45.6	9.0
HM-1.6	0.16	16.93	3.00	51.63	21.81	0.70	0.12	0.18	5.64	100.18	47.2	43.7	9.1
HM-1.7	0.16	16.76	3.03	52.03	21.87	0.70	0.10	0.13	5.50	100.28	47.0	44.1	8.9
HM-1.8	0.31	15.70	2.86	51.44	21.75	0.80	0.04	0.18	7.06	100.14	44.4	44.2	11.5
HM-1.9	0.21	17.11	3.14	51.67	21.77	0.67	0.09	0.14	5.57	100.37	47.6	43.5	8.9
HM-1.10	0.25	16.32	3.56	51.37	22.42	0.71	1.26	0.14	4.45	100.47	46.6	46.0	7.4
HM-1.11	0.25	15.40	3.50	50.77	21.99	0.90	0.07	0.19	7.22	100.29	43.6	44.7	11.8
HM-1.12	0.16	17.01	2.36	52.42	21.42	0.61	0.05	0.18	6.13	100.33	47.3	42.8	9.9

Label	Na_2O	MgO	Al_2O_3	SiO_2	CaO	TiO_2	Cr_2O_3	MnO	FeO	Total	En	Wo	Fs
HM-1.13	0.24	14.50	6.06	48.64	21.97	1.38	0.04	0.18	6.95	99.96	42.3	46.0	11.7
HM-1.14	0.22	16.43	4.24	51.22	23.06	0.73	0.73	0.04	4.23	100.91	46.4	46.8	6.8
HM-1.15	0.23	16.63	3.89	51.19	22.75	0.58	1.06	0.07	3.87	100.27	47.3	46.5	6.3
HM-1.16_1	0.21	14.88	5.94	49.01	21.60	1.12	0.43	0.18	6.93	100.30	43.3	45.1	11.6
HM-1.16_2	0.30	17.47	2.99	52.36	21.70	0.37	1.36	0.10	4.00	100.66	49.4	44.1	6.5
HM-1.16_3	0.36	15.67	4.14	50.19	19.04	0.40	0.16	0.20	7.39	97.55	46.6	40.7	12.7
HM-1.17	0.28	14.66	5.36	48.90	22.02	1.19	0.57	0.13	7.18	100.30	42.4	45.8	11.9
HM-1.18	0.17	18.07	1.76	53.08	21.94	0.41	0.69	0.10	4.40	100.61	49.7	43.4	6.9
HM-1.19	0.22	15.95	4.23	50.35	21.85	0.93	0.33	0.14	5.71	99.73	45.6	45.0	9.4
HM-1.20	0.27	14.37	5.63	48.82	21.97	1.38	0.17	0.15	6.89	99.67	42.1	46.3	11.6
HM-1.21	0.23	16.08	3.17	50.91	21.26	0.84	0.04	0.17	7.15	99.84	45.3	43.1	11.6
HM-1.22	0.22	15.99	3.07	51.39	21.30	0.80	0.01	0.17	7.20	100.15	45.1	43.2	11.7
HM-1.23	0.22	15.56	3.66	50.38	21.31	0.94	0.00	0.18	7.38	99.62	44.3	43.6	12.1
HM-1.24	0.17	17.01	3.17	51.38	21.77	0.75	0.49	0.12	5.20	100.08	47.7	43.9	8.4
HM-1.25	0.15	17.51	2.37	52.35	21.58	0.63	0.23	0.14	5.40	100.35	48.5	42.9	8.6
HM-1.26	0.32	15.28	3.31	51.15	21.74	0.79	0.21	0.16	6.90	99.87	43.8	44.8	11.4
HM-1.27	0.24	15.56	5.22	49.86	22.01	1.25	0.11	0.14	5.99	100.38	44.7	45.4	9.9
HM-1.28	0.27	15.01	5.32	49.36	21.46	1.29	0.04	0.13	6.64	99.52	43.8	45.1	11.1
HM-1.29_1	0.30	14.69	5.04	49.27	21.56	1.21	0.00	0.17	7.84	100.08	42.3	44.7	13.0
HM-1.29_2	0.14	17.81	2.43	52.19	21.33	0.47	0.53	0.11	4.82	99.82	49.6	42.7	7.7
HM-1.29_3	0.26	16.94	2.88	51.65	22.69	0.47	0.92	0.11	4.34	100.28	47.4	45.6	7.0
HM-1.29_4	0.22	17.63	2.02	52.78	22.63	0.35	0.97	0.10	3.62	100.34	49.0	45.2	5.8
HM-1.29_5	0.24	17.06	2.56	52.37	22.29	0.44	1.03	0.08	4.20	100.28	48.1	45.1	6.8
HM-1.29_6	0.24	16.46	3.70	50.80	22.21	0.70	0.49	0.09	5.05	99.74	46.6	45.2	8.2
HM-1.29_7	0.42	13.41	4.69	48.57	20.99	1.66	0.03	0.21	9.51	99.50	39.5	44.4	16.1
HM-1.30	0.12	17.86	1.86	52.70	21.63	0.46	0.47	0.14	4.75	99.99	49.4	43.0	7.6
HM-1.31	0.23	15.55	4.35	50.37	22.25	0.99	0.17	0.11	5.71	99.73	44.7	45.9	9.4
HM-1.32_1	0.29	14.69	5.01	49.07	21.69	1.32	0.09	0.18	7.53	99.87	42.5	45.0	12.5
HM-1.32_2	0.25	17.11	2.82	52.24	22.34	0.45	1.07	0.11	4.10	100.49	48.2	45.2	6.7
HM-1.32_3	0.23	15.69	4.19	51.05	22.22	0.77	0.08	0.14	5.94	100.30	44.7	45.5	9.7
HM-1.33	0.29	14.72	4.66	49.55	21.74	1.15	0.05	0.15	7.73	100.05	42.4	44.9	12.7
HM-1.34	0.20	17.38	2.88	52.61	21.51	0.63	0.15	0.16	5.78	101.30	48.0	42.7	9.2
HM-1.35_1	0.20	15.58	5.31	49.07	21.53	1.32	0.36	0.13	5.81	99.31	45.3	45.0	9.7
HM-1.35_2	0.29	16.40	2.86	51.34	22.24	0.48	1.09	0.12	4.56	99.38	46.8	45.6	7.5
HM-1.35_3	0.35	17.55	3.22	51.86	21.13	0.42	1.50	0.08	4.03	100.14	50.1	43.3	6.6
HM-1.36	0.23	15.90	2.96	50.83	21.00	0.94	0.04	0.21	7.75	99.86	44.8	42.6	12.6
HM-1.37	0.31	14.25	4.50	49.02	21.61	1.31	0.05	0.14	8.07	99.26	41.4	45.2	13.4
HM-1.38	0.26	16.24	4.10	50.36	21.67	0.85	0.26	0.18	5.61	99.53	46.3	44.4	9.3
HM-1.39	0.25	15.61	4.29	50.18	22.17	0.95	0.05	0.11	5.77	99.39	44.8	45.7	9.5
HM-1.40_1	0.35	14.31	3.53	49.48	21.17	1.33	0.05	0.20	9.14	99.55	41.2	43.8	15.1
HM-1.40_2	0.14	17.60	2.01	52.60	22.24	0.45	0.33	0.13	4.58	100.08	48.6	44.1	7.3
HM-1.40_3	0.20	17.86	1.89	52.88	22.29	0.35	0.94	0.08	3.87	100.36	49.5	44.4	6.2
HM-1.40_4	0.32	17.42	2.97	51.82	21.71	0.36	1.24	0.12	3.74	99.69	49.5	44.3	6.2
HM-1.40_5	0.29	18.02	2.11	52.93	21.73	0.29	0.89	0.11	3.99	100.37	50.1	43.5	6.4
HM-1.41_1	0.60	13.53	6.19	49.88	20.93	1.19	0.03	0.20	7.79	100.33	40.9	45.5	13.6
HM-1.41_2	0.23	15.92	4.50	50.50	22.02	0.85	0.13	0.13	5.76	100.05	45.4	45.2	9.4
HM-1.41_3	0.24	16.45	3.55	51.35	22.49	0.67	0.74	0.11	4.80	100.38	46.5	45.7	7.8
HM-1.41_4	0.22	16.98	2.41	52.24	22.95	0.41	1.04	0.06	3.77	100.09	47.7	46.3	6.0
HM-1.41_5	0.19	17.38	2.12	52.64	22.86	0.42	0.71	0.11	4.07	100.50	48.1	45.4	6.5
HM-1.42_1	0.30	14.08	4.01	48.88	21.41	1.44	0.03	0.22	8.93	99.30	40.7	44.5	14.8
HM-1.42_2	0.17	17.53	2.27	52.51	21.51	0.57	0.28	0.13	5.40	100.37	48.6	42.8	8.6
HM-1.42_3	0.23	17.12	2.43	51.87	22.77	0.43	1.07	0.12	3.85	99.89	47.9	45.8	6.2
HM-1.42_4	0.26	17.38	2.36	52.44	22.57	0.33	1.19	0.06	3.55	100.14	48.8	45.5	5.7
HM-1.42_5	0.20	17.13	2.38	52.31	22.94	0.41	0.67	0.11	4.07	100.22	47.6	45.9	6.5

Label	Na_2O	MgO	Al_2O_3	SiO_2	CaO	TiO_2	Cr_2O_3	MnO	FeO	Total	En	Wo	Fs
HM-1.43_1	0.25	14.70	4.90	49.05	22.04	1.17	0.08	0.14	6.94	99.27	42.6	45.9	11.5
HM-1.43_2	0.24	17.20	2.22	52.13	22.67	0.35	1.07	0.10	3.53	99.51	48.4	45.9	5.7
HM-1.43_3	0.25	18.45	1.76	53.08	21.34	0.26	0.88	0.11	3.72	99.84	51.4	42.7	6.0
HM-1.44	0.24	17.32	2.31	52.19	22.52	0.40	1.14	0.09	3.78	99.99	48.6	45.4	6.1
HM-1.45	0.27	15.78	5.05	49.50	22.02	1.18	0.41	0.12	5.68	100.01	45.3	45.4	9.3
HM-1.46	0.39	14.63	4.74	48.52	21.09	1.18	0.12	0.14	7.88	98.68	42.7	44.2	13.1
HM-1.47	0.24	16.41	3.66	50.77	22.11	0.77	1.13	0.12	4.64	99.85	46.9	45.4	7.6
HM-1.48	0.25	15.38	4.52	50.04	22.23	1.07	0.16	0.12	6.13	99.89	44.1	45.8	10.0
HM-1.49	0.28	14.91	4.55	49.74	21.82	1.12	0.06	0.16	7.19	99.81	42.9	45.2	11.9
HM-1.50	0.24	16.35	2.74	51.38	20.94	0.77	0.04	0.17	7.28	99.89	46.0	42.3	11.7
HM-1.51	0.17	16.56	3.01	51.26	21.61	0.74	0.03	0.18	5.76	99.33	46.7	43.8	9.4
HM-1.53	0.23	15.74	3.50	50.63	21.41	0.91	0.00	0.16	7.10	99.68	44.7	43.7	11.6
HM-2.1_1	0.22	16.69	3.56	51.55	22.04	0.71	0.35	0.11	4.90	100.14	47.2	44.8	8.0
HM-2.1_2	0.25	16.47	3.10	51.35	22.19	0.59	1.11	0.08	4.75	99.87	46.9	45.4	7.7
HM-2.1_3	0.17	17.90	1.70	52.59	21.79	0.39	0.55	0.10	4.03	99.23	49.9	43.6	6.5
HM-2.1_4	0.14	18.18	1.83	52.97	21.44	0.40	0.62	0.11	4.42	100.11	50.3	42.6	7.0
HM-2.2_1	0.34	14.26	3.83	49.45	21.28	1.50	0.02	0.22	8.29	99.20	41.5	44.5	13.9
HM-2.2_2	0.15	18.12	2.00	52.25	21.08	0.47	0.53	0.11	4.67	99.37	50.4	42.1	7.5
HM-2.2_3	0.20	17.64	2.30	52.02	21.48	0.48	0.91	0.14	4.34	99.51	49.6	43.4	7.1
HM-2.2_4	0.20	17.77	1.93	52.86	22.32	0.34	0.91	0.11	3.88	100.32	49.3	44.5	6.2
HM-2.3_1	0.37	13.48	3.80	48.69	20.97	1.80	0.00	0.25	9.28	98.65	39.8	44.5	15.8
HM-2.3_2	0.12	17.43	1.82	52.82	22.27	0.44	0.12	0.10	4.55	99.68	48.4	44.4	7.2
HM-2.3_3	0.17	17.50	1.67	52.81	22.41	0.36	0.64	0.11	3.92	99.58	48.8	44.9	6.3
HM-2.3_4	0.19	17.51	1.75	53.10	22.26	0.39	0.46	0.10	4.01	99.78	48.9	44.7	6.4
HM-2.3_5	0.14	17.45	1.76	52.89	22.39	0.38	0.44	0.12	4.21	99.78	48.5	44.7	6.7
HM-2.3_6	0.18	17.50	1.79	52.84	22.41	0.38	0.54	0.08	4.10	99.83	48.7	44.8	6.5
HM-2.3_7	0.24	16.58	3.27	51.13	22.35	0.62	0.89	0.10	4.53	99.72	47.0	45.6	7.4
HM-2.3_8	0.17	17.43	1.85	52.59	22.41	0.43	0.46	0.12	4.34	99.80	48.4	44.7	7.0
HM-2.3_9	0.17	17.41	1.95	52.23	22.01	0.47	0.34	0.10	4.84	99.52	48.4	43.9	7.7
HM-2.3_10	0.36	16.39	2.95	51.73	22.76	0.58	0.69	0.07	4.32	99.84	46.5	46.5	7.0
HM-2.3_11	0.22	16.29	3.91	50.26	22.30	0.85	0.70	0.12	4.97	99.61	46.3	45.6	8.1
HM-2.3_12	0.21	16.82	2.77	51.46	22.60	0.51	1.04	0.08	3.96	99.45	47.6	46.0	6.4
HM-2.4_1	0.28	15.47	2.80	50.32	21.67	1.00	0.02	0.15	7.12	98.84	44.0	44.3	11.6
HM-2.4_2	0.17	17.53	1.88	52.24	21.66	0.46	0.13	0.12	4.76	98.96	48.9	43.4	7.6
HM-2.4_3	0.16	17.94	1.82	52.55	21.64	0.43	0.31	0.13	4.48	99.45	49.7	43.1	7.2
HM-2.4_4	0.14	17.72	1.94	52.45	21.70	0.42	0.56	0.12	4.24	99.29	49.6	43.6	6.8
HM-2.5	0.24	15.96	3.98	50.16	22.05	0.85	0.89	0.07	4.55	98.74	46.4	46.1	7.5
HM-2.6	0.22	16.02	3.39	50.74	22.02	0.82	0.16	0.09	5.35	98.81	45.9	45.3	8.7
HM-2.7	0.34	13.94	3.05	49.82	21.16	1.56	0.02	0.26	9.14	99.29	40.5	44.2	15.3
HM-2.8	0.21	16.36	2.94	51.50	22.46	0.67	0.22	0.16	5.13	99.66	46.1	45.5	8.4
HM-2.9	0.28	15.04	4.10	49.94	21.79	1.29	0.04	0.15	7.00	99.64	43.3	45.1	11.6
HM-2.10	0.24	16.45	2.61	51.61	22.00	0.76	0.03	0.15	5.77	99.63	46.2	44.4	9.3
HM-2.11	0.25	16.30	2.67	51.43	22.00	0.79	0.06	0.14	5.83	99.48	46.0	44.6	9.4
HM-2.12	0.20	16.20	3.87	50.90	22.34	0.82	0.29	0.10	5.10	99.81	46.1	45.6	8.3
HM-2.13_1	0.24	16.58	3.14	50.89	22.31	0.61	0.59	0.11	5.38	99.85	46.5	44.9	8.6
HM-2.13_2	0.15	17.56	2.05	52.15	21.76	0.51	0.15	0.12	5.32	99.76	48.4	43.1	8.4
HM-2.13_3	0.20	16.39	3.46	50.80	22.41	0.71	0.69	0.12	4.97	99.73	46.4	45.6	8.1
HM-2.13_4	0.21	16.13	3.89	50.78	22.32	0.87	0.36	0.12	5.13	99.82	45.9	45.7	8.4
HM-2.14	0.14	17.60	2.32	52.36	21.34	0.57	0.29	0.13	5.35	100.10	48.9	42.6	8.5
HM-2.15	0.35	14.01	3.69	49.44	21.58	1.58	0.03	0.18	8.55	99.42	40.7	45.1	14.2
HM-2.16	0.28	15.96	3.87	50.42	22.22	0.89	0.15	0.12	5.71	99.62	45.3	45.4	9.3
HM-2.17	0.30	15.85	4.43	50.47	21.69	0.93	0.21	0.14	5.83	99.85	45.6	44.8	9.6
HM-2.18_1	0.41	14.12	3.57	49.50	21.53	1.47	0.02	0.21	8.58	99.39	40.9	44.8	14.3
HM-2.18_2	0.24	17.48	3.03	51.99	20.99	0.61	0.35	0.12	4.80	99.61	49.5	42.7	7.8

Label	Na_2O	MgO	Al_2O_3	SiO_2	CaO	TiO_2	Cr_2O_3	MnO	FeO	Total	En	Wo	Fs
HM-2.18_3	0.18	17.08	2.66	52.26	22.28	0.54	0.26	0.10	4.62	99.98	47.8	44.8	7.4
HM-2.18_4	0.19	17.77	1.67	53.19	22.46	0.38	0.57	0.08	3.97	100.27	49.1	44.6	6.3
HM-2.18_5	0.24	18.10	2.01	52.95	21.55	0.27	0.91	0.08	3.61	99.72	50.8	43.4	5.8
HM-2.18_6	0.32	15.75	4.82	50.41	22.38	0.57	0.24	0.09	5.22	99.80	45.3	46.2	8.6
HM-2.18_7	0.30	17.66	2.50	52.80	22.43	0.26	1.09	0.06	3.20	100.29	49.6	45.3	5.1
HM-2.18_8	0.25	17.59	2.76	52.69	22.23	0.31	0.39	0.08	3.82	100.12	49.2	44.7	6.1
HM-2.18_9	0.28	17.95	2.43	52.25	21.75	0.27	0.40	0.09	3.57	98.99	50.4	43.9	5.8
HM-2.18_10	0.29	17.40	2.98	52.75	21.94	0.37	0.46	0.07	4.21	100.48	48.9	44.3	6.8
HM-2.18_12	0.24	17.53	2.57	52.86	22.28	0.34	0.51	0.11	3.94	100.36	48.9	44.7	6.3
HM-2.18_13	0.40	15.57	5.10	50.51	22.01	0.52	0.22	0.14	5.70	100.17	44.9	45.6	9.5
HM-2.18_14	0.38	15.62	6.22	50.69	19.66	0.55	0.26	0.07	5.07	98.53	47.9	43.3	8.8
HM-2.18_15	0.26	16.28	3.47	51.09	22.47	0.68	0.65	0.14	4.82	99.85	46.2	45.9	7.9
HM-2.18_16	0.25	17.82	2.28	53.06	22.26	0.21	1.01	0.09	3.18	100.17	50.0	44.9	5.2
HM-2.18_17	0.27	17.15	3.65	51.80	22.08	0.49	0.30	0.11	3.98	99.81	48.6	44.9	6.5
HM-2.18_18	0.25	17.70	2.43	52.73	22.31	0.26	0.91	0.07	3.54	100.19	49.5	44.8	5.7
HM-2.18_19	0.31	15.77	4.71	50.61	22.61	0.66	0.29	0.10	4.80	99.86	45.4	46.7	7.9
HM-2.18_20	0.17	17.15	2.55	52.53	23.09	0.45	0.73	0.10	3.81	100.59	47.7	46.2	6.1
HM-2.19	0.25	14.85	4.76	49.93	21.34	1.17	0.07	0.19	7.25	99.80	43.2	44.6	12.1
HM-2.20	0.26	15.83	4.16	51.28	22.15	0.88	0.30	0.12	5.67	100.64	45.2	45.5	9.3
HM-2.21	0.25	15.45	4.66	50.14	21.77	1.03	0.28	0.11	5.88	99.58	44.8	45.4	9.8
HM-2.22	0.25	15.39	5.24	49.48	20.74	1.02	0.84	0.14	5.80	98.91	45.8	44.3	9.9
HM-2.23	0.24	16.51	2.86	51.90	22.12	0.74	0.02	0.12	5.65	100.15	46.3	44.6	9.1
HM-2.24	0.19	16.16	4.15	50.61	22.02	0.91	0.18	0.09	5.46	99.77	46.0	45.1	8.9
HM-2.25	0.23	16.25	3.40	51.08	22.24	0.68	0.55	0.11	4.96	99.50	46.3	45.6	8.1
HM-2.26	0.21	16.13	3.46	50.86	22.01	0.85	0.15	0.11	5.48	99.26	46.0	45.1	8.9
HM-2.27	0.31	14.48	4.20	49.49	21.82	1.37	0.02	0.15	7.32	99.17	42.2	45.6	12.2
HM-2.28	0.19	18.01	1.92	52.53	21.57	0.43	0.69	0.13	4.44	99.91	49.9	43.0	7.1
HM-2.29	0.23	16.00	3.95	50.31	21.15	1.04	0.04	0.14	6.43	99.29	45.9	43.6	10.6
HM-2.30	0.28	16.45	3.43	51.13	22.00	0.65	1.11	0.12	4.50	99.67	47.2	45.4	7.4
HM-2.31	0.23	16.21	3.72	50.95	22.40	0.80	0.29	0.11	5.13	99.85	46.0	45.7	8.3
HM-2.32	0.29	15.50	2.74	51.12	21.64	1.01	0.03	0.16	7.13	99.60	44.1	44.3	11.6
HM-2.33	0.15	17.70	1.96	52.28	20.82	0.47	0.45	0.10	4.72	98.65	50.0	42.3	7.7

Olivines

Label	Na_2O	MgO	Al_2O_3	SiO_2	CaO	TiO_2	Cr_2O_3	MnO	FeO	NiO	Total	Fo	Fa
HM-1.1_1	0.02	34.52	0.03	36.57	0.35	0.06	0.01	0.57	27.02	0.13	99.26	69.5	30.5
HM-1.1_2	0.02	44.68	0.03	39.02	0.25	0.03	0.03	0.21	15.01	0.21	99.49	84.1	15.9
HM-1.1_3	0.02	48.25	0.00	39.95	0.25	0.00	0.03	0.16	10.95	0.25	99.87	88.7	11.3
HM-1.1_4	0.02	48.66	0.06	39.83	0.30	0.01	0.06	0.15	10.32	0.23	99.65	89.4	10.6
HM-1.1_5	0.00	48.49	0.03	39.74	0.26	0.01	0.07	0.14	10.58	0.24	99.55	89.1	10.9
HM-1.1_6	0.02	47.66	0.04	39.49	0.23	0.02	0.02	0.16	11.61	0.19	99.44	88.0	12.0
HM-1.1_7	0.01	46.85	0.05	39.46	0.26	0.00	0.03	0.19	12.24	0.23	99.33	87.2	12.8
HM-1.1_8	0.00	47.01	0.05	39.30	0.23	0.02	0.05	0.19	12.56	0.23	99.66	87.0	13.0
HM-1.2_1	0.02	35.42	0.03	36.77	0.33	0.07	0.01	0.46	25.76	0.16	99.04	71.0	29.0
HM-1.2_2	0.02	45.67	0.02	39.29	0.26	0.02	0.00	0.18	13.94	0.21	99.62	85.4	14.6
HM-1.2_3	0.00	48.41	0.01	39.79	0.25	0.01	0.04	0.19	10.83	0.26	99.79	88.8	11.2
HM-1.2_5	0.00	47.49	0.06	39.89	0.38	0.02	0.04	0.16	11.22	0.23	99.48	88.3	11.7
HM-1.2_7	0.00	49.14	0.04	39.98	0.25	0.00	0.08	0.14	9.98	0.27	99.88	89.8	10.2
HM-1.5_1	0.01	34.17	0.02	36.69	0.31	0.04	0.00	0.55	27.09	0.15	99.04	69.2	30.8
HM-1.5_2	0.00	44.96	0.04	38.97	0.27	0.02	0.03	0.22	14.87	0.23	99.61	84.3	15.7

Label	Na_2O	MgO	Al_2O_3	SiO_2	CaO	TiO_2	Cr_2O_3	MnO	FeO	NiO	Total	Fo	Fa
HM-1.5_3	0.02	47.96	0.02	39.84	0.25	0.02	0.04	0.15	10.81	0.23	99.33	88.8	11.2
HM-1.5_4	0.01	48.65	0.03	39.97	0.27	0.00	0.01	0.15	10.00	0.25	99.34	89.7	10.3
HM-1.5_5	0.02	48.83	0.02	39.93	0.29	0.01	0.06	0.14	9.94	0.21	99.45	89.8	10.2
HM-1.5_6	0.01	48.61	0.01	39.87	0.26	0.02	0.05	0.12	10.03	0.23	99.21	89.6	10.4
HM-1.5_7	0.02	48.82	0.03	40.06	0.33	0.01	0.08	0.15	10.08	0.22	99.80	89.6	10.4
HM-1.5_8	0.01	48.56	0.05	39.84	0.29	0.01	0.08	0.15	10.24	0.23	99.47	89.4	10.6
HM-1.6_1	0.03	38.69	0.04	37.53	0.30	0.06	0.01	0.41	21.86	0.16	99.09	75.9	24.1
HM-1.6_2	0.01	44.95	0.03	38.99	0.25	0.03	0.02	0.20	14.65	0.23	99.37	84.5	15.5
HM-1.6_3	0.02	48.09	0.03	39.84	0.26	0.00	0.05	0.16	11.13	0.26	99.84	88.5	11.5
HM-1.6_4	0.03	49.04	0.03	39.88	0.27	0.02	0.08	0.14	9.96	0.26	99.71	89.8	10.2
HM-1.6_5	0.01	49.08	0.05	40.14	0.27	0.02	0.06	0.10	9.87	0.25	99.86	89.9	10.1
HM-1.6_6	0.04	48.92	0.01	40.03	0.26	0.01	0.10	0.10	9.98	0.27	99.71	89.7	10.3
HM-1.6_7	0.00	49.02	0.03	40.11	0.27	0.02	0.06	0.15	9.79	0.23	99.69	89.9	10.1
HM-1.7_1	0.01	36.35	0.04	37.08	0.32	0.05	0.05	0.50	24.64	0.19	99.23	72.5	27.5
HM-1.7_2	0.02	44.01	0.02	39.00	0.22	0.03	0.04	0.23	15.54	0.23	99.35	83.5	16.5
HM-1.7_3	0.01	47.18	0.04	39.54	0.26	0.01	0.04	0.15	11.96	0.26	99.45	87.6	12.4
HM-1.7_4	0.00	47.91	0.03	39.84	0.26	0.00	0.05	0.15	10.92	0.27	99.44	88.7	11.3
HM-1.8_1	0.02	35.40	0.03	36.96	0.33	0.06	0.00	0.50	25.21	0.14	98.65	71.5	28.5
HM-1.8_2	0.03	41.68	0.01	38.34	0.29	0.03	0.02	0.30	18.48	0.14	99.32	80.1	19.9
HM-1.8_3	0.09	45.78	1.25	38.93	0.33	0.01	0.03	0.21	14.26	0.21	101.11	85.1	14.9
HM-1.8_4	0.03	46.11	0.02	39.44	0.24	0.01	0.05	0.18	12.75	0.23	99.05	86.6	13.4
HM-1.8_5	0.03	47.42	0.04	39.74	0.26	0.01	0.06	0.19	11.69	0.30	99.73	87.9	12.1
HM-1.8_6	0.01	47.50	0.02	39.69	0.25	0.02	0.05	0.20	11.66	0.25	99.65	87.9	12.1
HM-1.8_7	0.02	46.72	0.02	39.63	0.27	0.02	0.07	0.20	12.23	0.27	99.45	87.2	12.8
HM-1.8_8	0.03	47.23	0.03	39.52	0.26	0.00	0.06	0.18	11.74	0.23	99.29	87.8	12.2
HM-1.8_9	0.01	47.32	0.02	39.73	0.25	0.01	0.04	0.17	11.39	0.29	99.24	88.1	11.9
HM-1.8_10	0.02	47.16	0.04	39.51	0.27	0.01	0.07	0.17	11.59	0.30	99.14	87.9	12.1
HM-1.8_11	0.03	46.62	0.04	39.53	0.26	0.02	0.07	0.17	12.38	0.27	99.38	87.0	13.0
HM-1.8_12	0.01	46.59	0.04	39.60	0.28	0.02	0.06	0.22	12.22	0.27	99.30	87.2	12.8
HM-1.8_13	0.03	47.93	0.03	39.89	0.26	0.01	0.06	0.16	10.60	0.30	99.27	89.0	11.0
HM-1.8_14	0.03	48.52	0.03	39.79	0.27	0.01	0.09	0.17	9.94	0.28	99.13	89.7	10.3
HM-1.8_15	0.01	49.12	0.02	40.14	0.26	0.00	0.08	0.16	9.70	0.28	99.77	90.0	10.0
HM-1.8_16	0.03	48.71	0.02	40.14	0.25	0.01	0.13	0.17	9.52	0.28	99.25	90.1	9.9
HM-1.8_17	0.00	48.84	0.04	40.04	0.27	0.03	0.07	0.14	9.57	0.28	99.28	90.1	9.9
HM-1.8_18	0.01	48.61	0.03	39.97	0.25	0.00	0.02	0.13	9.61	0.27	98.90	90.0	10.0
HM-1.8_19	0.04	48.70	0.00	39.97	0.26	0.01	0.07	0.18	9.78	0.24	99.23	89.9	10.1
HM-1.8_20	0.00	48.34	0.04	39.86	0.24	0.02	0.05	0.14	9.88	0.28	98.86	89.7	10.3
HM-1.9_1	0.02	35.08	0.04	36.78	0.31	0.04	0.01	0.48	25.27	0.15	98.18	71.2	28.8
HM-1.9_2	0.02	44.98	0.02	38.98	0.25	0.01	0.05	0.18	13.70	0.24	98.42	85.4	14.6
HM-1.9_3	0.02	47.84	0.02	39.67	0.28	0.00	0.03	0.16	10.48	0.27	98.78	89.1	10.9
HM-1.9_4	0.00	48.12	0.04	39.74	0.27	0.01	0.08	0.12	9.80	0.26	98.44	89.8	10.2
HM-1.9_5	0.02	48.75	0.02	39.73	0.24	0.02	0.06	0.13	9.79	0.25	99.02	89.9	10.1
HM-1.10	0.00	29.53	0.01	35.59	0.38	0.10	0.00	0.72	31.77	0.12	98.22	62.4	37.6
HM-1.11	0.03	32.21	0.03	35.99	0.37	0.06	0.00	0.63	28.80	0.12	98.24	66.6	33.4
HM-1.12	0.03	42.27	0.02	38.52	0.24	0.03	0.03	0.24	17.49	0.20	99.08	81.2	18.8
HM-1.13	0.01	29.78	0.00	35.37	0.31	0.16	0.03	0.71	32.07	0.15	98.59	62.3	37.7
HM-1.14	0.01	40.49	0.03	37.96	0.28	0.03	0.03	0.31	19.61	0.17	98.92	78.6	21.4
HM-2.1_3	0.02	42.29	0.04	38.42	0.37	0.03	0.03	0.29	17.44	0.18	99.11	81.2	18.8
HM-2.1_4	0.01	42.48	0.03	38.25	0.38	0.04	0.05	0.27	17.34	0.23	99.07	81.4	18.6
HM-2.1_5	0.01	42.59	0.03	38.22	0.34	0.03	0.01	0.27	17.75	0.21	99.44	81.1	18.9
HM-2.1_6	0.00	42.78	0.00	38.15	0.33	0.04	0.04	0.29	17.88	0.23	99.75	81.0	19.0
HM-2.2_1	0.01	42.72	0.01	37.72	0.33	0.02	0.05	0.24	17.96	0.17	99.24	80.9	19.1
HM-2.2_2	0.00	42.67	0.04	38.47	0.33	0.01	0.02	0.29	17.41	0.19	99.43	81.4	18.6
HM-2.2_3	0.01	42.88	0.03	38.55	0.32	0.03	0.07	0.28	16.77	0.22	99.15	82.0	18.0

Label	Na_2O	MgO	Al_2O_3	SiO_2	CaO	TiO_2	Cr_2O_3	MnO	FeO	NiO	Total	Fo	Fa
HM-2.2_4	0.00	42.54	0.02	38.61	0.35	0.02	0.08	0.29	16.90	0.23	99.05	81.8	18.2
HM-2.2_5	0.00	42.68	0.03	38.68	0.36	0.02	0.03	0.26	16.56	0.23	98.84	82.1	17.9
HM-2.2_6	0.00	43.02	0.02	38.79	0.37	0.02	0.04	0.30	16.76	0.21	99.51	82.1	17.9
HM-2.2_7	0.01	42.79	0.01	38.81	0.34	0.01	0.03	0.26	16.79	0.20	99.25	82.0	18.0
HM-2.2_8	0.01	42.46	0.03	38.87	0.33	0.02	0.00	0.27	16.83	0.21	99.04	81.8	18.2
HM-2.3	0.03	39.98	0.04	37.90	0.31	0.01	0.00	0.30	19.96	0.21	98.75	78.1	21.9
HM-2.4	0.03	42.56	0.05	38.36	0.32	0.02	0.06	0.28	17.50	0.27	99.46	81.3	18.7
HM-2.6_1	0.00	39.06	0.03	37.38	0.30	0.04	0.01	0.37	21.81	0.21	99.19	76.2	23.8
HM-2.6_2	0.01	39.32	0.13	40.69	0.43	0.03	0.04	0.29	17.19	0.16	98.28	80.3	19.7
HM-2.6_3	0.00	43.19	0.02	38.48	0.32	0.02	0.01	0.24	16.92	0.21	99.42	82.0	18.0
HM-2.6_4	0.02	42.98	0.02	38.55	0.30	0.03	0.04	0.24	16.87	0.22	99.27	82.0	18.0
HM-2.6_5	0.02	42.52	0.03	38.60	0.32	0.04	0.09	0.25	16.92	0.19	98.96	81.8	18.2
HM-2.6_6	0.01	41.48	0.04	38.44	0.33	0.01	0.14	0.27	17.66	0.19	98.58	80.7	19.3
HM-2.7	0.00	42.07	0.03	38.37	0.33	0.02	0.04	0.25	17.01	0.23	98.35	81.5	18.5
HM-2.8_1	0.02	34.40	0.02	36.50	0.32	0.06	0.00	0.47	26.59	0.16	98.54	69.8	30.2
HM-2.8_2	0.01	41.60	0.02	38.46	0.35	0.02	0.04	0.23	17.85	0.21	98.78	80.6	19.4
HM-2.8_3	0.01	42.29	0.03	38.35	0.34	0.05	0.00	0.28	17.19	0.22	98.75	81.4	18.6
HM-2.8_4	0.01	42.57	0.03	38.45	0.30	0.02	0.00	0.26	17.36	0.20	99.20	81.4	18.6
HM-2.8_5	0.00	42.39	0.03	38.46	0.32	0.03	0.01	0.22	17.33	0.20	99.00	81.3	18.7
HM-2.8_6	0.01	42.64	0.02	38.52	0.31	0.02	0.00	0.27	17.40	0.21	99.39	81.4	18.6
HM-2.8_7	0.00	42.36	0.03	38.62	0.30	0.03	0.01	0.27	17.36	0.20	99.19	81.3	18.7
HM-2.8_8	0.01	42.29	0.01	38.36	0.31	0.03	0.01	0.27	17.56	0.17	99.02	81.1	18.9
HM-2.8_9	0.03	42.59	0.03	38.57	0.33	0.02	0.00	0.31	17.30	0.21	99.39	81.4	18.6
HM-2.8_10	0.00	43.49	0.03	38.97	0.31	0.02	0.05	0.21	16.71	0.25	100.05	82.3	17.7
HM-2.32	0.00	43.32	0.02	38.44	0.29	0.03	0.07	0.28	15.77	0.20	98.43	83.0	17.0
HM-2.33	0.00	44.09	0.03	38.74	0.29	0.02	0.09	0.21	15.02	0.18	98.69	84.0	16.0
HM-2.34	0.00	43.93	0.03	38.66	0.29	0.04	0.05	0.25	15.59	0.21	99.05	83.4	16.6
HM-2.37	0.01	41.72	0.02	37.77	0.32	0.02	0.01	0.28	17.69	0.23	98.07	80.8	19.2
HM-2.1_1	0.11	35.99	0.00	37.62	0.34	0.05	0.00	0.44	26.19	0.14	100.87	71.0	29.0
HM-2.1_3	0.09	40.61	0.20	40.46	0.34	0.04	0.03	0.23	18.80	0.15	100.96	79.4	20.6
HM-2.1_4	0.03	44.36	0.02	39.35	0.29	0.01	0.03	0.23	16.26	0.15	100.74	82.9	17.1
HM-2.1_5	0.11	45.88	0.00	39.86	0.28	0.02	0.01	0.19	14.19	0.19	100.72	85.2	14.8
HM-2.1_6	0.20	46.93	0.03	40.26	0.28	0.01	0.11	0.19	12.76	0.18	100.95	86.8	13.2
HM-2.1_7	0.29	47.61	0.02	40.26	0.29	0.01	0.08	0.18	11.60	0.18	100.53	88.0	12.0
HM-2.1_8	0.04	48.13	0.03	40.49	0.25	0.02	0.09	0.11	11.31	0.18	100.66	88.4	11.6
HM-2.1_9	0.06	48.19	0.03	40.25	0.30	0.01	0.09	0.16	11.13	0.21	100.42	88.5	11.5
HM-2.1_10	0.05	48.33	0.03	40.44	0.33	0.00	0.06	0.14	10.90	0.21	100.49	88.8	11.2
HM-2.2_1	0.04	31.88	0.06	37.34	0.46	0.09	0.02	0.58	30.09	0.11	100.68	65.4	34.6
HM-2.2_2	0.09	37.43	0.00	37.83	0.34	0.04	0.03	0.40	24.24	0.12	100.51	73.4	26.6
HM-2.2_3	0.02	41.63	0.04	38.80	0.32	0.03	0.00	0.31	19.42	0.11	100.67	79.3	20.7
HM-2.2_4	0.02	43.69	0.00	39.44	0.28	0.01	0.06	0.28	16.99	0.14	100.92	82.1	17.9
HM-2.2_5	0.16	44.91	0.05	39.43	0.27	0.00	0.08	0.24	15.50	0.20	100.83	83.8	16.2
HM-2.2_6	0.04	45.71	0.01	39.86	0.25	0.01	0.16	0.23	14.27	0.19	100.74	85.1	14.9
HM-2.2_7	0.03	46.22	0.04	39.90	0.26	0.01	0.06	0.15	13.57	0.21	100.46	85.9	14.1
HM-2.2_8	0.05	45.61	0.15	39.75	0.36	0.03	0.29	0.16	12.49	0.18	99.08	86.7	13.3
HM-2.2_9	0.03	46.51	0.02	39.99	0.26	0.02	0.07	0.19	13.11	0.21	100.41	86.3	13.7
HM-2.2_10	0.03	46.99	0.04	40.18	0.25	0.03	0.05	0.20	13.03	0.19	101.00	86.5	13.5
HM-2.2_11	0.02	47.26	0.03	40.23	0.25	0.00	0.04	0.21	12.46	0.24	100.75	87.1	12.9
HM-2.2_12	0.01	47.40	0.02	40.28	0.24	0.01	0.07	0.16	12.25	0.20	100.64	87.3	12.7
HM-2.2_13	0.01	47.48	0.00	40.37	0.24	0.00	0.06	0.17	12.18	0.21	100.71	87.4	12.6
HM-2.2_14	0.02	47.51	0.01	40.41	0.25	0.00	0.07	0.20	11.94	0.21	100.62	87.6	12.4
HM-2.2_15	0.03	47.47	0.01	40.52	0.27	0.00	0.11	0.19	11.87	0.22	100.68	87.7	12.3

Label	Na_2O	MgO	Al_2O_3	SiO_2	CaO	TiO_2	Cr_2O_3	MnO	FeO	NiO	Total	Fo	Fa
HM-2.4_1	0.02	30.89	0.02	36.25	0.41	0.08	0.01	0.67	30.81	0.06	99.21	64.1	35.9
HM-2.4_2	0.03	35.80	0.01	37.25	0.34	0.04	0.03	0.48	25.52	0.10	99.61	71.4	28.6
HM-2.4_3	0.03	41.08	0.03	38.66	0.29	0.04	0.03	0.30	19.82	0.14	100.40	78.7	21.3
HM-2.4_4	0.00	44.02	0.01	39.42	0.26	0.01	0.04	0.24	16.28	0.18	100.47	82.8	17.2
HM-2.4_5	0.00	46.48	0.02	40.05	0.28	0.00	0.05	0.20	13.11	0.17	100.37	86.3	13.7
HM-2.4_6	0.01	47.85	0.03	40.20	0.27	0.00	0.07	0.20	11.47	0.20	100.30	88.1	11.9
HM-2.4_7	0.05	46.93	0.29	40.09	0.28	0.00	0.09	0.14	10.68	0.22	98.76	88.7	11.3
HM-2.4_8	0.02	48.81	0.05	40.45	0.26	0.00	0.06	0.15	10.36	0.22	100.37	89.4	10.6
HM-2.4_9	0.05	48.84	0.02	40.59	0.27	0.00	0.07	0.12	10.07	0.18	100.23	89.6	10.4
HM-2.4_10	0.03	49.04	0.02	40.75	0.30	0.00	0.08	0.15	10.06	0.24	100.66	89.7	10.3
HM-2.4_11	0.01	49.39	0.01	40.71	0.28	0.00	0.08	0.13	10.01	0.20	100.82	89.8	10.2
HM-2.4_12	0.01	49.32	0.04	40.66	0.29	0.01	0.07	0.15	10.08	0.20	100.81	89.7	10.3
HM-2.4_13	0.04	49.12	0.03	40.64	0.28	0.00	0.07	0.13	9.92	0.20	100.44	89.8	10.2
HM-2.4_14	0.04	49.07	0.01	40.79	0.28	0.01	0.09	0.11	10.00	0.18	100.60	89.7	10.3
HM-2.4_15	0.12	49.03	0.04	40.55	0.28	0.00	0.09	0.15	10.06	0.17	100.48	89.7	10.3
HM-2.4_16	0.05	49.00	0.00	40.61	0.29	0.01	0.06	0.18	9.99	0.19	100.38	89.7	10.3
HM-2.4_17	0.07	48.99	0.02	40.67	0.26	0.00	0.02	0.15	10.18	0.22	100.59	89.6	10.4
HM-2.4_18	0.06	49.11	0.02	40.56	0.29	0.00	0.11	0.13	10.10	0.21	100.59	89.7	10.3
HM-2.5_3	0.10	44.18	0.02	39.36	0.29	0.01	0.00	0.25	16.27	0.14	100.63	82.9	17.1
HM-2.5_5	0.05	47.55	0.05	40.28	0.23	0.00	0.01	0.15	11.88	0.21	100.41	87.7	12.3
HM-2.5_6	0.05	48.24	0.03	40.49	0.25	0.00	0.03	0.14	11.15	0.21	100.58	88.5	11.5
HM-2.5_7	0.13	48.35	0.06	40.40	0.26	0.01	0.05	0.16	10.66	0.21	100.28	89.0	11.0
HM-2.5_8	0.18	48.40	0.02	40.20	0.30	0.01	0.04	0.13	10.37	0.21	99.88	89.3	10.7
HM-2.5_9	0.31	48.08	0.04	40.35	0.30	0.00	0.03	0.10	10.15	0.19	99.55	89.4	10.6
HM-2.5_10	1.19	46.31	0.05	39.43	0.39	0.01	0.02	0.14	9.76	0.21	97.50	89.4	10.6
HM-2.5_11	0.15	48.76	0.04	40.37	0.29	0.00	0.07	0.15	10.01	0.20	100.04	89.7	10.3
HM-2.5_12	0.14	48.71	0.03	40.23	0.30	0.02	0.01	0.15	9.95	0.23	99.76	89.7	10.3
HM-2.5_13	0.02	49.34	0.03	40.55	0.28	0.00	0.05	0.12	9.90	0.23	100.53	89.9	10.1
HM-2.5_14	0.07	49.49	0.01	40.73	0.28	0.00	0.06	0.14	9.68	0.22	100.68	90.1	9.9
HM-2.5_15	0.02	49.70	0.03	40.85	0.26	0.00	0.06	0.15	9.52	0.23	100.83	90.3	9.7
HM-2.5_17	0.70	49.52	0.05	40.22	0.29	0.00	0.07	0.12	8.62	0.27	99.87	91.1	8.9
HM-2.5_18	0.02	50.34	0.04	40.91	0.27	0.00	0.05	0.08	8.45	0.27	100.44	91.4	8.6
HM-2.6_1	0.01	33.36	0.02	36.87	0.39	0.07	0.00	0.55	28.88	0.09	100.25	67.3	32.7
HM-2.6_2	0.05	41.66	0.03	38.91	0.31	0.02	0.03	0.30	19.23	0.15	100.69	79.4	20.6
HM-2.6_3	0.12	45.35	0.02	39.72	0.25	0.02	0.07	0.16	14.64	0.16	100.51	84.7	15.3
HM-2.6_4	0.05	47.44	0.03	40.30	0.25	0.02	0.07	0.17	12.25	0.21	100.78	87.4	12.6
HM-2.6_5	0.07	48.28	0.03	40.44	0.29	0.00	0.06	0.16	11.11	0.21	100.65	88.6	11.4
HM-2.6_6	0.01	48.86	0.04	40.51	0.26	0.00	0.06	0.13	10.63	0.20	100.71	89.1	10.9
HM-2.6_7	0.01	49.09	0.02	40.47	0.28	0.00	0.04	0.18	10.26	0.20	100.55	89.5	10.5
HM-2.6_8	0.00	49.21	0.03	40.61	0.28	0.00	0.11	0.16	10.29	0.20	100.89	89.5	10.5
HM-2.6_9	0.01	49.08	0.05	40.58	0.29	0.00	0.05	0.16	10.15	0.20	100.56	89.6	10.4
HM-2.6_10	0.01	49.41	0.03	40.55	0.26	0.00	0.09	0.15	10.15	0.23	100.89	89.7	10.3
HM-2.6_11	0.02	49.56	0.05	40.58	0.25	0.00	0.04	0.13	9.91	0.25	100.78	89.9	10.1
HM-2.6_12	0.00	49.28	0.02	40.70	0.25	0.00	0.05	0.11	9.86	0.27	100.54	89.9	10.1
HM-2.6_13	0.01	49.34	0.03	40.84	0.29	0.01	0.07	0.11	9.76	0.22	100.70	90.0	10.0
HM-2.6_14	0.03	49.50	0.02	40.48	0.27	0.00	0.09	0.13	9.57	0.22	100.31	90.2	9.8
HM-2.6_15	0.02	49.54	0.02	40.68	0.28	0.00	0.01	0.13	9.64	0.27	100.58	90.2	9.8
HM-2.6_16	0.04	49.39	0.04	40.71	0.29	0.00	0.08	0.15	9.76	0.28	100.75	90.0	10.0
HM-2.6_17	0.00	49.31	0.06	40.59	0.28	0.00	0.12	0.12	9.67	0.23	100.39	90.1	9.9
HM-2.6_18	0.01	49.49	0.02	40.79	0.25	0.00	0.08	0.14	9.57	0.21	100.57	90.2	9.8
HM-2.6_19	0.02	49.34	0.04	40.66	0.29	0.00	0.07	0.12	9.69	0.27	100.50	90.1	9.9
HM-2.6_20	0.01	49.11	0.02	40.51	0.29	0.00	0.08	0.13	9.87	0.21	100.23	89.9	10.1

Label	Na_2O	MgO	Al_2O_3	SiO_2	CaO	TiO_2	Cr_2O_3	MnO	FeO	NiO	Total	Fo	Fa
HM-2.7_1	0.04	30.33	0.03	36.15	0.35	0.08	0.00	0.72	32.78	0.11	100.59	62.3	37.7
HM-2.7_2	0.07	33.80	0.02	36.75	0.34	0.02	0.04	0.55	28.09	0.11	99.80	68.2	31.8
HM-2.7_3	0.05	35.49	0.03	37.32	0.34	0.04	0.03	0.50	26.23	0.11	100.14	70.7	29.3
HM-2.7_4	0.04	38.11	0.04	37.96	0.30	0.02	0.05	0.39	23.56	0.10	100.58	74.3	25.7
HM-2.7_5	0.05	40.02	0.02	38.41	0.28	0.02	0.03	0.35	20.50	0.18	99.85	77.7	22.3
HM-2.7_6	0.03	41.70	0.03	38.96	0.27	0.02	0.00	0.31	18.68	0.12	100.12	79.9	20.1
HM-2.7_7	0.02	42.99	0.02	39.24	0.27	0.01	0.00	0.23	17.41	0.16	100.35	81.5	18.5
HM-2.7_8	0.03	44.24	0.05	39.46	0.28	0.01	0.02	0.25	16.06	0.15	100.53	83.1	16.9
HM-2.8_1	0.03	33.78	0.03	36.87	0.36	0.06	0.00	0.55	27.89	0.11	99.68	68.3	31.7
HM-2.8_2	0.02	38.52	0.05	38.16	0.33	0.02	0.01	0.40	22.69	0.18	100.38	75.2	24.8
HM-2.8_3	0.03	43.08	0.04	38.99	0.24	0.01	0.05	0.25	16.99	0.16	99.83	81.9	18.1
HM-2.8_4	0.01	46.00	0.02	39.62	0.26	0.02	0.06	0.20	13.99	0.19	100.36	85.4	14.6
HM-2.8_5	0.01	47.88	0.02	40.21	0.26	0.01	0.06	0.19	11.46	0.18	100.28	88.2	11.8
HM-2.8_6	0.01	48.72	0.00	40.56	0.27	0.00	0.07	0.13	10.52	0.24	100.53	89.2	10.8
HM-2.8_7	0.02	48.83	0.04	40.62	0.28	0.01	0.08	0.13	10.40	0.23	100.63	89.3	10.7
HM-2.8_8	0.02	48.80	0.05	40.34	0.28	0.00	0.02	0.11	10.34	0.20	100.16	89.4	10.6
HM-2.3_1	0.00	32.05	0.01	36.65	0.37	0.05	0.02	0.65	30.13	0.12	100.04	65.5	34.5
HM-2.3_2	0.03	39.49	0.04	38.33	0.28	0.03	0.00	0.35	21.59	0.16	100.31	76.5	23.5
HM-2.3_3	0.04	45.16	0.02	39.57	0.28	0.03	0.03	0.23	15.19	0.21	100.75	84.1	15.9
HM-2.3_4	0.01	48.51	0.03	40.52	0.25	0.00	0.05	0.10	10.64	0.26	100.37	89.0	11.0
HM-2.3_5	0.02	50.50	0.03	40.95	0.25	0.00	0.05	0.13	8.27	0.27	100.49	91.6	8.4
HM-2.3_6	0.01	51.39	0.03	41.19	0.26	0.00	0.10	0.11	7.33	0.32	100.73	92.6	7.4
HM-2.3_7	0.01	51.48	0.05	41.08	0.25	0.00	0.08	0.09	6.82	0.33	100.19	93.1	6.9
HM-2.3_8	0.03	51.73	0.03	41.29	0.24	0.00	0.09	0.07	6.35	0.32	100.16	93.6	6.4
HM-2.3_9	0.00	51.95	0.01	41.26	0.26	0.00	0.11	0.07	6.45	0.34	100.47	93.5	6.5
HM-2.3_10	0.02	51.84	0.05	41.38	0.27	0.00	0.07	0.08	6.56	0.34	100.62	93.4	6.6
HM-2.3_11	0.03	51.61	0.03	41.30	0.23	0.00	0.07	0.09	6.80	0.32	100.48	93.1	6.9
HM-2.3_12	0.03	51.20	0.04	41.11	0.25	0.00	0.10	0.08	7.39	0.35	100.56	92.5	7.5

Feldspars

Label	Na_2O	MgO	Al_2O_3	SiO_2	K_2O	CaO	FeO	SrO	BaO	Total	An	Ab	Or
HM-1.1	3.49	0.12	31.04	50.67	0.40	13.74	0.95	0.09	0.01	100.51	66.9	30.8	2.3
HM-1.5	4.54	0.00	20.31	62.78	8.68	1.48	0.54	0.11	0.56	99.00	7.4	41.0	51.6
HM-1.6	4.50	0.01	20.39	63.16	8.97	1.57	0.40	0.00	0.06	99.05	7.7	39.9	52.4
HM-1.9	4.21	0.02	20.07	63.64	9.48	1.43	0.54	0.08	0.07	99.53	7.0	37.5	55.5
HM-1.10	3.81	0.05	20.12	62.95	10.07	1.35	0.65	0.05	0.01	99.07	6.7	34.1	59.2
HM-1.12	4.10	0.01	20.14	62.86	9.38	1.25	0.44	0.08	0.44	98.70	6.3	37.4	56.3
HM-1.13	4.26	0.02	19.95	63.06	9.53	1.11	0.51	0.14	0.20	98.79	5.5	38.2	56.3
HM-1.14	4.21	0.00	19.62	63.18	9.64	0.97	0.47	0.05	0.20	98.33	4.8	38.0	57.2
HM-1.17	4.07	0.01	20.19	62.26	9.60	1.40	0.47	0.15	0.67	98.84	6.9	36.5	56.6
HM-1.18	4.73	0.01	20.01	63.56	9.03	1.20	0.61	0.00	0.00	99.14	5.8	41.7	52.4
HM-1.19	3.88	0.04	20.40	62.27	9.83	1.47	0.49	0.15	0.61	99.13	7.3	34.8	58.0
HM-1.20	4.01	0.00	19.81	63.84	10.23	0.97	0.42	0.00	0.01	99.29	4.8	35.5	59.7
HM-1.22	3.86	0.01	19.84	62.43	9.96	0.98	0.38	0.12	0.95	98.55	5.0	35.2	59.8
HM-1.25	3.85	0.02	19.76	63.50	10.27	0.90	0.37	0.09	0.23	98.99	4.5	34.7	60.8
HM-1.26	3.83	0.01	19.68	63.23	10.08	0.96	0.50	0.12	0.41	98.82	4.8	34.8	60.3
HM-1.28	3.96	0.01	19.48	63.71	10.27	0.78	0.39	0.02	0.03	98.65	3.9	35.5	60.6
HM-1.30	4.18	0.03	19.88	62.81	9.52	1.50	0.38	0.08	0.23	98.61	7.3	37.1	55.6
HM-1.32	4.32	0.01	19.61	63.46	9.83	1.04	0.33	0.06	0.05	98.71	5.0	38.0	56.9
HM-1.34	3.60	0.01	19.33	63.67	10.95	0.75	0.39	0.01	0.00	98.72	3.7	32.1	64.2
HM-2.1	4.57	0.19	20.35	61.68	8.65	2.01	0.35	0.00	0.05	97.85	9.8	40.2	50.1
HM-2.3	4.42	0.01	19.17	63.99	9.81	0.66	0.15	0.00	0.00	98.21	3.3	39.3	57.4
HM-2.6	4.20	0.00	19.90	63.27	9.42	0.95	0.32	0.16	0.62	98.83	4.8	38.4	56.7
HM-2.7	4.05	0.13	19.58	63.42	9.90	0.76	0.45	0.13	0.78	99.21	3.8	36.9	59.3

Label	Na_2O	MgO	Al_2O_3	SiO_2	K_2O	CaO	FeO	SrO	BaO	Total	An	Ab	Or
HM-2.8	5.20	0.02	19.89	63.71	8.13	1.06	0.35	0.10	0.03	98.49	5.2	46.7	48.0
HM-2.9	5.03	0.03	19.95	63.63	8.74	1.19	0.29	0.01	0.01	98.88	5.8	44.0	50.3
HM-2.11	4.65	0.02	19.71	63.78	9.35	0.98	0.42	0.04	0.01	98.95	4.8	41.0	54.2
HM-2.13	4.29	0.02	20.23	63.34	9.41	1.42	0.30	0.10	0.10	99.21	7.0	38.1	54.9
HM-2.16	4.68	0.10	19.94	63.90	9.40	1.17	0.42	0.10	0.00	99.72	5.6	40.7	53.7
HM-2.17	4.24	0.48	19.46	63.91	9.63	0.78	0.69	0.00	0.00	99.19	3.9	38.5	57.5
HM-2.18	5.01	0.02	20.02	63.89	8.98	1.01	0.44	0.00	0.01	99.37	4.8	43.7	51.5
HM-2.19	4.49	0.01	19.91	63.59	9.51	0.94	0.44	0.13	0.44	99.45	4.6	39.8	55.6
HM-2.20	4.17	0.00	19.87	63.75	9.98	1.01	0.22	0.00	0.06	99.06	4.9	36.9	58.1
HM-2.21	4.63	0.11	19.98	63.39	8.95	0.96	0.23	0.03	0.04	98.34	4.8	41.9	53.3
HM-2.23	4.15	0.01	20.12	62.11	9.62	1.28	0.56	0.20	0.66	98.71	6.3	37.1	56.6
HM-2.24	4.90	0.02	19.85	63.38	8.75	1.10	0.38	0.00	0.04	98.42	5.4	43.5	51.1
HM-2.25	3.74	0.01	20.26	61.61	9.88	1.79	0.28	0.16	0.19	97.92	8.8	33.3	57.9
HM-2.26	4.71	0.01	20.23	63.07	8.55	1.65	0.25	0.00	0.00	98.49	8.1	41.9	50.0
HM-2.27	4.48	0.00	19.90	63.00	9.25	1.19	0.29	0.07	0.10	98.26	5.8	39.9	54.2
HM-2.1	4.29	0.01	19.76	64.79	9.48	1.15	0.40		0.01	99.89	5.7	38.4	55.9
HM-2.2	4.01	0.01	19.70	64.65	10.14	1.08	0.46		0.06	100.10	5.3	35.5	59.2
HM-2.3	3.72	0.08	30.46	51.87	0.35	13.71	0.95		0.05	101.19	65.7	32.2	2.0
HM-2.4	3.58	0.07	30.75	51.49	0.38	13.93	0.88		0.02	101.10	66.8	31.1	2.2
HM-2.5	3.90	0.08	30.35	52.04	0.37	13.33	0.89		0.03	100.99	64.0	33.9	2.1
HM-2.7	4.44	0.01	19.77	64.83	9.46	0.95	0.34		0.59	100.39	4.7	39.7	55.6
HM-2.9	3.72	0.13	30.47	51.58	0.47	13.25	0.87		0.05	100.54	64.5	32.7	2.7
HM-2.10	3.99	0.10	30.37	51.97	0.37	13.30	0.92		0.04	101.06	63.5	34.5	2.1
HM-2.11	4.86	0.04	21.19	63.09	7.00	2.56	0.63		0.05	99.41	13.0	44.7	42.3
HM-2.12	4.13	0.14	29.55	53.13	0.58	12.50	0.80		0.05	100.88	60.5	36.2	3.3
HM-2.13	3.75	0.10	30.37	51.92	0.30	13.48	0.86		0.04	100.82	65.4	32.9	1.7
HM-2.14	3.52	0.08	30.94	51.54	0.47	13.59	0.99		0.00	101.14	66.2	31.0	2.7
HM-2.15	4.50	0.00	20.29	65.07	9.56	1.12	0.44		0.13	101.10	5.4	39.5	55.1
HM-2.16	4.01	0.76	20.09	62.56	8.50	1.41	0.75		0.12	98.20	7.5	38.6	53.9
HM-2.17	5.35	0.08	28.35	55.29	0.43	10.55	0.83		0.07	100.95	50.9	46.7	2.4

Titano-magnetites

Label	SiO_2	TiO_2	Al_2O_3	Cr_2O_3	Fe_2O_3(c)	FeO	V_2O_3	MnO	MgO	ZnO	Total
HM-1.1	0.07	0.53	15.29	44.66	9.09	18.41	0.17	0.29	10.38	0	98.91
HM-1.2	0.08	21.85	1.81	0.01	23.08	47.72	1.02	0.75	1.73	0.08	98.11
HM-1.3	0.08	18.58	2.7	4.41	23.81	44.73	1.17	0.56	2	0.01	98.05
HM-1.4	0.08	21.47	1.9	0.08	22.83	47.97	0.91	0.7	1.24	0.01	97.19
HM-1.5	0.05	14.86	5.5	10.53	23.37	39.56	1.13	0.43	3.7	0.18	99.31
HM-1.6	0.04	12.71	6.6	14.44	22.1	37.1	1	0.44	4.06	0.09	98.57
HM-1.7	0.08	0.42	8.11	53.65	7.37	22.11	0.09	0.38	7.19	0.07	99.46
HM-1.8	0.08	19.39	1.97	0.02	27.47	46.09	0.98	0.55	1.4	0.16	98.12
HM-1.9	0.82	18.19	2.7	0	26.35	46.93	0.96	0.83	0.59	0.1	97.46
HM-1.10	0.09	21.22	1.44	0	23.2	47.93	0.71	1.46	0.31	0.23	96.59
HM-1.11	0.1	17.44	2.68	0.01	30.7	44.53	0.94	0.54	1.47	0.08	98.5
HM-1.12	0.04	0.6	12.08	48.57	7.74	23.81	0.15	0.38	6.69	0.09	100.16
HM-1.13	0.05	17.79	4.13	4.85	24.68	42.35	1.28	0.48	3.43	0.1	99.14
HM-1.14	1.62	16.6	4.19	5.32	22.98	41.46	1.17	0.45	4.54	0.07	98.4
HM-1.15	0.05	1.36	9.54	45.85	10.53	26.16	0.28	0.42	5.11	0.17	99.47
HM-1.16	0.04	0.52	10.14	51	7.17	24.04	0.14	0.34	6.19	0.17	99.75
HM-1.17	0.09	19.36	2.29	0.02	25.81	46.66	0.98	0.65	0.7	0.19	96.75
HM-1.18	0.04	0.62	13.43	46.68	8.58	19.66	0.24	0.31	9.38	0.05	98.99
HM-1.19	0.07	0.93	10.44	44.61	11.38	24.16	0.2	0.35	6.07	0.18	98.38

Label	SiO_2	TiO_2	Al_2O_3	Cr_2O_3	Fe_2O_3(c)	FeO	V_2O_3	MnO	MgO	ZnO	Total
HM-1.20	0.09	18.71	2.59	0	27.33	45.84	0.92	0.55	1.1	0.09	97.22
HM-1.21	0.12	18.41	2.42	0	26.73	45.22	1.01	0.61	0.89	0.22	95.64
HM-1.22	16	10.52	9.46	0	0	52.59	0.67	0.37	4.88	0	94.49
HM-1.23	0.04	0.65	14.01	45.42	8.81	18.15	0.2	0.25	10.22	0.05	97.79
HM-1.24	0.05	0.59	14.34	45.63	9.1	18.18	0.2	0.28	10.42	0	98.77
HM-1.25	38.23	0.02	0.29	1.41	2.19	8.71	0.03	0.02	47.46	0.01	98.37
HM-1.27	0.08	18.62	3.07	0.03	26.23	44.61	1.13	0.53	1.51	0.41	96.22
HM-1.28	0.12	17.67	3.1	0.22	28.07	44.98	1.05	0.6	0.84	0.45	97.12
HM-1.29	0.28	7.72	8.29	19.9	23.64	33.93	0.74	0.4	3.39	0.45	98.73
HM-1.30	0.08	17.41	3.11	0.57	29.32	44.78	0.95	0.53	1.25	0.06	98.05
HM-1.31	0.08	18.77	2.38	0	26.61	45.93	1.02	0.59	0.85	0.07	96.3
HM-1.32	2.11	18.38	3.22	0	19.93	45.92	1.01	1.55	1.29	0.05	93.46
HM-1.33	0.63	20.14	2.1	0.01	21.99	47.46	0.89	1.65	0.15	0.16	95.17
HM-1.34	0.07	19.3	1.93	0	27.04	45.95	0.76	0.75	1.08	0.15	97.03
HM-2.1	0.09	20.55	2.48	0.03	22.36	46.93	1.18	2.38	0.01	0.21	96.23
HM-2.2	0.48	20.77	2.22	0.01	20.93	46.46	1.18	3.15	0.15	0.15	95.49
HM-2.4	3.18	23.15	1.86	0	7.91	49.69	0.87	2.69	1.02	0.33	90.72
HM-2.5	0.08	1.24	12.23	43.11	11.02	19.11	0.27	0.25	9.62	0	96.92
HM-2.6	1.11	20.17	1.14	0.14	21.23	45.66	1	3.14	0.44	0.21	94.25
HM-2.7	2.39	19.83	2.31	0	17.99	47.24	0.89	2.49	0.87	0.25	94.25
HM-2.8	0.1	20.6	1.99	0.01	22.42	46.57	0.9	2.46	0.02	0.14	95.21
HM-2.9	0.2	20.89	2.17	0	21.17	46.78	0.91	2.49	0.07	0.13	94.82
HM-2.10	0.09	21.38	2	0.03	21.12	47.42	1	2.18	0.02	0.44	95.67
HM-2.11	0.04	0.77	13.66	43.24	11	21.39	0.38	0.27	8.38	0.09	99.22
HM-2.12	0.06	20.52	2.59	0.01	21.18	46.81	1.58	1.69	0.2	0.34	94.98
HM-2.13	0.04	2.19	24.89	25.76	13.03	21.69	0.67	0.22	10.09	0.05	98.64
HM-2.14	0.04	0.77	12.91	44.12	10.39	21.36	0.36	0.35	8.09	0.17	98.55
HM-2.15	0.12	19.18	1.95	0.04	25.02	45.98	1.09	1.58	0.01	0.4	95.37
HM-2.16	0.07	46.88	0.02	0	0	45.59	0.3	0.86	1.1	0	94.82
HM-2.17	0.26	21.33	2.1	0.03	20.89	47.26	0.79	2.58	0.11	0.21	95.54
HM-2.18	0.63	20.78	1.74	0	21.78	46.24	0.55	2.71	0.54	0.27	95.24
HM-2.19	0.17	20.02	2.3	0	23.67	46.55	1.11	2.35	0.04	0.24	96.46
HM-2.20	0.82	20.5	2.39	0.01	21.5	46.58	1.07	2.76	0.65	0.2	96.48
HM-2.22	0.07	21.35	1.99	0.02	22	47.67	1.03	2.49	0	0.22	96.83
HM-2.23	0.43	16.84	0.91	0	27.67	41.52	0.17	2.38	0.13	0.36	90.41
HM-2.26	0.18	25.32	1.64	0.01	15.72	51.51	1.18	2.28	0.3	0.46	98.6
HM-2.27	2.7	20.06	1.73	0.02	16.75	45.71	1.11	2.96	1.45	0.63	93.13

Spetch Rim Lamprophyre

Pyroxene

Label	Na_2O	MgO	Al_2O_3	SiO_2	CaO	TiO_2	Cr_2O_3	MnO	FeO	Total	En	Wo	Fs
SR-1a.1_1	0.44	14.39	3.80	48.46	22.97	2.53	0.00	0.11	7.19	99.89	41.1	47.2	11.7
SR-1a.1_2	0.26	16.72	1.44	53.03	23.64	1.13	0.00	0.11	5.17	101.50	45.6	46.3	8.1
SR-1a.1_3	0.27	16.67	1.35	52.85	23.61	1.11	0.01	0.09	5.08	101.03	45.6	46.4	7.9
SR-1a.1_4	0.28	16.61	1.39	52.74	23.61	1.07	0.01	0.08	5.02	100.82	45.6	46.6	7.9
SR-1a.2_1	0.53	14.98	3.14	49.69	23.27	2.53	0.00	0.12	6.33	100.59	42.4	47.4	10.2
SR-1a.2_2	0.24	16.86	1.21	53.19	23.29	1.03	0.09	0.10	4.89	100.90	46.3	46.0	7.7
SR-1a.2_3	0.37	15.08	3.03	50.09	23.58	1.97	0.02	0.12	6.56	100.81	42.2	47.4	10.5
SR-1a.3_1	0.42	14.90	3.42	49.85	23.27	2.20	0.02	0.11	6.98	101.16	41.9	47.0	11.2
SR-1a.3_2	0.27	16.61	1.63	52.85	23.73	1.11	0.07	0.07	4.97	101.30	45.5	46.7	7.7
SR-1a.3_3	0.26	16.62	1.35	53.22	23.79	1.06	0.04	0.09	4.88	101.33	45.5	46.8	7.7
SR-1a.3_4	0.27	16.58	1.36	52.78	23.76	1.07	0.07	0.06	4.85	100.81	45.5	46.9	7.6
SR-1a.4	0.37	15.30	2.80	50.02	23.08	2.17	0.00	0.10	6.71	100.54	42.8	46.5	10.7

Label	Na_2O	MgO	Al_2O_3	SiO_2	CaO	TiO_2	Cr_2O_3	MnO	FeO	Total	En	Wo	Fs
SR-1a.5	0.39	15.34	3.06	50.31	23.29	1.85	0.00	0.10	6.47	100.80	42.9	46.8	10.3
SR-1a.6	0.36	15.68	2.46	50.95	22.97	1.94	0.00	0.12	6.47	100.93	43.7	46.0	10.3
SR-1a.7	0.33	15.98	2.03	51.78	23.09	1.62	0.01	0.08	6.22	101.16	44.2	46.0	9.8
SR-1a.8_1	0.92	14.51	2.18	50.43	22.42	1.99	0.01	0.24	6.82	99.52	41.9	46.6	11.5
SR-1a.8_2	0.31	15.65	2.10	51.40	23.14	1.59	0.00	0.13	6.02	100.35	43.8	46.5	9.7
SR-1a.8_3	0.32	15.75	1.98	51.57	22.95	1.50	0.01	0.11	6.18	100.39	44.0	46.1	9.9
SR-1a.8_4	0.23	16.82	1.14	53.26	23.63	0.87	0.10	0.09	4.65	100.80	46.1	46.6	7.3
SR-1a.8_5	0.31	16.92	1.10	53.51	22.91	0.77	0.19	0.12	5.09	100.93	46.6	45.3	8.1
SR-1a.9_1	0.47	14.53	3.78	49.25	21.70	1.87	0.00	0.11	8.49	100.20	41.6	44.6	13.8
SR-1a.9_2	0.27	16.46	1.44	52.27	23.41	1.19	0.00	0.11	5.26	100.40	45.3	46.4	8.3
SR-1a.9_3	0.27	16.38	1.40	52.79	23.50	1.15	0.00	0.11	5.11	100.70	45.2	46.7	8.1
SR-1a.9_4	0.27	16.53	1.37	52.63	23.65	1.08	0.00	0.08	4.93	100.55	45.5	46.8	7.7
SR-1a.10	0.27	16.49	1.54	52.24	23.14	1.26	0.00	0.09	5.63	100.67	45.4	45.8	8.8
SR-1a.11	0.37	16.15	1.82	51.97	23.10	1.16	0.10	0.10	5.52	100.29	45.0	46.2	8.8
SR-1a.12	0.27	16.88	1.08	53.55	23.36	0.78	0.16	0.10	4.76	100.94	46.4	46.1	7.5
SR-1a.13	0.36	16.26	1.91	52.45	22.90	1.13	0.23	0.09	5.38	100.72	45.4	46.0	8.6
SR-1a.14_1	0.42	14.74	3.65	49.34	23.48	2.36	0.03	0.11	6.86	100.98	41.5	47.5	11.0
SR-1a.14_2	0.35	15.86	2.38	51.68	23.72	1.49	0.04	0.10	5.56	101.18	44.0	47.2	8.8
SR-1a.14_3	0.31	16.13	2.22	52.11	23.64	1.42	0.20	0.08	5.23	101.34	44.7	47.1	8.3
SR-1a.14_4	0.34	16.02	2.19	52.15	23.44	1.34	0.27	0.07	5.23	101.06	44.7	47.0	8.3
SR-1a.14_5	0.27	17.10	1.12	53.63	23.04	0.86	0.22	0.07	4.92	101.23	46.9	45.4	7.7
SR-1a.14_6	0.24	17.10	1.19	53.46	23.29	0.86	0.17	0.09	4.88	101.28	46.7	45.7	7.6
SR-1a.15	0.43	15.17	3.30	50.01	23.19	2.03	0.01	0.10	6.75	100.98	42.5	46.7	10.8
SR-1a.16	0.24	16.74	1.38	53.02	23.60	1.16	0.07	0.09	4.99	101.30	45.8	46.4	7.8
SR-1a.17	0.26	16.84	1.39	52.79	23.71	1.12	0.06	0.10	5.07	101.34	45.8	46.3	7.9
SR-1a.18	0.38	15.33	2.68	50.31	23.33	2.04	0.03	0.12	6.68	100.91	42.7	46.7	10.6
SR-1a.19	0.29	15.59	2.48	50.72	23.14	1.92	0.00	0.11	6.62	100.88	43.3	46.2	10.5
SR-1a.20	0.44	15.58	2.38	51.44	23.32	1.94	0.01	0.11	5.62	100.82	43.8	47.1	9.0
SR-1a.21	0.32	15.95	1.80	52.19	23.53	1.44	0.01	0.09	5.92	101.24	44.0	46.7	9.3
SR-1a.22	0.58	15.48	2.00	51.63	23.09	1.89	0.03	0.16	5.87	100.72	43.7	46.8	9.5
SR-1a.23_1	0.35	15.59	2.59	50.55	23.08	1.95	0.00	0.13	6.51	100.75	43.4	46.2	10.4
SR-1a.23_2	0.31	15.94	2.02	51.33	23.08	1.51	0.01	0.12	6.40	100.72	44.0	45.8	10.1
SR-1a.23_3	0.24	16.66	1.35	52.92	23.69	1.14	0.02	0.10	5.04	101.16	45.6	46.6	7.9
SR-1a.23_4	0.24	16.55	1.36	52.91	23.72	1.07	0.03	0.09	4.96	100.92	45.4	46.8	7.8
SR-1a.23_5	0.23	16.80	1.23	53.15	23.54	1.03	0.07	0.09	4.88	101.02	46.0	46.3	7.6
SR-1a.24	0.24	17.14	1.19	53.39	23.64	1.01	0.16	0.11	4.82	101.71	46.5	46.0	7.5
SR-1a.26_1	0.32	16.16	2.14	51.99	23.57	1.36	0.12	0.09	5.38	101.12	44.7	46.8	8.5
SR-1a.26_2	0.36	16.34	1.89	52.32	23.31	1.17	0.24	0.06	4.99	100.67	45.5	46.6	7.9
SR-1a.26_3	0.29	16.83	1.10	53.60	22.97	0.74	0.14	0.07	5.04	100.79	46.5	45.6	7.9
SR-1a.26_4	0.31	16.22	2.03	52.34	21.66	0.81	0.16	0.09	6.67	100.29	45.6	43.7	10.7
SR-1a.27	0.36	16.51	1.87	52.62	23.71	1.13	0.20	0.07	5.13	101.60	45.3	46.7	8.0
SR-1b.1	0.35	15.49	2.75	51.10	23.10	1.67	0.04	0.06	6.18	100.74	43.5	46.6	9.8
SR-1b.2	0.32	16.07	2.12	51.33	22.96	1.70	0.02	0.11	6.19	100.83	44.5	45.7	9.8
SR-1b.3	0.70	14.68	2.79	49.66	22.95	2.76	0.03	0.18	6.64	100.38	41.9	47.1	10.9
SR-1b.4	0.29	15.97	2.35	51.50	23.47	1.50	0.06	0.07	5.40	100.62	44.5	47.0	8.5
SR-1b.5	0.68	13.84	4.60	48.10	22.38	3.29	0.01	0.13	6.83	99.85	40.9	47.5	11.5
SR-1b.6	0.40	14.96	3.59	49.25	22.94	2.35	0.01	0.13	7.20	100.83	42.1	46.4	11.6
SR-1b.7	0.44	16.21	1.94	52.50	23.10	1.10	0.23	0.07	5.31	100.89	45.2	46.3	8.4
SR-1b.8	0.30	16.07	2.04	51.30	23.06	1.55	0.00	0.14	6.29	100.74	44.3	45.7	10.0
SR-1b.9	0.41	15.90	2.19	51.52	22.90	1.71	0.00	0.17	6.19	100.98	44.3	45.8	9.9
SR-1b.10	0.37	15.93	2.44	51.56	23.43	1.48	0.03	0.08	5.84	101.17	44.1	46.7	9.2
SR-1b.11	0.35	15.56	2.48	50.23	23.34	1.89	0.00	0.13	6.37	100.34	43.3	46.6	10.1
SR-1b.12	0.62	15.12	3.18	49.39	22.80	2.81	0.00	0.14	6.41	100.48	43.0	46.6	10.4
SR-1b.13	0.32	16.09	2.35	51.79	23.65	1.51	0.03	0.07	5.52	101.33	44.4	46.9	8.7

Label	Na_2O	MgO	Al_2O_3	SiO_2	CaO	TiO_2	Cr_2O_3	MnO	FeO	Total	En	Wo	Fs
SR-1b.14	0.32	16.15	2.21	51.31	23.58	1.40	0.04	0.07	5.41	100.49	44.6	46.9	8.5
SR-1b.15	0.26	16.66	1.38	52.62	23.82	1.10	0.04	0.08	4.97	100.92	45.5	46.8	7.7
SR-1b.16	0.35	15.24	3.18	49.45	22.84	2.40	0.03	0.15	7.01	100.65	42.7	46.0	11.3
SR-1b.17	0.41	15.24	3.23	49.70	22.86	2.41	0.00	0.13	6.99	100.97	42.7	46.1	11.2
SR-1b.18	0.41	15.49	2.88	49.90	23.00	2.28	0.00	0.13	6.37	100.45	43.4	46.4	10.2
SR-1b.19_1	1.16	13.77	3.14	48.82	21.80	3.08	0.01	0.23	7.78	99.79	40.6	46.2	13.2
SR-1b.19_2	0.33	16.22	2.12	51.99	23.60	1.35	0.14	0.07	5.19	101.00	44.9	46.9	8.2
SR-1b.19_3	0.29	16.94	1.10	53.12	23.29	0.84	0.16	0.09	4.73	100.56	46.6	46.0	7.4
SR-1b.19_4	0.25	16.78	1.22	53.00	23.49	1.00	0.06	0.06	4.76	100.62	46.1	46.4	7.4
SR-1b.19_5	0.25	16.56	1.48	52.61	23.57	1.20	0.00	0.11	5.22	100.98	45.4	46.4	8.2
SR-1b.20_1	0.54	15.17	2.64	50.46	23.34	2.25	0.00	0.15	6.21	100.77	42.7	47.2	10.1
SR-1b.20_2	0.29	15.61	2.25	50.75	23.26	1.70	0.00	0.13	6.31	100.30	43.4	46.5	10.1
SR-1b.20_3	0.30	16.07	1.74	52.04	23.61	1.42	0.00	0.11	5.73	101.03	44.3	46.7	9.0
SR-1b.20_4	0.26	16.32	1.51	52.36	23.21	1.21	0.05	0.10	5.44	100.45	45.2	46.2	8.6
SR-1b.20_5	0.27	16.68	1.34	52.70	23.47	1.08	0.00	0.08	4.93	100.56	45.9	46.4	7.7
SR-1b.21_1	0.35	15.78	2.45	50.88	23.30	1.82	0.00	0.11	6.06	100.76	43.9	46.5	9.6
SR-1b.21_2	0.32	15.91	2.17	51.30	23.24	1.69	0.00	0.12	6.25	101.00	44.0	46.2	9.9
SR-1b.21_3	0.30	16.36	1.69	52.24	23.39	1.31	0.00	0.15	5.59	101.02	45.0	46.2	8.8
SR-1b.21_4	0.25	16.78	1.22	53.06	23.48	0.98	0.09	0.07	4.72	100.66	46.2	46.4	7.4
SR-1b.21_5	0.26	16.91	1.23	52.94	23.50	0.96	0.12	0.07	4.67	100.66	46.4	46.3	7.3
SR-1b.21_6	0.30	16.99	1.10	53.55	23.27	0.80	0.11	0.12	4.79	101.04	46.6	45.9	7.5
SR-1b.21_7	0.38	16.12	2.32	51.70	23.30	1.31	0.22	0.07	5.42	100.85	44.8	46.6	8.6
SR-1b.21_8	0.42	16.12	2.18	52.18	23.27	1.28	0.23	0.06	5.25	100.98	45.0	46.7	8.3
SR-1b.21_9	0.36	15.26	3.28	50.07	23.25	2.02	0.05	0.10	6.50	100.89	42.8	46.8	10.4
SR-1b.21_10	0.41	14.84	3.62	49.34	23.21	2.12	0.00	0.10	6.98	100.63	41.8	47.0	11.2
SR-1b.22	0.75	14.53	2.94	49.40	22.75	2.89	0.00	0.19	7.00	100.45	41.6	46.8	11.6
SR-1b.23	0.43	16.02	2.12	52.11	23.10	1.27	0.22	0.08	5.45	100.81	44.8	46.5	8.7
SR-1b.24	0.68	14.96	2.72	50.24	23.00	2.44	0.01	0.19	6.31	100.55	42.6	47.0	10.4
SR-1b.25	0.32	15.89	2.15	51.26	23.31	1.77	0.00	0.11	6.12	100.93	44.0	46.4	9.7
SR-1b.26	0.32	15.83	2.14	51.08	23.22	1.56	0.01	0.11	6.37	100.65	43.8	46.2	10.1
SR-1b.27	0.35	15.86	2.47	51.06	23.29	1.55	0.00	0.11	5.76	100.45	44.2	46.6	9.2
SR-1b.28_1	0.42	14.87	3.51	49.35	23.14	2.25	0.00	0.10	6.75	100.38	42.1	47.1	10.9
SR-1b.28_2	0.34	15.72	2.23	51.02	23.00	1.36	0.00	0.08	5.35	99.11	44.5	46.8	8.6
SR-1b.28_3	0.33	16.30	2.18	52.17	23.37	1.33	0.11	0.08	5.19	101.05	45.2	46.6	8.2
SR-1b.28_4	0.35	16.56	1.61	52.48	23.41	0.98	0.25	0.09	4.85	100.58	45.8	46.5	7.7
SR-1b.29	0.30	16.03	1.96	51.15	23.16	1.53	0.01	0.13	6.19	100.44	44.3	46.0	9.8
SR-1b.30	0.27	16.76	1.37	52.74	23.83	1.09	0.00	0.09	4.97	101.12	45.6	46.6	7.7
SR-1b.31	0.34	15.46	2.77	50.26	23.49	1.87	0.00	0.09	6.16	100.44	43.1	47.1	9.8
SR-1b.32	0.33	16.09	2.28	51.67	23.50	1.51	0.08	0.09	5.41	100.96	44.6	46.8	8.6
SR-1b.33	0.30	16.30	1.84	51.58	23.22	1.48	0.00	0.13	5.83	100.68	44.9	45.9	9.2
SR-1b.34	0.46	14.40	3.70	47.86	22.92	2.92	0.03	0.14	7.51	99.95	41.0	46.8	12.2
SR-1b.35	0.44	15.37	2.38	50.53	23.40	2.08	0.01	0.14	6.16	100.51	43.0	47.1	9.9
SR-1b.36	0.29	15.79	2.23	50.96	23.06	1.72	0.02	0.10	6.25	100.42	43.9	46.1	9.9
SR-1b.37	0.28	16.48	1.38	52.46	23.61	1.18	0.03	0.13	5.13	100.68	45.3	46.6	8.1
SR-1b.38_1	0.89	14.52	2.45	50.07	22.66	2.58	0.02	0.17	6.65	100.00	41.9	47.0	11.0
SR-1b.38_2	0.31	15.42	2.60	50.20	23.00	2.01	0.01	0.14	6.52	100.21	43.2	46.3	10.5
SR-1b.38_3	0.31	15.81	2.08	50.73	23.28	1.58	0.01	0.10	6.03	99.93	44.0	46.5	9.6
SR-1b.38_4	0.31	15.89	1.99	51.02	23.22	1.53	0.04	0.08	6.09	100.15	44.1	46.3	9.6
SR-1b.39	0.30	15.26	2.43	50.58	23.22	1.80	0.01	0.10	6.20	99.89	43.0	47.0	10.0
SR-1b.40	0.28	16.30	1.79	51.52	23.46	1.40	0.03	0.11	5.65	100.54	44.8	46.3	8.9
SR-1b.41	0.27	16.89	1.19	53.09	23.54	0.99	0.14	0.06	4.64	100.80	46.4	46.4	7.2
SR-1b.42	0.25	16.75	1.36	52.64	23.59	1.08	0.03	0.12	5.01	100.82	45.8	46.3	7.9
SR-1b.43	0.37	15.68	2.29	51.06	23.18	1.56	0.02	0.16	5.94	100.25	43.9	46.6	9.6
SR-1b.44	0.29	16.14	2.13	51.51	23.46	1.42	0.04	0.07	5.52	100.59	44.7	46.6	8.7
SR-1b.45	0.67	15.07	2.48	50.60	22.89	2.35	0.00	0.19	6.07	100.33	43.0	47.0	10.0

Label	Na_2O	MgO	Al_2O_3	SiO_2	CaO	TiO_2	Cr_2O_3	MnO	FeO	Total	En	Wo	Fs
SR-1b.46	0.48	14.16	4.00	48.33	23.09	2.66	0.00	0.12	7.10	99.94	40.7	47.7	11.6
SR-1b.47	0.74	14.36	3.68	49.07	22.94	2.88	0.00	0.15	6.52	100.34	41.5	47.7	10.8
SR-1b.48	0.48	14.56	3.77	48.79	23.30	2.58	0.06	0.12	6.94	100.60	41.3	47.5	11.2
SR-1b.49	0.40	15.15	3.08	50.16	23.37	1.83	0.02	0.07	6.27	100.34	42.7	47.3	10.0
SR-1b.50	0.35	15.31	3.05	50.08	23.46	1.88	0.06	0.09	6.18	100.47	42.9	47.3	9.9
SR-1b.51	0.32	15.96	2.39	51.54	23.47	1.47	0.05	0.07	5.51	100.77	44.4	46.9	8.7
SR-1b.52	0.29	16.75	1.43	52.66	23.61	1.13	0.06	0.09	5.00	101.00	45.8	46.4	7.8

Feldspars

Label	Na_2O	MgO	Al_2O_3	SiO_2	K_2O	CaO	FeO	SrO	BaO	Total	An	Ab	Or
SR-1a.1	1.60	0.01	18.76	64.16	13.54	0.11	0.74	0.00	0.05	98.96	0.6	15.1	84.3
SR-1a.2	1.35	0.03	18.93	63.93	13.93	0.14	0.69	0.00	0.06	99.05	0.7	12.7	86.5
SR-1a.3	4.37	0.00	18.88	64.54	9.58	0.32	1.21	0.19	0.04	99.13	1.6	40.3	58.1
SR-1a.4	3.91	0.15	18.19	63.70	10.14	0.27	1.74	0.00	0.00	98.09	1.4	36.4	62.2
SR-1a.5	3.61	0.02	18.74	65.09	10.58	0.15	0.84	0.10	0.02	99.15	0.8	33.9	65.3
SR-1a.6	4.59	0.02	19.46	64.40	9.06	0.47	0.79	0.27	0.03	99.09	2.4	42.4	55.2
SR-1a.7	5.29	0.02	19.89	64.62	7.80	0.95	0.80	0.12	0.01	99.49	4.8	48.3	46.9
SR-1a.8	4.90	0.01	20.45	62.08	7.37	0.89	0.76	1.34	0.62	98.44	4.8	47.9	47.3
SR-1a.9	4.57	0.63	20.47	60.02	6.41	2.10	1.13	2.00	1.51	98.83	11.6	45.9	42.4
SR-1a.10	4.81	0.02	20.47	61.97	7.49	0.66	0.66	1.44	1.35	98.87	3.6	47.6	48.8
SR-1a.11	4.85	0.02	19.92	63.52	7.87	0.50	0.71	1.29	0.48	99.16	2.7	47.1	50.2
SR-1a.12	4.52	0.01	19.72	64.35	9.01	0.54	0.68	0.43	0.09	99.35	2.8	42.1	55.2
SR-1a.13	4.59	0.01	21.21	61.80	7.38	1.60	0.65	1.30	0.66	99.20	8.6	44.4	47.0
SR-1a.14	4.79	0.00	19.20	65.47	9.40	0.20	0.31	0.07	0.19	99.63	1.0	43.2	55.8
SR-1a.15	3.93	0.00	18.87	65.20	10.61	0.09	0.14	0.00	0.10	98.94	0.5	35.9	63.7
SR-1a.16	3.61	0.01	19.24	65.08	11.31	0.04	0.09	0.00	0.34	99.72	0.2	32.6	67.2
SR-1a.17	3.99	0.00	19.15	64.53	10.36	0.21	0.54	0.33	0.26	99.37	1.1	36.5	62.4
SR-1a.18	4.46	0.02	20.46	61.76	8.15	0.88	0.60	1.38	0.85	98.56	4.7	43.3	52.0
SR-1a.19	4.23	0.04	18.99	64.87	10.60	0.37	0.74	0.00	0.03	99.87	1.8	37.1	61.1
SR-1b.1	6.08	0.07	20.79	62.12	5.45	1.30	0.96	1.75	0.39	98.90	6.9	58.6	34.5
SR-1b.2	0.35	0.41	18.78	61.42	15.08	0.19	1.83	0.00	0.40	98.46	1.0	3.4	95.7
SR-1b.3	2.18	0.05	18.97	62.86	13.14	0.28	0.97	0.34	0.12	98.91	1.4	19.9	78.7
SR-1b.4	3.09	0.01	18.84	63.39	12.03	0.13	0.99	0.23	0.17	98.89	0.6	27.9	71.5
SR-1b.8	5.57	0.02	19.25	64.50	7.44	0.34	1.05	0.31	0.24	98.72	1.7	52.3	46.0
SR-1b.9	5.16	0.20	19.58	63.39	7.37	0.67	1.59	0.14	0.03	98.14	3.6	49.7	46.7
SR-1b.10	4.89	0.01	18.54	63.29	7.72	0.80	1.73	0.11	0.31	97.40	4.3	47.0	48.8
SR-1b.11	0.75	0.45	18.27	61.78	13.60	0.32	1.90	0.02	0.24	97.33	1.8	7.6	90.6
SR-1b.13	1.21	0.01	18.50	62.83	14.96	0.04	0.85	0.00	0.00	98.40	0.2	10.9	88.8
SR-1b.14	2.30	0.01	18.79	63.69	12.95	0.13	1.03	0.00	0.04	98.93	0.7	21.1	78.2
SR-1b.15	6.62	0.01	19.50	64.92	6.35	0.65	1.18	0.22	0.02	99.48	3.2	59.3	37.4
SR-1b.16	4.52	0.00	18.98	64.65	9.21	0.42	1.46	0.02	0.05	99.32	2.1	41.8	56.0

Phlogopite

Label	SiO_2	TiO_2	Al_2O_3	FeO	MnO	MgO	CaO	Na_2O	K_2O	F	Cl	H_2O(c)	Total
SR-1a.1_1	37.28	4.97	14.05	8.82	0.08	19.73	0.03	0.67	8.99	3.14	0.01	2.60	100.37
SR-1a.1_2	37.34	4.49	13.86	7.61	0.03	20.67	0.02	0.45	9.53	1.38	0.00	3.42	98.80
SR-1a.1_3	38.16	3.69	13.76	7.05	0.01	21.11	0.03	0.40	9.63	1.25	0.01	3.50	98.60
SR-1a.1_4	37.66	3.81	14.11	7.70	0.03	20.45	0.02	0.34	9.57	0.75	0.00	3.71	98.15
SR-1a.1_5	37.83	3.84	13.31	8.08	0.02	20.97	0.04	0.32	9.34	0.83	0.00	3.68	98.26
SR-1a.1_6	38.22	3.81	13.74	7.73	0.04	20.68	0.01	0.31	9.79	0.97	0.01	3.64	98.95
SR-1a.1_7	38.21	3.65	13.69	7.70	0.06	20.67	0.05	0.33	9.61	0.99	0.01	3.61	98.58
SR-1a.1_8	37.89	3.67	13.33	7.67	0.07	20.65	0.02	0.29	9.67	0.84	0.01	3.65	97.76
SR-1a.1_9	37.94	3.73	13.60	7.71	0.07	20.78	0.00	0.30	9.60	1.04	0.01	3.58	98.36

Label	SiO_2	TiO_2	Al_2O_3	FeO	MnO	MgO	CaO	Na_2O	K_2O	F	Cl	H_2O(c)	Total
SR-1a.1_10	37.97	3.70	13.83	7.69	0.08	20.80	0.04	0.37	9.43	0.86	0.00	3.67	98.44
SR-1a.2_1	37.04	5.14	13.81	9.26	0.07	19.30	0.05	0.68	9.18	3.29	0.00	2.51	100.33
SR-1a.2_2	37.17	4.48	13.77	7.73	0.07	20.61	0.02	0.48	9.37	1.50	0.00	3.35	98.55
SR-1a.2_3	37.80	3.98	13.83	7.24	0.01	20.99	0.04	0.46	9.55	1.28	0.01	3.48	98.67
SR-1a.2_4	37.50	3.75	13.89	7.39	0.08	20.73	0.07	0.40	9.49	0.87	0.00	3.64	97.81
SR-1a.2_5	37.89	3.83	13.66	7.70	0.06	20.59	0.05	0.37	9.50	1.03	0.01	3.58	98.27
SR-1a.2_6	37.96	3.59	13.64	7.92	0.03	20.59	0.07	0.31	9.26	1.12	0.01	3.53	98.03
SR-1a.2_7	37.92	3.68	13.74	8.05	0.04	20.79	0.05	0.32	9.46	0.85	0.01	3.68	98.59
SR-1a.3_1	36.10	7.47	13.59	10.96	0.09	16.04	0.22	0.89	8.13	3.14	0.02	2.51	99.16
SR-1a.3_2	37.91	3.88	13.78	7.11	0.03	21.16	0.07	0.41	9.44	1.48	0.00	3.39	98.66
SR-1a.3_3	37.77	3.61	14.04	6.91	0.01	20.71	0.23	0.42	8.80	0.95	0.01	3.60	97.06
SR-1a.3_4	38.42	3.69	13.75	7.11	0.03	20.41	0.14	0.36	9.01	1.05	0.00	3.57	97.54
SR-1a.3_5	37.53	3.72	13.80	6.96	0.02	20.75	0.15	0.36	9.22	1.00	0.00	3.56	97.07
SR-1a.4	37.57	3.65	13.88	7.66	0.06	20.54	0.09	0.78	9.27	4.01	0.00	2.16	99.67
SR-1a.5_1	37.20	4.91	13.59	9.03	0.05	19.58	0.03	0.64	9.27	3.09	0.00	2.60	99.99
SR-1a.5_2	38.20	3.69	13.73	6.96	0.05	21.26	0.05	0.49	9.47	1.25	0.00	3.51	98.66
SR-1a.5_3	37.98	3.75	13.98	7.07	0.02	21.15	0.03	0.45	9.37	1.37	0.00	3.45	98.62
SR-1a.5_4	38.26	3.80	13.76	6.93	0.04	21.04	0.05	0.45	9.53	1.40	0.00	3.44	98.70
SR-1a.5_5	38.20	3.73	13.86	6.98	0.03	20.88	0.04	0.47	9.41	1.78	0.01	3.24	98.63
SR-1a.5_6	37.75	3.74	13.70	7.71	0.06	20.37	0.03	0.59	9.15	2.56	0.00	2.84	98.50
SR-1b.1_1	36.79	4.85	13.72	8.95	0.07	19.56	0.07	0.71	9.05	3.34	0.02	2.45	99.58
SR-1b.1_2	37.78	3.86	13.62	7.15	0.02	21.13	0.04	0.61	9.30	1.81	0.03	3.21	98.56
SR-1b.1_3	37.71	3.62	13.66	6.98	0.04	21.20	0.04	0.43	9.60	1.28	0.03	3.45	98.04
SR-1b.1_4	37.70	3.64	13.85	6.98	0.07	20.78	0.06	0.39	9.64	1.05	0.01	3.55	97.72
SR-1b.1_5	37.81	3.75	13.50	6.80	0.05	21.03	0.02	0.31	9.82	1.12	0.01	3.52	97.74
SR-1b.1_6	37.74	3.80	13.64	6.75	0.03	20.79	0.05	0.29	9.85	1.04	0.02	3.55	97.55
SR-1b.1_7	37.74	3.76	13.71	6.81	0.01	20.77	0.04	0.34	9.85	1.04	0.03	3.55	97.65
SR-1b.1_8	37.55	3.68	13.67	6.74	0.01	20.83	0.05	0.30	9.72	1.04	0.04	3.53	97.16
SR-1b.1_9	37.51	3.79	13.87	6.89	0.00	20.89	0.03	0.32	9.72	0.91	0.01	3.62	97.56
SR-1b.1_10	37.57	3.77	13.87	6.86	0.00	20.77	0.03	0.28	9.73	0.86	0.03	3.63	97.40
SR-1b.2_1	37.56	3.80	13.50	8.45	0.15	20.12	0.10	0.73	9.30	3.59	0.03	2.34	99.67
SR-1b.2_2	37.89	3.76	13.91	7.04	0.03	20.96	0.04	0.47	9.47	1.47	0.00	3.38	98.42
SR-1b.2_3	37.78	3.75	13.97	7.11	0.01	20.61	0.07	0.40	9.58	0.97	0.01	3.60	97.86
SR-1b.2_4	37.49	3.72	13.66	7.15	0.05	21.09	0.05	0.35	9.83	1.25	0.01	3.46	98.11
SR-1b.2_5	37.63	3.75	13.96	7.03	0.08	20.94	0.07	0.35	9.60	1.39	0.00	3.41	98.21
SR-1b.3	37.66	3.72	13.78	7.89	0.06	20.62	0.09	0.90	9.03	4.25	0.01	2.06	100.07
SR-1b.4	37.74	3.69	13.88	7.31	0.06	20.71	0.07	0.76	9.18	2.60	0.01	2.83	98.84
SR-1b.5_1	36.96	4.91	13.82	8.77	0.09	19.91	0.07	0.74	9.10	3.51	0.01	2.41	100.30
SR-1b.5_2	37.70	4.11	13.73	7.42	0.00	21.15	0.02	0.54	9.53	2.01	0.01	3.14	99.36
SR-1b.5_3	38.36	3.64	13.58	6.90	0.00	21.34	0.02	0.56	9.69	1.76	0.02	3.26	99.13
SR-1b.5_4	37.84	3.90	13.57	7.25	0.00	21.24	0.02	0.47	9.65	1.49	0.01	3.38	98.82
SR-1b.5_5	37.94	4.02	13.60	7.35	0.04	21.16	0.05	0.49	9.48	1.81	0.01	3.23	99.18
SR-1b.6_1	36.62	6.18	13.67	9.75	0.09	18.08	0.09	0.71	9.01	3.30	0.01	2.48	99.99
SR-1b.6_2	37.27	4.59	13.91	7.85	0.04	20.51	0.02	0.50	9.48	2.68	0.01	2.81	99.67
SR-1b.6_3	37.80	3.99	13.65	7.29	0.02	21.36	0.03	0.51	9.66	1.42	0.00	3.43	99.16
SR-1b.6_4	38.00	3.70	13.71	7.04	0.01	21.10	0.01	0.46	9.67	0.88	0.00	3.66	98.24
SR-1b.6_5	39.62	3.27	14.30	7.30	0.01	19.26	0.10	0.44	9.26	0.94	0.01	3.66	98.17
SR-1b.7_1	35.29	8.36	13.66	9.81	0.13	16.12	0.08	0.62	8.12	2.45	0.01	2.80	97.45
SR-1b.7_2	37.91	3.66	13.74	6.97	0.03	21.17	0.01	0.52	9.48	1.75	0.02	3.24	98.50
SR-1b.7_3	37.95	3.68	13.91	7.00	0.04	20.91	0.02	0.39	9.62	1.31	0.01	3.45	98.29
SR-1b.7_4	38.16	3.77	13.85	7.96	0.00	20.34	0.14	0.39	9.28	1.04	0.02	3.59	98.54
SR-1b.7_5	39.37	3.56	13.89	7.41	0.06	19.73	0.10	0.59	9.16	1.50	0.01	3.40	98.78
SR-1b.7_6	36.92	4.31	14.90	8.16	0.02	19.56	0.02	0.65	9.38	1.38	0.01	3.42	98.73
SR-1b.7_7	37.06	3.53	14.59	8.52	0.05	19.75	0.05	0.53	9.08	1.72	0.02	3.22	98.12

Label	SiO_2	TiO_2	Al_2O_3	FeO	MnO	MgO	CaO	Na_2O	K_2O	F	Cl	H_2O(c)	Total
SR-1b.7_8	37.84	3.73	13.78	7.71	0.05	20.64	0.04	0.53	9.20	1.49	0.02	3.36	98.39
SR-1b.7_9	37.76	3.77	13.78	7.77	0.07	20.39	0.03	0.64	9.33	1.62	0.01	3.29	98.46
SR-1b.7_10	37.43	3.71	14.08	8.02	0.08	19.94	0.07	0.77	9.23	3.20	0.02	2.52	99.07
SR-1b.7_11	33.35	1.69	10.68	12.70	0.06	7.32	2.43	0.28	2.94	0.76	0.10	2.73	75.04
SR-1b.7_12	37.62	3.70	13.97	7.37	0.02	20.48	0.04	0.73	9.30	2.37	0.01	2.93	98.54
SR-1b.7_13	38.17	3.54	14.13	7.19	0.04	19.35	0.05	0.65	9.13	1.95	0.01	3.11	97.32
SR-1b.7_14	37.87	3.81	14.24	7.28	0.01	20.67	0.02	0.58	9.55	1.48	0.01	3.39	98.91
SR-1b.7_15	37.91	3.78	14.01	6.99	0.01	20.60	0.01	0.52	9.45	1.87	0.00	3.19	98.34
SR-1b.8_1	37.11	4.93	13.50	8.84	0.10	19.51	0.04	0.71	9.15	3.15	0.00	2.56	99.60
SR-1b.8_2	38.19	3.71	13.67	7.00	0.01	21.05	0.21	0.51	8.59	1.39	0.00	3.42	97.75
SR-1b.8_3	37.85	3.85	14.13	7.91	0.04	19.86	0.07	0.59	9.24	1.75	0.01	3.24	98.54
SR-1b.8_4	37.63	3.70	14.33	7.37	0.07	20.24	0.05	0.73	9.24	1.38	0.00	3.41	98.15
SR-1b.8_5	37.76	3.54	13.95	7.12	0.04	20.66	0.04	0.68	9.38	1.77	0.00	3.22	98.16
SR-1b.9_1	36.56	7.62	13.50	9.17	0.04	17.47	0.06	0.79	8.79	3.07	0.01	2.59	99.67
SR-1b.9_2	38.27	3.79	13.60	7.00	0.03	21.12	0.05	0.58	9.46	2.34	0.01	2.98	99.23
SR-1b.9_3	38.49	3.83	13.38	6.78	0.00	21.07	0.05	0.48	9.58	1.54	0.00	3.36	98.56
SR-1b.9_4	38.49	3.80	13.32	6.90	0.00	21.04	0.03	0.45	9.62	1.44	0.00	3.40	98.49
SR-1b.9_5	38.27	3.89	13.52	6.93	0.11	20.82	0.02	0.53	9.62	1.68	0.01	3.28	98.68
SR-1b.10_1	36.02	7.08	13.82	8.66	0.12	17.69	0.09	0.73	8.43	3.21	0.01	2.48	98.34
SR-1b.10_2	38.01	3.66	13.71	6.87	0.01	21.29	0.03	0.51	9.64	1.65	0.01	3.30	98.69
SR-1b.10_3	37.99	3.63	13.90	6.68	0.00	20.96	0.04	0.47	9.51	0.98	0.01	3.61	97.78
SR-1b.10_4	37.65	3.60	13.71	6.78	0.01	20.78	0.08	0.49	9.35	0.89	0.01	3.61	96.96
SR-1b.10_5	38.13	3.60	13.50	7.07	0.06	20.29	0.44	0.72	9.24	0.96	0.02	3.59	97.62
SR-1b.11	34.99	8.65	13.47	9.01	0.12	16.41	0.08	0.58	8.24	2.79	0.02	2.62	96.98
SR-1b.12	1.23	0.04	0.00	0.38	0.02	0.11	51.61	0.20	0.13	0.00	0.17	1.55	55.44

Mudcreek Lamprophyres

Pyroxenes

Label	Na_2O	MgO	Al_2O_3	SiO_2	CaO	TiO_2	Cr_2O_3	MnO	FeO	Total	En	Wo	Fs
MC-1.3	0.05	0.29	0.46	98.05	0.06	0.02	0.02	0.02	0.40	99.38	50.4	8.0	41.5
MC-1.4	0.03	0.53	0.56	96.84	0.12	0.00	0.00	0.02	0.64	98.75	53.5	9.0	37.5
MC-1.8	0.04	0.48	0.67	96.13	0.09	0.00	0.00	0.05	0.44	97.90	58.5	7.7	33.7
MC-2.1	0.30	16.56	2.70	51.61	22.40	0.98	0.45	0.14	5.41	100.56	46.3	45.0	8.7
MC-2.2	0.32	16.52	2.63	51.44	22.38	0.99	0.44	0.14	5.53	100.39	46.2	45.0	8.9
MC-2.3	0.19	17.55	1.29	53.24	22.27	0.61	0.23	0.16	5.03	100.56	48.1	43.9	8.0
MC-2.4	0.30	16.58	2.63	51.51	22.44	0.98	0.41	0.12	5.45	100.42	46.3	45.0	8.7
MC-2.5	0.27	17.29	2.05	52.53	21.94	0.78	0.51	0.13	5.20	100.70	48.0	43.7	8.3
MC-2.6	0.35	16.23	3.09	51.19	22.45	1.22	0.39	0.15	5.48	100.54	45.7	45.4	8.9
MC-2.7_1	0.29	16.68	2.53	51.54	22.49	0.91	0.53	0.15	5.14	100.27	46.6	45.1	8.3
MC-2.7_2	0.30	16.55	2.63	51.63	22.32	0.95	0.55	0.17	5.37	100.47	46.4	44.9	8.7
MC-2.7_3	0.29	16.95	2.18	52.14	22.13	0.83	0.60	0.15	5.19	100.46	47.3	44.4	8.3
MC-2.7_4	0.24	17.83	1.31	53.64	22.43	0.45	0.40	0.12	4.31	100.73	48.9	44.2	6.8
MC-2.7_5	0.33	17.19	1.96	53.10	22.52	0.62	0.63	0.10	4.49	100.93	47.8	45.0	7.2
MC-2.8	0.36	16.82	2.21	52.26	22.50	0.77	0.75	0.10	4.64	100.41	47.2	45.4	7.5
MC-2.9	0.32	16.78	2.60	51.32	22.43	0.92	0.79	0.12	5.01	100.29	46.9	45.1	8.1
MC-2.10	0.23	17.59	1.34	53.39	22.35	0.60	0.18	0.17	5.00	100.85	48.1	43.9	7.9
MC-2.11	0.25	17.28	1.68	52.23	21.46	0.85	0.05	0.19	6.47	100.46	47.4	42.3	10.3
MC-2.12	0.33	15.88	2.96	50.94	22.27	1.15	0.04	0.19	6.58	100.34	44.5	44.8	10.6
MC-2.13_1	0.40	15.78	3.28	49.23	21.62	1.55	0.03	0.18	7.65	99.74	44.2	43.5	12.3
MC-2.13_2	0.44	15.18	4.15	48.42	21.40	1.90	0.04	0.20	7.88	99.61	43.3	43.8	12.9
MC-2.13_3	0.47	15.14	3.75	49.35	21.17	1.86	0.05	0.17	8.02	99.98	43.3	43.5	13.2
MC-2.13_4	0.41	15.41	3.45	49.65	21.57	1.61	0.04	0.21	7.56	99.92	43.7	43.9	12.4
MC-2.13_5	0.38	16.03	2.68	51.06	21.84	1.22	0.27	0.18	6.36	100.01	45.3	44.4	10.4

Label	Na_2O	MgO	Al_2O_3	SiO_2	CaO	TiO_2	Cr_2O_3	MnO	FeO	Total	En	Wo	Fs
MC-2.13_6	0.33	16.42	2.45	51.33	22.41	1.15	0.18	0.14	5.79	100.20	45.8	44.9	9.3
MC-2.13_7	0.30	16.18	2.80	51.19	22.23	1.07	0.46	0.18	5.67	100.06	45.7	45.1	9.3
MC-2.13_8	0.06	22.83	12.50	34.36	0.65	0.01	0.16	0.09	17.61	88.27	68.7	1.4	29.9
MC-2.14_1	0.36	16.55	2.28	51.56	22.47	1.02	0.19	0.16	5.72	100.31	46.0	44.9	9.2
MC-2.14_2	0.34	16.61	2.31	51.59	22.13	1.05	0.17	0.15	6.02	100.37	46.2	44.2	9.6
MC-2.14_3	0.30	16.71	1.99	51.64	22.40	0.99	0.20	0.16	5.65	100.06	46.3	44.6	9.0
MC-2.14_4	0.29	16.60	2.26	51.52	22.27	1.03	0.16	0.15	5.82	100.09	46.2	44.5	9.3
MC-2.14_5	0.33	16.68	2.36	51.24	22.45	1.09	0.23	0.14	5.70	100.22	46.2	44.7	9.1
MC-2.14_6	0.35	16.53	2.46	51.05	22.28	1.13	0.25	0.13	5.70	99.87	46.2	44.7	9.1
MC-2.14_7	0.33	16.21	2.85	50.59	22.21	1.34	0.33	0.17	6.02	100.05	45.5	44.8	9.7
MC-2.14_8	0.34	16.02	2.83	50.55	22.11	1.35	0.30	0.14	6.12	99.77	45.2	44.9	9.9
MC-2.14_9	0.34	16.14	2.58	51.15	21.99	1.17	0.23	0.19	6.01	99.82	45.6	44.6	9.8
MC-2.14_10	0.37	16.25	2.52	51.05	22.06	1.14	0.25	0.17	6.17	99.98	45.6	44.5	10.0
MC-2.14_11	0.34	16.01	2.59	50.91	21.70	1.25	0.12	0.22	6.73	99.88	45.1	43.9	11.0
MC-2.14_13	0.33	15.31	3.59	48.89	19.12	1.14	0.18	0.15	8.56	97.28	45.1	40.5	14.4
MC-2.14_14	0.35	16.21	2.55	51.00	21.99	1.21	0.18	0.17	6.13	99.78	45.6	44.5	9.9
MC-2.14_15	0.36	16.00	2.86	50.50	22.09	1.33	0.27	0.15	6.14	99.70	45.2	44.8	10.0

Feldspars

Label	Na_2O	MgO	Al_2O_3	SiO_2	K_2O	CaO	FeO	SrO	BaO	Total	An	Ab	Or
MC-1.1	5.40	0.00	18.64	65.20	8.28	0.39	0.80	0.00	0.00	98.71	2.0	48.8	49.3
MC-1.2	5.91	0.01	18.88	65.47	6.92	0.83	0.94	0.00	0.01	98.96	4.2	54.1	41.7
MC-1.3	6.30	0.05	24.33	59.19	1.98	6.16	0.69	0.54	0.29	99.52	30.9	57.2	11.8
MC-1.4	5.94	0.74	25.41	56.73	1.17	7.11	1.18	0.80	0.21	99.29	36.9	55.8	7.2
MC-1.5	4.77	0.10	27.79	53.86	0.81	9.75	1.02	1.18	0.21	99.51	50.4	44.6	5.0
MC-1.6	4.56	0.11	28.33	53.28	0.66	10.79	1.06	0.97	0.08	99.84	54.4	41.6	4.0
MC-1.7	4.87	0.09	27.62	54.45	0.88	9.43	1.01	1.00	0.12	99.45	48.9	45.7	5.4
MC-1.8	5.49	0.28	26.16	56.76	1.07	7.89	1.07	0.72	0.26	99.70	41.3	52.0	6.7
MC-1.9	4.57	0.10	28.45	53.52	0.70	10.57	1.02	0.98	0.15	100.06	53.7	42.0	4.2
MC-1.10	5.03	0.08	27.44	54.70	0.93	9.28	0.74	1.17	0.21	99.58	47.6	46.7	5.7
MC-1.11	4.90	0.15	27.71	54.16	0.80	10.04	0.95	1.06	0.13	99.90	50.6	44.6	4.8
MC-1.12	5.24	0.15	25.32	53.59	1.05	10.61	0.82	0.85	0.18	97.81	49.7	44.5	5.8
MC-1.16	6.30	0.26	19.79	64.54	5.89	1.57	1.02	0.04	0.00	99.40	7.8	57.0	35.1
MC-1.17	6.56	0.54	23.68	59.52	1.87	5.53	1.21	0.50	0.20	99.61	28.2	60.5	11.4
MC-1.18	5.46	2.44	24.47	55.19	1.03	6.37	2.92	0.84	0.18	98.91	36.5	56.5	7.0
MC-1.19	4.99	0.10	27.30	54.94	0.99	9.23	0.84	1.01	0.32	99.73	47.5	46.5	6.1
MC-1.20	5.94	0.10	25.67	57.09	1.29	7.36	0.59	0.75	0.25	99.05	37.5	54.7	7.8
MC-1.21	5.96	0.07	25.57	57.41	1.35	7.51	0.65	0.81	0.20	99.52	37.7	54.2	8.1
MC-1.22	5.79	0.11	25.86	56.93	1.17	7.89	0.78	0.89	0.23	99.66	39.9	53.0	7.0
MC-1.23	4.79	0.08	27.60	54.51	0.85	9.73	0.73	1.01	0.17	99.47	50.1	44.7	5.2
MC-1.25	5.85	0.47	25.22	57.44	1.46	7.18	0.86	0.87	0.31	99.65	36.8	54.3	8.9
MC-1.26	4.95	0.10	27.52	54.70	0.91	9.48	0.76	1.17	0.26	99.86	48.6	45.9	5.6
MC-1.27	5.33	0.06	26.77	55.74	1.11	8.59	0.79	0.93	0.27	99.60	43.9	49.3	6.8
MC-1.28	4.64	0.11	28.23	53.79	0.78	10.19	0.84	1.11	0.14	99.83	52.2	43.0	4.8
MC-1.29	5.33	0.12	26.79	55.73	0.99	8.59	0.79	1.08	0.17	99.60	44.3	49.7	6.1
MC-1.30	6.30	1.05	24.45	57.60	1.01	5.96	1.47	0.71	0.14	98.70	32.1	61.4	6.5
MC-1.31	5.93	0.40	25.25	57.03	1.31	7.02	1.24	0.83	0.25	99.26	36.4	55.6	8.1
MC-1.32	5.67	0.06	26.08	56.12	1.09	8.52	1.13	0.84	0.16	99.67	42.4	51.1	6.5
MC-1.33	5.20	0.24	26.53	54.48	0.94	8.21	0.98	0.70	0.31	97.59	43.8	50.2	6.0
MC-1.34	5.49	0.07	26.78	55.45	0.91	9.19	0.91	0.94	0.17	99.90	45.5	49.2	5.3
MC-1.35	5.88	0.02	18.60	66.47	6.82	0.50	1.00	0.00	0.00	99.29	2.6	55.2	42.2
MC-1.36	5.78	0.04	26.00	57.48	1.25	7.77	0.82	0.91	0.24	100.30	39.4	53.0	7.6
MC-1.37	4.76	0.11	27.88	54.23	0.70	10.08	0.79	0.97	0.08	99.61	51.6	44.1	4.3
MC-1.38	6.23	0.05	24.76	58.81	1.75	6.47	0.84	0.50	0.25	99.66	32.6	56.9	10.5

Label	Na_2O	MgO	Al_2O_3	SiO_2	K_2O	CaO	FeO	SrO	BaO	Total	An	Ab	Or
MC-1.39	4.78	0.52	26.49	53.64	0.83	8.73	1.25	0.93	0.16	97.34	47.5	47.1	5.4
MC-1.40	5.69	0.07	26.19	56.78	1.22	8.12	0.80	0.94	0.22	100.03	40.9	51.8	7.3
MC-1.41	5.21	0.09	27.23	55.28	1.04	9.02	0.79	1.11	0.29	100.06	45.8	47.9	6.3
MC-1.42	4.98	0.06	19.49	64.15	8.12	0.91	0.63	0.05	0.38	98.77	4.6	46.0	49.4
MC-1.43	5.89	0.07	25.40	57.75	1.51	7.38	0.78	0.84	0.19	99.80	37.2	53.7	9.1
MC-1.44	5.55	0.02	18.62	65.59	7.92	0.37	1.01	0.06	0.00	99.14	1.9	50.6	47.5
MC-2.1	4.96	0.12	27.38	54.36	0.84	9.56	0.88	1.15	0.19	99.43	48.9	45.9	5.1
MC-2.2	5.21	0.07	27.16	54.57	0.92	9.12	0.78	1.15	0.18	99.16	46.4	48.0	5.6
MC-2.3	5.51	0.09	26.90	55.85	0.97	8.79	0.84	0.86	0.12	99.93	44.1	50.1	5.8
MC-2.4	5.24	0.09	26.86	55.06	1.00	8.94	0.76	0.97	0.22	99.13	45.6	48.4	6.1
MC-2.5	5.36	0.32	26.96	55.13	0.84	9.06	1.04	0.85	0.16	99.74	45.8	49.1	5.1
MC-2.6	5.15	0.60	26.83	54.87	0.93	8.75	1.23	0.88	0.14	99.38	45.7	48.6	5.8
MC-2.7	5.15	0.10	27.05	55.00	0.98	8.93	0.80	0.98	0.19	99.17	46.0	48.0	6.0
MC-2.8	5.08	0.11	27.37	54.29	0.77	9.63	0.80	0.99	0.17	99.20	48.8	46.5	4.6
MC-2.9	5.84	0.06	26.10	57.19	1.29	7.79	0.91	0.95	0.24	100.36	39.2	53.1	7.7
MC-2.10	5.05	0.09	27.34	54.82	0.85	9.51	0.81	1.05	0.20	99.72	48.4	46.5	5.1
MC-2.11	5.95	0.07	25.33	57.03	1.21	8.07	0.96	0.73	0.13	99.48	39.8	53.1	7.1
MC-2.12	6.49	0.04	24.71	58.88	1.63	6.57	0.80	0.46	0.11	99.70	32.4	58.0	9.6
MC-2.13	5.18	0.09	27.16	55.04	0.86	9.46	0.87	1.14	0.11	99.92	47.6	47.2	5.1
MC-2.14	5.09	0.88	26.33	54.41	0.91	8.71	1.56	1.12	0.17	99.16	45.8	48.5	5.7
MC-2.15	5.53	0.08	26.55	55.79	1.00	8.61	0.87	0.96	0.13	99.52	43.5	50.5	6.0
MC-2.16	6.05	0.19	23.51	59.86	1.77	6.14	0.89	0.49	0.27	99.18	32.0	57.0	11.0
MC-2.17	5.21	1.36	17.91	65.02	5.79	1.14	2.40	0.00	0.00	98.83	6.5	54.0	39.5
MC-2.18	4.77	0.00	18.79	65.98	8.92	0.37	0.78	0.00	0.00	99.63	1.9	44.0	54.1
MC-2.22	5.00	0.02	19.07	65.32	8.96	0.65	0.80	0.00	0.02	99.83	3.2	44.4	52.4
MC-2.23	5.16	0.13	18.51	65.42	8.57	0.38	1.10	0.00	0.02	99.30	1.9	46.8	51.2
MC-2.24	7.71	0.05	20.53	64.69	3.94	2.19	0.90	0.00	0.00	100.02	10.5	67.0	22.5
MC-2.25	5.35	0.08	18.98	65.21	8.47	0.54	0.76	0.00	0.07	99.45	2.7	47.7	49.7
MC-2.26	6.83	0.17	22.31	62.23	3.73	3.81	0.71	0.13	0.13	100.05	18.5	60.0	21.5
MC-2.27	5.37	0.09	26.88	54.88	1.01	8.89	0.84	1.39	0.25	99.61	44.9	49.0	6.1
MC-2.28	5.07	0.02	19.22	64.83	8.61	0.88	0.76	0.06	0.04	99.48	4.3	45.2	50.5
MC-2.29	5.09	0.10	27.02	55.03	1.09	8.98	1.06	1.10	0.22	99.67	46.1	47.3	6.7
MC-2.30	5.52	0.06	26.27	56.27	1.17	8.12	0.87	1.04	0.19	99.50	41.6	51.2	7.1
MC-2.31	5.17	0.07	26.90	55.17	0.97	8.83	0.86	1.16	0.16	99.29	45.6	48.4	6.0
MC-2.32	4.76	0.84	26.71	53.81	0.88	8.79	1.55	1.14	0.17	98.65	47.6	46.7	5.7
MC-2.34	4.71	0.00	19.88	63.72	8.25	1.19	0.63	0.12	0.43	98.93	6.1	43.6	50.3
MC-2.35	5.78	0.03	19.74	64.68	6.79	1.31	0.83	0.00	0.00	99.16	6.6	52.7	40.7
MC-2.36	5.63	0.08	26.23	56.70	1.15	8.03	0.86	0.98	0.14	99.81	41.0	52.0	7.0
MC-2.37	5.56	1.04	23.05	57.41	2.83	5.46	2.33	0.56	0.05	98.28	28.9	53.3	17.8
MC-2.38	6.02	0.05	25.09	58.23	1.62	6.73	0.86	0.66	0.24	99.50	34.4	55.7	9.9
MC-2.39	6.61	0.02	22.15	61.82	4.03	3.67	0.63	0.14	0.13	99.20	18.0	58.6	23.5
MC-2.40	6.01	0.07	25.55	57.95	1.39	7.39	0.74	0.74	0.15	99.99	37.1	54.6	8.3
MC-2.41	6.47	0.01	21.08	63.10	4.93	2.88	0.64	0.00	0.03	99.14	14.1	57.2	28.7
MC-2.42	5.76	0.07	25.84	57.27	1.30	7.73	0.79	0.84	0.22	99.82	39.2	52.9	7.8
MC-2.43	6.08	0.04	25.42	58.08	1.54	7.15	0.72	0.87	0.19	100.09	35.8	55.0	9.2

Phlogopite

Label	SiO_2	TiO_2	Al_2O_3	FeO	MnO	MgO	CaO	Na_2O	K_2O	F	Cl	H_2O(c)	Total
MC-1.1	36.28	5.50	14.43	9.04	0.12	18.36	0.26	0.88	8.01	2.96	0.05	2.61	98.50
MC-1.2	36.25	6.11	14.53	8.86	0.11	18.15	0.43	0.83	8.21	2.59	0.04	2.81	98.92
MC-1.3	34.86	5.22	13.68	7.87	0.15	18.07	2.80	0.81	7.91	3.05	0.07	2.47	96.96
MC-1.4	36.01	6.02	14.35	8.87	0.12	18.19	0.27	0.85	8.12	2.87	0.04	2.65	98.36
MC-1.5	35.79	5.92	14.28	9.05	0.16	17.97	0.25	0.91	8.18	3.00	0.04	2.56	98.11

Label	SiO_2	TiO_2	Al_2O_3	FeO	MnO	MgO	CaO	Na_2O	K_2O	F	Cl	H_2O(c)	Total
MC-1.6	36.95	4.97	14.55	8.16	0.09	19.42	0.03	0.86	8.52	2.84	0.05	2.71	99.15
MC-1.7	36.93	4.82	14.14	8.11	0.08	19.66	0.04	0.87	8.32	3.13	0.04	2.55	98.69
MC-1.8	35.50	5.64	14.31	10.79	0.17	17.89	0.11	0.72	7.46	2.95	0.04	2.57	98.15
MC-1.9	38.94	4.79	14.52	8.11	0.13	17.88	0.07	1.04	8.55	3.33	0.05	2.52	99.93
MC-1.10	36.45	6.02	14.44	8.14	0.11	18.07	0.13	0.82	8.31	2.13	0.03	3.00	97.65
MC-1.11	36.05	5.92	14.52	8.51	0.12	18.39	0.21	0.91	8.28	2.86	0.05	2.66	98.48
MC-1.13	35.39	6.09	14.45	9.47	0.10	18.02	0.06	0.81	7.77	2.32	0.05	2.87	97.40
MC-1.14	36.83	5.65	14.50	8.09	0.04	19.19	0.04	0.87	8.47	2.76	0.04	2.76	99.24
MC-1.15	36.17	5.97	14.46	8.13	0.09	18.56	0.32	0.83	8.26	2.58	0.04	2.80	98.21
MC-1.16	36.08	6.24	14.29	8.50	0.09	18.51	0.22	0.86	8.37	2.57	0.04	2.81	98.58
MC-1.17	36.43	6.39	13.94	10.18	0.18	17.56	0.14	0.79	8.36	2.87	0.06	2.67	99.57
MC-1.18	36.46	5.91	14.19	8.57	0.08	18.41	0.32	0.87	8.28	2.89	0.05	2.65	98.68
MC-1.20	36.05	6.00	14.31	8.63	0.10	18.33	0.21	0.84	8.34	2.87	0.05	2.64	98.37
MC-1.21	36.34	6.18	14.23	9.20	0.07	18.11	0.04	0.83	8.27	2.89	0.04	2.65	98.85
MC-1.22	36.33	6.28	14.36	8.68	0.13	18.48	0.05	0.93	8.43	2.67	0.05	2.78	99.17
MC-1.23	36.11	5.83	14.39	8.35	0.15	18.49	0.43	0.85	8.33	3.02	0.04	2.58	98.57
MC-1.24	36.01	6.38	14.24	9.68	0.14	17.49	0.29	0.81	8.30	2.81	0.06	2.67	98.88
MC-1.25	36.84	4.77	14.33	8.86	0.16	19.26	0.10	0.82	8.47	3.31	0.05	2.47	99.44
MC-1.26	36.23	5.97	14.25	9.81	0.20	17.82	0.37	0.82	8.48	3.22	0.05	2.50	99.72
MC-1.28	36.73	5.16	14.49	7.98	0.08	19.59	0.08	0.92	8.16	2.89	0.04	2.68	98.80
MC-1.29	37.30	5.41	14.17	8.22	0.09	19.11	0.10	0.85	8.23	2.69	0.04	2.79	99.00
MC-1.30	36.01	6.26	14.46	8.27	0.13	18.08	0.05	0.85	8.44	2.60	0.04	2.77	97.96
MC-1.31	35.95	6.07	14.17	9.61	0.19	17.38	0.15	0.82	8.47	3.16	0.04	2.49	98.50
MC-1.33	35.84	6.19	14.35	9.34	0.15	17.44	0.12	0.88	8.32	2.42	0.04	2.84	97.93
MC-1.34	35.87	6.45	14.46	9.33	0.14	17.49	0.18	0.85	8.49	2.58	0.05	2.78	98.67
MC-1.35	35.96	5.79	14.46	8.51	0.10	18.47	0.07	0.86	8.53	2.58	0.04	2.78	98.15
MC-1.36	36.11	6.02	14.36	9.10	0.08	17.86	0.10	0.85	8.41	3.18	0.04	2.50	98.61
MC-1.37	36.25	4.97	14.24	8.44	0.11	18.90	0.06	0.87	8.24	3.27	0.04	2.44	97.83
MC-1.38	36.27	5.17	13.87	7.86	0.12	18.77	0.93	0.81	8.35	2.89	0.05	2.62	97.71
MC-2.1	36.16	6.18	14.78	8.59	0.13	17.76	0.07	0.86	8.31	1.86	0.04	3.13	97.87
MC-2.2	35.47	6.08	15.00	8.43	0.06	18.02	0.09	0.92	8.28	2.48	0.04	2.82	97.69
MC-2.3	35.69	6.22	15.00	8.65	0.10	18.03	0.05	0.91	8.34	2.15	0.04	3.00	98.18
MC-2.4	36.12	6.26	14.89	8.26	0.11	18.38	0.21	0.90	8.13	1.88	0.03	3.15	98.32
MC-2.5	36.09	6.16	14.67	8.24	0.16	18.24	0.42	0.89	8.34	2.24	0.03	2.97	98.45
MC-2.6	36.06	4.50	14.22	10.86	0.13	18.70	0.37	0.66	6.92	1.96	0.04	3.05	97.47
MC-2.7	36.59	5.79	14.70	8.75	0.09	18.67	0.18	0.94	8.33	2.19	0.04	3.03	99.30
MC-2.8	35.58	5.96	13.79	10.85	0.13	17.56	0.31	0.67	7.12	1.96	0.04	3.02	96.99
MC-2.9	44.56	4.55	11.94	9.50	0.11	15.79	0.21	0.62	6.89	2.14	0.03	3.17	99.51
MC-2.10	36.33	5.85	14.91	8.87	0.10	18.40	0.07	0.87	7.95	2.10	0.04	3.05	98.54
MC-2.11	34.30	10.60	13.66	9.13	0.11	17.57	0.11	0.72	7.23	2.07	0.04	3.04	98.58
MC-2.12	36.96	5.68	14.29	8.57	0.10	18.95	0.04	0.82	8.41	2.10	0.04	3.07	99.03
MC-2.13	36.25	5.97	14.49	8.35	0.10	18.62	0.04	0.80	8.36	2.03	0.04	3.06	98.11
MC-2.14	36.41	5.85	14.66	8.33	0.07	18.84	0.07	0.86	8.32	2.35	0.03	2.94	98.73
MC-2.15	36.59	6.27	14.35	9.17	0.13	17.90	0.13	0.77	8.20	2.09	0.05	3.05	98.70
MC-2.16	36.21	5.39	14.86	8.41	0.13	18.71	0.20	0.84	8.34	2.25	0.02	2.97	98.33
MC-2.17	36.18	5.41	14.79	8.22	0.13	18.92	0.19	0.86	8.16	2.36	0.03	2.91	98.16
MC-2.21	36.39	4.76	14.41	9.99	0.09	18.96	0.19	0.73	7.54	2.05	0.04	3.04	98.19
MC-2.22	36.65	5.31	14.77	8.29	0.07	18.80	0.11	0.86	8.31	2.42	0.03	2.90	98.52
MC-2.23	36.38	5.70	14.89	8.24	0.10	18.55	0.08	0.84	8.45	2.53	0.03	2.84	98.63
MC-2.26_1	36.00	6.62	14.96	8.56	0.03	18.00	0.06	0.86	7.90	2.04	0.04	3.06	98.13
MC-2.26_2	37.00	3.36	14.73	8.03	0.05	19.80	0.03	0.81	8.87	2.28	0.02	2.95	97.93
MC-2.26_3	37.25	4.35	14.65	8.38	0.03	19.20	0.04	0.78	8.84	1.60	0.01	3.30	98.43
MC-2.26_4	38.01	3.94	13.48	8.93	0.05	19.64	0.02	0.74	8.97	1.68	0.02	3.26	98.74
MC-2.26_5	38.11	3.94	13.22	9.04	0.06	19.65	0.04	0.71	8.98	1.54	0.02	3.32	98.63

Label	SiO_2	TiO_2	Al_2O_3	FeO	MnO	MgO	CaO	Na_2O	K_2O	F	Cl	H_2O(c)	Total
MC-2.26_6	37.76	4.02	13.71	8.65	0.08	19.84	0.04	0.80	8.77	1.95	0.03	3.13	98.78
MC-2.26_7	37.95	3.94	13.26	8.76	0.03	19.38	0.06	0.74	8.85	1.46	0.02	3.33	97.78
MC-2.26_8	37.84	3.80	13.23	8.65	0.04	20.08	0.03	0.66	8.77	1.22	0.01	3.46	97.79
MC-2.27	35.54	6.40	14.91	9.16	0.08	17.89	0.10	0.80	8.46	2.09	0.04	3.03	98.50
MC-2.29	35.99	6.49	15.16	8.57	0.07	18.01	0.11	0.92	8.10	1.77	0.04	3.21	98.44
MC-2.30	36.27	5.80	14.69	9.36	0.10	18.24	0.05	0.84	8.16	2.35	0.04	2.92	98.82
MC-2.31	36.06	5.81	14.49	10.29	0.11	17.50	0.17	0.80	7.85	2.36	0.03	2.89	98.36
MC-2.32	35.64	6.39	15.03	8.83	0.13	17.71	0.08	0.85	8.06	2.09	0.02	3.02	97.85
MC-2.33	35.34	6.20	15.09	8.88	0.09	17.69	0.06	0.81	8.01	2.12	0.03	2.98	97.30
MC-2.34	36.52	5.43	14.20	9.08	0.08	18.64	0.05	0.88	8.56	2.34	0.03	2.92	98.73
MC-2.35	36.20	5.80	14.79	8.56	0.11	18.43	0.05	0.89	8.35	2.18	0.04	3.00	98.40
MC-2.36	35.71	5.97	15.06	8.95	0.12	18.30	0.14	0.83	8.25	2.14	0.03	3.01	98.51
MC-2.37	36.30	5.87	14.85	9.20	0.13	18.00	0.18	0.80	8.16	1.97	0.04	3.10	98.60
MC-2.38	35.71	6.49	14.80	8.81	0.11	17.55	0.12	0.89	8.33	2.16	0.03	2.98	97.98
MC-2.39	35.75	6.00	14.65	9.28	0.10	17.89	0.11	0.83	7.78	2.29	0.04	2.91	97.63
MC-2.40	35.79	5.52	14.43	10.20	0.13	18.06	0.56	0.66	7.29	1.60	0.04	3.23	97.51
MC-2.41	35.64	6.49	15.03	9.18	0.16	17.47	0.46	0.82	8.28	2.18	0.04	2.99	98.74
MC-2.42	35.67	6.54	14.89	9.12	0.15	17.26	0.31	0.83	8.22	1.72	0.04	3.19	97.94
MC-2.43	36.13	5.96	14.94	8.93	0.13	18.19	0.08	0.89	8.20	2.29	0.02	2.95	98.71
MC-2.44	35.49	6.18	15.24	8.29	0.10	18.01	0.13	0.83	8.22	1.93	0.04	3.09	97.55
MC-2.45	35.81	6.06	14.58	8.94	0.12	17.80	0.16	0.91	8.32	2.23	0.03	2.94	97.90
MC-2.46	35.69	6.30	14.81	8.11	0.11	18.15	0.08	0.93	8.21	2.28	0.02	2.92	97.61
MC-2.49	35.80	6.37	15.08	8.55	0.13	17.75	0.26	0.90	8.31	2.04	0.03	3.06	98.28
MC-2.50	36.17	5.62	14.91	9.36	0.12	18.10	0.16	0.82	8.04	2.08	0.04	3.04	98.46
MC-2.51	36.59	5.40	14.40	8.95	0.15	18.41	0.15	0.82	8.49	2.10	0.04	3.04	98.54
MC-2.53	35.65	5.95	15.13	8.54	0.10	18.04	0.14	0.82	7.99	2.00	0.03	3.05	97.44
MC-2.54	36.02	5.71	14.50	10.20	0.12	17.64	0.14	0.82	7.89	2.29	0.04	2.92	98.29
MC-2.24	39.42	4.44	12.57	8.98	0.17	15.04	11.65	2.33	1.25	1.05	0.05	3.67	100.62
MC-2.25	39.35	4.58	12.71	9.24	0.19	14.96	11.59	2.39	1.26	1.14	0.04	3.64	101.09

Titano-magetites

Label	SiO_2	TiO_2	Al_2O_3	Cr_2O_3	Fe_2O_3(c)	FeO	V_2O_3	MnO	MgO	ZnO	Total
MC-1.1	0.03	7.29	3.66	0	47.8	34.09	0.46	0.81	1.44	0.02	95.59
MC-1.2	0.06	7.22	3.15	0.01	47.98	33.53	0.51	0.93	1.42	0.2	95
MC-1.3	0.06	6.92	1.33	0.05	50.65	34.06	0.51	0.99	0.78	0.14	95.48
MC-1.4	0.23	8.2	4.38	0.03	43.18	36.35	0.3	0.87	0.25	0.32	94.09
MC-1.5	0.03	8.3	3.36	0.03	46.16	33.66	0.48	0.87	2.12	0.08	95.08
MC-1.6	1.98	5.89	1.68	0.02	48.16	35.43	0.67	0.63	1.27	0.2	95.92
MC-1.7	0.09	7.65	2.43	0	48.22	33.17	0.52	0.95	1.86	0.19	95.09
MC-1.8	0.05	7.46	2.79	0.01	48.52	32.49	0.43	0.94	2.19	0.2	95.08
MC-1.9	0.02	8.14	2.98	0.05	47.95	33.71	0.43	0.97	2.1	0.17	96.52
MC-1.10	0.07	7.88	3.46	0.06	47.63	35.23	0.42	0.82	1.27	0.15	97
MC-1.11	0.04	8.59	3.02	0.06	47.78	32.73	0.36	1	3.1	0.11	96.79
MC-1.12	0.06	9.01	2.95	0.08	46.15	34.57	0.35	1	2.1	0.09	96.37
MC-1.13	0.06	8.18	3	0.03	47.63	32.95	0.36	1.01	2.53	0.12	95.87
MC-1.14	0.08	6.67	0.92	0.02	52.45	34.66	0.63	0.84	0.63	0.11	97.02
MC-1.15	0.03	7.52	2.72	0.01	49.27	31.92	0.47	0.9	2.76	0.2	95.81
MC-1.16	0.07	7.8	2.41	0.05	48.37	33.32	0.47	1.02	1.88	0.23	95.63
MC-1.17	0.05	8.23	2.16	0.03	48.67	33.37	0.46	0.97	2.25	0.25	96.46
MC-1.18	0.06	6.32	1.33	0.05	52.48	34	0.48	0.91	0.71	0.14	96.48
MC-1.19	0.07	7.95	2.18	0.03	49.42	32.44	0.47	1.05	2.71	0.16	96.49
MC-1.20	0.05	7.22	2.8	0.03	49.98	33.49	0.45	0.97	1.78	0.18	96.96
MC-1.21	0.06	7.82	3.6	0.06	47.97	33.64	0.33	0.78	2.21	0.15	96.61

Label	SiO_2	TiO_2	Al_2O_3	Cr_2O_3	Fe_2O_3(c)	FeO	V_2O_3	MnO	MgO	ZnO	Total
MC-1.22	0.02	8.69	3.91	0.08	44.72	33.59	0.32	0.76	2.37	0.19	94.65
MC-1.23	0.05	8.33	3.8	0.09	45.31	34.89	0.28	0.71	1.49	0.09	95.04
MC-1.24	0.04	7.58	3.02	0.01	48.85	31.65	0.36	0.79	3.05	0.13	95.48
MC-1.25	0.04	7.25	4.29	0.01	47.2	33.76	0.35	0.79	1.65	0.09	95.43
MC-1.26	0.06	7.71	2.22	0.03	48.03	32.51	0.4	0.97	2.09	0.18	94.2
MC-1.27	0.07	8.88	4.92	0.04	43.03	35.11	0.27	0.65	1.81	0.12	94.9
MC-1.28	0.03	9.02	4.91	0.05	41.74	34.18	0.29	0.56	2.21	0.03	93.02
MC-1.30	0.05	8.64	4.11	0.05	45.4	34.13	0.28	1.06	2.09	0.24	96.05
MC-1.31	0.05	6.78	2.63	0.04	50.14	32.96	0.4	0.9	1.57	0.28	95.75
MC-1.32	0.04	7.61	2.56	0.02	48.28	33	0.45	0.88	1.94	0.2	94.97
MC-1.33	0.21	6.69	4.49	0.04	48.23	33.31	0.39	0.7	1.9	0.23	96.19
MC-1.34	0.07	6.78	1.32	0.01	51.78	33.85	0.51	0.88	1.06	0.21	96.47
MC-1.35	0.06	7.54	1.98	0.03	49.49	34.48	0.45	0.95	1.08	0.24	96.3
MC-1.36	0.15	7.23	1.78	0.02	50.14	33.36	0.49	0.96	1.62	0.22	95.95
MC-1.37	0.34	7.8	3.32	0.04	47.42	31.79	0.47	0.87	3.33	0.15	95.52
MC-1.38	0.24	6.99	2.93	0.07	48.42	34.24	0.36	0.8	1.13	0.17	95.36
MC-1.39	0.54	7.37	2.94	0.03	47.71	33.37	0.39	0.82	2.2	0.22	95.59
MC-2.1	1.74	1.19	0.47	0.07	57.94	32.53	0.24	0.17	0.02	0.13	94.5
MC-2.2	1.89	1.22	0.52	0.06	56.6	32.37	0.26	0.15	0.02	0.15	93.25
MC-2.3	1.38	2.66	0.65	0.07	56.39	33.65	0.41	0.22	0.04	0.21	95.68
MC-2.4	0.1	8.63	2.5	0	47.18	32.44	0.47	0.84	3.1	0.19	95.46
MC-2.5	1.32	2.09	0.35	0.03	58.06	33.13	0.38	0.16	0.03	0.15	95.69
MC-2.6	0.12	7.93	1.04	0.01	49.57	35.07	0.61	0.94	0.96	0.17	96.41
MC-2.7	0.91	3.66	0.73	0.06	55.97	33.92	0.41	0.25	0.18	0.2	96.28
MC-2.8	0.45	6.9	2.28	0.05	50.07	33.54	0.41	0.75	1.91	0.15	96.5
MC-2.9	0.06	52.9	1.95	0	0	34.32	0.08	0.23	5.02	0	94.57
MC-2.11	0.19	7.26	2.54	0.03	48.57	33.18	0.44	0.71	1.88	0.14	94.94
MC-2.12	0.04	9.36	3.7	0.06	44.95	32.25	0.43	0.84	3.82	0.09	95.55
MC-2.13	1.81	1.74	0.21	0.05	55.84	32.61	0.2	0.13	0	0.13	92.72
MC-2.14	0.03	8.14	2.82	0.03	47.01	32.84	0.4	1.03	2.25	0.16	94.71
MC-2.15	0.47	5.93	2.3	0.01	49.24	32.17	0.38	0.72	1.51	0.19	92.93
MC-2.16	1.52	1.31	0.25	0.1	57.65	31.99	0.24	0.22	0.01	0.05	93.34
MC-2.17	0.37	7.51	2.9	0.02	48.34	32.98	0.42	0.67	2.58	0.14	95.92
MC-2.18	1.44	1.56	0.22	0.07	58.05	32.41	0.26	0.21	0	0.07	94.3
MC-2.19	0.06	8.96	2.86	0.05	45.73	31.52	0.38	0.89	3.67	0.11	94.22
MC-2.20	0.07	8.62	3.24	0.04	46.35	32.08	0.36	0.87	3.38	0.03	95.05
MC-2.21	1.24	2.58	0.45	0.04	57.38	33.46	0.31	0.22	0	0.25	95.92
MC-2.22	1.24	2.72	0.6	0.03	57.49	33.9	0.36	0.17	0.01	0.26	96.78
MC-2.23	1.46	1.94	0.35	0.02	57.92	33.08	0.34	0.2	0.01	0.19	95.51
MC-2.24	0.03	7.93	2.32	1.17	47.45	33.34	0.38	0.89	2.08	0.12	95.7
MC-2.25	0.78	3.87	0.73	0.06	55.37	33.53	0.42	0.3	0.22	0.29	95.58
MC-2.26	1.76	1.52	0.43	0.06	57.89	33.15	0.29	0.15	0.01	0.15	95.4
MC-2.27	1.47	4.33	1.02	0.04	52.87	35.12	0.28	0.25	0.27	0.13	95.78
MC-2.28	1.45	1.74	0.49	0.04	58.16	32.91	0.3	0.2	0.01	0.13	95.43
MC-2.29	1.51	2.84	0.84	0.04	55.83	34.22	0.32	0.2	0	0.22	96.03
MC-2.30	1.47	1.91	0.59	0.04	57.13	32.94	0.35	0.18	0.02	0.13	94.76
MC-2.31	1.44	1.77	0.55	0.06	58.31	33.23	0.41	0.15	0.03	0.05	96
MC-2.32	1.31	2.57	0.51	0.06	57.11	33.36	0.42	0.21	0.16	0.22	95.93
MC-2.35	0.03	7.07	1.43	0	50.66	32.84	0.62	0.99	1.65	0.11	95.4
MC-2.37	1.16	3.56	1.15	0.02	54.03	33.19	0.46	0.34	0.39	0.35	94.65
MC-2.38	1.03	3.17	0.51	0.03	55.12	32.8	0.45	0.26	0.04	0.48	93.88
MC-2.39	0.02	7.82	2.04	0.02	48.05	32.52	0.56	1	2.04	0.33	94.4
MC-2.40	0.03	7.83	1.73	0	49.74	33.32	0.54	0.98	1.91	0.34	96.42
MC-2.41	0.93	3.67	1	0.03	56.68	34.15	0.45	0.34	0.31	0.24	97.79

Label	SiO_2	TiO_2	Al_2O_3	Cr_2O_3	Fe_2O_3(c)	FeO	V_2O_3	MnO	MgO	ZnO	Total
MC-2.42	0.68	6.08	2.04	0.03	51.82	33.43	0.44	0.61	1.89	0.14	97.16
MC-2.43	2.68	0.55	0.18	0.07	56.13	32.8	0.19	0.07	0.02	0	92.68
MC-2.44	1.57	2.56	0.98	0.02	56.46	34.15	0.35	0.19	0.04	0.22	96.54

Scott Butte Rhyolite Dike

Feldspars

Label	Na_2O	MgO	Al_2O_3	SiO_2	K_2O	CaO	FeO	SrO	BaO	Total	An	Ab	Or
GRD-1.1	7.53	0.00	25.28	59.99	0.22	6.40	0.05	0.00	0.00	99.46	31.5	67.2	1.3
GRD-1.2	7.06	0.00	25.07	59.52	0.23	6.40	0.03	0.00	0.08	98.38	32.9	65.7	1.4
GRD-1.3	7.63	0.00	24.55	60.69	0.30	5.80	0.03	0.00	0.03	99.04	29.0	69.1	1.8
GRD-1.4	7.57	0.00	25.24	60.00	0.25	6.20	0.01	0.00	0.04	99.33	30.7	67.8	1.5
SB-1.2	8.08	0.01	19.57	67.46	4.98	0.17	0.10	0.00	0.00	100.35	0.8	70.6	28.6
SB-1.3	5.68	0.01	19.39	66.60	8.43	0.06	0.09	0.01	0.02	100.30	0.3	50.4	49.3
SB-1.10	7.72	0.01	25.57	60.60	0.20	6.86	0.19	0.08	0.02	101.24	32.6	66.3	1.1
SB-1.14	7.65	0.00	25.43	61.12	0.21	6.21	0.13	0.09	0.03	100.88	30.6	68.2	1.2
SB-1.20	9.41	0.02	23.11	64.83	0.11	3.35	0.20	0.04	0.06	101.13	16.3	83.0	0.7
SB-1.21	8.30	0.02	24.10	62.58	0.34	4.94	0.05	0.02	0.06	100.42	24.2	73.8	2.0
SB-1.25	7.60	0.00	25.42	61.29	0.22	5.97	0.09	0.00	0.02	100.60	29.9	68.8	1.3
SB-1.31_1	7.46	0.00	25.72	60.12	0.18	6.61	0.05	0.02	0.04	100.20	32.5	66.4	1.1
SB-1.31_2	7.50	0.00	25.55	60.54	0.23	6.72	0.01	0.06	0.03	100.63	32.7	66.0	1.3
SB-1.31_3	7.27	0.00	25.94	60.07	0.19	6.97	0.05	0.15	0.03	100.67	34.2	64.7	1.1
SB-1.31_4	7.21	0.04	25.72	58.91	0.21	7.06	0.07	0.09	0.05	99.36	34.7	64.1	1.2
SB-1.31_5	7.59	0.02	25.75	60.22	0.20	6.85	0.04	0.15	0.01	100.84	32.9	66.0	1.2
SB-1.31_6	7.42	0.01	26.02	60.26	0.17	6.98	0.04	0.15	0.00	101.07	33.9	65.1	1.0
SB-1.31_7	7.58	0.01	25.74	60.37	0.20	7.13	0.04	0.08	0.00	101.16	33.8	65.0	1.1
SB-1.31_8	7.52	0.01	25.76	60.98	0.18	6.77	0.11	0.08	0.03	101.45	32.9	66.0	1.1
SB-1.34	7.56	0.01	25.77	60.12	0.18	6.86	0.03	0.03	0.00	100.55	33.0	65.9	1.1
SB-1.35	7.55	0.01	25.60	60.11	0.20	6.61	0.07	0.10	0.00	100.26	32.2	66.6	1.2
SB-1.36	7.62	0.01	25.58	60.91	0.20	6.66	0.04	0.07	0.01	101.11	32.2	66.7	1.2
SB-1.37	7.92	0.01	25.09	61.00	0.22	5.86	0.08	0.05	0.00	100.23	28.6	70.1	1.3
SB-1.40	7.94	0.00	25.02	61.49	0.28	5.78	0.10	0.09	0.01	100.72	28.2	70.1	1.6
SB-1.41	8.64	0.01	24.14	62.51	0.19	5.08	0.09	0.08	0.04	100.77	24.2	74.7	1.1
SB-1.56_4	7.62	0.02	25.07	60.44	0.20	6.53	0.05	0.06	0.01	100.01	31.8	67.1	1.1
SB-1.56_5	7.66	0.01	25.16	60.51	0.21	6.22	0.06	0.08	0.01	99.92	30.6	68.2	1.2
SB-1.56_6	7.56	0.00	25.11	60.55	0.22	6.20	0.05	0.13	0.02	99.85	30.8	67.9	1.3
SB-1.56_7	7.68	0.01	25.12	60.77	0.22	6.15	0.10	0.08	0.03	100.16	30.3	68.5	1.3
SB-1.56_8	8.03	0.02	24.44	61.07	0.24	5.50	0.16	0.08	0.03	99.56	27.1	71.6	1.4
SB-1.57_1	8.10	0.02	24.27	60.79	0.26	5.56	0.05	0.07	0.02	99.14	27.1	71.4	1.5
SB-1.57_2	7.91	0.00	24.61	61.09	0.26	5.88	0.02	0.08	0.05	99.91	28.7	69.8	1.5
SB-1.57_3	7.77	0.00	24.99	60.77	0.23	6.12	0.06	0.06	0.04	100.03	29.9	68.8	1.3
SB-1.57_4	7.72	0.01	25.22	60.90	0.20	5.93	0.03	0.06	0.01	100.08	29.5	69.3	1.2
SB-1.58_4	7.79	0.00	24.73	61.16	0.24	5.54	0.12	0.10	0.05	99.74	27.8	70.8	1.4
SB-1.58_5	7.98	0.01	24.77	61.31	0.25	5.44	0.11	0.07	0.03	99.98	27.0	71.5	1.5
SB-1.58_6	7.94	0.01	24.67	61.25	0.24	5.43	0.09	0.05	0.04	99.72	27.1	71.5	1.4
SB-1.58_7	7.95	0.01	24.45	61.26	0.26	5.54	0.11	0.13	0.06	99.76	27.4	71.1	1.5
SB-1.59_1	7.47	0.01	24.86	60.62	0.22	6.21	0.20	0.08	0.01	99.68	31.1	67.7	1.3
SB-1.59_2	7.22	0.00	25.73	60.10	0.20	6.69	0.14	0.10	0.00	100.18	33.5	65.3	1.2
SB-1.59_4	7.33	0.01	25.11	60.45	0.20	6.43	0.11	0.10	0.05	99.79	32.3	66.5	1.2
SB-1.59_5	7.42	0.02	25.02	60.91	0.21	6.29	0.08	0.08	0.01	100.03	31.5	67.2	1.2
SB-1.59_6	7.72	0.01	24.54	60.97	0.22	5.71	0.06	0.04	0.04	99.31	28.6	70.1	1.3

Label	Na_2O	MgO	Al_2O_3	SiO_2	K_2O	CaO	FeO	SrO	BaO	Total	An	Ab	Or
EMT-268.10_1	7.91	0.00	25.28	60.84	0.24	6.33	0.04	0.16	0.00	100.81	30.2	68.4	1.3
EMT-268.10_2	7.78	0.01	25.23	60.77	0.25	6.47	0.03	0.04	0.00	100.58	31.0	67.6	1.4
EMT-268.10_3	7.90	0.00	25.49	61.30	0.27	5.94	0.05	0.07	0.03	101.06	28.9	69.6	1.5
EMT-268.10_4	7.87	0.00	25.02	61.36	0.24	5.91	0.03	0.06	0.06	100.54	28.9	69.7	1.4
EMT-268.10_5	7.80	0.01	25.41	60.76	0.21	6.46	0.07	0.17	0.02	100.93	31.0	67.8	1.2
EMT-268.10_6	7.69	0.01	25.22	60.42	0.21	6.43	0.04	0.07	0.04	100.12	31.2	67.5	1.2
EMT-268.10_7	7.65	0.03	25.17	60.92	0.23	6.24	0.04	0.08	0.05	100.41	30.6	68.0	1.3
EMT-268.10_8	7.76	0.02	25.42	60.84	0.21	6.41	0.02	0.10	0.02	100.79	31.0	67.8	1.2
EMT-268.10_9	7.63	0.00	25.41	60.93	0.20	6.62	0.07	0.00	0.03	100.90	32.0	66.8	1.2
EMT-268.10_10	7.71	0.00	25.49	61.11	0.22	6.47	0.07	0.06	0.02	101.15	31.3	67.5	1.3
EMT-268.10_11	7.80	0.00	25.21	61.42	0.22	6.14	0.03	0.12	0.04	100.97	29.9	68.8	1.3
EMT-268.10_12	7.93	0.00	24.82	61.23	0.21	5.87	0.04	0.13	0.03	100.27	28.7	70.1	1.2
EMT-268.11_1	8.20	0.00	24.68	61.65	0.27	5.57	0.09	0.03	0.03	100.53	26.9	71.6	1.6
EMT-268.11_2	7.76	0.00	25.12	60.70	0.25	6.09	0.05	0.05	0.06	100.09	29.8	68.7	1.5
EMT-268.11_3	7.75	0.00	25.55	60.27	0.23	6.74	0.05	0.09	0.01	100.69	32.1	66.7	1.3
EMT-268.11_4	7.72	0.02	25.41	60.90	0.19	6.51	0.08	0.03	0.04	100.90	31.4	67.5	1.1
EMT-268.11_5	7.64	0.01	25.45	60.56	0.23	6.50	0.06	0.13	0.04	100.62	31.6	67.1	1.3
EMT-268.11_6	7.63	0.01	25.08	60.56	0.20	6.27	0.02	0.08	0.02	99.88	30.9	67.9	1.2
EMT-268.18_1	8.43	0.01	24.35	61.85	0.30	5.10	0.07	0.08	0.05	100.24	24.6	73.6	1.7
EMT-268.18_2	8.32	0.01	24.19	62.16	0.33	5.16	0.08	0.07	0.08	100.39	25.0	73.0	1.9
EMT-268.18_3	8.11	0.01	24.42	61.79	0.29	5.21	0.08	0.06	0.04	100.00	25.7	72.5	1.7
EMT-268.18_4	8.08	0.00	24.42	61.62	0.29	5.15	0.08	0.16	0.04	99.84	25.6	72.7	1.7
EMT-268.19_1	8.15	0.00	24.19	62.23	0.33	4.79	0.07	0.11	0.05	99.93	24.0	74.0	2.0
EMT-268.19_2	7.90	0.00	24.93	61.57	0.26	5.49	0.09	0.05	0.04	100.32	27.3	71.1	1.6
EMT-268.19_3	7.86	0.01	25.11	61.14	0.28	5.75	0.03	0.16	0.00	100.35	28.3	70.0	1.6
EMT-268.26_1	7.98	0.00	24.78	62.07	0.24	5.65	0.05	0.10	0.05	100.90	27.7	70.9	1.4
EMT-268.26_2	5.26	0.02	27.83	56.57	0.18	2.55	0.12	0.01	0.01	92.54	20.8	77.5	1.7
EMT-268.26_4	7.46	0.01	25.52	60.65	0.24	6.51	0.07	0.07	0.03	100.56	32.1	66.5	1.4
EMT-268.26_5	7.58	0.01	25.48	60.89	0.21	6.38	0.06	0.04	0.01	100.66	31.3	67.5	1.2
EMT-268.26_6	7.86	0.01	25.61	60.74	0.22	6.29	0.05	0.01	0.02	100.81	30.3	68.5	1.3
EMT-268.26_7	7.86	0.01	25.31	60.65	0.19	6.44	0.04	0.07	0.01	100.59	30.8	68.1	1.1
EMT-268.26_8	7.81	0.00	25.10	61.16	0.23	5.98	0.08	0.02	0.01	100.39	29.3	69.3	1.3
EMT-268.26_9	7.66	0.01	25.68	61.11	0.19	6.18	0.04	0.03	0.00	100.91	30.5	68.4	1.1
EMT-268.26_10	7.55	0.02	25.46	60.34	0.21	6.43	0.06	0.07	0.04	100.17	31.6	67.2	1.2
EMT-268.26_11	7.57	0.01	25.68	60.49	0.23	6.51	0.03	0.05	0.00	100.57	31.8	66.9	1.3
EMT-268.26_12	7.32	0.02	26.75	59.78	0.20	6.48	0.03	0.03	0.00	100.62	32.5	66.3	1.2
EMT-268.26_14	7.46	0.00	25.85	60.39	0.23	6.79	0.05	0.06	0.04	100.87	33.0	65.6	1.3
EMT-268.26_15	7.78	0.00	26.01	60.20	0.19	6.92	0.07	0.08	0.03	101.28	32.6	66.4	1.0
EMT-268.27_1	7.69	0.02	25.61	60.60	0.21	6.68	0.06	0.10	0.03	100.98	32.0	66.8	1.2
EMT-268.27_2	7.56	0.00	25.72	60.41	0.21	6.79	0.05	0.06	0.03	100.82	32.8	66.0	1.2
EMT-268.27_3	7.52	0.01	25.71	60.24	0.19	6.76	0.05	0.08	0.02	100.59	32.8	66.1	1.1
EMT-268.27_4	7.35	0.01	25.81	60.07	0.19	6.96	0.01	0.08	0.00	100.49	34.0	64.9	1.1
EMT-268.27_5	7.51	0.02	26.06	59.79	0.20	7.07	0.05	0.04	0.01	100.74	33.8	65.0	1.1
EMT-268.27_6	7.53	0.00	25.88	59.84	0.20	6.96	0.07	0.11	0.00	100.59	33.4	65.4	1.1
EMT-268.28_1	7.91	0.02	24.94	61.31	0.26	6.06	0.05	0.09	0.03	100.67	29.3	69.2	1.5
EMT-268.28_2	7.63	0.01	25.31	60.55	0.22	6.48	0.05	0.12	0.02	100.39	31.5	67.2	1.3
EMT-268.28_3	7.73	0.00	25.33	60.81	0.21	6.34	0.05	0.19	0.02	100.67	30.8	68.0	1.2
EMT-268.28_4	7.77	0.00	25.53	60.44	0.21	6.59	0.05	0.03	0.03	100.65	31.5	67.3	1.2
EMT-268.28_5	7.56	0.00	25.67	60.79	0.19	6.61	0.06	0.09	0.00	100.98	32.2	66.7	1.1
EMT-268.28_6	7.34	0.00	25.53	60.23	0.19	6.66	0.04	0.05	0.00	100.03	33.0	65.9	1.1
SB-2.10	8.23	0.00	24.47	61.64	0.29	5.27	0.05	0.06	0.00	100.01	25.7	72.6	1.7

Label	Na_2O	MgO	Al_2O_3	SiO_2	K_2O	CaO	FeO	SrO	BaO	Total	An	Ab	Or
SB-2.11	7.64	0.02	25.37	60.85	0.23	6.06	0.06	0.07	0.03	100.33	30.0	68.6	1.4
SB-2.12	7.72	0.02	25.38	60.94	0.27	5.62	0.06	0.10	0.04	100.15	28.2	70.1	1.6
SB-2.13	7.81	0.00	24.67	59.81	0.20	5.36	0.01	0.04	0.02	97.93	27.2	71.6	1.2
SB-2.14	7.40	0.01	24.52	59.25	0.21	5.52	0.04	0.09	0.01	97.05	28.8	69.9	1.3
SB-2.17	8.01	0.01	24.10	61.34	0.28	5.22	0.09	0.09	0.03	99.18	26.1	72.3	1.7
SB-2.20_1	7.66	0.01	24.66	60.55	0.23	6.08	0.02	0.10	0.01	99.31	30.1	68.5	1.4
SB-2.20_2	7.60	0.01	25.07	60.39	0.21	6.40	0.05	0.06	0.00	99.78	31.3	67.5	1.2
SB-2.20_3	7.62	0.01	25.06	60.79	0.23	6.33	0.01	0.09	0.03	100.16	31.0	67.6	1.3
SB-2.20_4	7.46	0.00	25.00	60.41	0.17	6.35	0.01	0.12	0.04	99.56	31.7	67.3	1.0
SB-2.20_5	7.40	0.00	25.23	60.57	0.21	6.41	0.05	0.12	0.00	99.99	32.0	66.8	1.3
SB-2.20_6	7.49	0.00	25.25	60.54	0.21	6.50	0.06	0.08	0.02	100.16	32.0	66.7	1.2
SB-2.21_1	7.94	0.01	24.67	61.26	0.30	5.85	0.09	0.10	0.03	100.24	28.4	69.8	1.7
SB-2.21_2	7.76	0.01	24.75	60.81	0.24	5.93	0.04	0.12	0.03	99.67	29.3	69.3	1.4
SB-2.21_3	7.70	0.00	24.77	61.15	0.26	6.06	0.03	0.10	0.01	100.09	29.9	68.6	1.5
SB-2.21_5	7.57	0.01	24.98	60.13	0.23	6.42	0.05	0.06	0.01	99.47	31.5	67.2	1.4
SB-2.21_6	7.65	0.00	25.26	60.56	0.22	6.28	0.05	0.04	0.00	100.06	30.8	67.9	1.3
SB-2.21_7	7.39	0.04	28.76	60.84	0.19	3.68	0.09	0.01	0.02	101.01	21.3	77.4	1.3
SB-2.21_8	7.54	0.02	25.11	60.34	0.20	6.30	0.04	0.08	0.03	99.66	31.2	67.6	1.2
SB-2.21_9	7.58	0.02	25.07	60.50	0.20	6.21	0.06	0.06	0.04	99.73	30.8	68.0	1.2
SB-2.21_10	7.38	0.00	25.60	59.82	0.21	6.95	0.04	0.09	0.03	100.13	33.8	65.0	1.2
SB-2.21_11	7.68	0.01	24.94	60.38	0.22	6.29	0.06	0.14	0.00	99.73	30.7	68.0	1.3
SB-2.21_12	7.81	0.00	24.68	60.91	0.24	6.06	0.05	0.07	0.05	99.87	29.6	69.0	1.4
SB-2.21_13	7.66	0.01	25.03	60.56	0.19	6.32	0.07	0.02	0.00	99.87	31.0	67.9	1.1
SB-2.21_14	7.60	0.00	25.42	60.26	0.23	6.69	0.04	0.02	0.00	100.26	32.3	66.4	1.3
SB-2.21_15	7.70	0.00	25.27	60.87	0.22	6.34	0.05	0.04	0.03	100.52	30.9	67.8	1.3
SB-2.27	7.59	0.01	25.09	60.67	0.20	6.22	0.05	0.10	0.02	99.95	30.8	68.0	1.2
SB-2.37_1	7.84	0.01	24.47	61.73	0.32	5.52	0.20	0.07	0.05	100.21	27.5	70.6	1.9
SB-2.37_2	7.81	0.02	24.25	61.14	0.25	5.52	0.12	0.11	0.05	99.27	27.7	70.8	1.5
SB-2.37_3	8.08	0.02	24.26	61.21	0.30	5.52	0.15	0.13	0.04	99.71	26.9	71.3	1.7
SB-2.37_4	8.30	0.00	23.80	61.84	0.30	4.77	0.11	0.08	0.06	99.26	23.7	74.5	1.8
SB-2.37_5	8.12	0.01	24.24	61.18	0.27	5.64	0.11	0.03	0.02	99.61	27.3	71.2	1.6
SB-2.39	7.79	0.02	24.28	61.64	0.23	5.37	0.09	0.14	0.04	99.59	27.2	71.4	1.4
SB-2.40	7.94	0.01	24.40	61.55	0.23	5.32	0.11	0.07	0.00	99.61	26.7	72.0	1.4
SB-2.41	7.79	0.02	24.92	61.79	0.23	5.33	0.17	0.08	0.08	100.41	27.1	71.5	1.4
SB-2a.2	8.28	0.24	23.03	62.44	1.00	3.00	1.35		0.19	99.52	15.6	78.2	6.2
SB-2a.3	8.36	0.23	23.15	62.73	0.97	3.03	1.22		0.20	99.89	15.7	78.3	6.0
SB-2a.6	3.88	0.01	18.70	65.74	10.30	0.30	0.08		0.17	99.18	1.5	35.9	62.6
SB-2a.7	8.14	0.00	23.71	62.07	0.40	4.93	0.29		0.05	99.59	24.5	73.1	2.4
SB-2a.9	6.45	0.00	20.56	64.52	5.38	1.87	0.02		0.14	98.94	9.4	58.5	32.1
SB-2a.10	3.33	0.02	17.81	67.37	10.46	0.22	0.02		0.24	99.47	1.2	32.2	66.6
SB-2a.11	7.98	0.02	24.72	61.04	0.36	5.68	0.09		0.04	99.94	27.6	70.3	2.1
SB-2a.12	6.01	0.00	14.26	76.62	1.50	1.24	0.12		0.09	99.85	8.9	78.2	12.9
SB-2a.13	7.37	0.02	17.47	71.51	1.16	1.72	0.13		0.06	99.44	10.5	81.2	8.4
SB-2a.16	7.80	0.31	24.17	60.65	0.39	5.28	0.52		0.06	99.18	26.6	71.1	2.3
SB-2a.18	3.49	0.03	16.95	68.37	9.62	0.07	0.07		0.00	98.60	0.4	35.4	64.2
SB-2a.21	2.56	0.03	14.71	73.52	8.30	0.20	0.01		0.51	99.85	1.4	31.5	67.1
SB-2a.22	4.53	0.01	19.88	64.80	9.07	0.98	0.03		0.22	99.51	4.9	41.0	54.1
SB-2a.23	8.36	0.02	24.34	61.90	0.39	5.11	0.12		0.05	100.29	24.7	73.1	2.2
SB-2a.24	3.08	0.00	17.47	67.84	10.66	0.09	0.08		0.21	99.43	0.5	30.4	69.1
SB-2a.25	4.71	0.02	19.08	65.79	9.08	0.20	0.13		0.45	99.48	1.0	43.6	55.3
SB-2a.26	7.72	0.01	19.64	67.25	1.17	2.84	0.04		0.08	98.76	15.6	76.7	7.7

Label	Na_2O	MgO	Al_2O_3	SiO_2	K_2O	CaO	FeO	SrO	BaO	Total	An	Ab	Or
SB-2a.27	8.47	0.00	23.66	62.05	0.49	4.81	0.02		0.03	99.55	23.2	74.0	2.8
SB-2a.28	8.30	0.00	23.85	62.37	0.43	4.82	0.02		0.03	99.81	23.7	73.8	2.5
SB-2a.29	7.93	0.06	22.87	62.45	1.48	4.00	0.09		0.10	98.97	19.9	71.4	8.8
SB-2a.30	7.83	0.02	21.33	64.96	2.99	2.44	0.08		0.14	99.79	12.1	70.2	17.7

Biotites

Label	SiO_2	TiO_2	Al_2O_3	FeO	MnO	MgO	CaO	Na_2O	K_2O	F	Cl	H_2O(c)	Total
GRD-1 30um	33.77	2.57	16.74	26.04	0.21	6.27	0.03	0.58	7.82	1.47	0.10	3.04	98.67
GRD-1	34.11	2.90	17.09	24.83	0.12	7.10	0.01	0.55	8.14	0.23	0.09	3.69	98.88
GRD-1 Core	34.46	2.76	16.90	25.40	0.08	7.24	0.00	0.65	8.27	0.34	0.11	3.66	99.86
GRD-1 Rim	34.08	2.70	16.91	24.47	0.12	6.97	0.00	0.63	8.28	1.08	0.12	3.24	98.62
SB-1.3_1	35.87	2.66	19.95	23.18	0.12	6.95	0.06	0.52	7.43	0.95	0.11	3.50	100.88
SB-1.3_2	36.16	2.53	18.82	23.06	0.11	6.99	0.06	0.59	7.40	0.91	0.11	3.48	99.80
SB-1.3_3	34.47	3.01	17.30	24.89	0.11	7.27	0.07	0.59	8.17	1.05	0.12	3.33	99.91
SB-1.3_4	33.95	2.64	18.32	24.40	0.11	7.14	0.10	0.50	7.93	0.98	0.11	3.35	99.09
SB-1.4	39.18	1.63	26.86	15.41	0.11	4.36	0.05	0.32	4.80	0.68	0.07	3.78	96.96
SB-1.5_1	34.60	2.94	17.94	25.75	0.13	6.56	0.04	0.74	8.03	1.59	0.11	3.11	100.84
SB-1.5_2	34.92	2.75	17.80	25.28	0.05	7.27	0.04	0.70	8.00	1.38	0.12	3.22	100.93
SB-1.5_3	34.79	2.76	17.79	25.22	0.06	7.36	0.04	0.72	7.84	1.72	0.11	3.05	100.71
SB-1.5_4	34.72	2.88	17.66	25.27	0.13	7.20	0.01	0.65	8.16	1.40	0.11	3.20	100.76
SB-1.5_5	34.19	2.91	17.79	25.53	0.07	6.87	0.02	0.69	8.08	1.57	0.12	3.08	100.24
SB-1.5_6	34.08	2.87	17.47	28.43	0.23	4.95	0.04	0.48	8.13	1.50	0.12	3.09	100.72
SB-1.5_7	34.20	2.86	17.43	27.82	0.27	5.09	0.03	0.61	8.19	1.81	0.14	2.93	100.58
SB-1.6_1	34.16	2.97	17.48	27.29	0.19	5.71	0.03	0.61	8.05	1.68	0.09	3.02	100.56
SB-1.6_2	34.52	2.97	17.72	25.83	0.12	7.00	0.03	0.72	8.07	1.44	0.11	3.18	101.08
SB-1.6_3	34.40	3.04	17.48	26.26	0.18	6.51	0.04	0.67	7.87	1.31	0.11	3.21	100.52
SB-1.6_4	33.88	2.98	17.61	27.57	0.19	5.64	0.04	0.56	8.10	1.37	0.11	3.16	100.60
SB-1.7_1	33.83	2.71	18.44	27.22	0.20	4.79	0.02	0.49	7.72	1.46	0.08	3.10	99.44
SB-1.7_2	34.11	3.10	17.78	25.49	0.12	7.00	0.02	0.64	8.07	1.19	0.13	3.27	100.38
SB-1.7_3	34.54	3.05	17.49	25.36	0.17	7.11	0.03	0.65	8.03	1.36	0.12	3.20	100.51
SB-1.7_4	34.82	3.14	17.21	24.87	0.12	7.05	0.04	0.54	7.98	0.73	0.12	3.49	99.77
SB-1.7_5	36.85	4.28	17.50	21.56	0.07	6.53	0.08	0.33	6.79	0.51	0.09	3.65	98.00
SB-1.7_6	35.35	3.08	17.18	24.75	0.06	7.25	0.04	0.56	7.85	0.65	0.11	3.56	100.14
SB-1.7_7	34.99	3.04	17.52	24.94	0.14	7.22	0.04	0.71	8.07	1.23	0.12	3.29	100.75
SB-1.7_8	34.89	3.06	17.85	24.75	0.08	7.02	0.02	0.60	7.87	0.96	0.10	3.41	100.17
SB-1.7_9	34.82	3.16	17.56	25.10	0.12	7.25	0.02	0.63	8.02	1.33	0.13	3.24	100.78
SB-1.7_10	34.54	2.92	17.82	26.92	0.29	5.88	0.01	0.65	7.88	1.82	0.17	2.97	101.08
SB-1.8_1	34.70	2.89	18.15	25.04	0.15	7.05	0.01	0.63	8.09	1.38	0.11	3.22	100.81
SB-1.8_2	34.31	3.00	17.90	25.43	0.18	7.32	0.03	0.62	7.99	1.07	0.12	3.35	100.84
SB-1.8_3	34.59	3.11	18.24	25.12	0.12	7.06	0.03	0.57	7.76	0.93	0.12	3.44	100.66
SB-1.8_4	35.11	3.00	17.63	25.05	0.12	7.36	0.03	0.54	7.77	1.36	0.12	3.23	100.72
SB-1.8_5	35.02	2.89	17.50	25.13	0.15	6.96	0.02	0.67	8.00	1.49	0.12	3.15	100.44
SB-1.9	33.78	2.87	17.42	26.86	0.19	6.08	0.05	0.65	7.97	1.32	0.10	3.17	99.88
SB-1.10	34.09	2.97	17.77	26.77	0.25	6.02	0.05	0.66	7.81	1.57	0.09	3.08	100.45
SB-1.11	33.74	3.02	17.29	26.59	0.16	6.18	0.04	0.61	8.04	1.48	0.13	3.08	99.71
SB-1.12	34.19	3.05	17.48	25.40	0.12	6.98	0.04	0.64	7.96	1.36	0.11	3.18	99.91
SB-1.13	34.26	3.01	17.54	26.18	0.17	6.57	0.03	0.68	7.71	1.47	0.12	3.13	100.22
SB-1.14	34.51	2.95	17.77	25.39	0.16	7.11	0.02	0.72	8.00	1.25	0.11	3.27	100.71
SB-1.15	35.09	2.63	18.29	25.56	0.24	5.95	0.01	0.66	7.92	1.75	0.10	3.03	100.48
SB-1.16_1	34.98	3.06	17.38	24.95	0.14	7.37	0.02	0.62	8.17	1.09	0.10	3.36	100.76
SB-1.16_2	34.67	3.16	17.65	25.22	0.07	7.09	0.01	0.62	8.13	0.95	0.13	3.41	100.68

Label	SiO_2	TiO_2	Al_2O_3	FeO	MnO	MgO	CaO	Na_2O	K_2O	F	Cl	H_2O(c)	Total
SB-1.16_3	36.15	2.67	20.43	22.63	0.13	6.21	0.01	0.51	7.01	1.45	0.10	3.26	99.94
SB-1.16_4	35.39	3.03	17.64	24.97	0.15	7.02	0.03	0.58	8.02	1.24	0.12	3.30	100.93
SB-1.16_5	34.39	3.02	17.22	25.72	0.11	6.92	0.03	0.69	8.23	1.51	0.13	3.12	100.41
SB-1.16_6	34.65	3.05	17.79	25.71	0.10	6.92	0.02	0.68	8.17	1.29	0.12	3.26	101.20
SB-1.16_7	34.68	3.04	17.57	25.89	0.14	7.10	0.03	0.72	8.33	1.25	0.13	3.28	101.59
SB-1.16_8	34.44	2.95	17.73	26.42	0.18	6.66	0.02	0.66	8.08	1.44	0.12	3.18	101.24
SB-1.17_1	33.51	2.96	18.04	26.38	0.20	6.29	0.03	0.71	8.04	1.70	0.13	3.00	100.25
SB-1.17_2	34.81	3.09	17.78	25.32	0.08	7.20	0.03	0.64	8.12	0.88	0.12	3.46	101.13
SB-1.17_3	39.00	2.27	24.22	16.69	0.02	5.55	0.06	0.12	6.05	0.60	0.08	3.80	98.20
SB-1.17_8	36.85	2.48	21.00	21.00	0.14	5.73	0.05	0.52	6.52	0.78	0.12	3.57	98.40
SB-1.17_9	35.25	2.86	19.11	23.49	0.14	6.12	0.04	0.51	7.72	1.15	0.12	3.32	99.33
SB-1.17_10	34.57	5.58	20.66	20.51	0.18	5.51	0.03	0.48	6.75	1.07	0.10	3.40	98.37
SB-1.17_11	34.57	3.16	18.84	24.22	0.11	6.48	0.03	0.59	7.82	1.65	0.14	3.08	99.95
SB-1.17_12	33.37	2.72	17.87	26.13	0.17	6.08	0.03	0.72	8.04	1.99	0.10	2.83	99.19
SB-1.18_1	33.84	2.82	17.58	26.42	0.22	5.77	0.05	0.63	8.00	1.66	0.10	2.99	99.36
SB-1.18_2	33.12	5.64	17.69	23.50	0.12	6.40	0.07	0.57	7.27	1.19	0.11	3.24	98.38
SB-1.18_4	36.20	2.78	18.38	22.10	0.14	6.23	0.06	0.42	7.66	0.67	0.14	3.52	98.01
SB-1.18_5	35.11	2.83	17.30	24.12	0.12	6.94	0.06	0.54	7.85	0.99	0.09	3.36	98.87
SB-1.18_7	34.58	3.00	17.49	23.33	0.10	6.95	0.10	0.34	6.83	0.53	0.12	3.51	96.61
SB-1.18_8	35.29	2.73	17.75	23.22	0.06	6.82	0.05	0.51	7.68	0.81	0.09	3.44	98.08
SB-1.18_9	34.77	2.70	17.68	23.91	0.12	7.13	0.03	0.58	7.78	1.03	0.12	3.33	98.70
SB-1.18_10	34.76	2.89	17.79	25.34	0.16	6.57	0.03	0.64	7.87	1.31	0.11	3.22	100.12
SB-1.19_1	34.30	2.84	18.33	25.71	0.26	5.24	0.02	0.55	7.78	1.44	0.09	3.12	99.05
SB-1.19_17	34.60	2.99	17.76	23.70	0.10	7.10	0.03	0.47	7.85	0.76	0.11	3.46	98.56
SB-1.19_18	34.80	2.74	19.18	23.55	0.15	5.87	0.03	0.48	7.38	0.99	0.09	3.36	98.18
SB-1.20_1	33.42	2.97	17.44	26.42	0.23	5.89	0.07	0.53	7.72	1.23	0.12	3.17	98.64
SB-1.20_2	33.40	3.11	17.43	24.83	0.09	6.93	0.05	0.63	7.73	1.22	0.11	3.19	98.18
SB-1.20_10	34.07	3.05	17.55	24.84	0.13	6.92	0.05	0.60	7.75	0.63	0.12	3.50	98.91
SB-1.20_11	33.49	2.95	17.44	25.44	0.12	6.64	0.05	0.65	7.82	1.01	0.12	3.29	98.56
SB-1.20_12	33.39	2.90	17.09	27.05	0.16	5.51	0.04	0.55	7.84	1.11	0.11	3.20	98.46
EMT-268.1_1	34.10	2.83	17.45	27.68	0.20	5.41	0.03	0.58	8.29	1.48	0.12	3.10	100.62
EMT-268.1_2	34.86	2.53	17.49	25.82	0.14	7.06	0.05	0.67	7.91	1.28	0.10	3.25	100.60
EMT-268.1_3	36.21	2.35	18.06	22.50	0.10	7.49	0.08	0.32	7.83	0.72	0.11	3.54	98.97
EMT-268.1_7	35.10	3.08	17.42	25.11	0.06	7.55	0.04	0.62	8.06	0.54	0.11	3.63	101.08
EMT-268.1_8	35.21	2.89	17.34	25.19	0.12	7.35	0.04	0.67	8.10	1.04	0.10	3.39	100.97
EMT-268.1_9	34.74	2.93	17.53	25.37	0.15	7.34	0.03	0.70	8.17	1.25	0.12	3.28	101.07
EMT-268.1_10	34.57	2.60	17.17	27.06	0.24	6.19	0.02	0.71	8.30	1.91	0.09	2.93	100.95
EMT-268.2	34.69	2.62	17.56	25.98	0.17	6.75	0.03	0.79	8.31	2.14	0.11	2.84	101.05
EMT-268.3_1	33.99	3.01	17.44	27.07	0.23	5.78	0.03	0.68	8.32	1.85	0.13	2.93	100.65
EMT-268.3_2	33.67	2.86	18.80	25.12	0.17	7.01	0.03	0.40	8.28	2.29	0.14	2.76	100.52
EMT-268.3_3	34.91	3.02	17.26	24.98	0.15	7.38	0.02	0.64	8.15	0.91	0.10	3.43	100.56
EMT-268.3_5	37.46	2.86	16.67	22.12	0.09	7.53	0.13	0.20	7.63	0.21	0.08	3.79	98.66
EMT-268.3_6	34.20	3.05	17.44	24.25	0.10	7.14	0.08	0.45	7.76	0.37	0.11	3.62	98.41
EMT-268.3_14	34.61	2.93	17.16	23.89	0.13	7.47	0.12	0.40	7.45	0.41	0.09	3.61	98.10
EMT-268.3_15	34.78	2.94	17.47	25.23	0.17	7.21	0.03	0.73	8.06	1.40	0.12	3.20	100.71
EMT-268.4_1	34.26	3.03	16.97	26.74	0.19	6.14	0.02	0.64	8.19	1.56	0.13	3.06	100.24
EMT-268.4_2	34.54	3.15	17.05	25.38	0.12	7.07	0.03	0.66	8.18	1.07	0.13	3.32	100.23
EMT-268.4_3	34.63	3.14	17.32	25.52	0.16	7.14	0.02	0.65	8.34	0.59	0.12	3.58	100.94
EMT-268.4_4	34.45	3.19	17.28	25.19	0.13	7.14	0.03	0.63	8.23	0.53	0.13	3.58	100.27
EMT-268.4_5	34.63	3.18	17.28	25.05	0.09	7.09	0.01	0.70	8.21	0.36	0.12	3.68	100.23
EMT-268.4_6	34.36	3.20	17.19	25.17	0.07	7.25	0.03	0.72	8.19	0.32	0.13	3.68	100.15

Label	SiO_2	TiO_2	Al_2O_3	FeO	MnO	MgO	CaO	Na_2O	K_2O	F	Cl	H_2O(c)	Total
EMT-268.4_7	34.68	3.15	17.33	25.50	0.07	7.22	0.02	0.71	8.02	0.55	0.13	3.60	100.74
EMT-268.4_8	34.70	3.11	17.49	25.56	0.12	7.32	0.04	0.65	8.18	0.88	0.13	3.45	101.24
EMT-268.4_9	34.28	2.99	17.45	25.57	0.15	7.00	0.01	0.68	8.30	0.98	0.12	3.37	100.47
EMT-268.4_10	34.39	2.96	17.20	27.54	0.24	5.74	0.03	0.63	8.38	1.83	0.13	2.96	101.22
EMT-268.5_1	33.50	2.97	17.24	27.73	0.21	5.48	0.03	0.58	8.52	1.39	0.12	3.11	100.27
EMT-268.5_2	34.19	3.05	17.30	25.58	0.12	6.83	0.03	0.64	8.21	1.37	0.12	3.17	100.02
EMT-268.5_3	34.21	3.08	17.30	25.35	0.13	7.11	0.02	0.70	8.10	1.10	0.12	3.30	100.03
EMT-268.5_4	34.43	3.10	17.52	25.75	0.14	7.19	0.01	0.73	8.24	1.08	0.13	3.35	101.18
EMT-268.5_5	34.71	3.05	17.19	25.20	0.09	7.21	0.02	0.70	8.13	0.89	0.11	3.43	100.33
EMT-268.5_6	34.40	3.11	17.38	25.47	0.11	7.06	0.02	0.71	8.25	1.06	0.11	3.34	100.54
EMT-268.5_7	34.84	3.03	17.23	25.20	0.11	7.17	0.01	0.77	8.22	1.12	0.12	3.32	100.64
EMT-268.5_8	34.82	2.98	17.08	26.91	0.18	6.23	0.02	0.72	8.27	1.68	0.10	3.06	101.32
EMT-268.7	34.82	2.93	17.41	25.20	0.15	7.06	0.03	0.55	8.34	0.40	0.12	3.66	100.47
EMT-268.8	34.42	2.89	17.93	25.48	0.15	6.71	0.02	0.57	8.31	1.21	0.11	3.28	100.55
EMT-268.9	34.27	2.84	17.33	25.06	0.15	6.37	0.04	0.74	8.17	1.88	0.11	2.89	99.03
EMT-268.10	34.60	2.90	17.10	25.34	0.19	6.66	0.02	0.79	8.28	1.78	0.11	2.98	99.96
EMT-268.11	34.54	2.93	17.39	25.87	0.21	6.30	0.01	0.57	8.23	1.62	0.11	3.05	100.13
EMT-268.12	34.41	2.91	17.11	26.07	0.21	6.01	0.03	0.65	8.16	1.34	0.15	3.15	99.59
EMT-268.13	34.96	2.89	17.30	24.55	0.09	7.43	0.03	0.75	7.97	1.16	0.14	3.29	100.04
EMT-268.14	35.12	2.87	16.75	24.38	0.07	7.72	0.03	0.68	7.90	1.09	0.11	3.32	99.56
EMT-268.15	34.23	2.89	17.17	26.24	0.15	6.19	0.03	0.63	8.02	1.45	0.11	3.10	99.59
EMT-268.16	33.96	2.84	17.10	25.98	0.14	6.21	0.02	0.70	8.21	1.65	0.13	2.99	99.20
EMT-268.17	34.53	2.96	17.20	25.46	0.15	6.78	0.01	0.74	8.28	1.39	0.12	3.17	100.16
EMT-268.18	35.06	2.96	17.14	24.84	0.18	7.09	0.04	0.72	8.14	1.44	0.12	3.17	100.25
EMT-268.19	34.91	2.86	17.61	24.91	0.20	7.15	0.00	0.79	8.01	1.86	0.13	2.98	100.60
EMT-268.20	35.59	3.00	16.70	24.66	0.10	7.44	0.03	0.80	8.21	1.14	0.14	3.33	100.63
EMT-268.21	34.90	3.04	17.19	24.87	0.16	7.31	0.03	0.84	8.19	1.85	0.13	2.98	100.67
EMT-268.22	34.56	2.89	17.25	25.21	0.13	6.88	0.02	0.81	8.19	2.06	0.13	2.84	100.08
EMT-268.23	34.54	2.81	17.29	25.55	0.16	6.39	0.02	0.76	8.02	1.94	0.14	2.88	99.67
EMT-268.24_1	34.43	2.93	17.32	25.40	0.12	6.35	0.02	0.79	8.18	1.83	0.12	2.94	99.63
EMT-268.24_2	34.88	2.94	17.23	25.00	0.14	6.87	0.03	0.77	8.08	1.52	0.12	3.11	100.04
EMT-268.24_3	34.57	2.95	17.07	24.67	0.08	7.06	0.03	0.68	8.13	1.30	0.13	3.19	99.29
EMT-268.24_4	34.68	2.83	17.15	25.08	0.13	7.06	0.02	0.66	8.11	1.19	0.12	3.26	99.77
EMT-268.24_5	34.48	2.79	16.99	25.21	0.13	6.54	0.03	0.61	8.16	1.56	0.13	3.04	98.98
EMT-268.24_6	34.50	2.93	16.75	26.88	0.26	5.77	0.03	0.65	8.21	1.61	0.14	3.02	100.04
EMT-268.25_1	34.08	2.79	17.33	25.82	0.17	6.55	0.09	0.73	7.73	1.61	0.13	3.02	99.34
EMT-268.25_2	34.50	2.63	17.43	25.01	0.12	7.14	0.12	0.56	7.43	1.04	0.13	3.31	98.96
EMT-268.25_3	35.12	2.73	17.81	24.98	0.11	7.12	0.16	0.50	7.41	0.51	0.12	3.62	99.96
EMT-268.25_4	34.64	2.84	17.45	25.19	0.12	6.98	0.06	0.71	7.88	0.60	0.14	3.54	99.86
EMT-268.25_5	34.44	2.90	17.66	25.75	0.10	6.90	0.09	0.64	7.57	0.26	0.12	3.72	100.01
EMT-268.25_6	36.08	2.77	17.99	23.07	0.06	7.29	0.11	0.26	7.71	0.44	0.10	3.68	99.36
EMT-268.25_7	34.84	2.91	17.76	23.81	0.10	7.21	0.12	0.35	7.62	0.17	0.13	3.75	98.66
EMT-268.25_8	34.94	2.87	17.48	24.75	0.09	7.23	0.10	0.53	7.65	0.35	0.11	3.68	99.61
SB-2.1_1	33.32	2.90	17.65	27.26	0.17	5.53	0.02	0.58	8.20	1.95	0.11	2.84	99.70
SB-2.1_2	34.31	2.91	17.40	25.74	0.14	6.50	0.02	0.71	8.05	2.16	0.11	2.79	99.90
SB-2.1_3	34.24	2.87	17.30	25.30	0.09	7.07	0.02	0.74	8.25	1.71	0.12	3.01	99.97
SB-2.1_4	34.24	2.79	18.06	25.28	0.17	7.02	0.01	0.73	8.23	1.53	0.11	3.12	100.64
SB-2.1_5	34.20	2.81	17.64	25.82	0.19	6.86	0.03	0.71	8.27	1.72	0.11	3.02	100.62
SB-2.1_6	34.62	2.85	17.46	25.42	0.12	6.89	0.02	0.71	8.28	2.06	0.12	2.86	100.53
SB-2.1_7	34.58	2.94	17.45	25.54	0.16	6.76	0.01	0.75	8.13	2.02	0.11	2.88	100.45
SB-2.1_8	34.74	2.95	17.36	25.20	0.11	6.87	0.03	0.73	8.17	1.91	0.11	2.94	100.30

Label	SiO_2	TiO_2	Al_2O_3	FeO	MnO	MgO	CaO	Na_2O	K_2O	F	Cl	H_2O(c)	Total
SB-2.1_9	34.23	2.92	17.27	25.69	0.14	6.33	0.01	0.77	8.02	2.20	0.12	2.75	99.50
SB-2.1_10	33.96	2.82	17.22	28.28	0.20	4.93	0.03	0.55	8.15	2.09	0.11	2.79	100.22
SB-2.2_1	34.10	2.86	17.20	27.07	0.17	5.64	0.03	0.64	8.02	1.75	0.10	2.96	99.79
SB-2.2_2	34.49	2.88	17.36	25.61	0.14	6.47	0.03	0.72	8.14	1.93	0.11	2.90	99.95
SB-2.2_3	33.98	2.95	17.63	25.71	0.12	6.67	0.03	0.69	8.15	1.68	0.10	3.02	100.00
SB-2.2_4	34.28	2.93	17.39	25.69	0.13	6.54	0.01	0.73	7.97	1.66	0.12	3.02	99.75
SB-2.2_5	34.40	2.99	17.64	26.01	0.14	6.52	0.02	0.69	8.07	1.55	0.11	3.10	100.58
SB-2.2_6	34.17	2.93	17.37	25.95	0.17	6.43	0.02	0.75	8.16	1.66	0.12	3.02	100.01
SB-2.2_7	34.02	2.95	17.46	26.10	0.19	6.35	0.03	0.73	8.19	1.68	0.13	3.01	100.09
SB-2.2_8	34.24	2.86	17.24	26.53	0.19	6.29	0.02	0.75	8.14	1.44	0.12	3.13	100.31
SB-2.2_9	33.92	2.90	17.68	26.18	0.14	6.14	0.04	0.76	7.98	1.31	0.11	3.18	99.77
SB-2.2_10	33.99	2.84	17.91	26.05	0.15	6.15	0.03	0.77	7.98	2.10	0.13	2.81	99.99
SB-2.2_11	33.98	2.86	17.50	26.66	0.19	6.00	0.01	0.79	8.21	2.21	0.12	2.75	100.33
SB-2.2_12	33.63	2.39	17.41	28.47	0.23	4.55	0.02	0.57	8.32	2.04	0.10	2.78	99.63
SB-2.3_4	33.24	2.46	17.55	27.26	0.16	5.79	0.02	0.51	7.67	2.06	0.10	2.76	98.69
SB-2.4_1	33.90	2.91	17.55	26.60	0.13	5.83	0.04	0.69	8.03	1.56	0.12	3.05	99.72
SB-2.4_2	34.31	2.89	17.46	25.34	0.10	7.19	0.05	0.62	7.68	1.05	0.12	3.32	99.67
SB-2.4_3	34.41	2.87	17.25	25.40	0.07	7.31	0.07	0.65	7.35	0.71	0.11	3.48	99.37
SB-2.4_4	34.20	2.84	17.41	24.84	0.14	7.59	0.12	0.57	6.88	0.73	0.11	3.46	98.58
SB-2.4_5	33.89	2.89	17.64	25.25	0.13	7.40	0.09	0.54	7.28	0.72	0.12	3.47	99.08
SB-2.4_6	34.31	2.78	17.37	24.88	0.09	7.58	0.14	0.58	6.99	0.36	0.11	3.64	98.65
SB-2.4_7	34.30	2.82	17.29	25.31	0.05	7.53	0.13	0.51	6.91	0.54	0.12	3.55	98.80
SB-2.4_8	33.90	2.92	17.40	25.40	0.11	7.20	0.10	0.60	7.42	0.66	0.12	3.48	99.01
SB-2.4_9	34.53	2.94	17.39	25.45	0.13	6.95	0.06	0.70	7.69	1.20	0.11	3.27	99.88
SB-2.4_10	33.95	2.88	17.30	26.98	0.18	5.76	0.05	0.64	7.88	1.73	0.11	2.97	99.67
SB-2.5_1	33.91	2.70	17.83	27.55	0.24	5.01	0.13	0.61	7.22	1.60	0.15	3.00	99.22
SB-2.5_2	34.46	2.82	17.44	26.54	0.16	5.93	0.03	0.71	8.01	1.82	0.10	2.95	100.20
SB-2.5_3	34.11	2.60	17.13	26.06	0.14	6.11	0.05	0.72	7.95	1.66	0.12	2.98	98.89
SB-2.5_4	34.25	2.78	17.52	26.24	0.17	6.16	0.04	0.71	7.97	1.63	0.12	3.03	99.89
SB-2.5_5	33.95	2.82	17.29	26.75	0.14	5.79	0.04	0.70	8.03	1.97	0.12	2.84	99.59
SB-2.5_6	34.13	2.71	16.41	29.30	0.17	4.00	0.04	0.54	8.13	1.55	0.12	2.99	99.41
SB-2.6_1	33.61	2.70	17.47	26.41	0.15	6.07	0.08	0.67	7.60	1.54	0.12	3.03	98.78
SB-2.6_3	33.75	2.80	17.26	26.46	0.16	6.18	0.06	0.71	8.02	1.50	0.12	3.06	99.43
SB-2.6_4	34.09	2.88	17.55	26.00	0.17	6.35	0.04	0.71	8.00	1.26	0.12	3.21	99.83
SB-2.6_5	32.94	2.81	17.18	26.78	0.17	5.59	0.05	0.61	7.89	1.74	0.18	2.86	98.02
SB-2.6_6	33.66	2.84	17.15	26.28	0.20	5.93	0.04	0.73	8.04	1.77	0.12	2.91	98.91
SB-2.6_7	33.56	2.81	17.39	26.55	0.16	5.87	0.07	0.66	7.85	1.64	0.12	2.98	98.95
SB-2.7_1	33.89	2.90	16.76	26.82	0.19	5.77	0.03	0.60	7.89	1.59	0.12	2.99	98.85
SB-2.7_2	33.95	2.92	17.03	25.57	0.10	6.47	0.04	0.69	7.84	1.44	0.14	3.08	98.63
SB-2.7_3	34.52	2.91	17.13	25.01	0.13	6.84	0.03	0.70	7.83	1.55	0.13	3.06	99.16
SB-2.7_4	34.37	2.88	17.05	25.30	0.10	7.05	0.02	0.68	7.83	1.27	0.12	3.20	99.31
SB-2.7_5	34.58	2.85	17.58	24.84	0.09	6.98	0.05	0.63	7.62	1.10	0.12	3.30	99.27
SB-2.7_6	34.80	2.87	17.31	24.63	0.11	6.98	0.05	0.65	7.50	0.88	0.12	3.40	98.91
SB-2.7_7	34.12	2.89	17.44	24.91	0.09	7.01	0.09	0.66	7.35	0.73	0.13	3.44	98.51
SB-2.7_8	34.29	2.99	17.24	25.21	0.09	6.99	0.07	0.65	7.75	0.97	0.11	3.35	99.28
SB-2.7_9	34.21	2.97	17.42	25.41	0.12	6.97	0.04	0.67	7.89	1.15	0.11	3.27	99.72
SB-2.7_10	33.93	2.63	17.24	26.26	0.21	5.99	0.06	0.65	7.90	1.45	0.12	3.07	98.87
SB-2.8_1	33.41	2.64	16.95	26.42	0.14	5.94	0.07	0.65	7.91	1.53	0.11	2.99	98.10
SB-2.8_2	33.86	2.80	17.12	25.61	0.12	6.60	0.03	0.70	7.83	1.70	0.10	2.96	98.69
SB-2.8_3	33.98	2.81	17.37	25.35	0.04	7.00	0.06	0.72	7.84	1.30	0.10	3.18	99.18
SB-2.8_4	34.23	2.88	17.18	25.13	0.14	7.07	0.03	0.76	8.03	1.30	0.12	3.19	99.47

Label	SiO_2	TiO_2	Al_2O_3	FeO	MnO	MgO	CaO	Na_2O	K_2O	F	Cl	H_2O(c)	Total
SB-2.8_5	34.04	2.88	17.20	25.68	0.16	6.51	0.03	0.73	8.03	1.47	0.12	3.09	99.31
SB-2.8_6	33.73	2.55	17.24	26.91	0.14	5.82	0.06	0.57	8.36	1.83	0.12	2.89	99.42
SB-2.9_1	34.00	2.83	17.21	27.38	0.18	5.55	0.03	0.64	8.21	1.72	0.13	2.96	100.09
SB-2.9_2	34.60	2.86	17.37	25.27	0.15	6.87	0.01	0.79	8.14	1.59	0.11	3.08	100.13
SB-2.9_3	34.40	2.77	17.71	25.20	0.13	6.83	0.01	0.74	8.17	1.50	0.12	3.12	100.03
SB-2.9_4	34.19	2.82	17.25	25.47	0.21	6.84	0.02	0.73	8.35	1.95	0.15	2.87	100.00
SB-2.9_5	34.61	2.92	17.55	25.06	0.11	6.90	0.04	0.78	7.97	1.53	0.11	3.11	100.03
SB-2.9_6	34.39	2.92	17.40	24.65	0.16	7.06	0.01	0.76	8.02	1.55	0.12	3.08	99.44
SB-2.9_7	34.25	2.84	16.99	25.14	0.20	6.75	0.01	0.74	8.12	1.90	0.13	2.88	99.12

Garnets

Label	SiO_2	TiO_2	Al_2O_3	Cr_2O_3	Fe_2O_3	FeO	MnO	MgO	CaO	Total	Pyr	Alm	Sps	Grs
GRD-1 #1.1	36.78	0.22	20.85		0.10	33.73	2.34	3.00	2.79	99.80	11.9	75.1	5.3	7.0
GRD-1 #1.2	37.27	0.25	21.05		0.00	33.40	2.32	3.07	3.01	100.36	12.2	74.3	5.2	7.8
GRD-1 #1.3	37.52	0.22	21.06		0.07	33.43	2.36	3.05	2.89	100.60	12.1	74.6	5.3	7.4
GRD-1 #1.4	37.42	0.19	21.22		0.00	33.76	2.33	2.97	2.75	100.64	11.8	75.3	5.3	7.3
GRD-1 #1.5	37.45	0.20	21.25		0.00	33.58	2.23	2.98	2.71	100.40	11.9	75.4	5.1	7.2
GRD-1 #1.6	37.45	0.18	21.21		0.00	34.18	2.24	2.80	2.69	100.74	11.2	76.3	5.1	7.2
GRD-1 #1.7	37.49	0.20	21.31		0.00	34.01	2.33	2.83	2.61	100.77	11.3	76.2	5.3	6.9
GRD-1 #1.8	37.66	0.20	21.26		0.00	34.05	2.25	2.86	2.63	100.91	11.4	76.2	5.1	7.0
GRD-1 #1.9	37.63	0.23	21.91		0.00	34.66	2.32	2.85	2.38	101.99	11.3	77.0	5.2	6.1
GRD-1 #1.10	38.58	0.20	21.91		0.00	34.45	2.45	2.92	2.21	102.71	11.6	76.8	5.5	5.7
GRD-1 #2.1	37.10	0.19	21.26		0.00	33.57	2.23	2.96	2.74	100.04	11.9	75.4	5.1	7.3
GRD-1 #2.2	37.51	0.19	21.15		0.00	34.04	2.22	2.96	2.70	100.77	11.7	75.8	5.0	7.2
GRD-1 #2.3	37.29	0.23	21.22		0.00	33.83	2.37	2.96	2.61	100.51	11.8	75.6	5.4	6.8
GRD-1 #2.4	37.16	0.23	20.94		0.15	34.01	2.45	2.95	2.63	100.52	11.7	75.6	5.5	6.3
GRD-1 #2.5	37.20	0.19	21.16		0.00	33.66	2.41	2.89	2.72	100.23	11.5	75.4	5.5	7.2
GRD-1 #2.6	37.07	0.20	21.16		0.00	33.86	2.29	2.79	2.69	100.05	11.2	76.1	5.2	7.1
GRD-1 #2.7	37.58	0.17	21.08		0.11	34.21	2.39	2.78	2.63	100.96	11.0	76.3	5.4	6.7
GRD-1 #2.8	37.74	0.20	21.28		0.00	34.70	2.36	2.69	2.61	101.57	10.6	76.9	5.3	6.8
GRD-1 #2.9	37.79	0.18	21.77		0.00	34.44	2.37	2.67	2.46	101.67	10.7	77.1	5.4	6.5
GRD-1 #2.10	38.69	0.18	21.97		0.00	34.23	2.30	2.53	2.39	102.29	10.3	77.7	5.3	6.4
GRD-1 #3.1	37.39	0.19	20.98		0.06	33.47	2.25	3.11	2.64	100.08	12.4	75.1	5.1	6.8
GRD-1 #3.2	37.40	0.16	21.04		0.06	33.67	2.41	2.93	2.73	100.40	11.7	75.3	5.4	7.1
GRD-1 #3.3	37.11	0.16	21.28		0.00	33.75	2.25	2.95	2.65	100.15	11.8	75.7	5.1	7.1
GRD-1 #3.4	37.29	0.14	21.26		0.00	34.12	2.38	2.92	2.66	100.76	11.5	75.7	5.3	7.1
GRD-1 #3.5	37.19	0.13	21.29		0.00	34.23	2.38	2.92	2.57	100.70	11.6	75.9	5.3	6.9
GRD-1 #3.6	37.39	0.17	20.94		0.19	34.25	2.22	2.87	2.48	100.50	11.4	76.6	5.0	6.0
GRD-1 #3.7	37.49	0.24	21.32		0.00	34.22	2.44	2.89	2.75	101.35	11.4	75.7	5.5	7.1
GRD-1 #3.8	37.52	0.14	21.26		0.00	34.42	2.35	2.86	2.46	101.00	11.3	76.5	5.3	6.6
GRD-1 #3.9	37.97	0.18	21.56		0.00	34.69	2.38	2.82	2.37	101.97	11.1	77.0	5.4	6.2
GRD-1 #3.10	38.87	0.19	22.17		0.00	34.46	2.41	2.85	2.31	103.26	11.3	76.9	5.4	6.0
EMT-268.1_1	37.19	0.15	20.56	0.02	0.46	34.32	2.30	2.78	2.34	100.12	11.1	76.9	5.2	5.3
EMT-268.1_2	37.28	0.19	20.52	0.00	0.49	34.26	2.36	2.79	2.45	100.34	11.1	76.5	5.3	5.5
EMT-268.1_3	37.33	0.17	20.64	0.01	0.74	34.13	2.35	2.87	2.47	100.72	11.4	76.2	5.3	4.8
EMT-268.1_4	37.30	0.17	20.72	0.02	0.55	34.19	2.40	2.77	2.49	100.62	11.0	76.4	5.4	5.4
EMT-268.1_5	37.37	0.20	20.85	0.00	0.14	34.19	2.35	2.86	2.50	100.47	11.4	76.2	5.3	6.7
EMT-268.1_6	37.29	0.19	20.94	0.01	1.19	34.02	2.41	2.86	2.50	101.41	11.4	76.0	5.5	3.6
EMT-268.1_7	37.28	0.20	21.20	0.00	0.52	34.21	2.45	2.81	2.39	101.05	11.2	76.4	5.5	5.3
EMT-268.2_1	37.05	0.21	20.81	0.04	0.67	34.10	2.36	2.79	2.37	100.39	11.2	76.6	5.4	4.7
EMT-268.2_2	37.11	0.16	20.90	0.00	1.07	33.95	2.40	2.81	2.45	100.85	11.2	76.3	5.5	3.8

Label	SiO_2	TiO_2	Al_2O_3	Cr_2O_3	Fe_2O_3	FeO	MnO	MgO	CaO	Total	Pyr	Alm	Sps	Grs
EMT-268.2_3	37.13	0.21	21.15	0.01	0.35	33.94	2.36	2.83	2.51	100.48	11.3	76.1	5.4	6.1
EMT-268.2_4	37.24	0.21	21.16	0.00	1.28	33.94	2.38	2.84	2.59	101.64	11.3	75.9	5.4	3.6
EMT-268.2_5	37.20	0.18	20.83	0.02	1.08	33.95	2.33	2.86	2.52	100.97	11.4	76.0	5.3	3.9
EMT-268.2_6	37.27	0.19	21.02	0.01	0.56	34.10	2.38	2.85	2.46	100.83	11.4	76.2	5.4	5.3
EMT-268.2_7	36.66	0.18	23.64	0.02	0.00	33.29	2.35	2.79	2.30	101.23	11.4	76.4	5.5	6.7
SB-2.1_1	36.81	0.15	20.91	0.00	0.94	33.77	2.44	2.73	2.38	100.12	11.0	76.5	5.6	4.1
SB-2.1_2	36.75	0.19	21.18	0.00	0.99	33.63	2.39	2.74	2.48	100.34	11.1	76.2	5.5	4.3
SB-2.1_3	36.90	0.24	21.38	0.00	1.06	33.87	2.38	2.82	2.36	101.01	11.4	76.4	5.4	3.7
SB-2.1_4	36.95	0.23	21.06	0.00	0.42	33.97	2.31	2.81	2.40	100.14	11.3	76.5	5.3	5.7
SB-2.1_5	36.87	0.22	21.22	0.00	0.91	33.62	2.34	2.81	2.56	100.53	11.3	75.9	5.3	4.7
SB-2.1_6	37.05	0.19	21.22	0.00	0.63	33.82	2.25	2.85	2.59	100.59	11.4	76.0	5.1	5.6
SB-2.1_7	36.83	0.20	21.20	0.01	0.92	33.48	2.38	2.81	2.60	100.43	11.3	75.7	5.4	4.8
SB-2.1_8	36.97	0.24	21.20	0.00	0.40	33.65	2.25	2.84	2.67	100.22	11.4	75.7	5.1	6.5
SB-2.1_9	37.05	0.20	20.89	0.00	0.67	33.55	2.34	2.86	2.69	100.26	11.5	75.4	5.3	5.7
SB-2.1_10	36.95	0.24	21.01	0.00	0.68	33.44	2.31	2.87	2.73	100.23	11.5	75.3	5.3	5.8
SB-2.1_11	37.04	0.19	21.15	0.05	0.43	33.44	2.39	2.82	2.80	100.31	11.3	75.2	5.4	6.6
SB-2.1_12	37.21	0.22	21.12	0.01	0.71	33.58	2.25	2.95	2.79	100.85	11.8	75.1	5.1	5.9
SB-2.1_13	37.07	0.22	20.92	0.00	1.02	33.19	2.31	2.97	2.88	100.58	11.9	74.6	5.3	5.2
SB-2.1_14	37.22	0.21	21.10	0.00	1.08	33.24	2.49	2.96	2.86	101.15	11.8	74.4	5.7	5.0
SB-2.1_15	37.14	0.22	20.94	0.01	0.78	33.50	2.31	2.89	2.82	100.61	11.6	75.1	5.2	5.7
SB-2.1_16	37.07	0.21	21.03	0.02	0.66	33.47	2.29	2.94	2.72	100.41	11.8	75.2	5.2	5.8
SB-2.1_17	37.22	0.22	20.83	0.02	0.50	33.61	2.29	2.98	2.72	100.39	11.9	75.2	5.2	6.2
SB-2.1_18	37.14	0.20	21.10	0.01	0.29	33.78	2.26	2.85	2.69	100.31	11.4	75.8	5.1	6.8
SB-2.1_19	37.09	0.20	21.18	0.01	0.51	33.71	2.38	2.82	2.64	100.54	11.3	75.7	5.4	6.1
SB-2.1_20	37.10	0.20	20.96	0.00	0.30	33.91	2.38	2.78	2.55	100.18	11.1	76.1	5.4	6.4
SB-2.1_21	36.95	0.19	21.21	0.03	0.82	33.61	2.34	2.85	2.58	100.58	11.4	75.8	5.3	4.9
SB-2.1_22	37.09	0.22	21.26	0.00	0.44	33.97	2.30	2.82	2.51	100.60	11.3	76.3	5.2	5.9
SB-2.1_23	36.89	0.19	21.23	0.01	0.85	33.85	2.30	2.78	2.47	100.57	11.2	76.4	5.2	4.6
SB-2.1_24	36.81	0.21	21.44	0.00	0.93	33.80	2.32	2.74	2.48	100.71	11.0	76.5	5.3	4.4
SB-2.1_25	37.19	0.16	21.27	0.00	0.00	34.42	2.32	2.72	2.34	100.42	10.9	77.2	5.3	6.7
SB-2.2_1	36.79	0.16	21.10	0.02	0.42	33.97	2.41	2.64	2.36	99.88	10.7	77.0	5.5	5.5
SB-2.2_2	37.05	0.16	21.08	0.02	0.70	34.05	2.33	2.74	2.46	100.57	11.0	76.6	5.3	4.9
SB-2.2_3	36.85	0.28	20.99	0.00	0.80	33.78	2.31	2.69	2.66	100.36	10.8	76.2	5.3	5.3
SB-2.2_4	36.91	0.16	20.81	0.00	0.69	33.78	2.31	2.76	2.52	99.94	11.1	76.3	5.3	5.2
SB-2.2_5	36.89	0.21	21.03	0.00	0.74	33.65	2.42	2.80	2.51	100.24	11.3	76.0	5.5	5.0
SB-2.2_6	36.98	0.21	21.19	0.00	0.75	33.70	2.35	2.86	2.52	100.54	11.5	75.9	5.4	5.1
SB-2.2_7	36.90	0.21	21.26	0.02	0.90	33.58	2.29	2.85	2.60	100.61	11.5	75.8	5.2	4.8
SB-2.2_8	37.06	0.25	21.19	0.00	0.35	33.71	2.26	2.87	2.67	100.36	11.5	75.7	5.1	6.6
SB-2.2_9	37.06	0.23	20.94	0.05	0.76	33.27	2.39	2.94	2.80	100.43	11.8	74.7	5.4	5.7
SB-2.2_10	36.95	0.23	21.00	0.00	0.63	33.19	2.41	2.95	2.74	100.10	11.8	74.8	5.5	6.0
SB-2.2_11	37.10	0.19	20.99	0.00	0.42	33.48	2.41	2.94	2.64	100.17	11.8	75.2	5.5	6.3
SB-2.2_12	37.26	0.26	21.18	0.00	0.29	33.53	2.33	2.95	2.84	100.63	11.8	74.9	5.3	7.2
SB-2.2_13	37.23	0.18	21.13	0.00	0.58	33.69	2.41	2.88	2.66	100.76	11.5	75.4	5.5	5.9
SB-2.2_14	37.15	0.22	21.12	0.00	0.79	33.61	2.30	2.94	2.67	100.80	11.8	75.3	5.2	5.3
SB-2.2_15	37.19	0.19	21.23	0.00	0.32	33.71	2.35	2.86	2.70	100.55	11.4	75.5	5.3	6.8
SB-2.2_16	37.22	0.19	21.01	0.00	0.92	33.85	2.32	2.84	2.66	101.01	11.4	75.8	5.3	4.9
SB-2.2_17	37.04	0.19	21.17	0.01	0.61	33.77	2.32	2.78	2.64	100.53	11.1	75.9	5.3	5.8
SB-2.2_18	37.11	0.18	21.09	0.01	0.21	33.90	2.42	2.81	2.49	100.22	11.2	76.1	5.5	6.5
SB-2.2_19	37.15	0.18	21.33	0.00	0.21	34.10	2.36	2.79	2.44	100.56	11.1	76.5	5.4	6.4
SB-2.2_20	37.28	0.18	21.25	0.00	0.27	34.50	2.30	2.73	2.38	100.89	10.9	77.1	5.2	6.0

Appendix 3: $^{40}Ar/^{39}Ar$ Age Dating Results

Sample SR-1; Phlogopite Separate; Measured $^{40}Ar/^{36}Ar_a$= 298.9; J= 0.00479±0.1% (1-sigma)

Temperature (°C)	$^{40}Ar_R$	$^{39}Ar_K$	$^{40}Ar/^{39}Ar$	$^{39}Ar/^{37}Ar$	$\%^{40}Ar_R$	$\%^{39}Ar$	Apparent Age (Ma ± 1 sigma)		
650	0.07641	0.01450	5.269	6.07	25.0	0.7	44.97	±	2.58
750	0.17493	0.03101	5.641	11.98	69.3	1.4	48.09	±	0.37
850	0.54352	0.09543	5.695	59.93	86.7	4.4	48.56	±	0.35
900	0.81449	0.14089	5.781	98.08	91.7	6.5	49.27	±	0.12
950	1.71858	0.29633	5.800	109.03	94.0	13.7	49.43	±	0.11
1000	1.88496	0.32624	5.778	128.13	94.9	15.1	49.25	±	0.08
1050	1.59552	0.27678	5.765	109.88	93.8	12.8	49.14	±	0.08
1100	1.56163	0.27565	5.665	112.72	94.6	12.8	48.30	±	0.07
1150	1.70226	0.30193	5.638	67.41	96.3	14.0	48.07	±	0.09
1200	1.21327	0.21610	5.614	37.16	96.8	10.0	47.87	±	0.07
1300	1.03681	0.18444	5.621	15.51	96.4	8.5	47.93	±	0.34
Total Gas			5.707				48.65	±	0.14

Plateau Test Results

Age (Ma)		Error	Step #	% of Total Gas	Plateau Min (Ma)	Plateau Max (Ma)	Wtd. Mean
48.67	±	0.17	2-11	99.3	48.82	49.43	x

Sample BB-1; Phlogopite Separate; Measured $^{40}Ar/^{36}Ar_a$= 298.9; J= 0.004803±0.1% (1-sigma)

Temperature (°C)	$^{40}Ar_R$	$^{39}Ar_K$	$^{40}Ar/^{39}Ar$	$^{39}Ar/^{37}Ar$	$\%^{40}Ar_R$	$\%^{39}Ar$	Apparent Age (Ma ± 1 sigma)		
650	0.02217	0.00698	3.177	0.85	8.6	0.4	27.32	±	2.32
750	0.01129	0.01032	1.094	0.52	18.2	0.6	9.45	±	0.57
850	0.39517	0.06938	5.696	0.53	71.4	4.1	48.69	±	0.25
900	0.94407	0.16516	5.716	62.17	91.4	9.8	48.86	±	0.30
950	1.46976	0.25646	5.731	129.92	96.3	15.3	48.99	±	0.08
1000	1.80592	0.31460	5.740	178.28	97.4	18.7	49.07	±	0.10
1050	1.63105	0.28265	5.771	139.69	95.9	16.8	49.32	±	0.08
1100	1.19113	0.20617	5.777	92.57	91.5	12.3	49.38	±	0.10
1150	0.66523	0.11637	5.717	64.16	88.4	6.9	48.86	±	0.10
1200	0.70443	0.12385	5.688	40.08	88.8	7.4	48.62	±	0.14
1300	0.72411	0.12887	5.619	26.48	89.1	7.7	48.04	±	0.07
Total Gas			5.690				48.64	±	0.15

Plateau Test Results

Age (Ma)		Error	Step #	% of Total Gas	Plateau Min (Ma)	Plateau Max (Ma)	Wtd. Mean
48.97	±	0.14	3-11	99.0	48.04	49.38	x

Sample SB-1; Biotite Separate; Measured $^{40}Ar/^{36}Ar_a$= 298.9; J= 0.004765±0.1% (1-sigma)

Temperature (°C)	$^{40}Ar_R$	$^{39}Ar_K$	$^{40}Ar/^{39}Ar$	$^{39}Ar/^{37}Ar$	$\%^{40}Ar_R$	$\%^{39}Ar$	Apparent Age (Ma ± 1 sigma)		
650	0.06200	0.01661	3.732	70.86	16.6	1.0	31.80	±	0.75
750	0.66041	0.12499	5.284	161.68	49.8	7.9	44.86	±	0.14
850	0.95299	0.15773	6.039	292.27	84.0	9.9	51.18	±	0.09
900	0.53040	0.08783	6.039	259.03	86.2	5.5	51.18	±	0.33
950	0.54028	0.08906	6.066	213.75	79.2	5.6	51.41	±	0.18
1000	0.60814	0.10032	6.062	211.05	78.0	6.3	51.37	±	0.17
1050	1.11909	0.18470	6.059	346.63	76.5	11.6	51.34	±	0.09
1100	2.51082	0.41670	5.997	277.80	80.8	26.4	50.83	±	0.08
1150	1.82211	0.30577	5.959	215.35	86.3	19.3	50.51	±	0.08
1300	0.59265	0.09975	5.941	30.39	87.2	6.3	50.36	±	0.11
Total Gas			5.928				50.25	±	0.12

Plateau Test Results

Age (Ma)		Error	Step #	% of Total Gas	Plateau Min (Ma)	Plateau Max (Ma)	Wtd. Mean
50.93	±	0.14	3-10	91.1	50.36	51.41	x

Sample SB-2; Biotite Separate; Measured $^{40}Ar/^{36}Ar_a$= 298.9; J= 0.00479±0.1% (1-sigma)

Temperature (°C)	$^{40}Ar_R$	$^{39}Ar_K$	$^{40}Ar/^{39}Ar$	$^{39}Ar/^{37}Ar$	$\%^{40}Ar_R$	$\%^{39}Ar$	Apparent Age (Ma ± 1 sigma)		
650	0.22299	0.04919	4.533	49.30	28.7	2.9	38.75	±	0.42
750	0.76938	0.1293	5.950	262.62	85.2	7.7	50.70	±	0.21
850	1.30591	0.21724	6.011	450.04	95.9	12.9	51.21	±	0.08
900	0.71900	0.12040	5.972	342.48	95.9	7.2	50.88	±	0.10
950	0.63334	0.10594	5.978	341.15	95.6	6.3	50.93	±	0.08
1000	1.09279	0.18076	6.045	250.08	96.1	10.8	51.50	±	0.08
1050	2.34080	0.39109	5.985	585.52	97.9	23.2	50.99	±	0.08
1100	2.23784	0.37615	5.949	682.34	98.3	22.4	50.69	±	0.12
1150	0.81185	0.08544	5.991	95.65	98.2	5.1	51.04	±	0.12
1300	0.14660	0.02576	5.700	25.05	87.1	1.5	48.59	±	1.69
Total Gas			5.936				50.58	±	0.14

Plateau Test Results

Age (Ma)		Error	Step #	% of Total Gas	Plateau Min (Ma)	Plateau Max (Ma)	Wtd. Mean
50.97	±	0.11			50.69	51.50	x

Sample MC-2; Phlogopite Separate; Measured $^{40}Ar/^{36}Ar_a$= 298.9; J= 0.00477±0.1% (1-sigma)

Temperature (°C)	$^{40}Ar_R$	$^{39}Ar_K$	$^{40}Ar/^{39}Ar$	$^{39}Ar/^{37}Ar$	$\%^{40}Ar_R$	$\%^{39}Ar$	Apparent Age (Ma ± 1 sigma)		
650	0.00058	0.0081	0.717	1.00	0.3	0.1	6.16	±	13.44
750	0.01757	0.00396	4.435	0.23	27.4	0.7	37.77	±	3.12
850	0.10303	0.01785	5.773	0.93	68.2	3.2	49.00	±	1.39
900	0.26173	0.04611	5.676	24.47	90.2	8.1	48.20	±	0.15
950	0.59735	0.10554	5.660	67.78	94.9	18.6	48.06	±	0.07
1000	0.66870	0.11815	5.660	88.74	95.5	20.9	48.06	±	0.26
1050	0.52308	0.09263	5.647	54.53	93.4	16.4	47.95	±	0.14
1100	0.33556	0.05975	5.616	32.79	88.4	10.5	47.69	±	0.07
1150	0.22033	0.03935	5.599	22.55	87.7	6.9	47.55	±	0.14
1300	0.45939	0.08225	5.589	7.01	77.7	14.5	47.43	±	0.19
Total Gas			5.627				47.79	±	0.36

Isochron Age Regressions

York 1	Slope	Slope error	Y intercept	Intercept error	Value	Error (2 sigma)	
n = 8 (3-10)	5.6292	0.057142	303.61	15.566			
Age (Ma)					47.80	0.244	
Initial $^{40}Ar/^{36}Ar$					304	7.78	
Radiogenic $^{40}Ar/^{39}Ar$					5.63	0.0286	
York 2	Slope	Slope error	Y intercept	Intercept error	Value	Error (2 sigma)	mswd
n = 8 (3-10)	5.6356	0.0002027	300.75	0.091331			136
Age (Ma)					47.86	0.0472	
Initial $^{40}Ar/^{36}Ar$					301	0.0457	
Radiogenic $^{40}Ar/^{39}Ar$					5.64	0.000101	

Sample MB-1; Whole Rock; Measured $^{40}Ar/^{36}Ar_a$= 298.9; J= 0.004957±0.1% (1-sigma)

Temperature (°C)	$^{40}Ar_R$	$^{39}Ar_K$	$^{40}Ar/^{39}Ar$	$^{39}Ar/^{37}Ar$	$\%^{40}Ar_R$	$\%^{39}Ar$	Apparent Age (Ma ± 1 sigma)		
600	1.40827	0.25385	5.548	2.00	78.5	20.2	48.94	±	0.10
700	0.61866	0.10846	5.704	6.69	92.3	8.6	50.30	±	0.17
800	0.75610	0.13791	5.482	8.08	88.1	10.9	48.37	±	0.07
900	0.44640	0.08267	5.400	4.20	91.8	6.6	47.65	±	0.18
1000	0.73147	0.13679	5.347	2.78	95.8	10.9	47.20	±	0.28
1100	0.83575	0.16260	5.140	0.62	92.8	12.9	45.39	±	0.15
1200	0.32841	0.25941	5.121	0.12	92.5	20.6	45.22	±	0.07
1300	0.61159	0.11782	5.191	0.03	91.2	9.4	45.83	±	0.21
Total Gas			5.349				47.21	±	0.14

Isochron Age Regressions

York 1	Slope	Slope error	Y intercept	Intercept error	Value	Error (2 sigma)	
n = 8 (all)	5.2315	0.27489	362.38	122.46			
Age (Ma)					46.19	1.2	
Initial $^{40}Ar/^{36}Ar$					362	61.2	
Radiogenic $^{40}Ar/^{39}Ar$					5.23	0.137	
York 2	Slope	Slope error	Y intercept	Intercept error	Value	Error (2 sigma)	mswd
n = 8 (all)	5.2095	0.0001730	369.85	0.12954			624
Age (Ma)					46.00	0.0454	
Initial $^{40}Ar/^{36}Ar$					370	0.0648	
Radiogenic $^{40}Ar/^{39}Ar$					5.21	0.0000065	

Sample MB-3; Whole Rock; Measured $^{40}Ar/^{36}Ar_a$= 298.9; J= 0.00485±0.1% (1-sigma)

Temperature (°C)	$^{40}Ar_R$	$^{39}Ar_K$	$^{40}Ar/^{39}Ar$	$^{39}Ar/^{37}Ar$	$\%^{40}Ar_R$	$\%^{39}Ar$	Apparent Age (Ma ± 1 sigma)		
600	1.49148	0.26650	5.597	1.99	85.5	25.3	48.31	±	0.14
700	1.39029	0.23304	5.966	6.02	96.1	22.1	51.46	±	0.08
800	1.07511	0.10761	5.731	7.86	91.1	17.8	49.45	±	0.10
900	0.67785	0.12051	5.625	4.18	95.8	11.4	48.55	±	0.55
1000	0.47170	0.08412	5.608	1.81	93.5	8.0	48.41	±	0.07
1100	0.34873	0.06559	5.317	0.42	85.6	6.2	45.93	±	0.23
1200	0.37883	0.07384	5.131	0.04	77.0	7.0	44.34	±	0.29
1350	0.11794	0.02389	4.936	0.00	46.6	2.3	42.68	±	0.07
Total Gas							48.69	±	0.17

Isochron Age Regressions

York 1	Slope	Slope error	Y intercept	Intercept error	Value	Error (2 sigma)	
n = 8 (all)	5.7018	0.19791	246.72	35.559			
Age (Ma)					49.21	0.844	
Initial $^{40}Ar/^{36}Ar$					247	17.8	
Radiogenic $^{40}Ar/^{39}Ar$					5.70	0.0990	
York 2	Slope	Slope error	Y intercept	Intercept error	Value	Error (2 sigma)	mswd
n = 8 (all)	5.7203	0.00000433	236.82	0.062351			607
Age (Ma)					49.37	0.0487	
Initial $^{40}Ar/^{36}Ar$					237	0.0312	
Radiogenic $^{40}Ar/^{39}Ar$					5.72	0.0000422	

Sample CB-1; Whole Rock; Measured $^{40}Ar/^{36}Ar_a$= 298.9; J= 0.004902±0.1% (1-sigma)

Temperature (°C)	$^{40}Ar_R$	$^{39}Ar_K$	$^{40}Ar/^{39}Ar$	$^{39}Ar/^{37}Ar$	$\%^{40}Ar_R$	$\%^{39}Ar$	Apparent Age (Ma ± 1 sigma)		
600	1.57985	0.34729	4.549	1.82	81.8	21.7	39.79	±	0.06
700	1.66263	0.30136	5.517	3.61	86.6	18.9	48.14	±	0.07
750	0.72371	0.13539	5.345	4.25	82.0	8.5	46.66	±	0.08
800	0.77093	0.14635	5.268	4.48	86.7	9.2	45.99	±	0.07
900	0.90452	0.17369	5.200	3.13	87.5	10.9	45.41	±	0.07
1000	1.06599	0.20553	5.185	1.77	87.3	12.9	45.28	±	0.07
1150	0.69356	0.19285	4.538	0.20	79.9	9.6	39.69	±	0.30
1300	0.60560	0.13406	4.517	0.02	73.2	8.4	39.51	±	0.13
Total Gas							43.80	±	0.10

Isochron Age Regressions

York 1	Slope	Slope error	Y intercept	Intercept error	Value	Error (2 sigma)	
n = 8 (all)	5.9751	0.90738	15.297	254.29			
Age (Ma)					52.08	3.9	
Initial $^{40}Ar/^{36}Ar$					15.3	127	
Radiogenic $^{40}Ar/^{39}Ar$					5.98	0.0454	
York 2	Slope	Slope error	Y intercept	Intercept error	Value	Error (2 sigma)	mswd
n = 8 (all)	5.9677	0.001140	16.98	0.30451			1020
Age (Ma)					52.02	0.0515	
Initial $^{40}Ar/^{36}Ar$					17.0	0.152	
Radiogenic $^{40}Ar/^{39}Ar$					5.97	0.00057	

Sample HM-2; Whole Rock; Measured $^{40}Ar/^{36}Ar_a$= 298.9; J= 0.004905±0.1% (1-sigma)

Temperature (°C)	$^{40}Ar_R$	$^{39}Ar_K$	$^{40}Ar/^{39}Ar$	$^{39}Ar/^{37}Ar$	$\%^{40}Ar_R$	$\%^{39}Ar$	Apparent Age (Ma ± 1 sigma)		
600	0.29498	0.07913	3.728	0.72	44.5	1.9	32.69	±	0.42
700	1.34910	0.26057	5.178	1.79	91.9	6.2	45.24	±	0.14
800	3.29171	0.63872	5.154	2.95	95.7	15.2	45.02	±	0.07
900	3.39196	0.65327	5.192	2.89	97.6	15.5	45.37	±	0.07
1000	2.67079	0.51960	5.140	2.05	96.6	12.3	44.92	±	0.07
1100	3.38495	0.66581	5.084	2.20	97.9	15.8	44.43	±	0.07
1200	5.22186	1.03885	5.027	1.01	97.7	24.7	43.94	±	0.07
1300	1.79579	0.35690	5.032	0.13	95.6	8.5	43.98	±	0.12
Total Gas			5.080				44.40	±	0.08

Isochron Age Regressions

York 1	Slope	Slope error	Y intercept	Intercept error	Value	Error (2 sigma)	
n = 8 (all)	5.1789	0.071054	204.68	16.214			
Age (Ma)					45.26	0.31	
Initial $^{40}Ar/^{36}Ar$					205	8.11	
Radiogenic $^{40}Ar/^{39}Ar$					5.18	0.0355	
York 2	Slope	Slope error	Y intercept	Intercept error	Value	Error (2 sigma)	mswd
n = 8 (all)	5.1773	0.0002098	205.77	0.07198			300
Age (Ma)					45.24	0.0447	
Initial $^{40}Ar/^{36}Ar$					206	0.036	
Radiogenic $^{40}Ar/^{39}Ar$					5.18	0.000105	

Sample BD-1; Whole Rock; Measured $^{40}Ar/^{36}Ar_a$= 298.9; J= 0.00489±0.1% (1-sigma)

Temperature (°C)	$^{40}Ar_R$	$^{39}Ar_K$	$^{40}Ar/^{39}Ar$	$^{39}Ar/^{37}Ar$	$\%^{40}Ar_R$	$\%^{39}Ar$	Apparent Age (Ma ± 1 sigma)		
600	0.03281	0.02497	1.314	0.97	6.6	2.5	11.56	±	1.10
700	0.53814	0.17657	3.048	0.83	31.6	17.8	26.69	±	0.04
800	0.68236	0.17896	3.813	0.56	62.0	18.1	33.33	±	0.30
900	0.64630	0.17266	3.743	0.44	71.7	17.4	32.72	±	0.06
1000	0.36989	0.10150	3.644	0.31	67.0	10.2	31.86	±	0.05
1100	0.25355	0.07214	3.515	0.27	60.2	7.3	30.74	±	0.22
1200	0.78334	0.22496	3.482	0.10	61.9	22.7	30.46	±	0.05
1350	0.13899	0.03892	3.572	0.11	65.9	3.9	31.24	±	0.19
Total Gas			3.478				30.42	±	0.18

Isochron Age Regressions

York 1	Slope	Slope error	Y intercept	Intercept error	Value	Error (2 sigma)	
n = 8 (all)	3.8982	0.12815	255.55	10.717			
Age (Ma)					34.07	0.556	
Initial $^{40}Ar/^{36}Ar$					256	5.36	
Radiogenic $^{40}Ar/^{39}Ar$					3.90	0.0641	
York 2	Slope	Slope error	Y intercept	Intercept error	Value	Error (2 sigma)	mswd
n = 8 (all)	3.8814	0.001353	256.79	0.13628			315
Age (Ma)					33.92	0.0341	
Initial $^{40}Ar/^{36}Ar$					257	0.0681	
Radiogenic $^{40}Ar/^{39}Ar$					3.88	.000676	

Sample CM-2; Whole Rock; Measured $^{40}Ar/^{36}Ar_a$= 298.9; J= 0.004902±0.1% (1-sigma)

Temperature (°C)	$^{40}Ar_R$	$^{39}Ar_K$	$^{40}Ar/^{39}Ar$	$^{39}Ar/^{37}Ar$	$\%^{40}Ar_R$	$\%^{39}Ar$	Apparent Age (Ma ± 1 sigma)		
600	0.53110	0.14197	3.741	4.35	63.8	7.0	32.75	±	0.07
700	2.17509	0.53455	4.069	3.85	92.6	26.3	35.63	±	0.06
800	2.63301	0.51975	5.066	1.73	97.0	25.5	44.25	±	0.09
850	1.36041	0.25559	5.323	1.22	97.2	12.6	46.47	±	0.13
900	0.91669	0.17189	5.333	1.17	96.9	8.4	46.55	±	0.13
1000	0.54532	0.10589	5.150	0.97	92.5	5.2	44.97	±	0.20
1100	0.53267	0.10761	4.950	0.96	86.2	5.3	43.25	±	0.47
1300	0.98492	0.19803	4.971	0.50	71.3	9.7	43.43	±	0.07
Total Gas			4.755				41.57	±	0.11

Sample LM-1; Whole Rock; Measured 40Ar/36Ara= 298.9; J= 0.004795±0.1% (1-sigma)

Temperature (°C)	$^{40}Ar_R$	$^{39}Ar_K$	$^{40}Ar/^{39}Ar$	$^{39}Ar/^{37}Ar$	$\%^{40}Ar_R$	$\%^{39}Ar$	Apparent Age (Ma ± 1 sigma)		
600	1.73007	1.08784	1.590	4.73	31.7	52.0	13.70	±	0.02
700	0.48341	0.20433	2.366	—	46.3	9.8	20.5	±	0.10
800	0.64015	0.19122	3.348	0.54	64.2	9.1	28.73	±	0.07
900	0.36906	0.10836	3.406	0.47	62.4	5.2	29.22	±	0.39
1000	0.27005	0.09151	2.951	0.63	52.4	4.4	25.35	±	0.31
1100	0.35570	0.14022	2.537	0.81	44.7	6.7	21.81	±	0.04
1300	0.68389	0.26875	2.545	0.70	44.8	12.8	21.88	±	0.09
Total Gas			2.166				18.64	±	0.06

Plateau Test Results

Age (Ma)		Error	Step #	% of Total Gas	Plateau Min (Ma)	Plateau Max (Ma)	Wtd. Mean
21.89	±	0.07	6-7	19.5	21.01	21.80	

Sample LWC-1; Whole Rock; Measured $^{40}Ar/^{36}Ar_a$= 298.9; J= 0.004878±0.1% (1-sigma)

Temperature (°C)	$^{40}Ar_R$	$^{39}Ar_K$	$^{40}Ar/^{39}Ar$	$^{39}Ar/^{37}Ar$	$\%^{40}Ar_R$	$\%^{39}Ar$	Apparent Age (Ma ± 1 sigma)		
500	0.00974	0.00069	14.193	0.57	33.4	0.1	120.76	±	28.75
700	0.53283	0.08018	6.645	0.46	77.8	7.8	57.55	±	0.26
800	1.50736	0.23967	6.289	0.39	94.2	23.4	54.51	±	0.08
900	1.39331	0.22865	6.094	0.35	96.2	22.4	52.84	±	0.08
1000	0.80505	0.13299	6.054	0.39	93.9	13.0	52.50	±	0.29
1100	1.12706	0.18826	5.987	0.61	94.9	18.4	51.93	±	0.13
1200	0.69241	0.13084	5.292	0.30	90.5	12.8	45.98	±	0.25
1300	0.10379	0.02174	4.774	0.04	64.9	2.1	41.53	±	1.03
Total Gas			6.033				52.32	±	0.18

Sample CAU-1; Whole Rock; Measured $^{40}Ar/^{36}Ar_a$= 298.9; J= 0.004853±0.1% (1-sigma)

Temperature (°C)	$^{40}Ar_R$	$^{39}Ar_K$	$^{40}Ar/^{39}Ar$	$^{39}Ar/^{37}Ar$	$\%^{40}Ar_R$	$\%^{39}Ar$	Apparent Age (Ma ± 1 sigma)		
600	0.12354	0.02047	6.035	1.56	18.7	1.0	52.08	±	0.12
700	1.06219	0.25094	4.233	1.04	76.4	11.7	36.68	±	0.07
750	1.02650	0.20049	5.120	1.00	95.1	9.4	44.28	±	0.07
800	2.41393	0.47287	5.102	0.92	98.4	22.1	44.15	±	0.07
850	1.82599	0.36612	4.987	0.99	98.2	17.1	43.14	±	0.07
900	1.81427	0.36879	4.919	1.01	98.0	17.3	42.56	±	0.08
950	1.33429	0.27278	4.891	0.99	97.7	12.8	42.32	±	0.07
1000	0.53957	0.11076	4.871	0.83	95.5	5.2	42.15	±	0.34
1100	0.34324	0.07394	4.642	0.62	89.2	3.5	40.19	±	0.25

*last fraction was collected to at too low a temperature

Isochron Age Regressions

York 1	Slope	Slope error	Y intercept	Intercept error	Value	Error (2 sigma)	
n = 9 (all)	4.8582	0.21435	301.51	30.497			
Age (Ma)					42.04	0.918	
Initial $^{40}Ar/^{36}Ar$					302	0.152	
Radiogenic $^{40}Ar/^{39}Ar$					4.86	0.107	
York 2	Slope	Slope error	Y intercept	Intercept error	Value	Error (2 sigma)	mswd
n = 9 (all)	4.8907	0.00001070	267.84	0.067009			942
Age (Ma)					42.32	0.0418	
Initial $^{40}Ar/^{36}Ar$					268	0.0335	
Radiogenic $^{40}Ar/^{39}Ar$					4.89	0.0000535	

Sample CBU-2; Whole Rock; Measured $^{40}Ar/^{36}Ar_a$= 298.9; J= 0.004845±0.1% (1-sigma)

Temperature (°C)	$^{40}Ar_R$	$^{39}Ar_K$	$^{40}Ar/^{39}Ar$	$^{39}Ar/^{37}Ar$	$\%^{40}Ar_R$	$\%^{39}Ar$	Apparent Age (Ma ± 1 sigma)		
600	0.07884	0.05624	1.402	6.36	14.6	2.2	12.21	±	0.10
700	2.36657	0.57074	4.147	3.39	83.0	22.2	35.88	±	0.06
800	4.33980	0.79241	5.477	1.60	97.0	30.9	47.24	±	0.07
850	2.73399	0.53491	5.111	0.87	97.6	20.8	44.13	±	0.07
900	0.97305	0.19575	4.971	0.66	94.9	7.6	42.93	±	0.16
950	0.75644	0.15231	4.966	0.50	93.7	5.9	42.89	±	0.17
1000	0.46215	0.09343	4.946	0.53	89.7	3.6	42.72	±	0.27
1200	0.81332	0.17061	4.767	0.48	82.5	6.6	41.19	±	0.16
Total Gas			4.880				42.16	±	0.10

Plateau Test Results

Age (Ma)		Error	Step #	% of Total Gas	Plateau Min (Ma)	Plateau Max (Ma)	Wtd. Mean
42.88	±	0.20	5-7	17.2	42.72	42.93	

Sample CAU-2; Whole Rock; Measured $^{40}Ar/^{36}Ar_a$= 298.9; J= 0.00484±0.1% (1-sigma)

Temperature (°C)	$^{40}Ar_R$	$^{39}Ar_K$	$^{40}Ar/^{39}Ar$	$^{39}Ar/^{37}Ar$	$\%^{40}Ar_R$	$\%^{39}Ar$	Apparent Age (Ma ± 1 sigma)		
600	0.41048	0.05540	7.409	3.23	28.0	2.1	63.56	±	0.10
700	2.04847	0.40443	5.065	1.70	67.1	15.6	43.69	±	0.07
800	1.51668	0.29651	5.115	1.46	95.7	11.4	44.12	±	0.07
900	5.81549	1.16737	4.982	1.18	98.6	44.9	42.98	±	0.07
1000	1.45226	0.30371	4.782	1.13	97.4	11.7	41.28	±	0.16
1100	0.98010	0.21136	4.637	1.24	96.3	8.1	40.04	±	0.21
1200	0.51590	0.12047	4.282	0.72	93.0	8.1	37.01	±	0.15
1350	0.16539	0.03939	4.198	0.21	84.0	4.6	36.29	±	0.19
Total Gas			4.966			1.5	42.85	±	0.10

Isochron Age Regressions

York 1	Slope	Slope error	Y intercept	Intercept error	Value	Error (2 sigma)	
n = 4 (1-4)	4.9781	0.18636	30.03	16.574			
Age (Ma)					42.95	.796	
Initial $^{40}Ar/^{36}Ar$					330	8.29	
Radiogenic $^{40}Ar/^{39}Ar$					4.98	0.0932	
York 2	Slope	Slope error	Y intercept	Intercept error	Value	Error (2 sigma)	mswd
n = 4 (1-4)	5.0074	0.0004029	322.55	0.073131			380
Age (Ma)					43.20	0.0427	
Initial $^{40}Ar/^{36}Ar$					323	0.0366	
Radiogenic $^{40}Ar/^{39}Ar$					5.01	0.000201	

Sample HEC-1; Whole Rock; Measured $^{40}Ar/^{36}Ar_a$= 298.9; J= 0.004827±0.1% (1-sigma)

Temperature (°C)	$^{40}Ar_R$	$^{39}Ar_K$	$^{40}Ar/^{39}Ar$	$^{39}Ar/^{37}Ar$	$\%^{40}Ar_R$	$\%^{39}Ar$	Apparent Age (Ma ± 1 sigma)		
600	2.04281	0.41601	4.910	2.39	73.9	17.1	42.26	±	0.09
700	1.48458	0.23792	6.240	1.78	97.4	9.8	53.53	±	0.08
800	5.33362	0.88396	6.034	1.36	96.6	36.3	51.79	±	0.08
900	3.58688	0.61928	5.792	1.04	98.9	25.4	49.74	±	0.08
1000	0.93992	0.16561	5.675	0.59	97.0	6.8	48.76	±	0.17
1100	0.37931	0.06818	5.563	0.68	94.1	2.8	47.80	±	0.42
1200	0.11399	0.02047	5.569	0.51	94.3	0.8	47.86	±	0.29
1350	0.13435	0.02450	5.483	0.25	87.2	1.0	47.12	±	3.43
Total Gas			5.754				49.42	±	0.13

Isochron Age Regressions

York 1	Slope	Slope error	Y intercept	Intercept error	Value	Error (2 sigma)	
n = 8 (all)	5.9425	0.19886	115.11	86.403			
Age (Ma)					51.02	0.843	
Initial $^{40}Ar/^{36}Ar$					115	43.2	
Radiogenic $^{40}Ar/^{39}Ar$					5.94	0.0994	
York 2	Slope	Slope error	Y intercept	Intercept error	Value	Error (2 sigma)	mswd
n = 8 (all)	5.9389	0.0003023	115.78	0.13686			624
Age (Ma)					50.99	0.0503	
Initial $^{40}Ar/^{36}Ar$					116	0.0684	
Radiogenic $^{40}Ar/^{39}Ar$					5.94	0.000151	

Sample HEC-2; Whole Rock; Measured $^{40}Ar/^{36}Ar_a$= 298.9; J= 0.004875±0.1% (1-sigma)

Temperature (°C)	$^{40}Ar_R$	$^{39}Ar_K$	$^{40}Ar/^{39}Ar$	$^{39}Ar/^{37}Ar$	$\%^{40}Ar_R$	$\%^{39}Ar$	Apparent Age (Ma ± 1 sigma)		
500	0.46409	0.10878	4.266	2.95	50.3	4.9	37.13	±	0.07
700	2.16202	0.38296	5.698	1.96	90.8	17.4	49.43	±	0.08
800	4.96715	0.84362	5.888	1.42	98.2	38.3	51.05	±	0.08
900	2.97972	0.52498	5.676	1.04	98.9	23.8	49.24	±	0.08
1000	0.96495	0.17299	5.578	0.87	96.3	7.9	48.40	±	0.12
1100	0.44617	0.08395	5.315	0.92	91.9	3.8	46.14	±	0.07
1200	0.35258	0.06889	5.118	0.53	90.5	3.1	44.46	±	0.25
1300	0.07937	0.01669	4.755	0.12	61.5	0.8	41.34	±	0.57
Total Gas			5.645				48.98	±	0.09

Sample LEC-1; Whole Rock; Measured $^{40}Ar/^{36}Ar_a$= 298.9; J= 0.00491±0.1% (1-sigma)

Temperature (°C)	$^{40}Ar_R$	$^{39}Ar_K$	$^{40}Ar/^{39}Ar$	$^{39}Ar/^{37}Ar$	$\%^{40}Ar_R$	$\%^{39}Ar$	Apparent Age (Ma ± 1 sigma)		
500	0.04293	0.00664	6.461	0.53	24.9	0.6	56.34	±	0.36
700	0.55956	0.08868	6.310	0.49	81.9	8.2	55.04	±	0.21
800	1.32216	0.22177	5.962	0.49	92.5	20.5	52.05	±	0.08
900	0.95462	0.16713	5.712	0.29	94.9	15.5	49.90	±	0.10
1000	0.66942	0.11908	5.622	0.26	92.4	11.0	49.12	±	0.08
1100	1.06696	0.19205	5.556	0.42	94.4	17.8	48.55	±	0.13
1200	1.23525	0.24275	5.089	0.39	92.3	22.5	44.52	±	0.07
1300	0.18951	0.04254	4.454	0.06	73.0	3.9	39.03	±	0.89
Total Gas			5.590				48.84	±	0.14

Sample LEC-2; Whole Rock; Measured $^{40}Ar/^{36}Ar_a$= 298.9; J= 0.00497±0.1% (1-sigma)

Temperature (°C)	$^{40}Ar_R$	$^{39}Ar_K$	$^{40}Ar/^{39}Ar$	$^{39}Ar/^{37}Ar$	$\%^{40}Ar_R$	$\%^{39}Ar$	Apparent Age (Ma ± 1 sigma)		
600	0.17264	0.02895	6.047	0.63	46.1	3.0	53.42	±	0.09
700	0.81659	0.13355	6.115	0.85	85.5	13.9	54.01	±	0.08
800	1.07710	0.18172	5.927	0.58	92.6	19.0	52.38	±	0.11
900	0.79632	0.14124	5.638	0.18	91.8	14.7	49.85	±	0.24
1000	0.58476	0.10434	5.604	0.17	90.1	10.9	49.56	±	0.17
1100	1.05254	0.19182	5.487	0.35	90.3	20.0	48.54	±	0.08
1200	0.72630	0.14475	5.018	0.29	80.8	15.1	44.44	±	0.07
1350	0.15396	0.03293	4.680	0.04	60.3	3.4	41.48	±	0.33
Total Gas			5.611				49.62	±	0.12

Isochron Age Regressions

York 1	Slope	Slope error	Y intercept	Intercept error	Value	Error (2 sigma)	
n = 8 (all)	5.5929	0.46773	284.96	69.869			
Age (Ma)					49.46	2.04	
Initial $^{40}Ar/^{36}Ar$					285	34.9	
Radiogenic $^{40}Ar/^{39}Ar$					5.59	0.234	
York 2	Slope	Slope error	Y intercept	Intercept error	Value	Error (2 sigma)	mswd
n = 8 (all)	5.6322	0.00009648	261.82	0.056496			1220
Age (Ma)					49.81	0.0491	
Initial $^{40}Ar/^{36}Ar$					262	0.0282	
Radiogenic $^{40}Ar/^{39}Ar$					5.63	0.0000482	

Appendix 4: CIPW Norms

Marshall Butte

Bulk Data	MB-1 XRF	MB-2 XRF	MB-2 ICP-AES	MB-3 XRF	MB-3 ICP-AES
SiO_2	43.10	43.31	43.13	42.65	42.36
TiO_2	2.59	2.53	2.53	2.59	2.56
Al_2O_3	11.03	11.33	11.37	11.32	11.30
Fe_2O_3	1.73	1.73	1.78	1.75	1.79
FeO	8.64	8.66	8.88	8.77	8.96
MnO	0.19	0.22	0.23	0.20	0.20
MgO	12.42	12.07	12.16	12.40	11.87
CaO	13.94	13.54	13.56	13.98	13.73
Na_2O	3.53	3.41	3.37	3.61	3.66
K_2O	1.08	1.00	0.96	0.99	0.97
P_2O_5	0.90	0.90	0.83	0.91	0.87
Total	99.14	98.69	98.80	99.17	98.29
Norms					
Q	0	0	0	0	0
Or	0.71	5.91	5.17	0	0
Ab	0	0.48	0	0	0
An	11.06	12.66	13.04	11.76	11.52
Lc	4.44	0	0.40	4.59	4.51
Ne	16.18	15.37	15.46	16.55	16.79
Di	41.87	39.04	39.17	41.41	40.65
Hy	0	0	0	0	0
Ol	15.37	15.84	16.26	15.65	15.18
Mt	2.51	2.51	2.58	2.54	2.60
Il	4.92	4.81	4.80	4.92	4.87
Ap	2.13	2.13	1.98	2.16	2.07
Cs	0	0	0	0	0.05
C	0	0	0	0	0
Silica	undersaturated	undersaturated	undersaturated	undersaturated	undersaturated

Marshall Butte (cont.)

Bulk Data	MB-3r ICP-AES	MB-4 XRF	EMT-169 ICP-AES	EMT-77 ICP-AES
SiO_2	41.98	45.30	43.16	48.51
TiO_2	2.51	2.03	2.47	0.92
Al_2O_3	11.35	12.19	11.25	12.40
Fe_2O_3	1.75	1.70	1.80	1.74
FeO	8.76	8.50	9.02	8.70
MnO	0.20	0.18	0.19	0.18
MgO	11.91	11.03	12.05	14.85
CaO	13.53	13.49	13.85	10.15
Na_2O	3.56	2.26	3.44	1.59
K_2O	0.98	0.49	0.80	0.32
P_2O_5	0.85	0.81	0.84	0.14
Total	97.38	97.98	98.86	99.51
Norms				
Q	0	0	0	0
Or	0	2.90	4.71	1.87
Ab	0	13.02	0	13.48
An	12.09	21.67	12.92	25.74
Lc	4.55	0	0.00	0
Ne	16.32	3.31	15.75	0
Di	39.67	32.18	40.58	19.13
Hy	0	0	0	18.26
Ol	15.44	16.72	15.80	16.51
Mt	2.54	2.47	2.62	2.52
Il	4.78	3.85	4.69	1.75
Ap	2.02	1.92	1.99	0.32
Cs	0.01	0	0	0
C	0	0	0	0
Silica	undersaturated	undersaturated	undersaturated	saturated

Corporate Butte

Bulk Data	CB-1 XRF	CB-1 ICP-AES	EMT-149 ICP-AES	EMT-25 ICP-AES
SiO_2	44.06	43.66	43.99	42.61
TiO_2	2.30	2.25	2.29	2.26
Al_2O_3	11.35	11.05	15.06	11.26
Fe_2O_3	1.65	1.70	1.67	1.68
FeO	8.23	8.52	8.37	8.39
MnO	0.19	0.19	0.17	0.19
MgO	11.30	11.68	9.01	11.54
CaO	14.67	14.57	14.50	14.36
Na_2O	3.40	3.19	3.68	3.09
K_2O	1.21	1.14	0.83	1.10
P_2O_5	0.84	0.76	0.82	0.78
Total	99.19	98.72	100.38	97.25
Norms				
Q	0	0	0	0
Or	2.29	1.09	4.88	0
Ab	0	0	1.41	0
An	12.13	12.48	22.14	13.63
Lc	3.81	4.44	0	5.08
Ne	15.59	14.61	16.08	14.16
Di	44.32	44.04	36.01	41.83
Hy	0	0	0	0
Ol	12.37	13.57	11.30	13.84
Mt	2.39	2.47	2.43	2.43
Il	4.36	4.27	4.34	4.29
Ap	1.98	1.80	1.95	1.84
Cs	0	0	0	0.07
C	0	0	0	0
Silica	undersaturated	undersaturated	undersaturated	undersaturated

Hudspeth Mill Intrusion

Bulk Data	HM-1 XRF	HM-2 XRF	HM-2 ICP-AES	HM-2r ICP-AES	EMT-43 ICP-AES
SiO_2	48.46	49.44	49.37	48.71	49.26
TiO_2	1.02	1.03	1.04	1.01	0.97
Al_2O_3	12.13	12.38	12.33	12.28	11.55
Fe_2O_3	1.42	1.39	1.47	1.41	1.43
FeO	7.08	6.96	7.34	7.05	7.14
MnO	0.15	0.15	0.16	0.15	0.15
MgO	12.20	12.19	12.71	12.42	13.58
CaO	10.02	10.16	10.11	10.15	10.66
Na_2O	2.09	2.23	2.21	2.17	1.92
K_2O	2.36	2.60	2.52	2.47	2.26
P_2O_5	0.76	0.77	0.71	0.70	0.65
Total	97.69	99.31	99.94	98.53	99.57
Norms					
Q	0	0	0	0	0
Or	13.95	15.36	14.89	14.62	13.33
Ab	16.59	15.97	15.30	14.86	14.96
An	16.75	16.09	16.28	16.46	16.22
Lc	0	0	0	0	0
Ne	0.59	1.57	1.83	1.90	0.72
Di	22.45	23.47	23.43	23.48	25.91
Hy	0	0	0	0	0
Ol	21.62	21.09	22.47	21.62	23.01
Mt	2.05	2.02	2.13	2.04	2.07
Il	1.93	1.96	1.97	1.93	1.84
Ap	1.80	1.82	1.68	1.67	1.55
Cs	0	0	0	0	0
C	0	0	0	0	0
Silica	undersaturated	undersaturated	undersaturated	undersaturated	undersaturated

Hudspeth Mill Intrusion (cont.) ***Mudcreek Lamprophyres***

Bulk Data	EMT-172 ICP-AES	MC-1A ICP-AES	MC-2A ICP-AES	EMT-231A ICP-AES
SiO_2	49.47	54.91	51.41	47.55
TiO_2	1.03	2.23	2.21	2.51
Al_2O_3	12.64	12.57	11.93	13.25
Fe_2O_3	1.45	1.73	1.75	2.04
FeO	7.24	8.66	8.77	10.21
MnO	0.16	0.23	0.28	0.36
MgO	11.80	5.21	6.26	6.34
CaO	10.14	7.56	11.78	11.46
Na_2O	1.77	2.27	2.32	2.30
K_2O	2.44	2.63	2.63	2.51
P_2O_5	0.76	0.99	1.07	0.97
Total	98.90	99.01	100.42	99.51
Norms				
Q	0	0	0	0
Or	14.44	15.53	15.53	14.85
Ab	14.97	11.07	19.66	15.97
An	19.33	16.37	14.38	18.40
Lc	0	0	0	0
Ne	0	4.39	0	1.91
Di	20.91	12.06	30.35	26.42
Hy	6.48	0	8.71	0
Ol	16.97	13.39	1.30	12.01
Mt	2.10	2.51	2.54	2.96
Il	1.96	4.24	4.19	4.77
Ap	1.79	2.36	2.54	2.30
Cs	0	0	0	0
C	0	0	0	0
Silica	saturated	undersaturated	saturated	undersaturated

Black Butte Area Lamprophyres

Bulk Data	BB-1A ICP-AES	EMT-288A ICP-AES	EMT-102A ICP-AES	EMT-227A ICP-AES	EMT-68A ICP-AES
SiO_2	49.82	35.48	49.17	42.15	48.04
TiO_2	4.37	4.96	4.13	4.78	4.67
Al_2O_3	10.96	10.08	10.84	9.82	11.87
Fe_2O_3	1.91	2.08	1.92	2.37	2.03
FeO	9.53	10.42	9.62	11.84	10.13
MnO	0.13	0.74	0.13	0.55	0.10
MgO	6.72	9.43	8.88	9.64	7.50
CaO	8.63	18.23	7.53	11.84	7.30
Na_2O	2.05	2.02	2.25	1.43	2.26
K_2O	2.80	1.78	2.55	1.88	2.51
P_2O_5	1.53	2.79	1.45	2.22	1.38
Total	98.44	98.01	98.47	98.51	97.80
Norms					
Q	3.31	0	0.16	0	0.73
Or	16.55	0	15.06	11.10	14.85
Ab	17.33	0	19.06	12.07	19.13
An	12.45	13.19	11.93	14.83	14.83
Lc	0	8.25	0	0	0
Ne	0	9.26	0	0	0
Di	16.56	20.60	12.87	23.85	10.02
Hy	17.65	0	25.40	2.21	23.23
Ol	0	25.47	0	16.79	0
Mt	2.76	3.02	2.79	3.43	2.94
Il	8.30	9.42	7.85	9.09	8.88
Ap	3.61	6.61	3.44	5.26	3.27
Cs	0	5.18	0	0	0
C	0	0	0	0	0
Silica	oversaturated	undersaturated	oversaturated	saturated	oversaturated

Scott Butte Rhyolite Dike

Bulk Data	SB-1 XRF	SB-2 XRF	SB-2 ICP-AES	EMT-16 ICP-AES	EMT-268 ICP-AES
SiO_2	75.26	75.91	77.23	76.20	75.96
TiO_2	0.06	0.06	0.08	0.07	0.06
Al_2O_3	14.95	14.49	15.31	14.65	14.61
Fe_2O_3	0.21	0.24	0.23	0.55	0.39
FeO	0.41	0.48	0.46	1.09	0.78
MnO	0.01	0.01	0.00	0.01	0.01
MgO	0.77	0.48	0.74	0.64	0.49
CaO	0.90	1.14	0.82	0.93	1.14
Na_2O	3.11	3.56	3.12	3.91	3.52
K_2O	2.34	2.61	2.39	2.48	2.44
P_2O_5	0.08	0.10	0.05	0.06	0.05
Total	98.10	99.07	100.43	100.59	99.43
Norms					
Q	45.15	42.07	46.99	40.53	42.68
Or	13.83	15.42	14.13	14.68	14.39
Ab	26.32	30.12	26.39	33.09	29.79
An	3.93	5.01	3.76	4.21	5.34
Lc	0	0	0	0	0
Ne	0	0	0	0	0
Di	0	0	0	0	0
Hy	2.41	1.80	2.37	3.03	2.22
Ol	0	0	0	0	0
Mt	0.30	0.35	0.33	0.79	0.56
Il	0.12	0.11	0.15	0.14	0.12
Ap	0.19	0.23	0.12	0.15	0.12
Cs	0	0	0	0	0
C	5.86	3.97	6.21	3.98	4.22
Silica	oversaturated	oversaturated	oversaturated	oversaturated	oversaturated